BOND MECHANISMS IN FIBER REINFORCED CEMENT-BASED COMPOSITES

by

A. E. Naaman, G. Namur, H. Najm and J. Alwan

A Report on Research Sponsored by the
Air Force Office of Scientific Research
Grant No. F49620-87-C-0063

Report No. UMCE 89-9
August 1989

Department of Civil Engineering
The University of Michigan
Ann Arbor, MI 48109-2125

SECURITY CLASSIFICATION OF THIS PAGE

UNCLASSIFIED

REPORT DOCUMENTATION PAGE

1a REPORT SECURITY CLASSIFICATION: Unclassified	1b RESTRICTIVE MARKINGS:
2a SECURITY CLASSIFICATION AUTHORITY:	3 DISTRIBUTION/AVAILABILITY OF REPORT: Approved for public release, distribution unlimited
2b DECLASSIFICATION/DOWNGRADING SCHEDULE:	
4 PERFORMING ORGANIZATION REPORT NUMBER(S):	5 MONITORING ORGANIZATION REPORT NUMBER(S): AFOSR-TR- 89-1276
6a NAME OF PERFORMING ORGANIZATION: University of Michigan. / 6b OFFICE SYMBOL (If applicable):	7a NAME OF MONITORING ORGANIZATION: AFOSR
6c ADDRESS (City, State, and ZIP Code): Civil Engineering Department, Ann Arbor, MI 48109-2125	7b ADDRESS (City, State, and ZIP Code): Bolling Air Force Base, Washington, DC 20332
8a NAME OF FUNDING/SPONSORING ORGANIZATION: AFOSR / 8b OFFICE SYMBOL (If applicable): NA	9 PROCUREMENT INSTRUMENT IDENTIFICATION NUMBER: F49620-87-C-0063
8c ADDRESS (City, State, and ZIP Code): Civil Engineering, Bolling Air Force Base, Washington, DC 20332	10 SOURCE OF FUNDING NUMBERS: PROGRAM ELEMENT NO 61102F; PROJECT NO 2302/C2; TASK NO C2; WORK UNIT ACCESSION NO

11 TITLE (Include Security Classification)

BOND MECHANISMS IN FIBER REINFORCED CEMENT-BASED COMPOSITES

12 PERSONAL AUTHOR(S)

A. E. Naaman, G. Namur, H. Naim, and J. Alwan

13a TYPE OF REPORT	13b TIME COVERED	14 DATE OF REPORT (Year, Month, Day)	15 PAGE COUNT
Final	FROM 7/1/87 TO 8/30/89	1989, August	233

16 SUPPLEMENTARY NOTATION

17 COSATI CODES		
FIELD	GROUP	SUB-GROUP

18 SUBJECT TERMS (Continue on reverse if necessary and identify by block number)
Fiber concrete, cement composites, SIFCON, bond, interfaces, mathematical modeling, constitutive modeling, pull-out test, friction, latex, fly ash, microsilica, shear, (JES)

19 ABSTRACT (Continue on reverse if necessary and identify by block number)

This report presents a comprehensive investigation of the mechanisms of bond in steel fiber reinforced cement based composites. Following a state-of-the-art review on bond in reinforced and prestressed concrete as well as fiber reinforced concrete, the results of an experimental and an analytical program are described. The experimental program focuses primarily on the behavior of fibers under pull-out conditions. Pull-out load versus end slip behavior and bond shear stress versus slip relationship are studied extensively. The bond shear stress versus slip relationship is assumed to be a constitutive property of the interface. Variables influencing the shear stress versus slip response include different types of fibers (smooth, hooked, deformed), different additives to the cement matrix (fly ash, microsilica, latex), different embedment lengths, different fiber diameters, and the medium from which the fiber

(OVER)

20 DISTRIBUTION/AVAILABILITY OF ABSTRACT	21 ABSTRACT SECURITY CLASSIFICATION
☒ UNCLASSIFIED/UNLIMITED ☐ SAME AS RPT ☐ DTIC USERS	

22a NAME OF RESPONSIBLE INDIVIDUAL	22b TELEPHONE (Include Area Code)	22c OFFICE SYMBOL
Dr. Spencer T. Wu	(202) 767-6962	AFOSR/NA

DD FORM 1473, 84 MAR — 83 APR edition may be used until exhausted. All other editions are obsolete.

SECURITY CLASSIFICATION OF THIS PAGE

UNCLASSIFIED

19. (Continued)

is pulled out (plain concrete, fiber reinforced concrete and SIFCON). The analytical program addresses three complementary problems. In the first model the general solution of the pull-out problem is developed, namely: for a given bond shear stress slip relationship, a pull-out load versus end slip response is predicted and, inversely, for a given experimental pull-out load versus end slip curve, a shear stress versus slip relationship is derived. The second and third models address the problem of a representative unit of composite consisting of a prism of matrix with a single fiber along its axis. The second model assumes a given bond shear stress versus slip relationship while the third model is based on a mechanism of force transfer between the fiber and the matrix similar to the truss model in shear. The two models lead to predictions equations for the normal stress distribution in the fiber and the matrix and the shear stress distribution at their interface. Both the experimental and the analytical studies lead the way to numerous research topics that need further understanding and analysis.

UNIVERSITY OF MICHIGAN
DEPARTMENT OF CIVIL ENGINEERING
ANN ARBOR, MICHIGAN, 48109-2125

BOND MECHANISMS IN FIBER REINFORCED CEMENT-BASED COMPOSITES

by

A. E. Naaman, G. Namur, H. Najm and J. Alwan

A Report on Research Sponsored by the
Air Force Office of Scientific Research
Grant No. F49620-87-C-0063

Report No. UMCE 89-9
August 1989

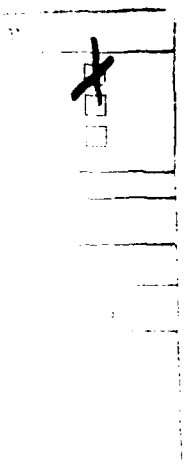

A-1

TABLE OF CONTENTS

LIST OF FIGURES

Figure

LIST OF TABLES

LIST OF NOTATIONS

A_c	=	area of concrete in a reinforced concrete specimen
$\mathring{A}_c$	=	area of composite
A_f	=	area of fiber
A_m	=	area of matrix
A_s	=	area of steel rebar
d	=	diameter of reinforcement
D	=	diameter of reinforced concrete cylinder
D_u	=	diameter of representative unit
E_f	=	modulus of elasticity of fiber
E_m	=	modulus of elasticity of matrix
E_s	=	modulus of elasticity of steel rebar
f_c	=	tensile stress in concrete in a reinforced concrete specimen
f_f	=	tensile stress in fiber
f_m	=	tensile stress in matrix
f_s	=	tensile stress in steel rebar
f_t	=	tensile strength of matrix
F	=	tensile force in fiber
F_b	=	tensile force in the fiber in the bonded zone
F_d	=	tensile force in the fiber in the debonded zone
F_o	=	force acting on representative unit of composite

F_f^* = fraction of F_o that is proportional to the fiber relative stiffness

F_m^* = fraction of F_o that is proportional to the matrix relative stiffness

ℓ = fiber length

ℓ_d = half the debonded length

ℓ_t = distance from center of fiber to point where debonding starts

L = length of reinforced concrete cylinder

n = modular ratio

P = pull-out force

P_b = bonded force

P_c = force acting on composite specimen

P_d = debonded force

P_{crit} = critical pull-out load

P_p = peak pull-out force

r = radial distance from center of fiber to centroid of disk whose interior diameter is that of the fiber, and exterior diameter is that of representative unit

S = local slip between fiber/reinforcement and matrix

S_b = back slip

t = interfacial shear flow

t_b = shear flow in the bonded region

t_f = interfacial frictional shear flow

t_{max} = maximum interfacial shear flow(strength)

t_l = maximum interfacial shear flow

T = tensile force in matrix

T_{max} = maximum tensile force in matrix

V_f = fiber volume fraction

α = angle between axis of fiber and compressive matrix strut in the mechanical model

χ = fraction of the total force acting on the representative unit that is taken by the fiber tips

χ_{crit} = critical value of χ for which the force distributions in the fiber and the matrix are uniform

δ_f = local displacement of fiber

δ_m = local displacement of matrix

Δ = end slip

Δ_p = pull-out slip at peak

Δ_o = pull-out slip at full debonding

ε_c = local strain in concrete in a reinforced concrete specimen

ε_f = local strain of fiber

ε_m = local strain of matrix

ε_s = local strain in steel rebar

κ = Bond Modulus

κ_1 = Bond Modulus Index

κ_d = decaying frictional bond modulus

ν = Poisson's ratio for matrix

ρ = Debonding Index

σ_c = stress applied to the composite specimen

$(\sigma_c)_{cr}$ = stress applied to the composite specimen that would create cracking

$(\sigma_c)_{deb}$ = stress applied to the composite specimen that would enhance debonding at the interface between fibers and the matrix

τ = shear stress at interface between fiber and matrix

τ_f = frictional bond shear stress at the interface between fiber and matrix

τ_{max} = bond strength of the interface between fiber and matrix

τ_1 = maximum theoretical shear stress at interface between fiber and matrix(applied)

Ω = bonding factor

ψ = perimeter of reinforcement

CHAPTER I

EXECUTIVE SUMMARY

1.1 INTRODUCTION

Cementitious materials such as mortar and concrete are brittle and have an inherent weakness in resisting tension. They are known to crack under low levels of tensile strains. The addition of discontinuous fibers to such matrices leads to a drastic improvement in their toughness. It is generally agreed that the fiber contribute primarily to the post-cracking response of the composite by bridging the cracks and providing resistance to crack opening. The transmission of forces between the fibers and the matrix is achieved through interfacial bond, defined as the shearing stress at the interface between the fiber and the surrounding matrix. Bond has been recognized as a major factor in composite action. There is hardly any property of the composite that is not dependent on bond. Thus there exists a genuine need to provide a fundamental undestanding of bond and bond mechanims in fiber reinforced cement composites.

The nature of bond in today's fiber reinforced cementitious composites is very complex because of the presence and the combined action of several bond components. These include: 1) physical and chemical adhesion between fiber and matrix, 2) the mechanical component of bond such as in deformed, crimped and hooked fibers, 3) fiber to fiber interlock, or entanglement, which exists in SIFCON even before addition of the matrix, and 4) friction which is greatly influenced by confinement. The addition of latex to a cement matrix may add significantly to the magnitude of the "adhesion" component of bond especially in the precracking state. The shear stress-slip relation of a smooth fiber may be

substantially different from that of a hooked or deformed fiber. Both may lead to the same maximum shear yet have drastically different slip characteristics and pull-out energies. All the above factors must be accounted for to better undestand the behavior of fiber reinforced cement composites and develop models to predict their mechanical and fracture properties.

1.2. OBJECTIVES

The main objective of this research is to investigate the various fundamental mechanisms of bond, generate a related comprehensive experimental data base, and develop rational analytical models to describe bond in fiber reinforced cement based composites. A particular focus is placed at characterizing bond by a bond shear stress versus slip relatiohship. Such a relationship is considered to be a constitutive property of the interface, and, for given conditions, is considered to be location independent. It is also the objective of this research to better assess the shear stress distribution along the fiber as well as the distribution of normal stresses in the fiber and the matrix.

1.3 SUMMARY

Following is a brief summary of what was achieved in this study:

1. A review of the state-of-the-art on bond in conventional reinforced and prestressed concrete was carried out. Particular attention was given to the study and determination of a bond shear stress versus slip relationship (Chapter II) which is believed to be a characteristic property of the interface to the same extent as a stress-strain curve in compression or tension. It is observed that the derivative of the slip between the reinforcement and the surrounding matrix is the difference between the strain in the fiber and that in the matrix at a given point along the reinforcement. Experimental approaches to the determination of a shear stress-slip relationship are described, and existing models for bond shear stress distribution are evaluated, discussed and compared (Chapter III). The most important factors

affecting bond are reviewed. It is observed that, while the concept of a bond shear stress versus slip relationship has been applied to conventional reinforcement, such a relationship has so far not been developed for fiber reinforced concrete.

2. A state-of-the-art review on bond in fiber reinforced cement composites is presented in Chapter IV. The review addresses both experimental work and analytical studies. Factors affecting bond and bond mechanisms in cement based composites are discussed. Observations which are either agreed upon or a subject of disagreement between researchers are pointed out.

3. A basic analytical study of a typical pull-out test is developed in Chapter V. The test consists in a fiber embedded in a matrix and being pulled out at its free end. The study is subdivided into two parts, one dealing with what is defined as the primal problem and the other dealing with the dual or reciprocal problem. The primal problem focuses on predicting the pull-out load versus end slip response of a pull-out test based on the knowledge of an idealized bond shear stress versus slip relationship. For small values of slip, the idealized relatiohship is assumed to be linear perfectly frictional, and characterized by three parameters, namely a shear modulus, a maximum shear strength which includes adhesion and friction, and a frictional shear stress which may be different from the shear strength. The dual problem, which is the reciprocal of the primal problem, predicts a bond shear stress versus slip relationship based on an experimentally obtained pull-out curve. For large slips, in both problems, decaying friction was considered. It was modeled using the concept of misfit which accounts for the influence of normal pressure due to shrinkage of the matrix, and including the effect of fiber Poisson's ratio. The solution of the dual problem forms the basis for the interpretation of the results of the experimental program undertaken in this investigation.

4. A comprehensive experimental program on pull-out and pull-through tests is described in Chapter VI. . The pull-out load versus end slip response was carefully measured. Parameters included three

different types of fibers (smooth, deformed, hooked), three different mortar matrices with low, medium, and high strengths, one slurry paste matrix, and additives such as latex, fly ash, and microsilica. Also the medium from which the fiber was pulled out included a control mix without fibers, mixes with 1%, 2% and 3% fibers by volume, and a SIFCON matrix containing about 11% fibers by volume. For smooth fibers, five different diameters and three different embeddment lengths were investigated. Chapter VI also contains comparisons between experimental pull-out load versus slip curves and curves predicted by the analytical model developed in Chapter V. Typical bond shear stress versus slip curves are derived using the analytical approach described in Chapter V and are input in the solution equations of the primal problem to predict typical pull-out load versus slip curves and compare them with the experimentally observed curves.

5. Two different and independent analytical models were developed in Chapters VII and VIII. These models are also independent of the pull-out problem described in Chapter V and VI. Both models assume that the composite has a square packing distribution of fibers and that a representative unit made out of a prism of matrix containing one fiber can be analysed in lieu of the composite as a whole. The first model is based on an assumed bond stress versus slip relationship that consists of a linear ascending portion followed by a constant purely frictional portion. It leads to prediction equations for the stress distribution in the fiber, the matrix and the interface. Two numerical examples illustrating the application of the procedure are described in Chapter VII. The second model developed in Chapter VIII is based on a mechanism of force transfer between the fiber and the matrix. The mechanism is similar to the truss analogy method, except that the matrix is assumed uncracked and the external tensile force is applied to the fiber. Thus the model applies particularly well to the case of continuous fibers or long fibers bridging more than one crack. The model leads to prediciton equations for the interfacial shear stresses as well as the normal stresses in the fiber and in the matrix. It also led to the analytical

prediction of a bond modulus as well as the prediction of the precracking strength of the composite. Chapter VIII also contains a parametric evaluation of various composite properties using the model.

1.4 CONCLUDING REMARKS

Specific and detailed conclusions related to the experimental investigation as well as to the analytical models developed in this study can be found at the end of Chapters V to VIII. The following conclusions address more generally the overall objective of this research.

1. For conventional reinforcing bars and prestressing strands, the bond shear stress versus slip relationship can be determined experimentally by instrumenting the bar along its length using for instance, strain gages. Such an approach cannot be used in the case of small fibers. In this study, bond shear stress versus slip relationship were derived indirectly from a pull-out test in which the load and the slip were measured simultaneously.

2. A methodology was developed to derive a bond shear stress versus slip relationship for various types of smooth fibers. A typical relationship would be elastic linear up to a maximum shear stress, τ_{max}, then drops suddently to a maximum frictional stress, τ_f, then decays exponentially to zero with increasing slip. It is observed that for hooked fibers, the relationship can be obtained from superimposing two relationships, one characteristic of a smooth fiber without the hook and the other characteristic of the hook alone. In a hooked fiber, the hook tends to straighten under pull-out leading to a characteristic load versus slip response. However, the slip at which the load is maximum is substantially larger than that for which the load is maximum for a smooth fiber. Deformed fibers have mechanical deformations uniformely distributed along their length. The fibers used in this study were dented along segments about 0.2 in long each. Thus they had a section that varied every 0.2 in. They too seem to respond through the surperpositon of two mechanisms,

one due to the adhesion similar to that of a smooth fiber, and the other due to the mechanical bearing against the surrounding matrix induced by the variation in cross section.

3. For small values of slip, such as encountered up to the peak pull-out load in a typical pull-out test, the bond shear stress versus slip relationship can be assumed to have, as a first approximation, a constant frictional property. That is, the decay in friction with the slip is ignored. Such an assumption greatly simplifies the analytical model and leads to a negligeable error.

4. The medium (slurry, plain matrix, fiber reinforced matrix) from which a fiber pulls-out influences the pull-out load versus slip curve. It was observed that the presence of fibers tends to improve primarily the post peak response in fiber reinforced mortar, and the peak load as well as the post peak behavior in SIFCON. The addition of latex to the matrix leads to a significant improvement in the peak load (up to four times), but has no effect on the post-peak response. The addition of microsilica does not seem to improve the bond characteristics of smooth fibers beyond what is predicted from the induced improvement in matrix strength. The addition of fly ash to the matrix led to very small improvement in the overall response.

5. Everything else being equal, the slip at maximum load for hooked or deformed fibers is one to two orders of magnitude larger than that of a smooth fiber. This is due to the mechanical contribution of the hook in hooked fibers and the non-uniform section in deformed fibers. As a result, the pull-out work up to the peak load for hooked and deformed fibers can be ten to twenty times that of a smooth fiber.

6. Everything else being equal, the pull-out work of a hooked or a deformed fiber up to complete pull-out can be three to four times that of a smooth fiber.

7. A deformed fiber shows in the post peak load response a cyclic behavior that is characteristic of the way the non uniform section moves in its surrounding tunnel of matrix.

8. Observed values of maximum pull-out loads on single fibers lead to the following ranges for the maximum bond stress calculated as the maximum pull-out load divided by the embedded surface area: from 150 to 400 psi for smooth fibers, from 500 to 1000 psi for hooked fibers, and from 400 to 950 psi for deformed fibers. It should be observed that, although differences between smooth fibers and deformed and hooked fibers are significant, they tend to be smaller when the whole composite is considered. This is because the pull-out load per fiber decreases when the number of fibers pulling out from the same area increases. The addition of latex to the matrix led to bond stresses as high as about 1400 psi. However, the frictional stress was similar to that obtained without latex.

9. Observed frictional shear stress values for smooth fibers ranged from about 170 to 290 psi for the range of variables tested in this study.

10. For smooth fibers, bond shear modulus (obtained from the slope of the initial portion of the shear stress versus slip curve) varied from about 1×10^6 to 9×10^6 lb/in3.

1.5 RECOMMENDATIONS FOR FUTURE WORK

Following is a list of recommendations for future research related to bond in fiber reinforced cement composites. The list is by no means exhaustive but reflects several areas that were touched upon in this investigation.

1. There is need to better understand frictional decay with the extent of slip and to model the mechanisms involved. A model based on damage mechanics may be most approriate. This should help in better predicting the descending branch of the load versus slip response in a typical pull-out test. The analytical work may be coupled with an experimental investigation using, for instance, a

comprehensive microscopic analysis of the history of debonding with slip.

2. There is a need to better understand the mechanical component of bond for a deformed or a hooked fiber and to model such behavior. It is observed that the maximum contribution of the mechanical component of bond occurs much after the maximum adhesion-friction is developed. This contribution seems to significantly improve the pull-out work up to the peak load.

3. The phenomenon of fiber entanglement or interlock found in highly reinforced fiber cement composites such as SIFCON, should be more thoroughly addressed both experimentally and analytically.

4. The models developed in Chapters VII and VIII in which a tensile prism containing one fiber is analysed, assumed that the load is applied to the fiber and transferred to the matrix. The reciprocal problem should be addressed, that is, to apply the load to the matrix and study the stress transfer to the fiber. The two solutions should help in modeling the behavior of the composite before and after cracking. Such a study can also be coupled with a finite element solution to check the validity of the model.

5. The effect of strain rate on the shape of the bond shear stress versus slip curve should be investigated. Such a study would provide a better understanding of the effects of strain rate on the mechanical properties of the composite.

6. There is need to investigate the modulus of elasticity of the composite and to develop a rational prediction model whereas the bond shear stress versus slip relationship, which characterizes the interface, is accounted for to the same extent as the properties of the matrix and the fiber.

7. The theory developed in Chapter V regarding the pull-out process should be used in a fracture mechanics framework to predict the post-cracking response of the composite. The shear stress versus slip relationship can be suitably integrated with the constant crack

opening angle assumption to predict the onset of fracture and the fracture energy.

1.6 ACKNOWLEGMENT

This study was supported by Grant # F49620-87-C0063 from the Air Force Office of Scientific Research to the University of Michigan, Ann Arbor. Dr. Spencer T. Wu was the Air Force program Director. The support of AFOSR is gratefully acknowledged. Any opinions, findings, and conclusions expressed in this report are those of the authors and do not necessarily reflect the views of the sponsor.

The authors also would like to thank the following people from the Civil Engineering Department at the University of Michigan: students D. Otter, M. Founas, K. Soubra, and H. Hammoud for their valuable help in calibrating the electronic instrumentation, setting up the data acquisition system, and plotting much of the raw data; laboratory technicians R. Spence, K. Schmidt, D. Bigelow and R. Birch for their assistance and advice during the course of the experimental investigation.

CHAPTER II

BOND SHEAR STRESS - SLIP RELATIONSHIP

2.1 GENERAL

The general relationship between local bond stress and slip for different types of tension reinforcement is illustrated in Fig. 2.1. All types of reinforcement display a similar behavior up to the point where the adhesion breaks (ascending branch). Plain bars will slide out; the failure is hence of a sliding nature. As for ribbed bars, further loading mobilizes the mechanical interlocking between the lugs and the concrete. The effects of lug spacing and depth on the stress-slip relationship will be discussed farther ahead. This, in effect, creates circumferential tensile cracks in the surrounding concrete (see Fig. 2.2), and thus reduces the stiffness of the bond stress-slip relationship (i.e. the slope of the ascending portion of the curve becomes smaller). The existence of these internal cracks has been proven experimentlally by Goto [18]. For unconfined concrete or in the case of a small volume of surrounding concrete, the internal cracks propagate to the surface resulting in bond failure. On the other hand, if the concrete is well confined, the load can be increased beyond the creation of these cracks, up to a point where the maximum bond stress (i.e. the bond strength) is reached. At this stage, shear cracks develop as shown in Fig. 2.3. After the maximum bond stress is reached, further slip causes a reduction in the bond resistance until bond stresses all become of a frictional nature. The friction that takes place is actually between the rough concrete at the cylindrical surface where the shear cracks developed [14].

It is worth noting that there is a general tendency to believe that the shear stress-slip relationship is of a local nature, meaning that this rela-

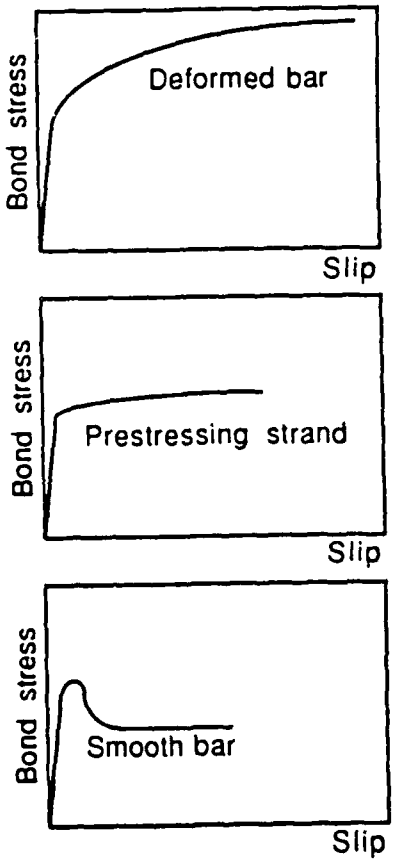

Fig. 2.1 - General relationship between bond stress and slip for different types of tension reinforcement.

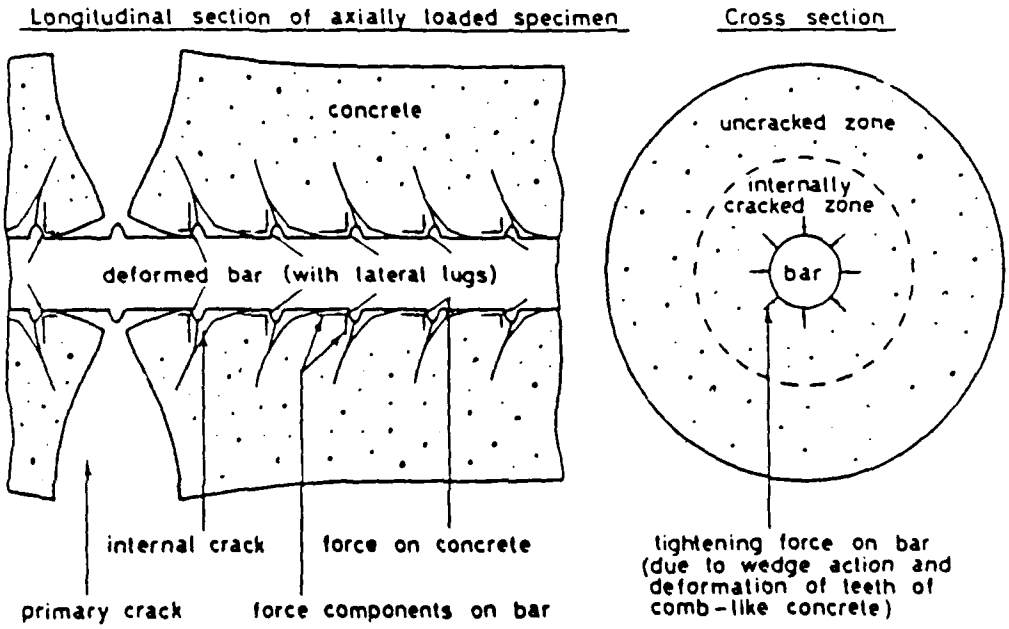

Fig. 2.2 - Internal bond cracks and forces acting on concrete (From Ref. 18).

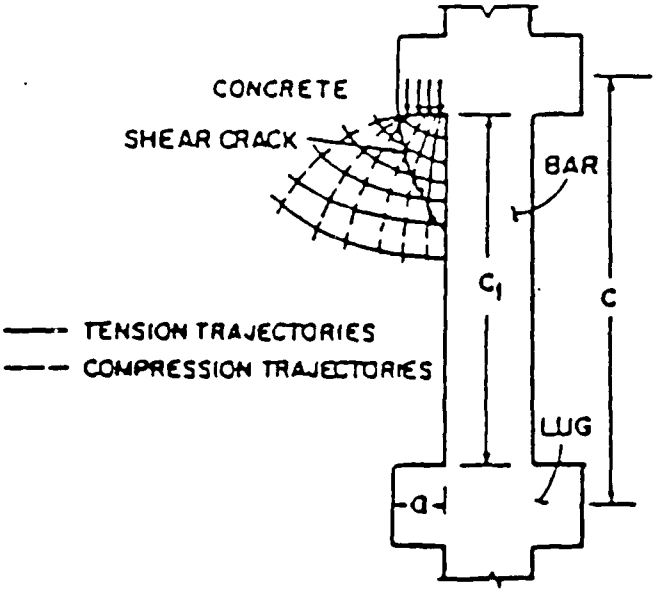

Fig. 2.3 - Shear cracks in concrete keys between lugs (From Ref. 14).

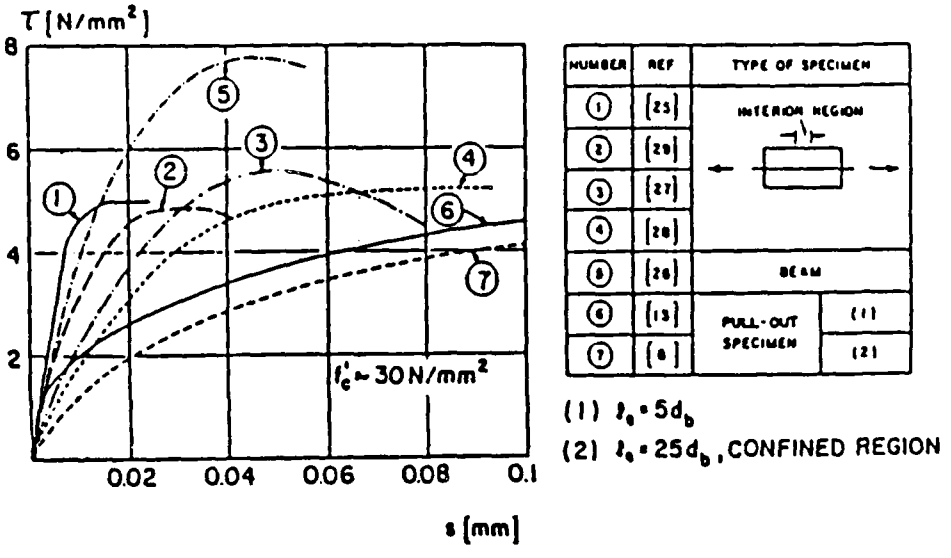

Fig. 2.4 - Local bond stress-slip relationships for reinforcing steel bars after different researchers (From Ref. 14).

tionship is not unique, but depends instead on the location [1,16,23,25,45,55]. However, Edwards and Yannopoulos [12] stated that "the maximum bond stress value would not vary with distance from a loaded end, or a crack face, in a concrete member." Mirza and Houde [37] reported similar findings.

2.2 MODELS AND STUDIES OF STRESS-SLIP RELATIONSHIPS

Extensive experimental studies were undertaken in recent years to determine the characteristic behavior of local bond stress-slip relationship of deformed reinforcing steel bars [11,14,37,45,46], and several mathematical models were proposed. However, depending on the case, the characteristic behavior of the bond stress-slip relationship shows significant scatter. This scatter can be illustrated in Fig. 2.4.

Nilson [45] carried out tests on 6x6x18 in. prism specimens to study the local bond stress-slip relationship on concrete-steel interfaces. #8 bars were used in these tests. All specimens were subjected to concentric tension forces acting on both ends of the embedded bar. As was mentioned earlier, it was concluded from this study that the bond stress-slip relationship varies along the embedment length, and is thus not unique. The following equations were suggested by Nilson to relate the bond stress to the slip and the distance from the loaded end:

$$\tau_x = 3100\,(1.43\,c + 1.5)\,S_x\,\sqrt{f'_c} \qquad (2.1)$$

$$\tau_x \leq (1.43\,c + 1.5)\,\sqrt{f'_c} \qquad (2.2)$$

where τ_x is the local bond stress in psi, c and S_x represent the distance from the loaded end (in.) and the slip respectively, and f'_c is the concrete compressive strength in psi. The slip is the relative displacement between the concrete and the steel bar.

Comparisons between Eq. 2.1 and the experimental results for different values of c are shown in Fig. 2.5.

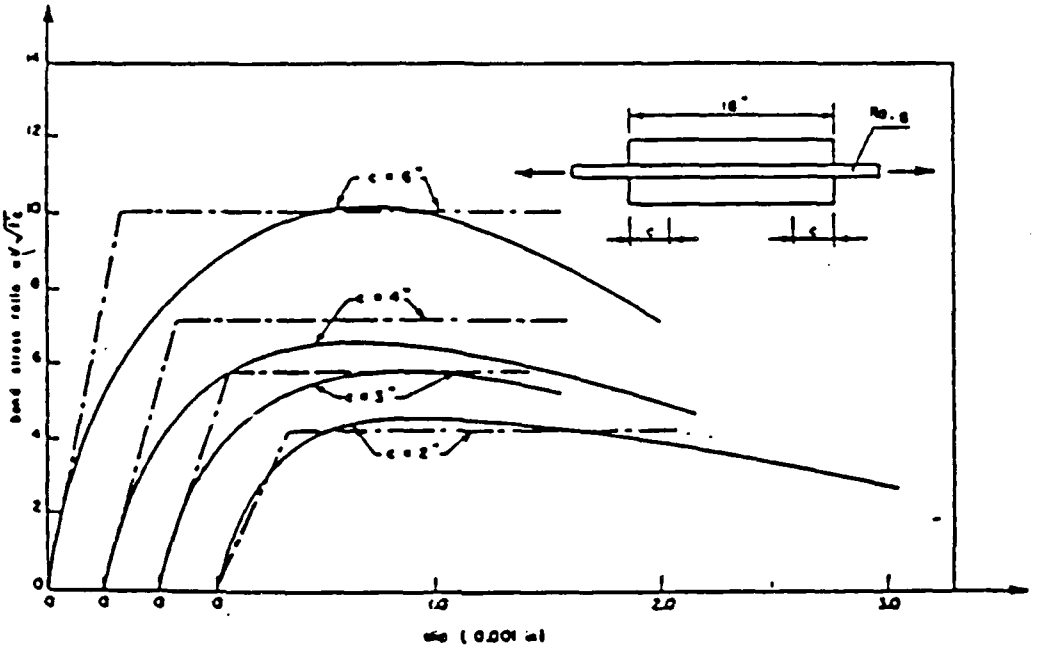

Fig. 2.5 - Comparison between Eqs. 2.1 and 2.2 and experimental data (From Ref. 45).

Mirza and Houde [37] tested 62 pull-out tension specimens reinforced with steel bars ranging from #4 to #8. Different concrete strengths and different size prisms were studied. The authors found out that the bond stress is independent of the distance from the loaded end. This is in contradiction with what was stated by Nilson. Mirza and Houde suggested the following expression for the bond stress-slip relationship:

$$\tau_x = 1.95\text{x}10^6 S_x - 2.35\text{x}10^9 S_x^2 + 1.39\text{x}10^{12} S_x^3 - 0.33\text{x}10^{15} S_x^4 \qquad (2.3)$$

where τ_x is the local bond stress in psi, normalized to $\sqrt{f'_c}$ (f'_c = 5000 psi) and S_x is the local slip in inches. Concrete strengths other than 5000 psi can be accounted for by multiplying the right hand side of Eq. 2.3 by $\sqrt{\frac{f'_c}{5000}}$.

Recently, an extensive study was conducted by Eligehausen, Popov and Bertero [14] to determine the local bond stress-slip relationship under generalized excitations. Pull-out tests were conducted on concrete specimens with small embedment lengths (5 times the bar diameter). Different bar diameters d_b (#6 to #10) and different concrete strengths (4000 to 8000 psi) were used. In addition, the effect of bar spacing and the amount of confining reinforcement, to simulate the conditions prevailing in an actual joint, were also studied. The authors observed that confinement helps restrain the propagation of the secondary internal tensile cracks around the bar lugs, and thus increase the bond strength significantly. Specimens with no confining reinforcement developed a peak bond stress of about 6 MPa as opposed to the 13.5 MPa developed in confined specimens. It was also observed that the bar diameter has little influence on the maximum bond strength. Moreover, it was observed that for a given slip, the bond strength increases linearly with $\sqrt{f'_c}$. The following expression was suggested for the ascending portion of the local bond stress-slip curve:

$$\tau_x = \tau_{max} \left(\frac{S_x}{S_1}\right)^{0.4} \qquad (2.4)$$

where :

τ_x = local bond stress

τ_{max} = maximum bond strength

S_x = local slip

S_1 = local slip corresponding to τ_{max}.

The average observed values [14] of τ_{max} and S_1 were respectively 13.5 MPa and 1.0 mm for a 30 MPa concrete strength. Typical plots of the bond stress-slip relationship for the monotonic loading are shown in Fig. 2.6.

Stocker and Sozen [58] carried out pull-out tests on 1/2" prestressing strands with short embedment length (0.5-2 in.) and different concrete strengths. The average value of maximum bond strength in their study was about 0.4 ksi for a 2500 psi concrete strength, 0.56 ksi for 6000 psi concrete and 0.58 ksi for a 7500 psi concrete.

Edward and Picard [11] tested a total of 12 specimens to study the bond characteristics of 1/2" prestressing strands. The embedment length of the strands was 1.5" and the average concrete cube strength of all the specimens was 9640 psi. It was observed that the average value of the maximum bond strength decreases with increasing concrete cover. This observation was attributed to the settlement of the concrete under the strand which was held in a horizontal position during casting. They concluded that the bond-slip relationship for strands is almost linear up to the peak bond stress and remains constant and equal to its maximum value thereafter, provided no longitudinal cracks appear in the specimens. The maximum bond stress in this test varied between 0.33 and 0.67 ksi, and the stiffness of the bond stress-slip curve varied between 665 and 879 k/in^3. Typical plots of bond stress-slip relationships in their test is shown in Fig. 2.7.

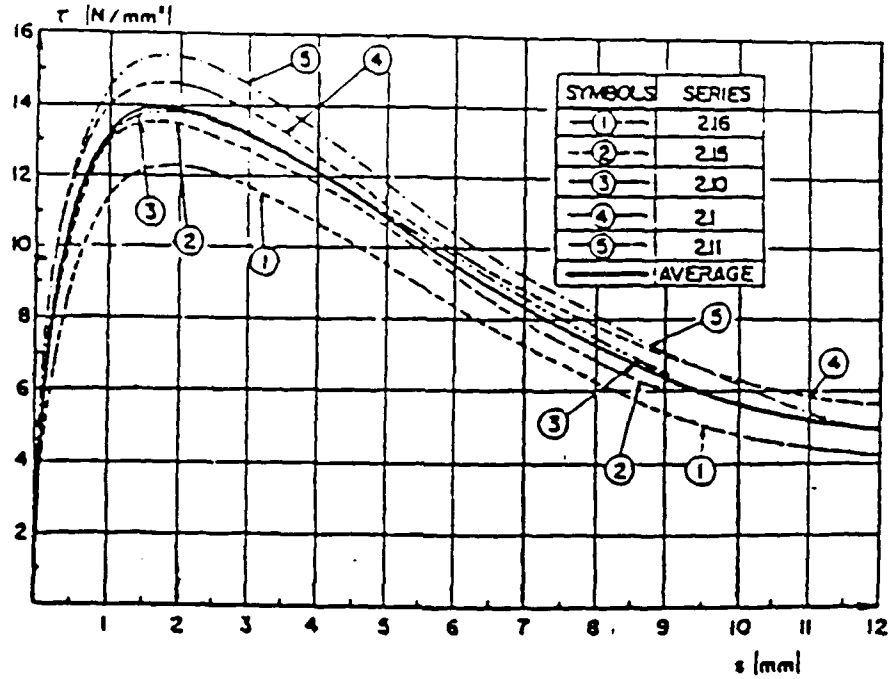

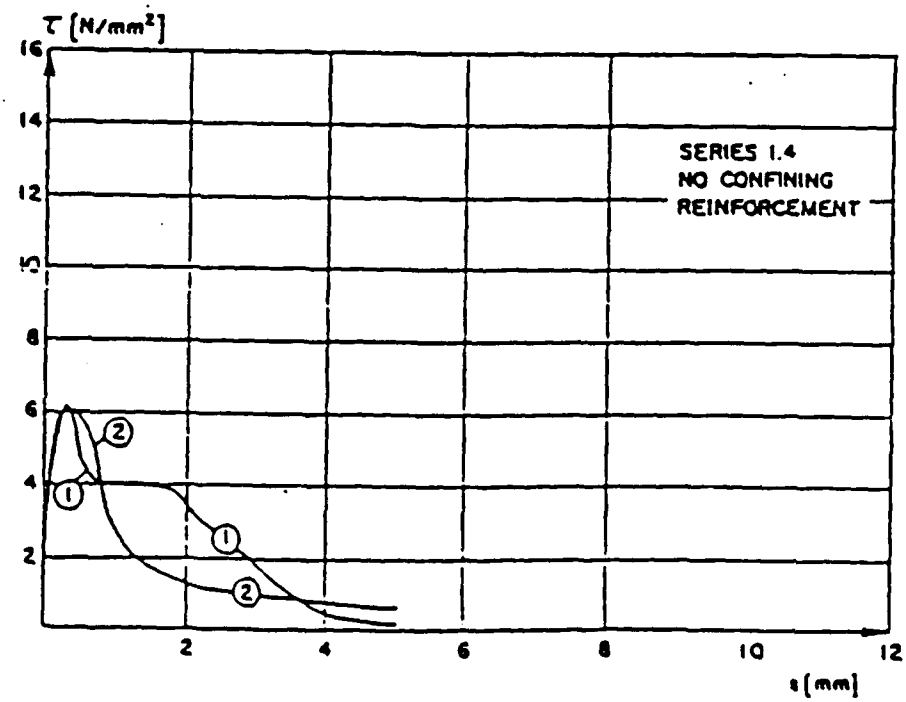

Fig. 2.6 - Bond stress-slip relationships for reinforcing steel bars (From Ref. 14).

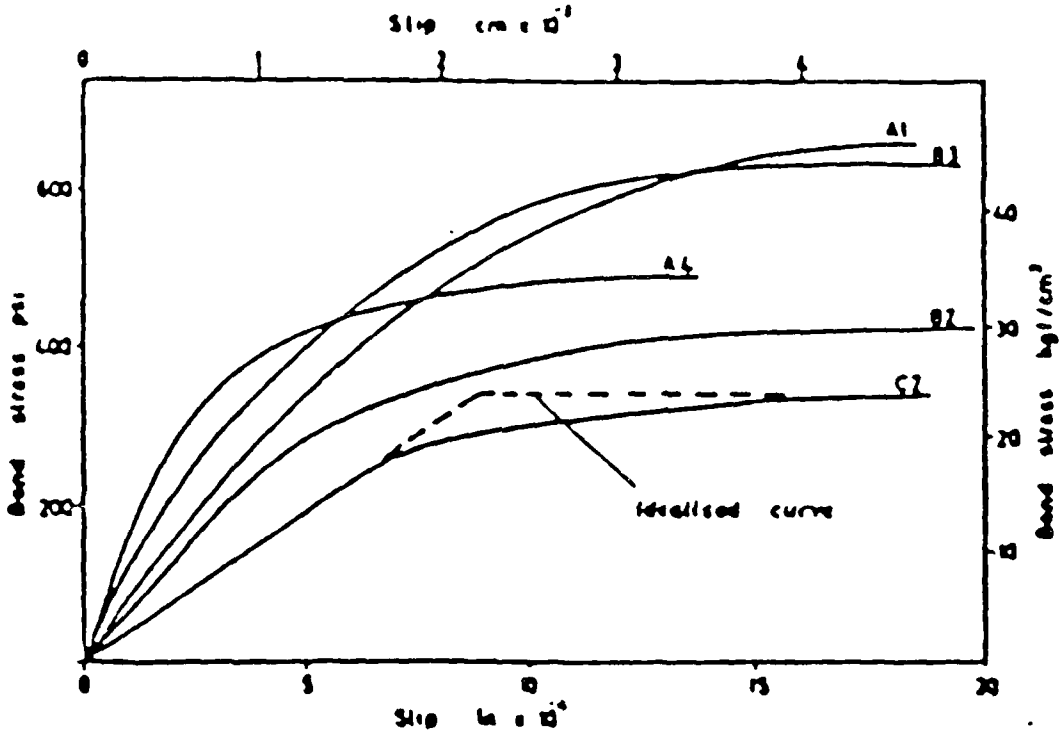

Fig. 2.7 - Local bond stress-slip relationship for prestressing strands (From Ref. 11).

2.3 EXPERIMENTAL APPROACH: STRESS-SLIP THROUGH STRAIN MEASUREMENT

Another approach to the problem is the experimental way, which is easy conceptually, but rather difficult to perform, especially in the case of fiber reinforcement. It was used by Nilson [45] to obtain stress-slip curves.

The experimental determination of the force-displacement relationship in bond has two components: the bond stress must be found, and the slip between steel and concrete must be measured. Since both these quantities vary with distance along the bar at any load, it is desirable to establish each as a continuous function of distance.

The average unit bond stress, expressed in units of force per unit interfacial area, is an appropriate parameter. This stress is given by:

$$\tau = \frac{dT}{\psi\, dx} \tag{2.5}$$

$$= \frac{A_s\, df_s}{\psi\, dx} \tag{2.6}$$

Eq. (2.6) can be easily restated in terms of the tensile strain ε_s in the steel:

$$u = \frac{A_s\, E_s\, d\varepsilon_s}{\psi\, dx} \tag{2.7}$$

where:

τ = average bond stress at location considered

dT = change in bar tension in length dx

ψ = bar perimeter

A_s = bar cross-sectional area

df_s = change in steel tensile stress in length dx

E_s = modulus of elasticity of steel

Bond stress at any location along the interface, at any load, is thus proportional to the slope of the steel strain distribution curve at that point and that load. Eq. 2.7 assumes that steel is still in the elastic range. In reinforced concrete, this fact is usually true because reinforced concrete members are usually designed in such a way that under working loads, the stress level in steel does not exceed 50% of yield. This assumption is also sound in the case of steel fiber reinforced concrete since it has been established that steel fibers usually pull-out before they yield.

To get the shear stress-slip relationship using this method, all is needed is the strain distribution for both steel and concrete along the steel, be it a reinforcing bar or a fiber. Indeed, bond slip can be found indirectly as the difference between the steel displacement and that of concrete, at any location on the interface, with respect to some transverse reference plane. In case of reinforced concrete, this plane should be the median of the portion of the bar between two primary cracks. In the case of fiber reinforced concrete, if the fiber is not crossed by any crack, the reference plane would simply be the median of the fiber, otherwise this plane would be the plane of the crack. The displacement function for the concrete and the steel may be obtained by integration of the strain functions.

Nilson [45] obtained the steel strain distribution as follows. The reinforcing bar was sawed longitudinally on a diametral plane, and slots milled along the centerline of each cut surface. Electric resistance gages were then attached at close intervals along the bottom of each slot, after which the two halves of the bar were rejoined using epoxy cement. As for the concrete, he used electric resistance strain gages cemented between two thin polyester resin blocks. The outer surface of the resin is coated with coarse grit material to provide good bonding with the concrete. Such gages were embedded in test specimens at intervals along the interface, and 1/2 in. from it.

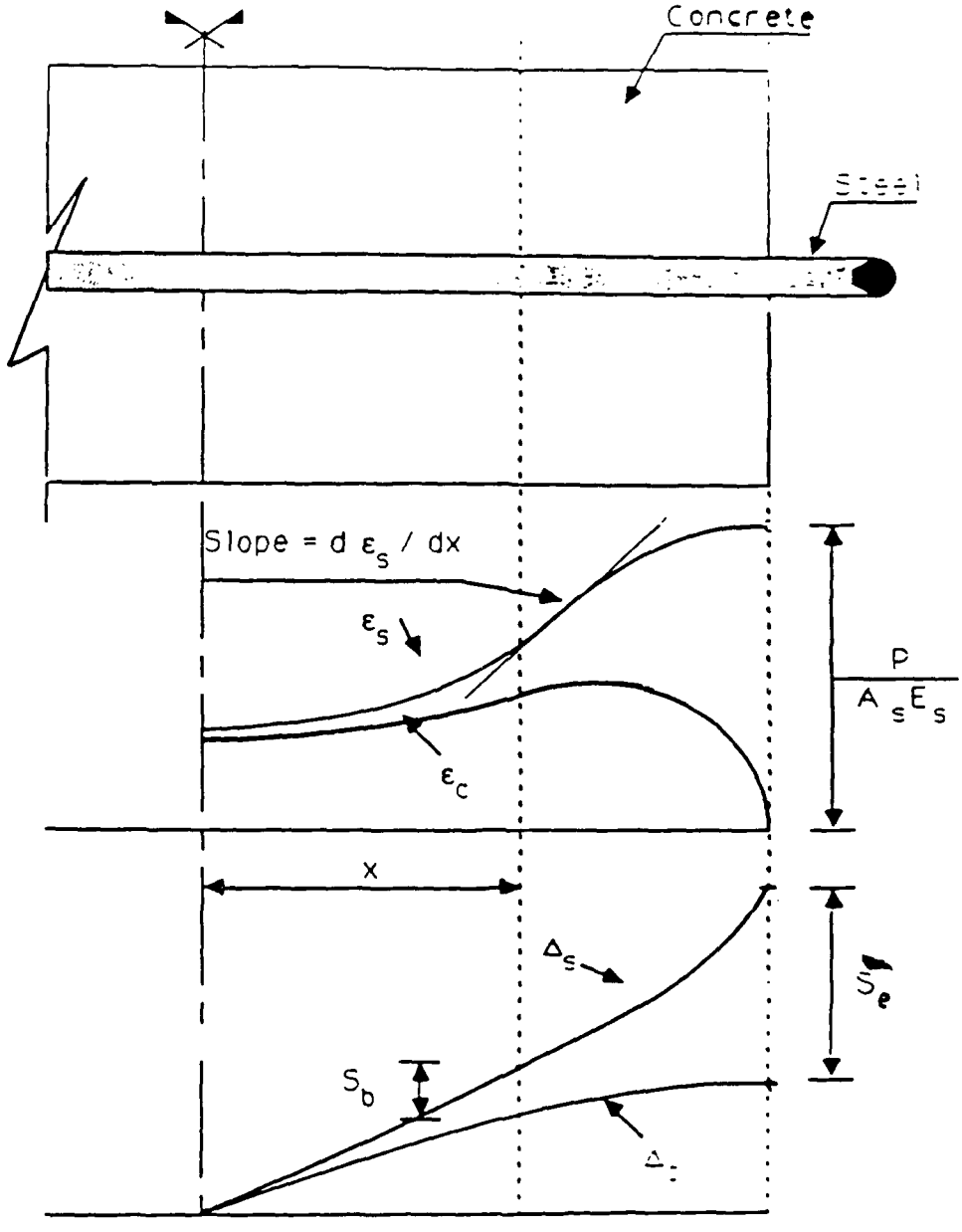

Fig. 2.8 - Determination of slip from strain functions (Reproduced from Ref. 45).

In Fig. 2.8, the variation of steel strain is plotted as a function of distance, and so is the concrete strain. Integration of each strain function along the bar length provides the displacement of the steel and the concrete, measured from the reference plane.

With the bond stress calculated from the slope of the steel strain curve using Eq. 2.7, and the bond slip found by numerical integration, one point on the bond stress-slip curve is established. By increasing the load incrementally, subsequent points may be obtained for larger bond stress and slip, hence defining the complete curve at a given location.

CHAPTER III

EXISTING MODELS FOR BOND SHEAR STRESS DISTRIBUTION

3.1 GENERALITIES

In composite materials, the study of bond is an unavoidable step towards the understanding of the way forces are transmitted from the matrix to the reinforcement. The idea of reinforcing cementitious matrices stems from this concept. Since these matrices fail at much lower tensile strains than steel does, once the matrix (concrete or mortar) cracks, the tension that cannot be taken by the matrix is transmitted to the reinforcement (reinforcing bars, prestressed strands or discontinuous fibers). If there was no bond between the matrix and the reinforcement, i.e. a condition of free frictionless slippage, then the composite would fail as soon as the matrix cracks, and the reinforcement would not have taken any share of the tension. Bond is needed for tension, as well as for compression, although the force transmission and the mode of failure are different for the two cases.

In the case of fiber-reinforced concrete, bond is important in many respects. There is hardly any formula giving the tensile strength of a fiber-reinforced composite that does not contain a bond term. The bond is also important for the understanding of strain rate effects on the tensile properties of fiber reinforced concrete. This bond is usually the average bond stress along the interface which cannot be determined accurately unless the bond stress distribution along the interface is known. Various approaches have been used by researchers to determine bond stress distributions. In this chapter, three different analytical methods used in the determination of the bond stress distribution along reinforcing bars in rein-

forced concrete are reviewed. §3.5 briefly discusses a new approach to the bond action between concrete and a typical deformed steel bar. All methods presented are briefly compared to each other in §3.6 with regards to accuracy, practicality, and simplicity.

Usually, it is the average shear stress along the interface rather than the stress distribution that is needed. However, when the shear stress distribution along the interface is known, a simple integration (mathematical or numerical) gives the value of the average bond. The following three sections outline three different methods for finding the stress distribution along an interface.

3.2 ANALYTICAL METHOD BASED ON ASSUMED BOND SHEAR STRESS-SLIP RELATIONSHIP

The idea behind this method is simple conceptually, and the mathematics involved are not particularly cumbersome. This method requires an analytical relationship between the bond shear stress and the slip. It also assumes that the bond shear stress-slip relationship is unique. While this assumption may not be exact, as was pointed out earlier in Chap. 2, the fact remains, however, that this method is still valid, especially when the shear stress distribution is used for averaging the bond, as long as an average stress-slip relationship is used. The detailed mathematical aspects of this method as applied to fiber-reinforced cementitious composites are developed in Chap. 5. The essence of this method, as well as the underlying rationale are briefly described next.

It is first noted that the rate of change of the slip along the reinforcement-matrix interface is the difference between the strain in the reinforcement and the strain in the matrix. This same relationship can be expressed in function of the stresses in the reinforcement and the matrix, assuming Hooke's law applies for both of them. The stress in the matrix can be related to the stress in the reinforcement in a linear manner, so that the rate of change of the slip with distance can be expressed as a function of the stress in the reinforcement. The second derivative of the slip with respect to distance is, therefore, proportional to the rate of change of the

stress in the reinforcement with distance, which is directly related to the shearing stress through the bond-slip $(\tau\text{-}S)$ relationship assumed known. Using the $(\tau\text{-}S)$ relationship, the problem is reduced to a second degree differential equation, the solution of which provides the slip distribution with distance. This slip distribution, along with the bond shearing stress-slip relationship gives the bond shear stress distribution.

This method does not involve any mathematical approximations so long as the differential equation obtained can be analytically solved, which is not necessarily true. Furthermore, this approach yields an analytical expression for the bond stress, rather than discrete values at select points along the interface. The shear stresses at different points along the interface can be obtained by plugging the value of the distance from the point of interest to the reference point into the expression of the shear stress.

The above described method has at least one disadvantage, in that it cannot accommodate bond shear stress-slip relationships that cannot be expressed analytically. Therefore, $(\tau\text{-}S)$ relationships expressed graphically are to be modeled mathematically first, before this method can be applied. Such a modeling will inevitably introduce an error, the effect of which might be significant depending on the level of simplification adopted. It is worth mentioning that this method has been widely used.

3.3 NUMERICAL METHOD BASED ON EXPERIMENTALLY DERIVED BOND STRESS-SLIP RELATIONSHIP

Tassios and Yannopoulos [62] derived a computerized method capable of determining in a direct and analytical way the stress distributions in the reinforcement, in the matrix, as well as the bond stress distribution along the interface. It can also determine all the corresponding deformation characteristics. Examples of applications regarding pull-out tests under monotonic loading, axially loaded elements under both monotonic and cyclic loading, and flexural members under reversible loading were given.

Fig. 3.1 shows the interrelationship between the stress in the reinforcement, the stress in the matrix, the shearing stress and the slip.

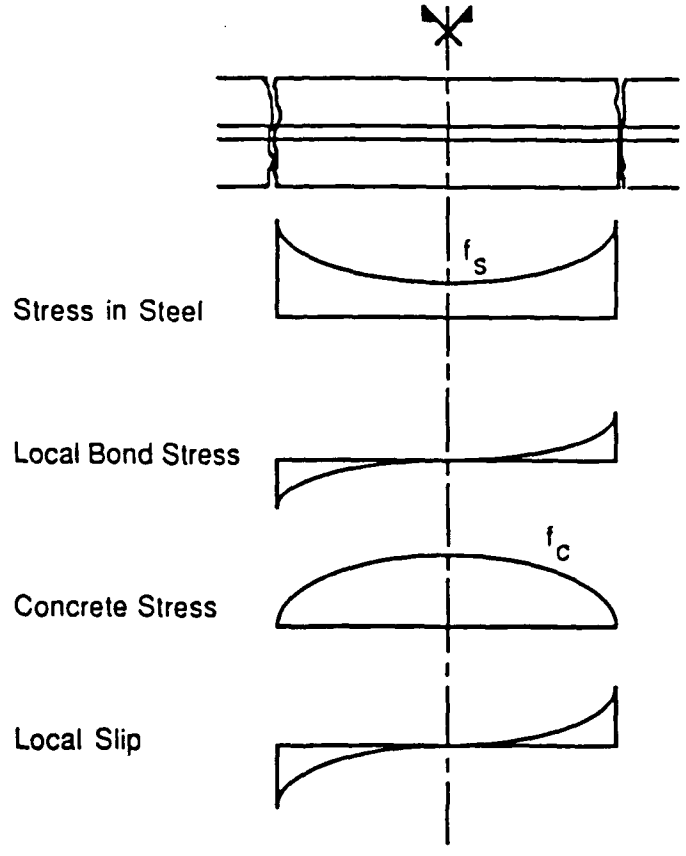

Fig. 3.1 - Schematic distributions of stresses and local slip along cracked element (Reproduced from Ref. 62).

For the axially loaded element shown in Fig. 3.2, the following elementary equations may be derived:

$$\Delta\sigma_s = \frac{4\,\tau}{\psi}\,\Delta x \tag{3.1}$$

$$\Delta\sigma_c = \frac{A_s}{A_c}\,\Delta\sigma_s \tag{3.2}$$

$$\Delta S = (\varepsilon_s - \varepsilon_c)\,\Delta x \tag{3.3}$$

where the subscripts s and c refer to the steel reinforcement and the concrete respectively, σ is the normal stress, ε is the strain, A is the area, S is the slip, τ is the bond stress along the interface, and ψ is the reinforcement perimeter.

It is assumed here that there is a unique relationship between local bond τ and local slip S at every point of a bar inserted in a mass of concrete. An axially tensioned reinforced concrete element after cracking is considered.

A typical pullout element (Fig. 3.3) is studied analytically by dividing its length into a number of parts of sufficiently small length Δx, and applying the basic relationships of Eqs. 3.1 - 3.3 at each consecutive section. In the case of axially loaded elements, only half of their length needs to be considered because of symmetry.

The following algorithm is applied to compute the values of σ_s, σ_c, S, and τ at section i+1, knowing the corresponding values at section i and assuming that τ is uniformly distributed over the elementary length Δx:

$$\sigma_{s,i+1} = \sigma_{s,i} - \frac{4\,\tau_i}{\psi}\,\Delta x \tag{3.4}$$

$$\sigma_{c,i+1} = \sigma_{c,i} - (\sigma_{s,i+1} - \sigma_{s,i})\,\frac{A_s}{A_c} \tag{3.5}$$

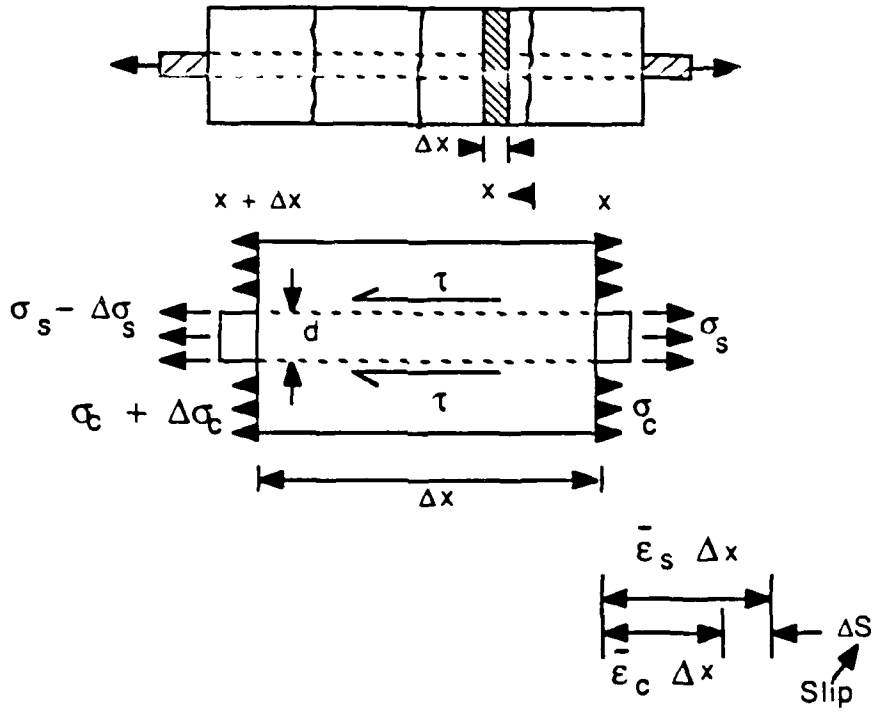

Fig. 3.2 - Stresses and strains on a finite length of a reinforced concrete element (Reproduced from Ref. 62).

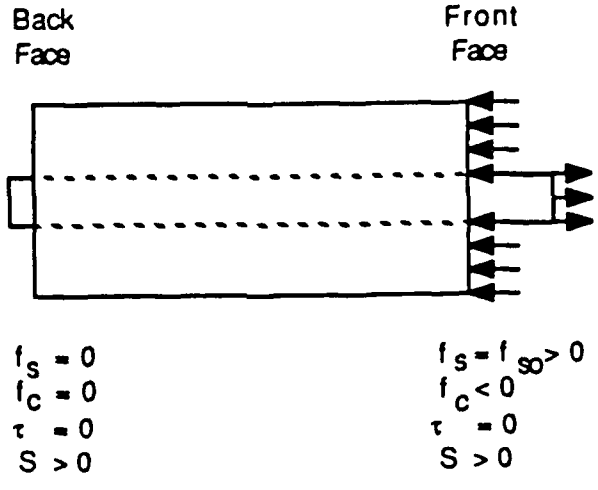

Fig. 3.3 - Typical pull-out element (Reproduced from Ref. 62).

With $\varepsilon_{s,i+1}$ and $\varepsilon_{s,i}$ corresponding to $\sigma_{s,i+1}$ and $\sigma_{s,i}$ respectively in the σ_s - ε_s curve, and $\varepsilon_{c,i+1}$ and $\varepsilon_{c,i}$ corresponding to $\sigma_{c,i+1}$ and $\sigma_{c,i}$ respectively in the σ_c - ε_c curve:

$$S_{i+1} = S_i - (\varepsilon_{s,i+1} + \varepsilon_{s,i}) \frac{\Delta x}{2} + (\varepsilon_{c,i+1} + \varepsilon_{c,i}) \frac{\Delta x}{2} \qquad (3.6)$$

where τ_{i+1} corresponds to S_{i+1} in the $(\tau - S)$ curve.

The boundary conditions for the pullout element are shown in Fig. 3.3. Using the above algorithms and boundary conditions, the values of $\sigma_{s,i}$, $\sigma_{c,i}$, S_i, and τ_i can be computed at each section for any given back slip S_b, starting from the back face ($S_1 = S_b$) and ending at the front one.

As can be seen from the above description, the numerical method is flexible, easy, and short if a computer is used. Furthermore, it can accommodate all kinds of stress-slip relationships, no matter how complicated they are, without modeling anything. Finally, the error introduced can be reduced by reducing the value of Δx. The above method is very powerful and useful, and can accommodate more complex situations, such as cyclic loading.

The main shortcoming in this method is the back slip S_b that cannot be determined. The authors did not suggest any way to determine the value of S_b. Another possible disadvantage of this method is that the shear stress along the interface (or axial stress in the reinforcement or matrix) cannot be found at any point, but only at specific points or "stations". This means that the bond stress curve obtained is only defined by discrete points, joined by straight lines, or perhaps by a best fit curve. Another source of error is that the integration needed to obtain the average bond stress, has to be done numerically. The error can be reduced by including more stations per interface.

3.4 ANALYTICAL METHOD BASED ON ASSUMED BOND STRESS DISTRIBUTION

surement of local bond stress and local slip along a stressed reinforcing bar of a tension member is difficult and very sensitive to experimental error. Moreover, the relationship between bond stress and local slip has been observed to vary from section to section [45]. The authors of this work were basically trying to find the shear stress distribution at the interface of the reinforcing bar and the surrounding concrete, as well as the normal stresses in the bar and the concrete for the bar shown in Fig. 3.4. They introduced a differential equation relating the second derivative of the local slip to the local bond stress, along with five boundary conditions, namely that:

1. At $x = \frac{s}{2}$, $S_x = 0$.

2. At $x = 0$, $\frac{dS_x}{dx} = -\epsilon_s$

3. At $x = L_t$, $\frac{dS_x}{dx} = 0$.

4. At $x = 0$, $\frac{d^2S_x}{dx^2} = 0$.

5. At $x = \frac{s}{2}$, $\frac{d^2S_x}{dx^2} = 0$.

where S_x is the local slip, s is the length of the specimen, ϵ_s is the strain in the steel, and L_t is the transfer length, defined as the embedment length required to satisfy the condition that at $x = L_t$, the strains in the steel and the concrete are equal to each other.

The authors then noted that if a stress-slip relationship is to be assumed, and if it is assumed that the local bond stress is linearly dependent on the local slip, then the resulting solution would be of the form:

$$S_x = A e^{kx} + B e^{-kx} \qquad (3.7)$$

where A and B are constants to be determined from the boundary conditions, and k is a constant dependent on the material properties and cross-sectional dimensions.

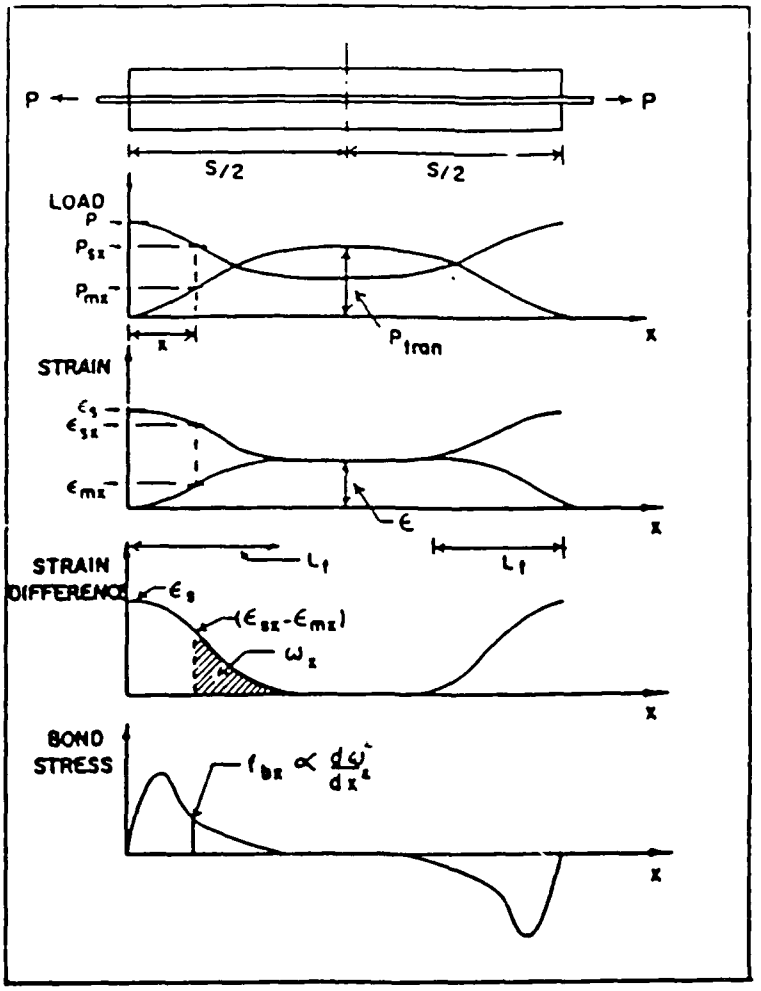

Fig. 3.4 - Load , strain, slip, and bond stress distribution (From Ref. 56).

The problem lies in the fact that Eq. 3.7 has only two unknown coefficients, whereas five boundary conditions are to be satisfied simultaneously. Two observations were made by Somayaji and Shah namely that : 1) the relationship between the local bond stress and the local slip is not unique, 2) it is experimentally difficult to obtain a precise relationship between the local bond stress and local slip that can be mathematically modeled. These problems led them to the following alternative approach.

Instead of assuming a relationship between the bond stress and the slip, an exponential bond stress distribution is assumed leading to the following:

$$\frac{d^2 S_x}{dx^2} = A e^x + B e^{-x} + C \qquad (3.8)$$

Integrating the above equation twice leads to the following expression for the local slip S_x:

$$S_x = A e^x + B e^{-x} + C \frac{x^2}{2} + D x + E \qquad (3.9)$$

where the five coefficients A, B, C, D, and E can be found from the five boundary conditions mentioned earlier. After determining the coefficients, one can evaluate the strains in steel and concrete at any section by successively differentiating Eq. 3.9, and using the relationships between the strains in the reinforcement and the matrix, and the local slip. In solving a typical pull-out problem, the five coefficients were found to depend on the transfer length L_t, as well as the crack spacing or the segment length s. It was also noted that in the course of the development of this theory, a linear relationship between the transfer length and transfer load was assumed, which assumption is not unreasonable.

This approach is unique, and Somayaji and Shah are the only investigators to have adopted it. The authors believe that the method can be substantially improved if Eq. 3.8 is replaced by:

$$\frac{d^2 S_x}{dx^2} = A' e^{kx} + B' e^{-kx} \qquad (3.10)$$

Then, by integrating twice, the following expression for the local slip is obtained:

$$S_x = A e^{kx} + B e^{-kx} + C x + D \qquad (3.11)$$

where $A = A' / k^2$ and $B = B' / k^2$.

k in these expressions is a function of the cross-section, and should in fact reflect the stress-slip relationship.

This method overall is simple and easy to implement. However, it lacks power and accuracy. As can be noted, the expressions obtained depend only on the boundary conditions. In other words, the shear stress distribution obtained using this method is independent of the stress-slip relationship, meaning that the stresses in the steel and the concrete, as well as the shear distribution along the interface are independent of the bond properties of the interface. It is true that because of the analytical nature of this method, the shear stress can be found "exactly" at every point, but again, this accuracy is in contradiction with the rough assumption made as a starting point that the slip distribution satisfies Eq. 3.9. Finally it should be mentioned that Somayaji and Shah were able to derive a stress-slip curve from the assumption made in Eq. 3.9.

3.5 YANKELEVSKY'S THEORITICAL APPROACH

So far, all the methods outlined in this chapter have in common that the bond shear stress distribution is dictated by the relationship between the stress and the slip. Of course, the stress distribution and the stress-slip curve are interrelated in that one can always be derived from the other. However, assuming one in order to obtain the other is not the only valid approach. Indeed, Yankelevsky [65] adopted a completely different path to study the bond between a deformed steel reinforcing bar and the surrounding concrete.

Yankelevsky's work was centered on the problem of axially loaded specimens, where a single reinforcing deformed bar is encased concentrically in a long concrete cylinder with the bar ends exposed. Goto [18]

performed an interesting series of tests in which such specimens were loaded in tension and found that shortly after primary lateral cracks formed, internal cracking began (Fig. 2.2). These numerous cracks form cones with their apexes near bar lugs. The angle of internal cracking is generally within the range of 45° to 80° to the bar axis and many crack angles reach 60°. These cracks were found to start at a steel stress level of about 100 MPa (14 ksi).

The model in question, which is closely related to Goto's experimental observations, represents the interaction between uncracked concrete and a deformed bar through a mechanical system; conceivably it could be modified to apply to cracked concrete in between two cracks.

Fig. 3.5 shows a concrete cylinder having a length L and a diameter D, in which a deformed steel bar is centrally located. A tensile force F_o is applied to the steel bar ends. A differential element dx of the steel bar is located to the left of the axis of symmetry. The applied tensile force pulls to the left all the segments located to the left of the axis of symmetry. It is assumed that the surrounding concrete resists the pull by inclined compressive forces dC (Fig. 3.6), thus reducing the axial force F in the bar along the x coordinate.

The structural model through which the resisting force dC is transferred to the concrete is shown in Fig. 3.6. Concrete segments in compression AB and A'B' are inclined to the steel bar segment at angle α and react on the rod by a force dC per unit length in the hoop direction. The circumference BB' is the locus of segment centroids of a typical disc EE' (Fig. 3.6). The centroid B (or B') in Fig. 3.6 is the location of the resultant tensile force to equally distributed tensile stress in concrete in the axial direction. The compressive force dC' per unit length of the circumference BB' in the inclined segment AB (Fig. 3.6) at B is in equilibrium with a radial force dN per unit length of the circumference BB' in the disc EE' and with the longitudinal tensile force per unit length dQ. By such a mechanism, the tensile force F in the steel bar is reduced at a rate of dF/dx and is increased at an equal rate of dT/dx in the concrete. T is the total tensile force and equal to 2π r Q, where the centroid location r (Fig. 3.6) is given by:

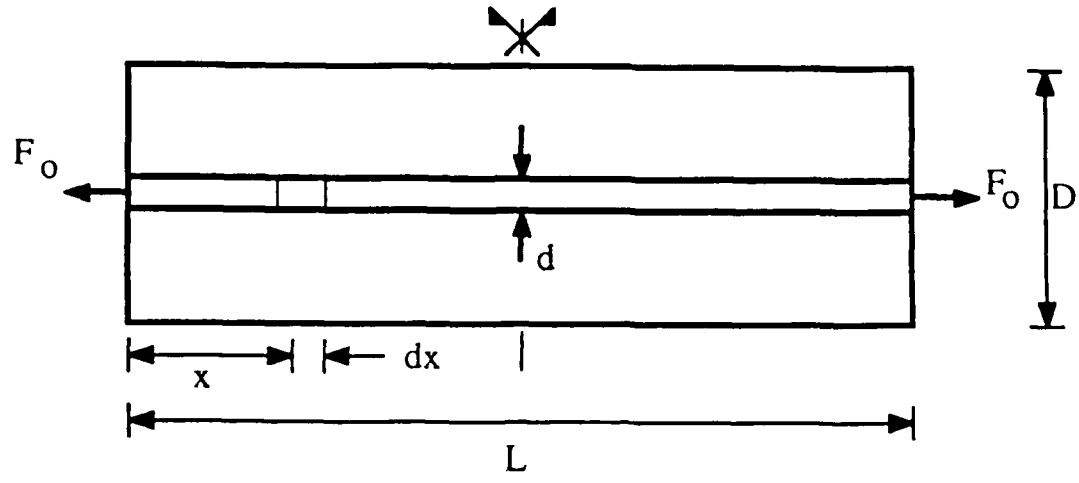

Fig. 3.5 - Schematic representation of Yankelevsky's specimen (Reproduced from Ref. 65).

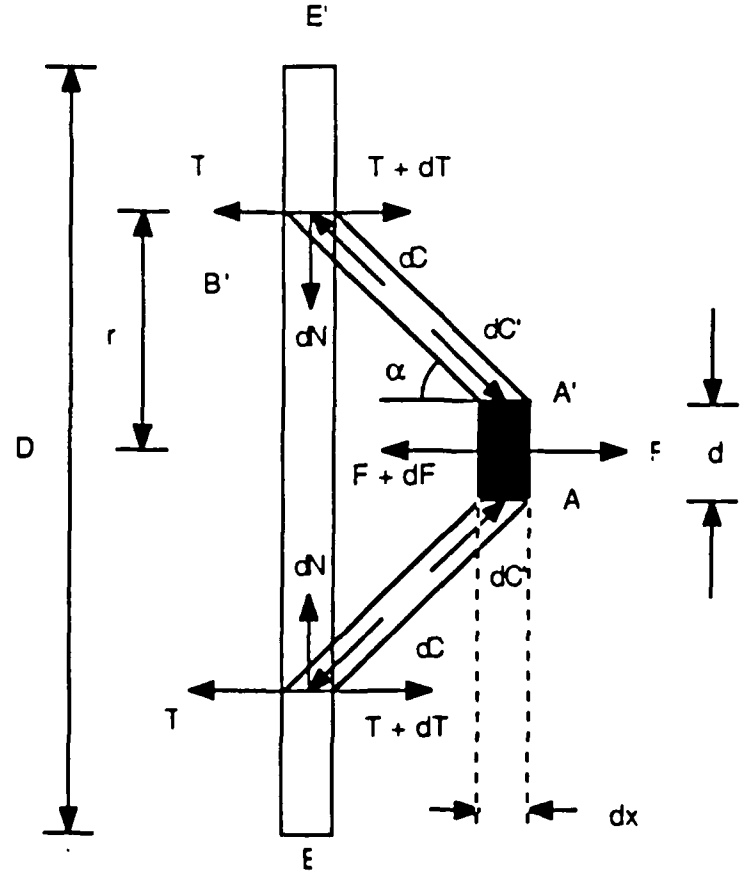

Fig. 3.6 - Structural model of Yankelevsky (Reproduced from Ref. 65).

$$r = \frac{D}{3} \cdot \left(\frac{1 + \frac{d}{D} + \frac{d^2}{D^2}}{1 + \frac{d}{D}} \right) \qquad (3.12)$$

For the common cases where d«D, r can be taken as D / 3.

From this point, static equilibrium and compatibility are used to relate the forces together. A differential equation in F (the axial force in the steel) is obtained and solved. The solution obtained was:

$$F = C_1 e^{\beta x} + C_2 e^{-\beta x} + \frac{n A_s}{A_c + n A_s} F_o \qquad (3.13)$$

where n is the modulus ratio ($n = E_s / E_c$) and β is a constant dependent on the modulus of elasticity of steel, on that of concrete, as well as the dimensions of the specimen.

It is found that the third term in the right hand side of Eq. 3.6 (say F_s) is the portion of the total force F_o which is carried by the steel bar ac*cording to its relative stiffness, the other portion* (say $F_c = F_o - F_s$) being carried by the concrete. Strain in the steel bar at X=0 (Fig. 3.5) has its highest value, and strain in the concrete there is zero. As distance from bar end increases, the strain in the concrete increases and that in the steel decreases. At a distance l from the bar end, the strains in the concrete and steel become equal. In that section, the force in the steel is F_s, whereas the force in the concrete is $T = F_c$, and bond stresses approach zero.

The two constants C_1 and C_2 are found from the following boundary conditions:

(1) At $X = 0$, $F = F_o$ (3.14)

(2) At $X = l$, the shear stress is zero, hence:

$$\frac{dF}{dx} = 0 \qquad (3.15)$$

Using these two conditions, Eq. 3.13 becomes:

$$F = F_c \frac{e^{-2\beta l}}{1 + e^{-2\beta l}} e^{\beta x} + F_c \frac{1}{1 + e^{-2\beta l}} e^{-\beta x} + F_s \qquad (3.16)$$

For high values values of l (practically for $\beta l > 4$), the first term has a negligible contribution and Eq. 3.16 simply becomes

$$F = F_c e^{-\beta x} + F_s \qquad (3.17)$$

From Eq. 3.17, and using the fact that $F_o = F + T = F_s + F_c$, the following is found:

$$f_s = \frac{1}{A_s} \{ F_o - F_c [1 - e^{-\beta x}] \} \qquad (3.18)$$

$$\tau = - \frac{\beta}{\pi d} \frac{A_c}{A_c + nA_s} F_o e^{-\beta x} \qquad (3.19)$$

where f_s is the stress in the steel, and τ is the shearing stress at the interface.

Yankelevsky verified these expressions againt results of tests run at Berkeley (Fig. 3.7), and the results compared very well with his theory. Indeed, this approach is powerful, and the assumptions made are sound. However, the approach is limited to the uncracked concrete case.

3.6 GENERAL OVERVIEW

As far as accuracy is concerned, the new theory presented in §3.5 seems to be the most accurate, without being inconsistent. The analytical method presented in §3.2 is apparently exact; it is, however, based on an analytical stress-slip relationship that is probably not very accurate, nor is it always available. This fact introduces an inconsistency between the mathematical rigidity of the derivation of the bond distribution, and the inaccuracy of the stress-slip relationship, on which the results are based. The numerical method presented in §3.3 is the most powerful, while practical and realistic, for it can accommodate a wide variety of cases, including a graphical stress-slip relationship (thus no mathematical model

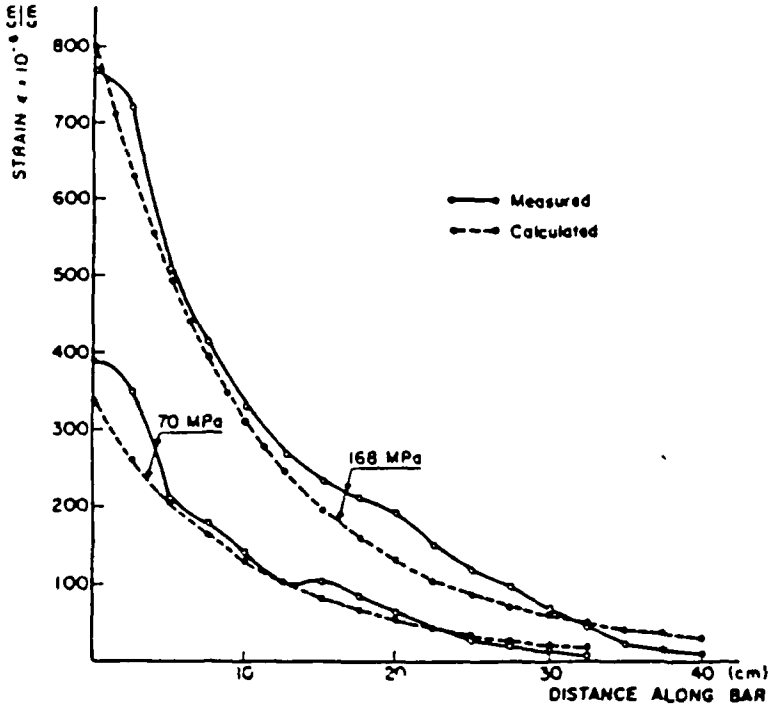

Fig. 3.7 - Predicted strain along bar compared to Berkeley test results (From Ref. 65).

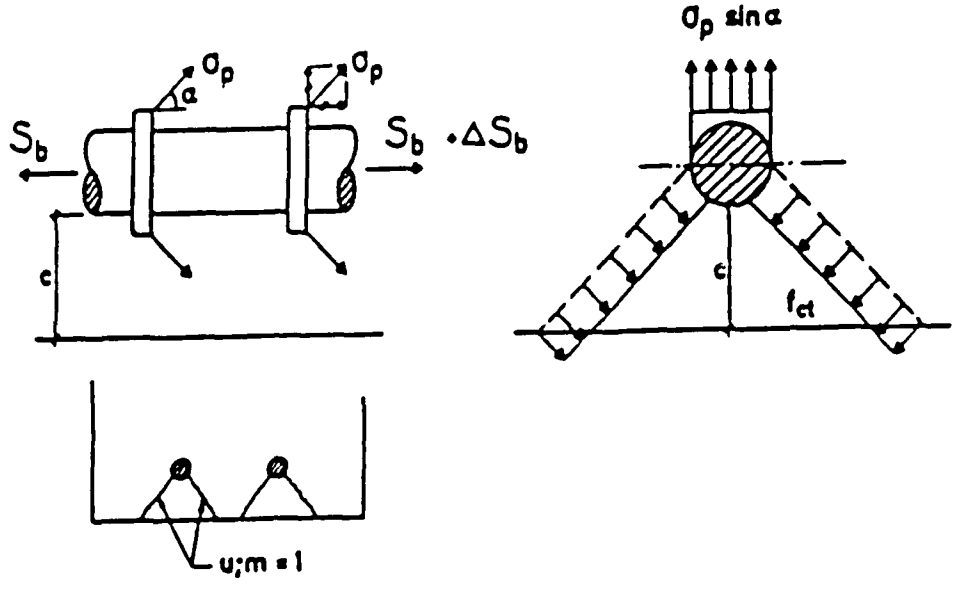

Fig. 3.8 - Splitting forces and bond splitting failure with deformed bars (From Ref. 30).

is needed) and a cyclic case of loading. The assumed bond distribution method of §3.4 is not realistic, and lacks consistency and soundness.

As far as practicality and ease of use is concerned, the new theoretical method in §3.5 is the easiest to use since it involves simple mathematical expressions.

The authors have extended this new approach to the case of fiber-reinforced cementitious composites (see Chap. 8) as one of two different methods of predicting the interfacial bond distribution in FRC.

3.7 FACTORS AFFECTING BOND IN REINFORCED CONCRETE

3.7.1 General

As was emphasized earlier, it is very important to understand bond to be able to explain the behavior of composites, especially under tensile type loading. The composites in question can be anything typically represented by a weak brittle matrix and a stronger ductile reinforcement. While the main focus of this study pertains primarily to bond in fiber-reinforced cementitious composites, bond in reinforced concrete and prestressed concrete cannot be ignored, and ought to be addressed, if briefly. While it is true that reinforced and prestressed concrete and fiber reinforced concrete fall under the category of cementitious composites, they display to a large extent a different behavior, notably in the case of bond mechanisms.

Factors affecting bond in reinforced concrete are numerous. Some of them are obvious, while others are harder to comprehend. The problem of bond in reinforced concrete is far from being fully understood, even less so for the case of fiber-reinforced composites. Moreover, there is not always a consensus between researchers as to what factors affect bond and in what way. In this work, only three factors affecting bond will be discussed, even though more factors are recognized. Those three factors were chosen because of their importance, and because they have been addressed in the past. They are: the texture of the steel reinforcement (plain versus deformed), the concrete cover, and the confinement. One section will be devoted to each, and finally, §3.7.5 will summarize the conclusions.

3.7.2 Texture of The Steel Reinforcement

This is the most important and the most significant factor affecting bond properties of reinforced concrete, but also of other cementitious composites. One can sense the difference between smooth and deformed reinforcing bars in bond. It is clear that deformed bars will display a better bond performance than smooth (plain) bars. It is also important to understand that the behavior of deformed bars is completely different from that of plain bars.

The classical concept of bond is that it consists of adhesion between the reinforcement and the surrounding concrete and bond failure is caused by the failure of this adhesion. Traditional design methods and code rules concerning bond and anchorage of reinforcement are based upon this concept and result in provisions for allowable bond stress values or corresponding development lengths necessary for developing the full design strength in the bars.

This concept is originally based on bond tests, usually pull-out tests, with smooth reinforcing bars, and in such cases the concept corresponds relatively well to the real function. For deformed bars, tests of this kind and this concept of bond are however quite wrong, especially for bond failure in an ordinary beam case where the bar is placed near a surface with normal concrete cover. In this case the failure is preceded and finally caused by longitudinal cracking due to the compressive forces radiating out with a certain inclination α from the surface deformation lugs (see Fig. 3.8). These forces in turn produce tensile stresses in the surrounding concrete and cause successive splitting cracks following some critical splitting surface line between the reinforcing bars and the surface of the concrete member. The final failure takes place when these cracks have propagated all along the anchorage zone along the bar. Depending on the arrangement of the reinforcement and its location relative to the concrete surface, the covering layer, etc..., these splitting lines can form different patterns (Fig. 3.9). This concept of splitting line was introduced by Losberg and Olson [30] who found that the bond force is closely related to

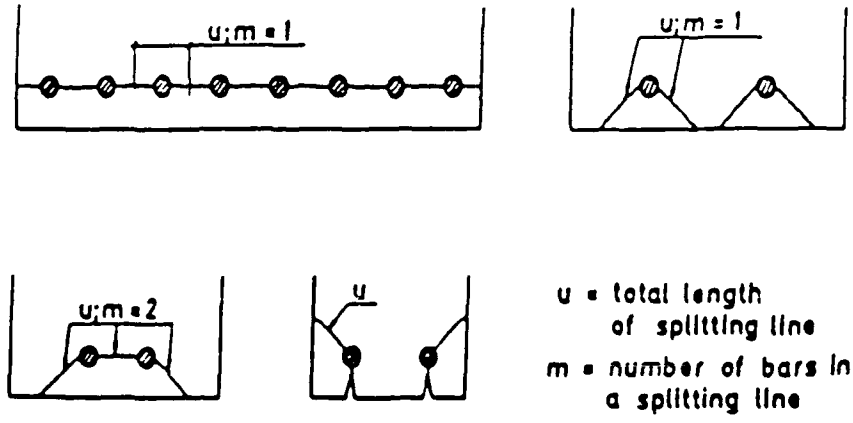

Fig. 3.9 - Splitting line patterns in some cases of reinforcement arrangement (From Ref. 30).

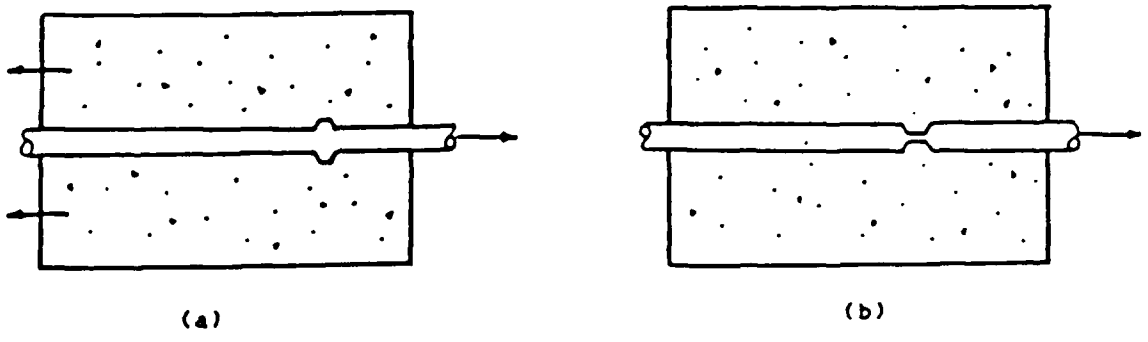

Fig. 3.10 - Single rib and single concrete tests (From Ref. 31).

the length u of the splitting line (Fig. 3.9) and the concrete tensile strength (splitting strength) f_{ct}.

In general, bond can be thought of as the shearing stress or force between a bar and the surrounding concrete. Bond is made up of three components:

(a) Chemical adhesion

(b) Friction

(c) Mechanical interlock between concrete and steel

Bond between concrete and plain bars consists primarily of the first two elements, although there is some mechanical interfacial friction due to the roughness of the bar surface. Deformed bars, however, depend foremostly on mechanical interlocking for superior bond properties. Nevertheless, friction and chemical adhesion are not necessarily negligible in the case of deformed bars, but are somewhat secondary.

To obtain a clear understanding of the bond of a deformed bar in concrete, the bond forces as well as the slip will be examined. Unless the strain in the concrete and the steel is the same and constant over a length, a deformed bar attempts to move or slip in relation to the surrounding concrete. Initially, chemical adhesion combined with mechanical interaction prevents significant slippage. After adhesion is destroyed, and slip occurs, the ribs of a bar restrain this movement by bearing against the concrete between the ribs; this concrete will be called the concrete key (Fig. 3.10). Friction, which would occur after slip is induced in the case of plain bars, does not occur here because of the presence of the ribs.

Slip of a deformed bar can occur in two ways:

(a) the ribs can push the concrete away from the bar (wedging action)

(b) the ribs can crush the concrete

It was determined experimentally from pull-out tests on bars with only a single concrete key (Fig. 3.10) that the movement of the ribs is

about the same for all ribs with face angles greater than 40° (the face angle of ribs is measured with respect to the bar axis). These tests included specimens with ribs having face angles of 90° (and even 105°) in which case the rib cannot push the concrete outward, hence preventing any wedging action). The friction between the rib face and the concrete is evidently sufficient to prevent relative movement at the interface when face angles are larger than about 40 to 45°. It follows that slip is due almost entirely to the crushing of the porous concrete paste (mortar) in front of the ribs if the rib face angles are larger than about 40°. It is understandable that crushing of the concrete does occur, since the average bearing pressure exerted by these ribs is very large.

Bars with ribs having face angles less than about 30° exhibit markedly different load-slip relationships (Fig. 3.10). Here the friction between the rib face and the concrete is not sufficient to prevent relative movement. Thus, slip is mainly due to the relative movement between the concrete and steel along the face of the rib, and, to a lesser extent, to some crushing of the mortar.

Slip caused by relative movement (in addition to that caused by crushing) also occurs when the frictional properties of the rib face are reduced by grease. In other words, bars with ribs having face angles greater than about 45°, but where the friction is impaired, exhibit load-slip curves which are similar to that for a rib with flat rib face angle. The extent to which slip properties are affected by grease depends nevertheless on the face angle; ribs with flatter face angles are understandably more affected by poor frictional properties.

For the more common case of good frictional properties and a rib face angle greater than 40°, slip occurs by progressive crushing of the concrete paste structure in front of the rib. This does not appear to produce significant wedging action until considerable crushing has occured, at which time a wedge of crushed concrete (compacted powder) becomes lodged in front of the rib and moves along with it. This, in effect, produces a rib with a face angle of 30 to 40°. Such wedges of compacted concrete powder have been observed in front of ribs that had carried high bond forces; Rehm [53] states that crushing extends in front of the rib for a

length of 5 to 7 times the height of the rib, although the compacted powder that moves with the rib extends at most 2 times the height of the rib.

It is interesting to note (Fig. 3.11) that the bond modulus (slope of bond-slip curve) upon reloading is considerably higher than that displayed initially. This was observed by Rehm [53]. This behavior can best be explained by the fact that during the second loading, the rib bears against a compacted nonporous crushed concrete, as opposed to the porous, intact concrete during the initial loading.

It should be pointed out here that it is not possible to produce extensive crushing and wedge action in front of every rib without having transverse and longitudinal cracking, caused by the forces produced by the ribs bearing on the concrete.

As can be deduced by what preceded, the bond behavior of deformed bars is in essence very different from that of smooth bars, and surface deformations improve the bond performance of bars. Also, it is the angle of the rib, rather than its size, that dictates the general behavior of deformed bars. Many researchers were thus misled all along when they assumed that a deformed bar with closely spaced lugs has a higher bond strength than a similar one with a larger rib spacing.

3.7.3 Concrete Cover Effect

Another important factor affecting bond in reinforced concrete is the thickness of concrete binding the steel bar. Conceptually, it is easy to visualize how the cover makes a difference in the bond strength and properties of the interface. The concrete surrounding a steel bar in tension is subjected to compressive stresses. When the concrete cover is very small for instance, then the concrete might fail under the compressive forces that are acting on it. However, if the concrete cover is very large, say infinitely large, then this does not mean that the bond at the interface of the concrete and the steel is infinitely strong.

The problem has hence to be viewed in the following manner. If the cover is too small, then the concrete governs the bond, and the failure of

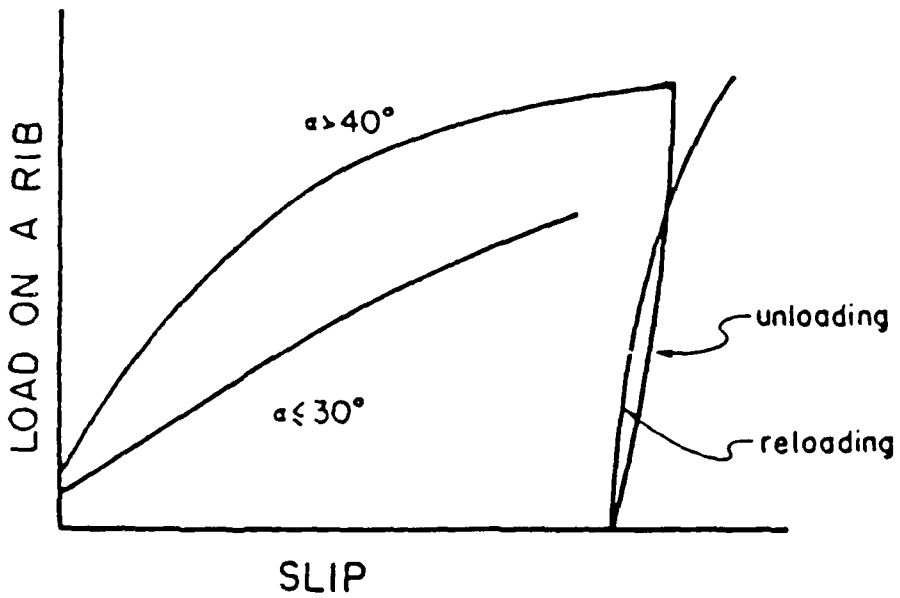

Fig. 3.11 - Sketch of load slip curves for ribbed bars (From Ref. 31).

the interface is that of the concrete. Beyond a certain value for the cover, the bond is dictated by the strength of the adhesion at the interface. In other words, even though the concrete surrounding the steel will remain intact, the bond between the concrete and the steel will eventually fail. No discussion of this threshold value can be found in the available literature on bond, hence the weakness of most bond theories.

Orangun, Jirsa, and Breen [46] derived the following equation from a non-linear regression analysis of test data:

$$\frac{\tau_{max}}{\sqrt{f'c}} = 1.2 + 3.0\,\frac{c}{d_b} + 50\,\frac{d_b}{L} \qquad (3.20)$$

where τ_{max} is the bond stress capacity (psi), c is the smallest concrete cover or half the bar spacing, d_b is the bar diameter, L is the embedment length, and f'_c is the concrete cylinder strength (psi).

The major flaw of this equation is that it predicts an infinite bond strength for a steel reinforcing bar embedded in a very huge matrix of concrete (since the cover then tends to infinity). It also predicts an infinitely large bond strength for small embedment lengths.

Kemp and Wilhelm [28] presented the following equation:

$$\tau_{bv} = \sqrt{f'_c}\left(2.64 + 2.37\,\frac{c}{d_b}\right) \qquad (3.21)$$

where τ_{bv} is the average bond stress at first visible crack (psi), c is the concrete cover (in), d_b is the bar diameter (in), and f'_c is the concrete compressive strength (psi).

This concept, directly relating the bond strength (or average bond) to the concrete cover lacks in that it only works for small covers. For larger covers, it is the adhesion between the steel and the concrete that governs the strength of the interface.

In conclusion, the concrete cover influences bond in a sense that it needs to be large enough not to create problems at the interface (namely causing a splitting mode of failure). However, the equations presented in

this section cannot be used for all cases, but need to be modified to accommodate the fact that beyond a certain value, concrete cover has hardly any effect on bond.

3.7.4 Effect of Confinement on Bond

The confinement effect can be not so different from that of the concrete cover. When an external pressure is applied to the concrete surrounding the steel subjected to tension, the compressive capacity of the concrete increases by up to 20% of its original value, which makes the interface stronger in resisting splitting. In this respect, the effect of confinement is exactly the same as that of the concrete cover.

However, the confinement reinforces the bond capacity of the interface no matter what the concrete cover is, even when the mode of failure is not of the splitting type. Indeed, after the adhesion between the concrete and the steel breaks, frictional stresses develop along the interface. These stresses are directly related to the normal stresses acting on the steel. This means that for the same slip, more frictional stresses would be needed to develop along the interface, which implies that the tensile capacity of the system is increased.

Finally, it can be stated that confinement of the concrete around the steel subjected to tension is helpful in increasing the bond capacity of the interface and the tensile strength of the system. Such a confinement is usually provided by tranverse steel reinforcement which, by preventing the concrete from expanding, induces a confining pressure.

CHAPTER IV

OVERVIEW OF BOND IN FIBER-REINFORCED CONCRETE

4.1 GENERAL

Bond in fiber-reinforced concrete is a discipline in itself. However, it is very useful to look at bond in reinforced concrete before attempting to solve the bond problem with fibers since fibers feature a completely different behavior than conventional reinforcement.

The main difference between fiber-reinforced concrete and conventional reinforced concrete lies in the fact that, unlike reinforcing bars, fibers are not continuous. Moreover, since many fibers are near each other, their interaction must be considered. In the more extreme case of Slurry Infiltrated Fiber Concrete (SIFCON), interaction may include fiber entanglement. The fiber entanglement modifies the behavior of the whole composite. A long and single steel fiber embedded in concrete and subjected to a direct tensile load (typical pull-out test), will behave like a steel reinforcing bar in the same condition and undergoing the same kind of loading. However, even in the case of normal fiber-reinforced concrete (as opposed to SIFCON), a single fiber, in the presence of the many other discontinuous fibers in a concrete matrix, behaves differently. The very fact that to date, no complete analytical model of the behavior of discontinuous fibers in a cementitious matrix has been developed yet, shows how intricate the problem of bond in fiber-reinforced concrete is.

The analytical work in fiber-reinforced concrete is not the only problem a researcher might encounter. Indeed, the experimental work can be at least equally as streneous. The best example is the problem of

measuring strains and/or displacements along the interface of a steel fiber with concrete. It seems almost impossible to make any actual measurement, mainly because of the size of the fiber, not to mention the interaction among fibers. One possible way of solving the problem will be to use the following procedure:

(1) To analytically model the behavior of a single fiber in a concrete matrix.

(2) To use results of experiments to evaluate some of the parameters involved in the theory.

(3) To generalize the theory to the case of multiple fibers, and possibly SIFCON in a semi-empirical way.

(4) To use the model thus obtained in conjunction with other theories to predict the overall behavior of the specimen under tensile loading.

This study will only address the first part of the problem, i.e. the analytical model for a single fiber will be developed, and then experimental data would be used to substantiate it.

The remaining part of this chapter will deal with the differences between fibers and rebars in bond, as well as the properties of bond in fiber-reinforced concrete.

4.2 TYPES OF BOND IN FIBER-REINFORCED CONCRETE

Depending on the type of stress transferred accross an interface, two types of bond are identified: the tensile bond and the shear bond.

The tensile bond resists displacement caused by forces acting perpendicular to the interface. This kind of bond is of no major interest in this study, and will thus be overlooked in the remaining part of this report.

The shear bond controls the transfer of stresses parallel to the longitudinal axis of the reinforcement (rebar or fiber). In an uncracked com-

posite, the shear bond transfers stresses from the matrix back into the reinforcement. When the matrix cracks and the load is carried by the fibers bridging the crack, the shear bond enables the load to be transferred back into the uncracked parts of the matrix. Shear bond also resists the pull-out of the reinforcement from the matrix and is therefore one of the main factors influencing the mechanism and mode of failure of a composite. Two types of shear bond are capable of transferring stresses acting along the interface: the elastic shear bond which includes adhesion if any, and the frictional shear bond. When the elastic shear stress at the interface between the reinforcement and the matrix exceeds the bond strength of the interface, bond becomes frictional in nature and the adhesion is broken.

Elastic Shear Bond: If an elastic shear bond exists at an interface and the shear stress does not exceed the strength of the bond, then the shear stresses are directly related to the relative slip between the reinforcement and the matrix. Bartos [4] stated that when elastic bond is prevailing, "the longitudinal displacements of the fibre and matrix at the interface remain compatible." A compatibility of displacements would imply zero slip, which would then mean that no shear stresses are developed at the interface, hence implying an infinitely large bond modulus.

Frictional Shear Bond: The frictional shear bond resists displacements along the interface parallel to the length of the fiber, and may or may not depend on the local slip. If the frictional bond is perfectly plastic (theoretical case), then the stress will be completely independent of the slip. The frictional bond is characterized by an initial value of the bond, referred to as the bond strength τ_{max}, which has to be exceeded for the elastic bond to break and for the frictional stresses to take place.

4.3 BOND IN FIBER REINFORCED CONCRETE

4.3.1 Uncracked Composite

When a fiber-reinforced specimen is subjected to a tensile load, the tensile stresses are transmitted from the matrix to the fibers and the fibers undergo tension. Depending on the strength of the bond between the fiber

and the matrix, the bond may or may not fail under a given load. It is possible that the following happens before cracking of the matrix:

1- The load is so low (or the chemical adhesion is so strong) that the adhesive bond does not break, and there is no relative displacement between the fiber and the matrix.

2- The load breaks the chemical adhesion between the matrix and the fiber; however the bond strength of the fiber is not attained, so that a condition of elastic bond prevails along the interface.

4.3.? Cracked Composite

Bond remains a very important factor in determining the properties of a composite even in its post-cracking stage, but its function changes. The change is most significant in the case of discontinuous fibers. In the pre-cracking stage, when the elastic shear bond was intact, the maximum shear flow occured at the ends of the fibers. The stresses were transferred from the matrix to the fibers. In the post-cracking stage, the fibers bridging a crack are pulled out and the interfacial shear stress changes; the maximum stress now occurs at the point where the fibers enter the matrix i.e at the crack. If the frictional shear bond is perfectly plastic before the start of the cracking, it is likely to stay this way in the post cracking stage.

4.4 FIBER DEBONDING

Fundamental information on the nature and strength of the interfacial bond between the fiber and the matrix in a fiber-reinforced composite material is usually obtained using the single-fiber concentric pull-out test specimen and configuration shown schematically in Fig. 4.1. Stress distributions in this specimen are similar to those within and on the surface of a fiber normal to and bridging a matrix crack in a composite. The similarity holds, assuming that the failure is by matrix tensile fracture followed by fiber-matrix debonding and fiber pull-out, i.e. the common failure mode for discontinuous fiber composites with a brittle or elastic matrix. However, the values and the exact stress distribution are obviously

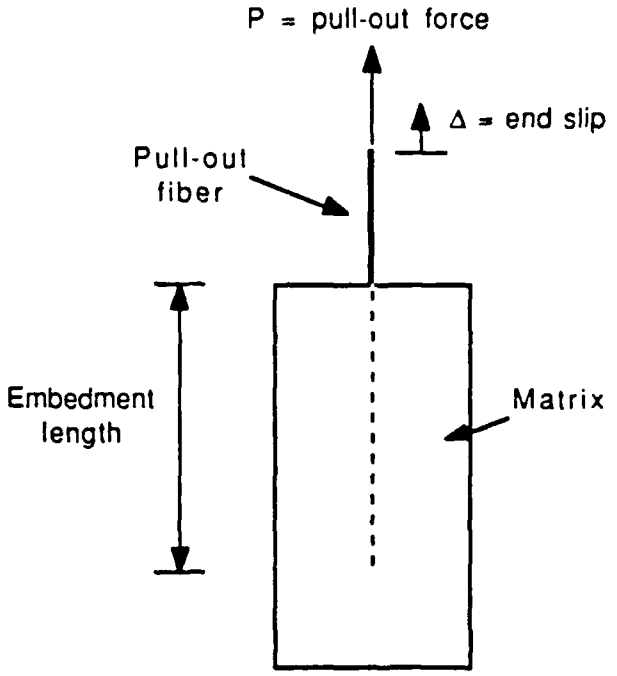

Fig. 4.1 - Typical single-fiber concentric pull-out test specimen.

different for a single fiber does not behave as it does in the presence of a large number of neighboring fibers.

Resistance to the debonding and pull-out processes is primarily a function of the fiber-matrix interfacial bond shear strength and the interfacial bond area. Theoretical analyses of this resistance were initially developed for ductile or plastically deforming matrices and a uniform interfacial shear stress along the length of the embedded fiber was assumed. Under this assumption, sudden failure of the interfacial bond occurs when its shear strength is reached and the debonding load, that is the peak load observed in the pull-out test, is directly proportional to the embedded fiber length.

However, theoretical analyses of the stress conditions in a pull-out test specimen with a brittle or elastic matrix show that the distribution of shear stress along the interface is not uniform, and that the relationship between the debonding or the pull-out load and the embedded length of fiber in the specimen is more complex than indicated above. Furthermore, the variation of the peak pull-out load with the embedded length is nonlinear, and consequently, it cannot be inferred that the true value of the interfacial bond strength can be obtained simply from this load and the nominal interfacial area. In fact, as will be shown in Chap. 6, the peak pull-out load is related to the frictional bond shear stress as well as the bond strength.

What preceded indicates that even though the pull-out load is not linearly related to the embedment length, the embedded length has to be included in any bond model.

4.5 FACTORS AFFECTING BOND IN FIBER-REINFORCED CONCRETE

The problem of bond in fiber-reinforced concrete is hardly understood at all. All ideas presented so far are incomplete. Experimental invetigations have been carried out [10, 19, 35,.40, 50, 59], but as will be seen in what follows, corresponding results were not always consistent. Following is a brief presentation of some of the findings.

4.5.1 Experimental Investigation

Naaman and Shah [40] reported that the bond efficiency in a pull-out test of steel fibers inclined with respect to the line of stress is at least as good as that of fibers parallel to the direction of stress. They also found that fiber efficiency decreases with the number of fibers being pulled out simultaneously from the same area.

Gokoz and Naaman [16] noticed that for steel fibers where a pull-out mode of failure was observed, the postpeak response is almost insensitive to the loading velocity. They also reported that the peak pull-out load, which is indicative of the elastic bond at the interface, is strain-rate sensitive.

It was reported by Gray and Johnston [19] that the direction of casting has a substantial influence on the bond strength. They stated that vertically-cast specimens have a higher interfacial bond strength than horizontally cast specimens. They also found out that an increase in the sand-cement ratio in the mortar matrix has contrasting effects on the strength of the interfacial bond in the vertically and horizontally-cast specimens. For the vertically-cast specimens, there is a decrease in the apparent interfacial bond strength. They explained that "this reduction in bond strength is almost certainly a result of a change in the relative proportions of cement paste and aggregate in the matrix with a change in the sand-cement ratio." For the horizontally-cast specimens there is an increase in the apparent bond strength with an increase in the sand-cement ratio. This was explained by what the authors called the water gain, i.e. "the accumulation of water under the embedded fiber due to the tendency of the bleed water in the mortar matrix to rise during and after consolidation." Water gain is known to have a weakening effect on the cement paste-aggregate bond in plain concretes.

It was also noted by Gray and Johnston [19] that the average interfacial bond strength increases slightly, but not significantly, with an increase in the fiber withdrawal rate, which is not in contradiction with the

findings of Gokoz and Naaman [16] who stated that bond in fibers is rate-independent.

Maage [35] found out that the bond properties between steel fibers and cement-based matrices are of mechanical nature, where the anchoring effect is essentially more important than the adhesive effect. He also said that the mean pull-out load per fiber is unaffected by the number of fibers. This finding is questionable, since this would imply that N fibers have N times more strength than one single fiber, which is not the case as reported by Naaman and Shah [40]. Maage ascerts that, "based on the weakest link theory, it should be reasonable that the pull-out load per fiber would decrease when the number of fibers in the area increased." This of course is an indication of the variability often encountered in fiber bond tests.

Pinchin [50], who carried out tests on wires, stated that a compaction of the concrete surrounding a fiber would actually increase the frictional bond. This property is discussed in Chap. 3 for the case of reinforced concrete. He also determined that the pull-out load increases linearly with the confinement. Another interesting finding is that deformed fibers are less sensitive to pressure than plain (straight) fibers. He also showed analytically that the pull-out load is proportional to the fiber-matrix misfit, which he defined as the difference between the radius of the wire and that of the hole in the matrix in the absence of the wire.

Burakiewicz [10] reported that the shape of the load-displacement curve depends on the fiber type, and that hooked fibers show smaller scatter in bond strength than all the other types he tested. He also observed that the pull-out of hooked and indented fibers requires more energy than that of plain fibers, which implies that deformed fibers have a higher bond strength than straight fibers. He also stated that there is no significant influence on the bond strength of vibration and orientation of fibers during setting and hardening of the matrix, which is in contradiction with the findings of Gray and Johnston [19]. He finally noted that bond strength seems to depend on the rate of loading of the matrix, which contradicts the findings of Gokoz and Naaman [16].

Gopalaratnam and Abu-Mathkour [66] investigated experimentally the effect of the following three parameters on the fiber pull-out characteristics: fiber embedment length, fiber diameter and matrix quality. They observed that the average bond strength is inversely related to the embedment length and that the average bond strength of an interface increases with an increase in fiber diameter. They also observed that the peak pull-out load for identical fibers being pulled out from matrices of increasing compressive strength does not necessarily increase. Their reasoning is that the frictional bond strength may be unrelated to the matrix compressive strength.

4.5.2 Analytical investigation

Few studies have addressed the analytical modeling aspects of bond in cement composites. Most often in such cases, some aspects of the problem were overlooked.

Romualdi and Batson [54] assumed that "in the absence of a crack, the strain in the concrete due to remote tension is equal to the strain in the wires," hence implying zero slip between the wires and the surrounding concrete.

Aveston, Mercer, and Sillwood [3] assumed frictional shear bond with no debonding, hence ignoring the elastic bond that develops for shear stresses not exceeding the bond capacity of the interface.

Kar and Pal [27], on the other hand, assumed a linear shear stress distribution along the fiber, with a maximum at the point where a crack intersects the fiber.

Swamy and Mangat [61] made a similar assumption concerning the linearity of the shear stress distribution at the interface. However, it can be shown that a linear bond-slip relationship does not lead to a linear bond shear stress distribution at the interface.

Larson and Bayasi [69] developed a special test to measure bond strength of carbon fiber embedded in a cementitious matrix. They observed that bond strength increases with the water-binder ratio of the matrix which is attributed to an improvement in workability. They found out that the bond strength decreases with addition of microsilica and increases drastically with the addition of latex.

Parameswaran and Rajagopalan [48] recognized the fact that there is no strain compatibility between the matrix and the reinforcement once debonding occurs but didnot extend this assumption to the pre-debonding phase. Indeed, at any point, the existance of a mechanical shear stress must always be accompanied with a corresponding slip.

More recently, a study by Gopalaratnam and Shah [17] addressed the problem of the tensile response of steel fiber-reinforced mortar. Bond was incorporated in the study of the pull-out behavior of fibers. However, in an attempt to apply shear lag theory to the problem of fiber pull-out, they ignored the normal tensile stresses in the matrix, hence creating a serious flaw in the analytical part of the study.

Nammur et al. [43] performed a fundamental study of the pull-out problem and related the pull-out curve to the interfacial bond-slip relationship. They derived a method of analytically predicting the bond-slip curve from an experimental pull-out curve. The method is presented with some improvement in detail in Chap. 5.

Mandel, Wei and Said [67] developed a procedure to determine the coefficient of adhesion, and the energy release rate per unit area of crack surface at the crack front required for unstable growth of a crack along the fiber-matrix interface. This procedure uses the results of the pull-out test.

Li and Wang [70] developed a theoritical model to predict the load-crack seperation relationship for synthetic fiber reinforced concrete. The distinctive feature of the model lies in the recognition that the fiber matrix bond strength at any point on the fiber is a function of the slippage accumulation at that fiber segment.

Shah and Jenq [71] investigated the interfacial bond properties between fibers and matrix through analysis of pull-out tests. The bonding between fibers and matrix was assumed to be perfect before the pull-out load is applied. Griffith energy criterion was used to govern the crack propagation at the interfacial region where debonding begins. They also developed a fracture model that predicts the progressive failure of the interfacial bond. However, the proposed model doesnot account for friction in the debonded zone.

Gao, Mai, and Cotterell [72] studied the interface between the matrix and the fiber with a new fracture mechanics-based debonding criterion by including the friction in the debonded region. In their study they defined several basic concepts such as the threshold value of the interface pressure, friction zone as well as strong and weak fibers.

Gopalaratnam and Chang [73] formulated the pull-out problem in one dimension with a view to focus on the nonlinear interfacial response. In general, their work was narrowed to the effect of the softening of the interface on the pull-out strength, composite ductility, energy absorption and the stability of the debonding process.

What preceded gives an indication about what could affect the bond performance of a fiber in a concrete matrix. It also shows how far away the current state of the art of bond in fiber-reinforced concrete is from being scientifically reliable and accurate. As was mentioned earlier, this is partly due to the difficulties involved in performing experiments and making measurements when small discontinuous fibers are used.

CHAPTER V

ANALYTICAL STUDY OF PULL-OUT PROBLEM

5.1 OBJECTIVE

The main objective of the experimental part of this study is to generate bond shear stress-slip curves from experimentally obtained pull-out curves for various fibers and matrix types. Furthermore, an attempt is to be made at experimentally characterizing the thus-obtained bond shear stress-slip curves.

An analytical study of the mechanics of the pull-out test is first presented, so as to make it possible to relate a typical pull-out curve $(P\text{-}\Delta)$ to a bond shear stress-slip $(\tau\text{-}S)$ relationship. A bond-slip relationship is first assumed, and a pull-out curve is hence derived. The problem of obtaining $(\tau\text{-}S)$ from a given $(P\text{-}\Delta)$ curve would be the reciprocal to the above mentioned problem.

5.2 STATEMENT OF THE PROBLEM

The analysis that follows pertains to a pull-out test whereby a tensile force P is applied to the tip of a fiber embedded over a length ℓ in a cementitious body (Fig. 5.1).

Initially, it is assumed that the relationship between the bond shear stress at the interface between the fiber and the matrix, and the relative slip between the same components is as shown in Fig. 5.2. A more accurate

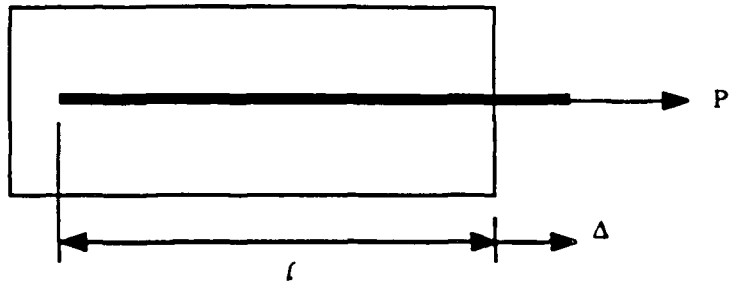

Fig. 5.1 - Pull-out test configuration.

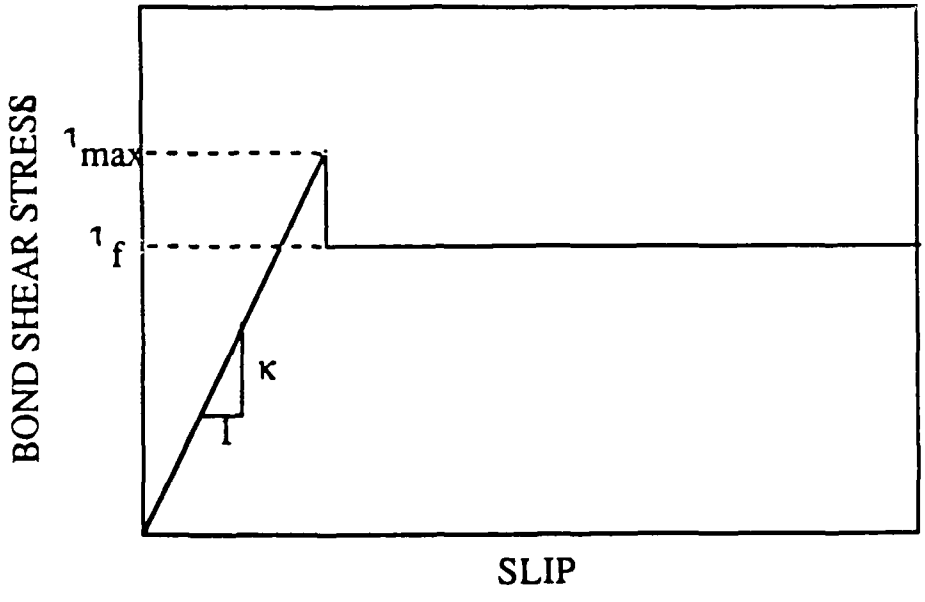

Fig. 5.2 - Assumed bond shear stress versus slip relationship.

relationship will be introduced later in this chapter. Thus, it is assumed that the bond-slip curve is linear elastic up to the point where the bond strength τ_{max} of the interface is reached, beyond which stage purely frictional conditions prevail, with a constant frictional shear stress equal to τ_f. It is also assumed that τ_f cannot exceed τ_{max}, that is the value of τ_f ranges between zero and τ_{max}. While it is understood that a constant bond stress equal to τ_f cannot be sustained forever, it is furthermore assumed that slips causing the bond stress to diminish significantly beyond τ_f will not be attained.

5.3 MATHEMATICAL DERIVATION

5.3.1 Basic Equations

The free body diagram of an infinitesimal segment of fiber (Fig. 5.3) leads to the following equation:

$$dF - \tau \psi \, dx = 0 \tag{5.1}$$

where F is the local force in the fiber at a distance x from the embedded end of the fiber, ψ is the perimeter of the fiber, and τ is the local shear stress at the interface between the fiber and the matrix.

Eq. 5.1 can be rewritten as:

$$\frac{dF}{dx} = \tau \psi \tag{5.2}$$

The product $\tau \psi$ is the shear force per unit length, or the shear flow t at the interface. Hence:

$$t = \tau \psi \tag{5.3}$$

Furthermore, the local tensile force F in the fiber can be related to the local strain in the fiber ε_f thru the following equation:

$$F = A_f E_f \varepsilon_f \tag{5.4}$$

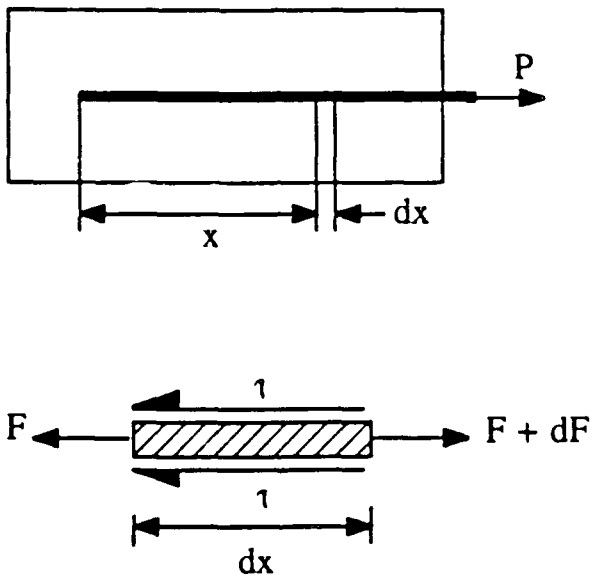

Fig. 5.3 - Free body diagram of an infinitesimal segment of fiber.

where A_f and E_f are respectively the area and the elastic modulus of the fiber, and ε_f is the local strain in the fiber.

Moreover, in the elastic region, the local shear stress τ can be related to the local slip S through the bond modulus κ as follows:

$$\tau = \kappa S \tag{5.5}$$

$$= \kappa (\delta_f - \delta_m) \tag{5.6}$$

where δ_f and δ_m are the local displacement in the fiber and the matrix respectively.

To satisfy static equilibrium, the total force P applied at the free tip of the fiber has to be resisted at any section by the local force in the fiber F, as well as the local force in the matrix T, or:

$$P = F + T \tag{5.7}$$

$$= A_f E_f \varepsilon_f + A_m E_m \varepsilon_m \tag{5.8}$$

where A_m and E_m are respectively the area and the elastic modulus of the matrix, and ε_m is the local strain in the matrix.

Differentiating Eqs. 5.2 and 5.6 leads to:

$$\frac{d^2F}{dx^2} = \frac{\psi \, d\tau}{dx} \tag{5.9}$$

$$\frac{d\tau}{dx} = \kappa \left(\frac{d\delta_f}{dx} - \frac{d\delta_m}{dx} \right) \tag{5.10}$$

Combining Eqs. 5 9 and 5.10, and recognizing the fact that the first derivative of the local displacement function is the local strain, it can be proven that:

$$\frac{d^2F}{dx^2} = \psi \kappa (\varepsilon_f - \varepsilon_m) \tag{5.11}$$

From Eq. 7.8, ε_m can be expressed as a function of ε_f as in:

$$\varepsilon_m = \frac{1}{A_m E_m} (P - A_f E_f \varepsilon_f) \quad (5.12)$$

Replacing ε_m in Eq. 5.11 by the right hand side of Eq. 5.12 leads to:

$$\frac{d^2F}{dx^2} = \frac{\psi \kappa}{A_m E_m} [A_m E_m \varepsilon_f - (P - A_f E_f \varepsilon_f)] \quad (5.13)$$

$$= -K P + K [A_m E_m + A_f E_f] \varepsilon_f \quad (5.14)$$

$$= -K P + K [A_m E_m + A_f E_f] \frac{F(x)}{A_f E_f} \quad (5.15)$$

$$= -K P + K Q F(x) \quad (5.16)$$

where:

$$K = \frac{\psi \kappa}{A_m E_m} \quad (5.17)$$

and

$$Q = \frac{A_m E_m + A_f E_f}{A_f E_f} -$$

$$= 1 + \frac{A_m E_m}{A_f E_f} \quad (5.18)$$

Eq. 7.16 is a second degree differential equation in F of the form:

$$\frac{d^2F}{dx^2} - \lambda^2 F = -K P \quad (5.19)$$

in which

$$\lambda = \sqrt{KQ} \quad (5.20)$$

The solution to this differential equation is of the form:

$$F(x) = A' e^{\lambda x} + B' e^{-\lambda x} + \frac{P}{Q} \quad (5.21)$$

The unknown coefficients A' and B' are determined from the following boundary conditions:

1) $F(0) = 0$ (5.22)

2) $F(\ell) = P$ (5.23)

Eqs. 5.22 and 5.23 are equivalent to the following two equations in A' and B':

$$A' + B' + \frac{P}{Q} = 0 \tag{5.24}$$

$$A' e^{\lambda \ell} + B' e^{-\lambda \ell} + \frac{P}{Q} = P \tag{5.25}$$

The solution to the system of equations described in Eqs. 5.24 and 5.25 is:

$$A' = \frac{P}{1 - e^{-2\lambda \ell}} \left((1 - \frac{1}{Q}) e^{-\lambda \ell} + \frac{1}{Q} e^{-2\lambda \ell} \right)$$

and $$B' = \frac{P}{1 - e^{-2\lambda \ell}} \left(-(1 - \frac{1}{Q}) e^{-\lambda \ell} - \frac{1}{Q} \right)$$

Introducing the coefficients A and B, equal to $\frac{A'}{P}$ and $\frac{B'}{P}$ respectively, we get:

$$A = \frac{1}{1 - e^{-2\lambda \ell}} \left((1 - \frac{1}{Q}) e^{-\lambda \ell} + \frac{1}{Q} e^{-2\lambda \ell} \right) \tag{5.26}$$

and $$B = \frac{1}{1 - e^{-2\lambda \ell}} \left(-\left(1 - \frac{1}{Q}\right) e^{-\lambda \ell} - \frac{1}{Q} \right) \tag{5.27}$$

Using these expressions for A and B, the force F(x) in the fiber, and the interfacial shear flow t(x) can be respectively expressed as:

$$F(x) = P \left(A e^{\lambda x} + B e^{-\lambda x} + \frac{1}{Q} \right) \tag{5.28}$$

$$t(x) = \frac{dF}{dx}$$

$$= P \lambda \left(A e^{\lambda x} - B e^{-\lambda x} \right) \tag{5.29}$$

As can be seen from Eq. 5.29, the interfacial shear flow t is a direct function of the load P. Furthermore, the shear flow is a direct function of the shear stress as in Eq. 5.3. Also, the maximum shear stress (or flow) for a given load will always occur at the point where the fiber penetrates the matrix, or at $x = \ell$.

5.3.2 Critical Force

Given the bond-slip relationship, there will be a critical force P_{crit} that will induce a shear stress at $x = \ell$ equal to τ_{max}, or a shear flow equal to t_{max} where:

$$t_{max} = \tau_{max} \Psi \tag{5.30}$$

To find P_{crit}, the shear flow at $x = \ell$, or $t(\ell)$ has first to be evaluated:

$$t(\ell) = P \lambda \left(A e^{\lambda \ell} - B e^{-\lambda \ell}\right) \tag{5.31}$$

$$= \frac{P}{1 - e^{-2\lambda \ell}} \left(\left(1 - \frac{1}{Q}\right)(1 + e^{-2\lambda \ell}) + \left(\frac{1}{Q}\right) 2e^{-\lambda \ell}\right) \tag{5.32}$$

Setting $t(\ell)$ equal to t_{max} yields the value of P_{crit}; thus:

$$P_{crit} = \frac{\tau_{max} \Psi}{\lambda} \left(\frac{1 - e^{-2\lambda l}}{\left(1 - \frac{1}{Q}\right)(1 + e^{-2\lambda \ell}) + \left(\frac{1}{Q}\right) 2e^{-\lambda \ell}} \right) \tag{5.33}$$

When a force $P \leq P_{crit}$, elastic bond conditions prevail at the interface, and no debonding occurs; in other words, the fiber remains fully bonded to the surrounding matrix.

5.3.3 Elastic Displacement

The displacement of the free end of the fiber (at $x=\ell$) can be evaluated using the following equation:

$$\Delta = \int_0^{\ell} \left(\varepsilon_f(x) - \varepsilon_m(x)\right) dx$$

$$= \int_0^{\ell} \left(\frac{F(x)}{A_f E_f} - \frac{P - F(x)}{A_m E_m}\right) dx$$

$$= \int_0^{\ell} \frac{-P}{A_m E_m} dx + \int_0^{\ell} \frac{F(x)}{A_f E_f + A_m E_m} dx$$

$$= \frac{-P \ell}{A_m E_m} + \frac{Q}{A_m E_m} \int_0^{\ell} F(x) dx \qquad (5.34)$$

To carry out the integral in Eq. 5.34, F(x) is replaced by the right hand side of Eq. 5.28. Δ is found to be as follows:

$$\Delta = \frac{P (Q - 2)}{\lambda A_m E_m} \left(\frac{1 - e^{-\lambda \ell}}{1 + e^{-\lambda \ell}}\right) \qquad (5.35)$$

As can be seen from Eq. 5.35, there is a linear relationship between the applied force P and the displacement of the fiber free end. Moreover, in a pull-out curve, the slope of the ascending linear portion of the curve is given by:

$$\left(\frac{P}{\Delta}\right) = \frac{\lambda A_m E_m}{(Q - 2)} \frac{1 + e^{-\lambda \ell}}{1 - e^{-\lambda \ell}} \qquad (5.36)$$

5.3.4 Debonding Zone

When the applied force P exceeds P_{crit}, a region identified as "zone of debonding" will develop and grow as the applied force P increases. In other words, two interfacial zones will adjacently coexist, one that is bonded and one that is debonded, i.e. one where debonding has occurred because the shear stresses have exceeded τ_{max}. Fig. 5.4 shows typical bond shear stress distribution for cases with different values of P. The forces resisted by these two individual zones will be identified as bonded

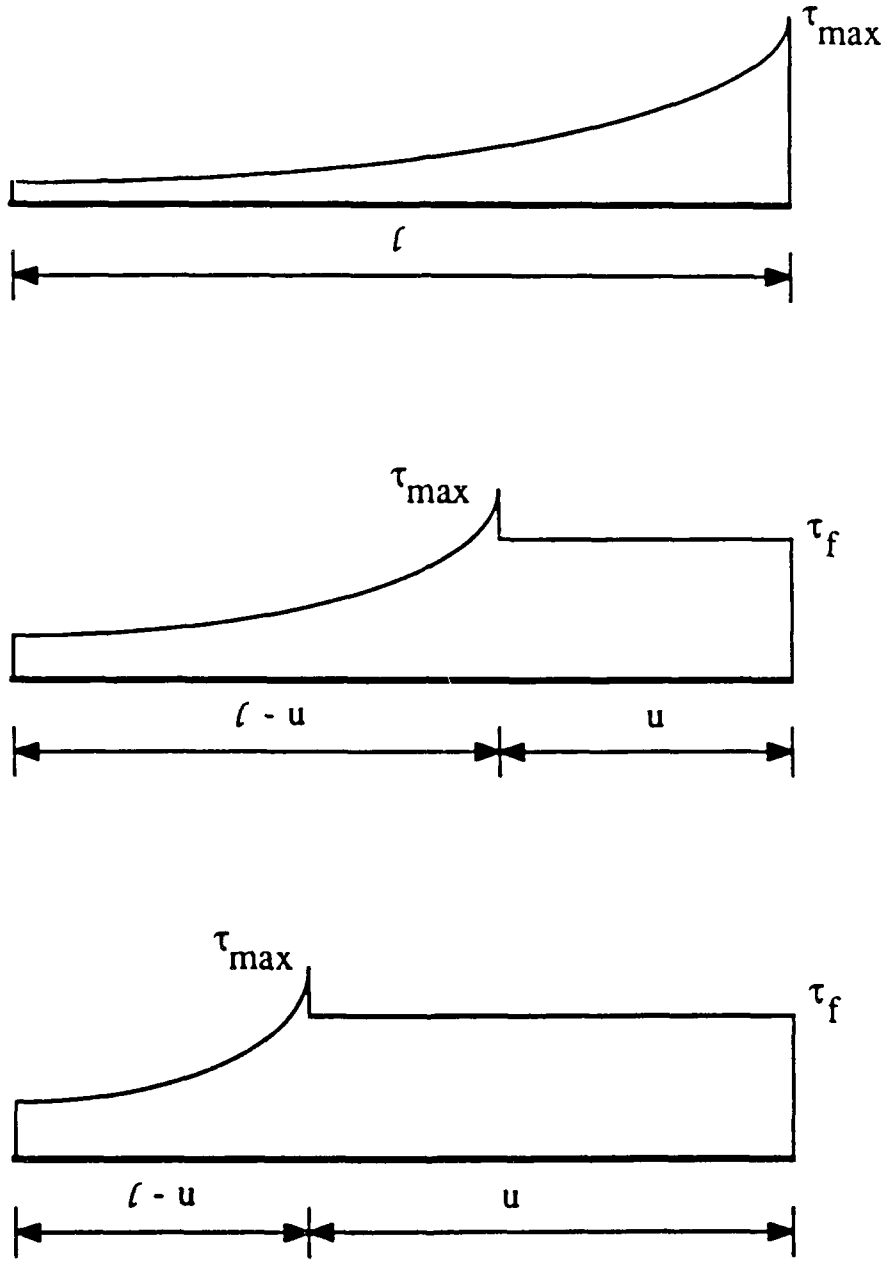

Fig. 5.4 - Typical bond stress distributions for cases where:
(a) $P = P_{crit}$
(b) $P = P_1 > P_{crit}$
(c) $P = P_2 > P_1$.

force P_b and debonded force P_d respectively. To satisfy static equilibrium, it can be inferred that for any load $P \geq P_{crit}$,

$$P = P_b + P_d \tag{5.37}$$

Based on the assumed bond shear stress - slip relationship shown in Fig. 5.2, the interfacial shear stress prevailing in the zone of debonding is constant and equal to τ_f. This means that the normal force distribution in the fiber is linear, decreasing at the rate of t_f per unit length, where:

$$t_f = \tau_f \Psi \tag{5.38}$$

In this study, the length of the zone of debonding will be noted by u. The length of the bonded zone is hence $(\ell - u)$. Over this bonded length, the same shear stress distribution prevails as in the case where $P \leq P_{crit}$, except that the force is $P' = (P - t_f u)$, and the length is $(\ell - u)$. Therefore, the shear flow distribution along the interface of the bonded length can be expressed as:

$$t_b(x) = (P - t_f u)\,\lambda\,(A^* e^{\lambda x} - B^* e^{-\lambda x}) \tag{5.39}$$

where

$$A^* = \frac{1}{1 - e^{-2\lambda(\ell-u)}}\left(\left(1 - \frac{1}{Q}\right) e^{-\lambda(\ell-u)} + \frac{1}{Q} e^{-2\lambda(\ell-u)}\right) \tag{5.40}$$

and

$$B^* = \frac{1}{1 - e^{-2\lambda(\ell-u)}}\left(-\left(1 - \frac{1}{Q}\right) e^{-\lambda(\ell-u)} - \frac{1}{Q}\right) \tag{5.41}$$

The relationship between P and u can be obtained by setting the value of the shear flow at $x = (\ell - u)$ equal to t_{max}, or:

$$(P - t_f u)\,\lambda\,(A^* e^{\lambda(\ell - u)} - B^* e^{-\lambda(\ell - u)}) = t_{max} \tag{5.42}$$

or, replacing A^* and B^* by their respective values given in Eqs. 5.40 and 5.41, P can be found explicitly as:

$$P = t_f u + \frac{t_{max}}{\lambda} \frac{1 - e^{-2\lambda(\ell - u)}}{\frac{2}{Q} e^{-\lambda(\ell - u)} + \left(1 - \frac{1}{Q}\right)\left(1 + e^{-2\lambda(\ell - u)}\right)} \tag{5.43}$$

Since the force resisted by the debonded zone can be easily found as:

$$P_d = t_f u \tag{5.44}$$

then, P_b, which is equal to the difference between the total force P (given in Eq. 5.43) and P_d (as per Eq. 5.44), can hence be found as:

$$P_b = \frac{t_{max}}{\lambda} \frac{1 - e^{-2\lambda(\ell - u)}}{\frac{2}{Q} e^{-\lambda(\ell - u)} + \left(1 - \frac{1}{Q}\right)\left(1 + e^{-2\lambda(\ell - u)}\right)} \tag{5.45}$$

To determine the distribution of the force in the fiber in the bonded zone, F_b, the shear flow distribution in that zone is integrated:

$$F_b(x) = \int_0^x t_b(y)\, dy \tag{5.46}$$

$$= (P - t_f u)\lambda \int_0^x \left(A^* e^{\lambda y} - B^* e^{-\lambda y}\right) dy$$

$$= (P - t_f u)\left(A^* e^{\lambda x} + B^* e^{-\lambda x} - A^* + B^*\right) \tag{5.47}$$

Naturally, Eq. 5.47 holds for values of x between 0 and $(\ell - u)$. x = 0 at the fiber's embedded end, and x = $(\ell - u)$ at the point of demarcation between the bonded and debonded zones. Fig. 5.5 shows the interfacial bond shear stress and the fiber normal force distribution under conditions of partial debonding.

The force distribution in the debonded zone can be expressed as:

$$F_d(z) = P - t_f z \tag{5.48}$$

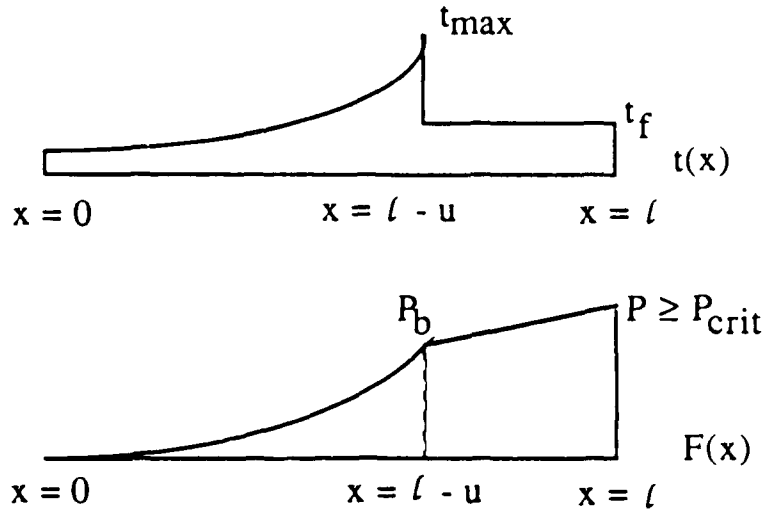

Fig. 5.5 - Bond stress and normal force distributions under partially debonded conditions.

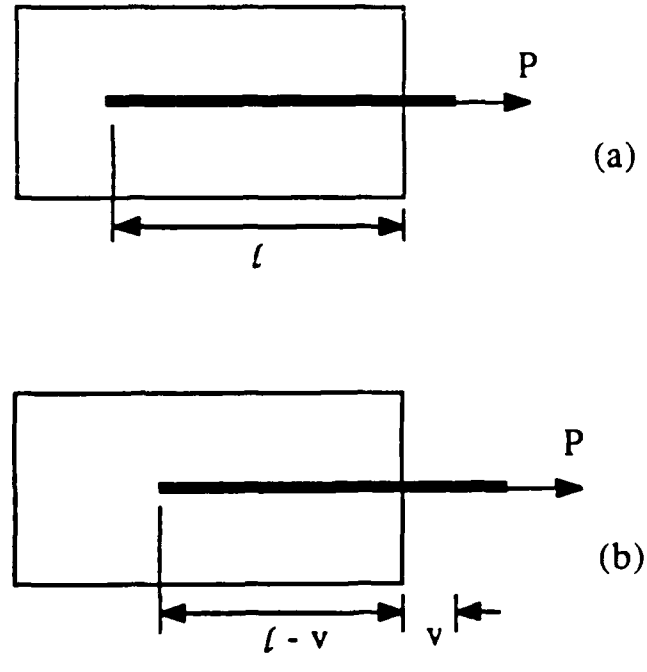

Fig. 5.6 - Pull-out test under: (a) pre-peak conditions, and (b) dynamic pull-out conditions.

Equation 5.48 holds for values of z between 0 at the free end, and u at the point of demarcation between the bonded and debonded zones.

To find the displacement at the free end, Eq. 5.34 is still valid, except that the integral will be carried out separately over each of the two zones, thus:

$$\Delta = \frac{-P\ \ell}{A_m\ E_m} + \frac{Q}{A_m\ E_m}\left(\int_0^u F_d(x)\ dx + \int_0^{\ell-u} F_b(x)\ dx\right) \quad (5.49)$$

in which $F_d(z)$ and $F_b(x)$ are as given in Eqs. 5.48 and 5.47 respectively. The integral in Eq. 5.49 yields:

$$\Delta = \frac{\left(P(Q-1)u - \frac{t_f u^2}{2}(Q-2) + \left(P - t_f u\right)\left(\frac{1-e^{-\lambda(\ell-u)}}{1+e^{-\lambda(\ell-u)}}\right)\frac{Q-2}{\lambda} - t_f u\ell\right)}{A_m E_m} \quad (5.50)$$

5.3.5 Dynamic Mechanism of Pull-Out

The value of tne length of the debonded zone u goes from zero at the onset of debonding to ℓ at complete debonding (purely frictional bond shear stresses at the interface). For each value of u, one value for the pull-out load and the corresponding end slip exists.

Once u has reached ℓ, a dynamic mechanism of pull-out develops. The relationship between the pull-out load and the slip can now be derived. If the rigid body displacement of the fiber is referred to as v (Fig. 5.6), then the pull-out force is:

$$P = t_f\,(\ell - v) \quad (5.51)$$

The force F within the fiber at a distance x from the point at which the fiber penetrates the matrix is:

$$F(x) = t_f\,(\ell - v - x) \quad (5.52)$$

The dynamic pull-out slip Δ is now equal to the total rigid body movement of the fiber v, added to the elastic elongation within the fiber, or:

$$\Delta = \int_0^{\ell-v} \left(\varepsilon_f(x) - \varepsilon_m(x)\right) dx + v$$

$$= \int_0^{\ell-v} \left(\frac{F(x)}{A_f E_f} - \frac{P - F(x)}{A_m E_m}\right) dx + v$$

$$= \int_0^{\ell-v} \frac{-P}{A_m E_m} dx + \int_0^{\ell-v} \frac{F(x)}{A_f E_f + A_m E_m} dx + v$$

$$= \frac{-P(\ell-v)}{A_m E_m} + \frac{Q}{A_m E_m} \int_0^{\ell-v} F(x)\, dx + v \qquad (5.53)$$

The dynamic pull-out slip Δ, as given by Eq. 5.53, is almost equal to the fiber rigid body movement v. This suggests an almost perfectly linear relationship between the applied pull-out force P, and the dynamic pull-out slip Δ, of the form:

$$P = t_f(\ell - \Delta) \qquad (5.54)$$

As is demonstrated in Chap. 6, pull-out tests conducted in the lab suggested a descending branch that is not linear, but decays more rapidly (Fig. 5.7), which suggests a decay in the the frictional bond. In other words, the assumption that the bond shear stress remains constant after the bond strength τ_{max} is reached is not correct. However, it is acceptable at small values of slip.

An alternative convenient way to look at the descending branch would be to assume that the bond shear stress versus slip curve is as shown in Fig. 5.8. Therefore, it is assumed that at some point after the

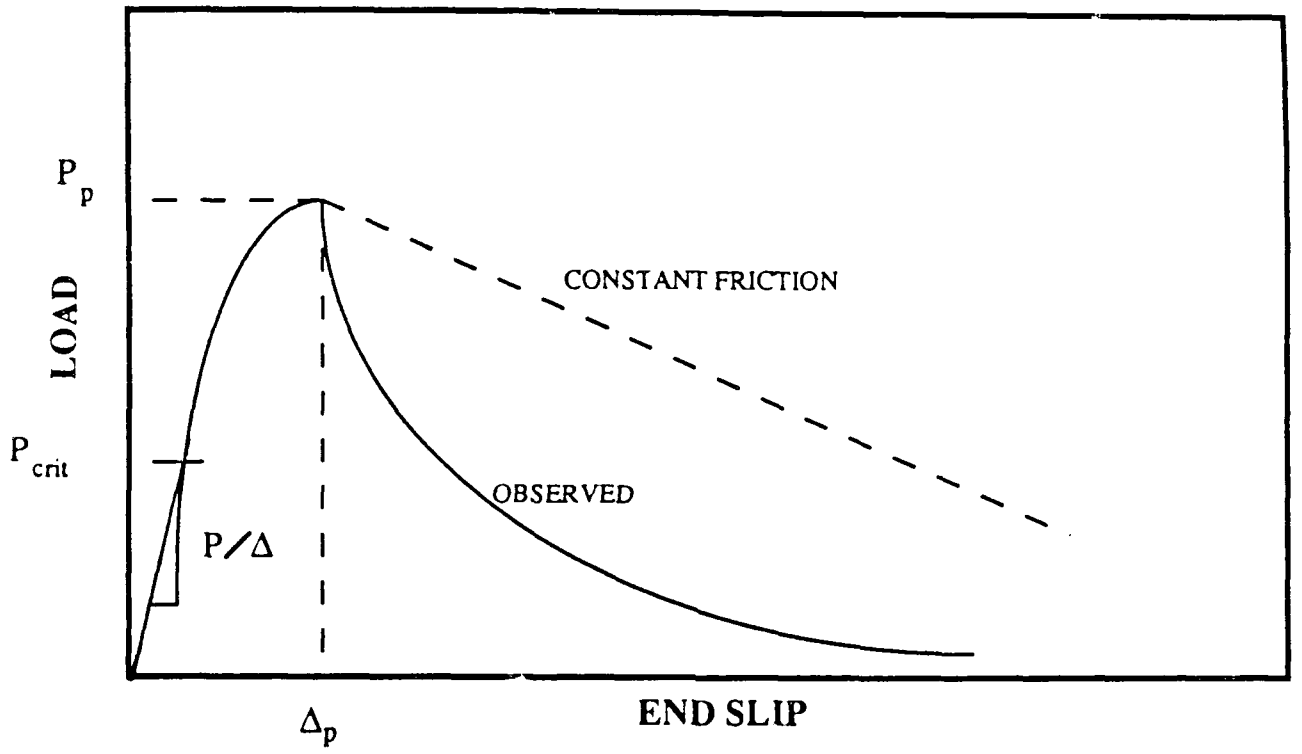

Fig. 5.7 - Schematic representation of a typical pull-out curve.

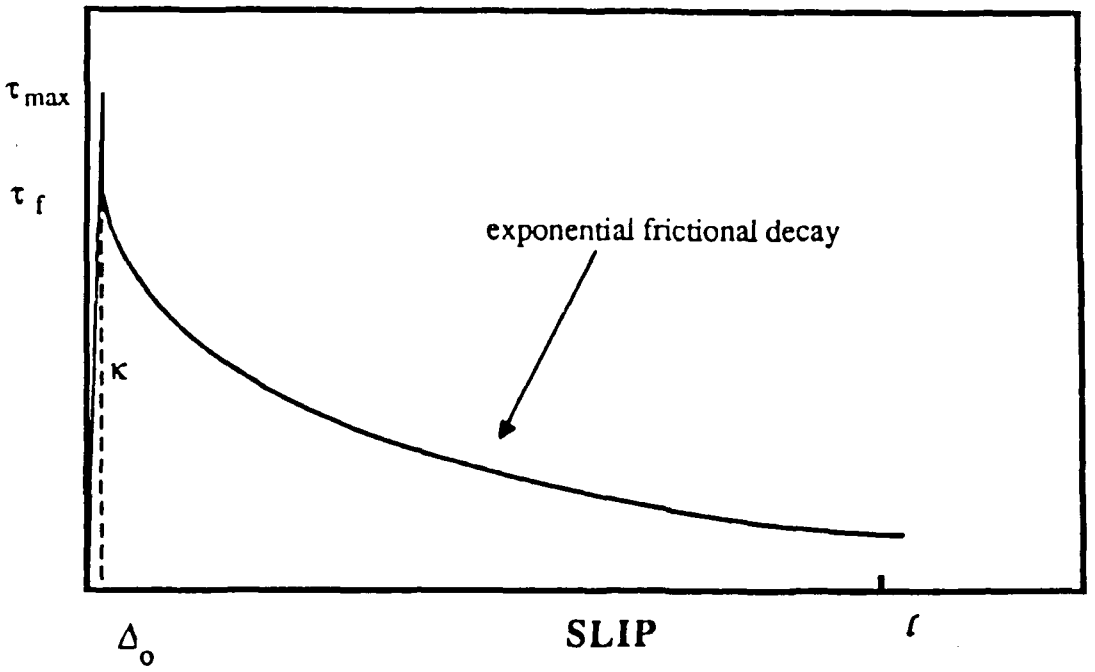

Fig. 5.8a - Alternative bond shear stress versus slip relationship with frictional decay.

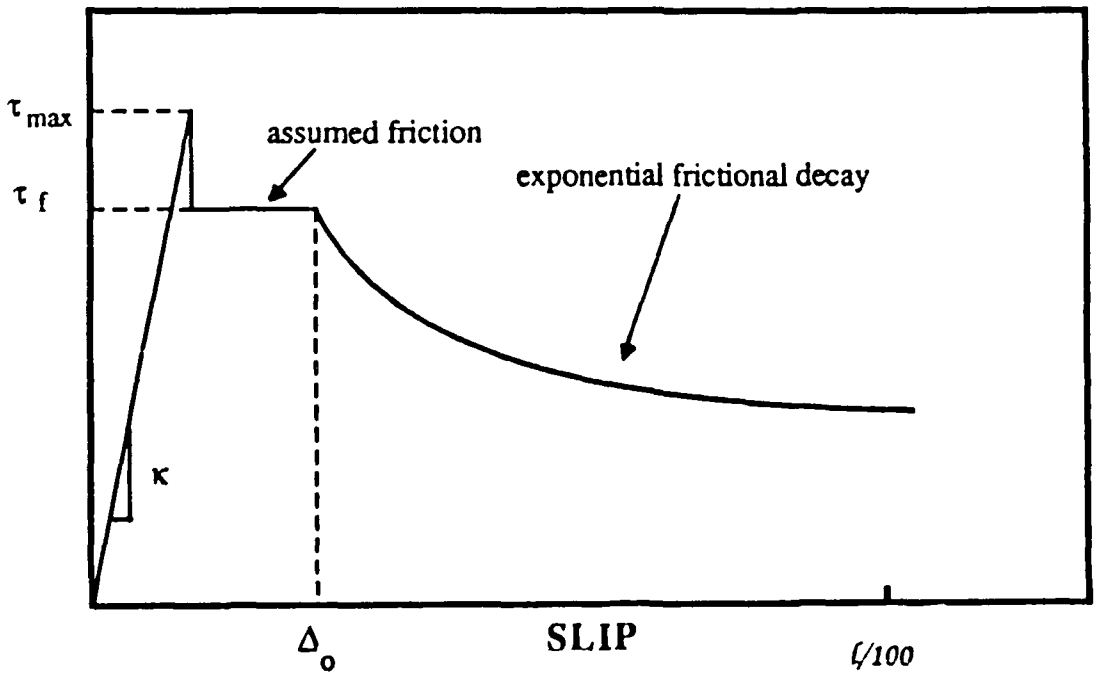

Fig. 5.8b - Alternative bond shear stress versus slip relationship with frictional decay when smaller scale.

bond strength τ_{max} is reached, the frictional shear stress starts decreasing with the slip. In what follows, it will be assumed that the slip for which the friction starts decaying is the slip Δ_o that corresponds to the case of full debonding, which is the onset of the dynamic mechanism. Δ_o is assumed small in comparison to the embedded length. Under this assumption, the equations given in this chapter, that pertain to both the fully bonded case and the the case of partial bonding are still applicable. At this stage, a state of complete failure of the elastic bond between the fiber and the matrix exists. Thus, the only phenomenon that describes the resistance of the fiber against pull-out is friction.

5.3.5.1 Normal Contact Pressure. The frictional stress is equal to the normal contact pressure on the steel fiber multiplied by a coefficient of friction:

$$\tau_d = \mu P_N \tag{5.55}$$

in which P_N is the normal contact pressure between the fiber and the matrix.

From examining the free body diagram of the embedded fiber in Fig. 5.6, one can write from equilibrium that:

$$dF = \tau_d \psi \, dx \tag{5.56}$$

where dF is the differential of the local force in the fiber at a distance x.

So if we divide Eq. 5.56 by the cross sectional area of the fiber we get:

$$df_f = \frac{2 \tau_d}{r_f} dx \tag{5.57}$$

Substituting the right hand side of Eq. 5.55 in Eq. 5.57 leads to:

$$df_f = \frac{2 \mu P_N}{r_f} dx \tag{5.58}$$

But from the shrink fit theory [Timoshinko], the interfacial contact pressure P_N in a shrink fit configuration (Fig. 5.9) with no load on the fiber and for $r_f << r_m$ is given by:

$$P_N = \frac{\varepsilon_{mr}}{\frac{(1 + \nu_m)}{E_m} + \frac{(1 - \nu_f)}{E_f}} \tag{5.59}$$

where ε_{mr} is the radial shrinkage strain in the matrix in addition to, if present, the strain due to any externally applied confining load.

The radial shrinkage strain ε_r in the matrix can be expressed as:

$$\varepsilon_{mr} = \frac{\delta}{r_f} \tag{5.60}$$

δ in Eq. 5.60 represents the matrix-fiber misfit. The misfit was defined by Pinchin [50] as "the difference between the fiber and the hole radius in the absence of the fiber" (Fig. 5.9).

$$\delta = r_f - r_o \tag{5.60-a}$$

5.3.5.2 Poisson's Effect. However, when the fiber is loaded longitudinally with a stress f_f, it will be subjected to a Poisson's contraction ε_{fr} such that:

$$\varepsilon_{fr} = \frac{f_f}{E_f} \nu_f \tag{5.61}$$

This strain ε_{fr} will obviously reduce the interfacial contact pressure caused by the original matrix strain, thus:

$$\varepsilon_{eff} = \varepsilon_{mr} - \varepsilon_{fr} \tag{5.62}$$

$$= \frac{\delta}{r_f} - \frac{f_f}{E_f} \nu_f \tag{5.63}$$

substituting the right hand side of Eq. 5.63 in Eq. 5.59, and solving the resulting differential equation, the stress in the fiber can be expressed as follows:

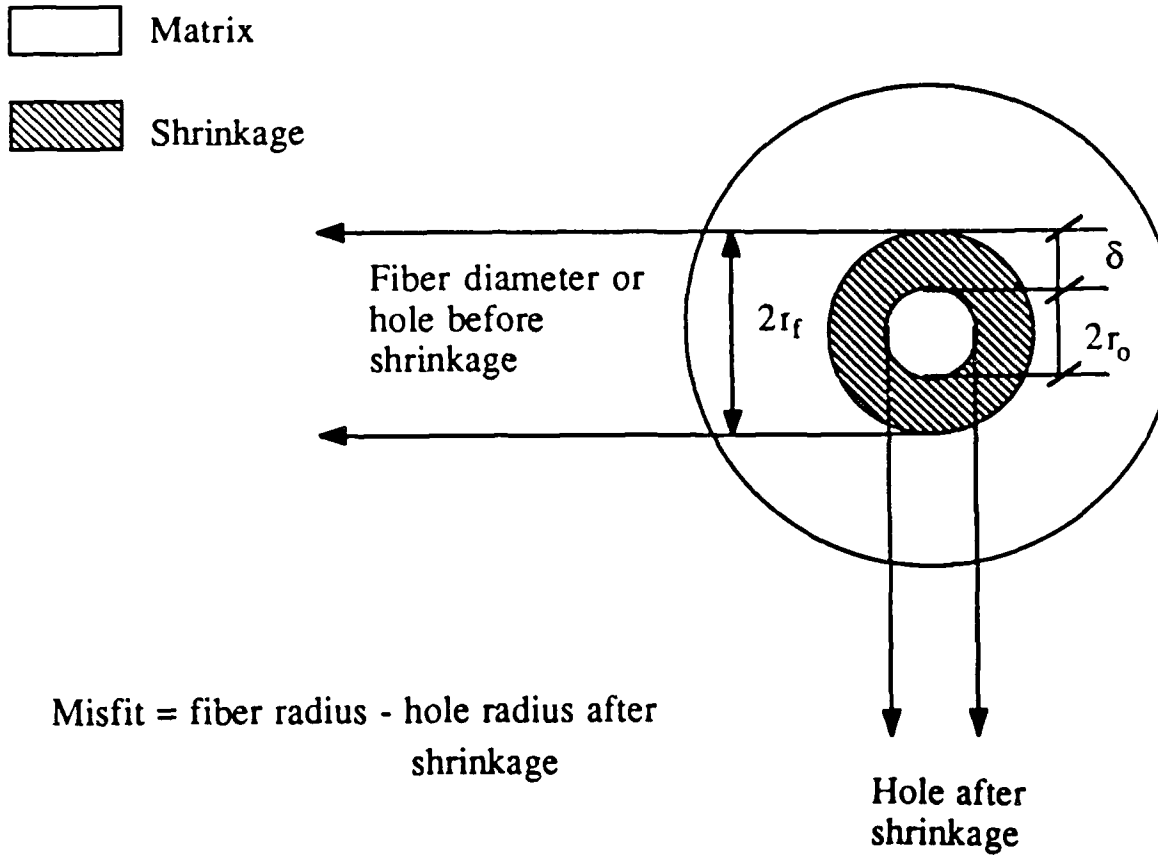

Fig. 5.9 - Fiber - matrix misfit

$$f_f = \left(1 - \mathrm{Exp}\left(\frac{-2\ \nu_f\ \mu\ x}{E_f\ r_f\left(\frac{(1+\nu_m)}{E_m} + \frac{(1-\nu_f)}{E_f}\right)}\right)\right)\frac{\delta\ E_f}{r_f\ \nu_f} \qquad (5.64)$$

where x is the embedded length of the fiber.

Multiplying Eq. 5.64 by the cross sectional area of the fiber yields an equation for the pull-out load as a function of the embedded length x:

$$P = \left(1 - \mathrm{Exp}\left(\frac{-2\ \nu_f\ \mu\ x}{E_f\ r_f\left(\frac{(1+\nu_m)}{E_m} + \frac{(1-\nu_f)}{E_f}\right)}\right)\right)\frac{\delta\ E_f\ \pi\ r_f}{\nu_f} \qquad (5.65)$$

5.3.5.3 Effect of Decay in Misfit δ. It is observed that δ, the fiber-matrix misfit, deteriorates (i.e. decreases) as the fiber is pulled out. This is due to a combined action of abrasion and compaction of cement and sand particles surrounding the fiber since the steel fiber is harder than the matrix.

Several attempts were made in this study to model the decay in misfit. A linear and a parabolic function were considered. The best results were obtained when the decreasing trend of the misfit was assumed exponential, as suggested by comparison with experimental pull-out curves. The following expression for the fiber-matrix misfit δ is proposed in this study:

$$\delta = \delta_o \frac{e^{-(\Delta-\Delta_o)^\eta} - \xi e^{-(\ell)^\eta}}{1 - \xi e^{-(\ell-\Delta+\Delta_o)^\eta}} \qquad (5.66)$$

in which:

Δ_o = relative slip of the fiber under conditions of full debonding

Δ = the end slip

δ_o = the initial fiber-matrix misfit = $r_f - r_o$

ξ = a dimensionless constant to give the analytical descending branch the same asymptotic value as the experimental one.

The initial fiber-matrix misfit δ_o is calculated by equating the pull-out load that corresponds to an embedded length $x = \ell$ in Eq. 5.65. That is P is replaced by $t_f . \ell$. Hence:

$$\delta_o = \frac{t_f \ell v_f}{E_f \pi r_f}\left(1 - \mathrm{Exp}\left(\frac{-2 v_f \mu \ell}{E_f r_f\left(\frac{(1+\nu_m)}{E_m} + \frac{(1-\nu_f)}{E_f}\right)}\right)\right)^{-1} \tag{5.67}$$

Δ_o can be obtained from Eq. 5.50, with a $P = t_f \ell$, and $u = \ell$, or:

$$\Delta_o = \frac{(Q-2)\, t_f \ell^2}{2 A_m E_m} \tag{5.68}$$

Fig. 5.10 shows a typical plot of the variation of the misfit as related to the relative slip between the fiber and the matrix. This plot pertains to a smooth fiber of diameter 0.01 inches pulled out from a high strength cementitious matrix containing 2% by volume steel fibers of the same kind as the one being pulled out. Additional information on this series can be looked up in chapter 6, tables 6.3 through 6.5.

In pull-out tests the embedded length of the fiber is equal to the difference between the original embedded length and the additional end slip, i.e. $x = \ell - (\Delta - \Delta_o)$. On the other hand, in pull-through tests the embedded length of the fiber is constant and equal to the original embedded length, i.e. $x = \ell$

5.3.5.4 Frictional Shear Value. The above described methodology makes it possible to find an equivalent value for the frictional shear bond for any given pull-out load, or end slip Δ, since:

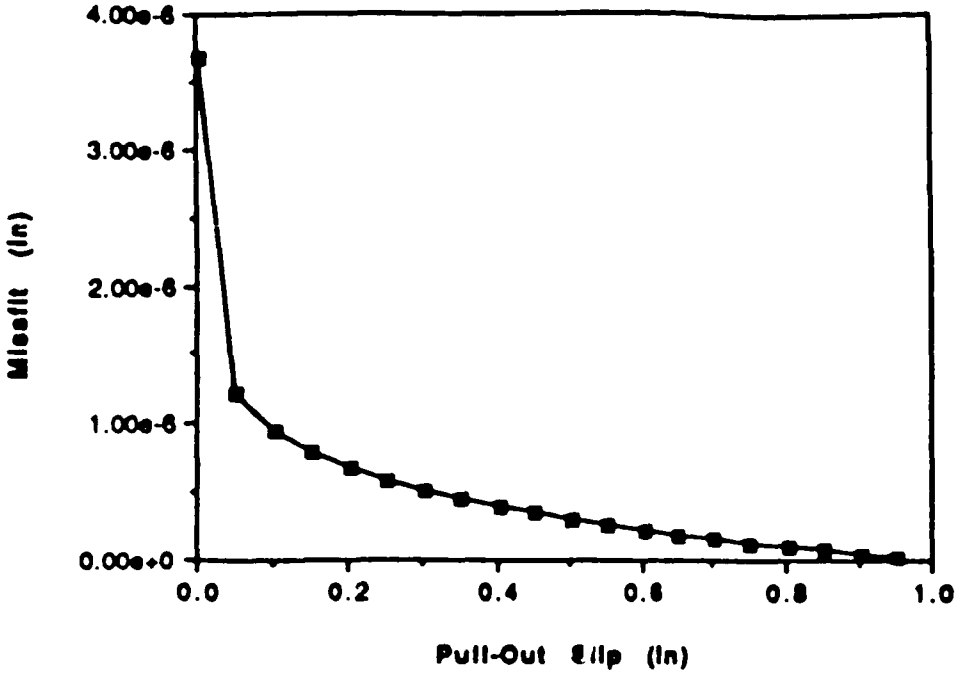

Fig. 5.10 - Deterioration function of the misfit (H2SF series)

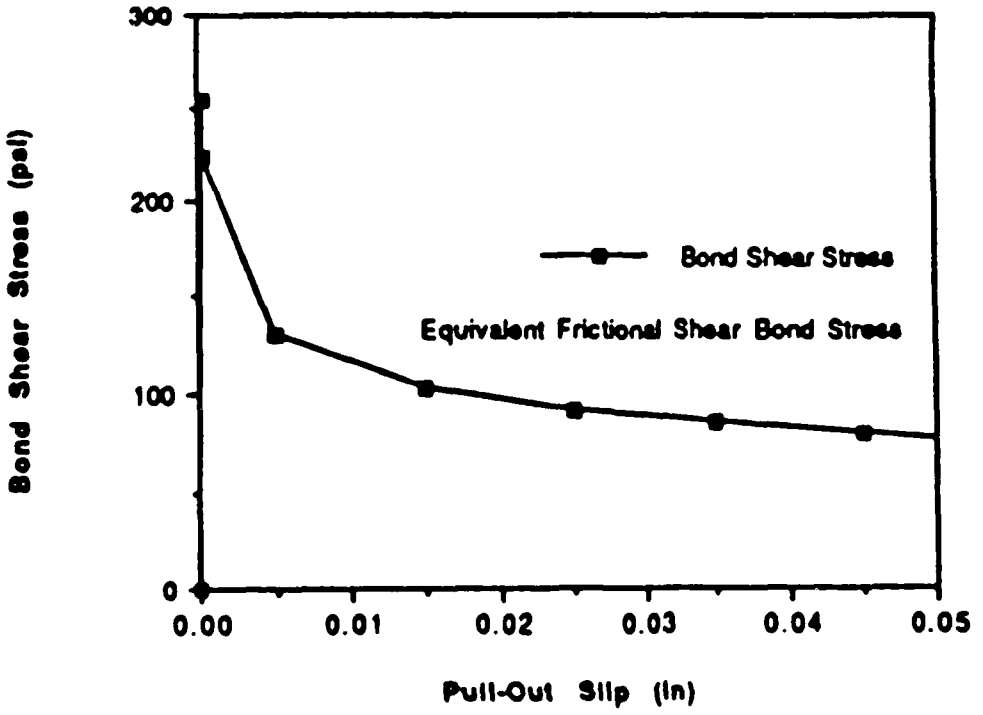

Fig. 5.11 - Equivalent frictional shear bond (H2SF series)

$$P = \psi \tau_d(x) x$$

or

$$\tau_d(x) = \frac{P}{\psi x}$$

$$= \frac{P}{\psi (\ell - \Delta + \Delta_o)}$$

The value of P obtained from Eq. 5.65 can be divided by the corresponding embedded length, thus giving an equivalent value for the frictional shear bond for a given slip, hence:

$$\tau_d(\Delta) = \left(1 - \mathrm{Exp}\left(\frac{-2 \nu_f \mu (\ell - \Delta + \Delta_o)}{E_f r_f\left(\frac{(1 + \nu_m)}{E_m} + \frac{(1 - \nu_f)}{E_f}\right)}\right)\right) * \frac{\delta_o \left(e^{-(\Delta-\Delta_o)^\eta} - \xi e^{-(\ell)^\eta}\right) E_f \pi r_f}{\psi \left(1 - \xi e^{-(\ell-\Delta+\Delta_o)^\eta}\right)(\ell - \Delta + \Delta_o) \nu_f} \quad (5.69)$$

which is valid for $\Delta \geq \Delta_o$.

A typical plot of τ_d versus x where $x=\ell-\Delta+\Delta_o$ is shown in Fig. 5.11.

The initial frictional stress τ_f, is equal to $\tau_d(\Delta_o)$, hence:

$$\tau_f = \left(1 - \mathrm{Exp}\left(\frac{-2 \nu_f \mu \ell}{E_f r_f\left(\frac{(1 + \nu_m)}{E_m} + \frac{(1 - \nu_f)}{E_f}\right)}\right)\right) \frac{\delta_o E_f \pi r_f}{\psi \ell \nu_f} \quad (5.70)$$

Hence, the decaying frictional stress τ_d can be expressed as:

$$\tau_d(\Delta) = \tau_f \frac{e^{-(\Delta-\Delta_o)^\eta} - \xi e^{-(\ell)^\eta}}{1 - \xi e^{-(\ell-\Delta+\Delta_o)^\eta}} * \frac{\left(1 - \mathrm{Exp}\left(\frac{-2\,\nu_f\,\mu\,(\ell - \Delta + \Delta_o)}{E_f\, r_f\left(\frac{(1+\nu_m)}{E_m} + \frac{(1-\nu_f)}{E_f}\right)}\right)\right)}{\left(1 - \mathrm{Exp}\left(\frac{-2\,\nu_f\,\mu\,\ell}{E_f\, r_f\left(\frac{(1+\nu_m)}{E_m} + \frac{(1-\nu_f)}{E_f}\right)}\right)\right)} \quad (5.71)$$

5.4 PREDICTION OF PULL-OUT CURVE (PRIMAL PROBLEM)

For a given bond shear stress versus slip relationship of the type discussed above (Fig. 5.8), a complete pull-out curve can be predicted. The predicted pull-out curve (Fig. 5.7) is divided into three distinct regions and can be obtained using the following procedure:

1. Pre-critical region: it is a linear portion; the critical point (P_{crit}, Δ_{crit}) is enough to describe this linear zone, which extends from the origin to the critical point.

2. Partial debonding region: for each value of the length of the debonding zone u, one point on the curve can be found by computing the corresponding pull-out force and end slip (Eqs. 5.43 and 5.50). As many points as needed within this range can be found, so long as the value of u is bound between 0 and the fiber length ℓ.

3. The pull-out region: for each value of the end slip Δ ($\Delta_o \le \Delta \le \ell$), or ($0 \le (\Delta - \Delta_o) \le \ell$), a value for the pull-out load can be determined from Eq.5.65, hence leading to one point on the pull-out curve. When $(\Delta - \Delta_o)$ reaches the value of ℓ, the force would be equal to zero.

5.5 PREDICTION OF BOND-SLIP CURVE (DUAL PROBLEM)

Given an experimental pull-out curve for a given fiber, the bond shear stress versus slip curve can be theoretically obtained, assuming that it is of the type described in Fig. 5.8, i.e. linear elastic ascending branch, followed by a purely frictional region, and then a deteriorating frictional zone(see Eq. 5.70). The whole curve can hence be described by five parameter., namely the bond modulus κ, the bond strength τ_{max}, the constant frictional bond stress τ_f, the value of the slip at which the bond starts to deteriorate Δ_o, and the decaying frictional parameters ξ and η, describing the deteriorating frictional zone.

The bond modulus κ is determined from the slope of the linear ascending portion of the pull-out curve, which can be obtained graphically. Furthermore, the value of Q (Eq. 5.18) can be evaluated from the physical and mechanical properties of the fiber and the matrix. Judgment and common sense are to be used in evaluating the area of the matrix A_m. Indeed, only a fraction of the matrix cross sectional area is effective if the proportion of the specimen's cross sectional area to that of the fiber is relatively large. However, it can be shown that the solution to the dual problem is insensitive to the value of A_m. Once Q and the slope $\left(\frac{P}{\Delta}\right)$ are known, λ can be solved for in Eq. 5.36 by iteration or by some numerical procedure. Having found λ, and using Eq. 5.20, K can now be solved for:

$$K = \frac{1}{Q} \lambda^2 \tag{5.71}$$

Finally, the value of the bond modulus κ can be derived from Eq. 5.17:

$$\kappa = \frac{1}{\psi} A_m E_m K \tag{5.72}$$

The next step would be to evaluate the bond strength of the interface τ_{max} as well as the frictional bond τ_f. The peak load P_p and the corresponding end slip Δ_p are to be studied first. The peak load will

generally occur under partial debonding conditions. The value of u corresponding to that case is the value of u that would maximize P. Hence, for $u = u_p$, we have:

$$\left(\frac{dP}{du}\right)_{@\ u = u_p} = 0$$

where P is as given in Eq. 5.43:

$$P = t_f u + \frac{t_{max}}{\lambda} \frac{1 - e^{-2\lambda(\ell - u)}}{\frac{2}{Q} e^{-\lambda(\ell - u)} + \left(1 - \frac{1}{Q}\right)\left(1 + e^{-2\lambda(\ell - u)}\right)}$$

To make the differentiation easier, a change of variables is in order. Introducing the variable X defined as:

$$X = e^{-\lambda(\ell - u)} \tag{5.73}$$

$$\text{then} \quad \frac{dX}{du} = \lambda e^{-\lambda(\ell - u)} \tag{5.74}$$

$$\text{and} \quad \frac{dP}{du} = \frac{dP}{dX}\frac{dX}{du}$$

$$\text{thus} \quad \left(\frac{dP}{dX}\right)_{@\ X = X_p} = 0 \tag{5.75}$$

where

$$X_p = e^{-\lambda(\ell - u_p)} \tag{5.76}$$

$$P(X) = \frac{t_f}{\lambda} \ln(X) + t_f \ell + \frac{t_{max}}{\lambda} \frac{1 - X^2}{\frac{2}{Q} X + \left(1 - \frac{1}{Q}\right)\left(1 + X^2\right)} \tag{5.77}$$

$$\left(\frac{dP}{dX}\right)_{@\ X = X_p} = \frac{t_f}{\lambda X_p} + \frac{t_{max}}{\lambda} \frac{\frac{-2}{Q} X_p^2 - 4\left(1 - \frac{1}{Q}\right) X_p - \frac{2}{Q}}{\left(\left(1 - \frac{1}{Q}\right) X_p^2 + \frac{2}{Q} X_p + \left(1 - \frac{1}{Q}\right)\right)^2} \tag{5.78}$$

$$\text{also} \quad P(X_p) = \frac{t_f}{\lambda}\ln(X_p) + t_f\,\ell + \frac{t_{max}}{\lambda}\,\frac{1 - X_p^2}{\frac{2}{Q}\,X_p + \left(1 - \frac{1}{Q}\right)\left(1 + X_p^2\right)} \tag{5.79}$$

$$\text{and} \quad \Delta(X_p) = \frac{P(Q-1)\left(\frac{\ln(X_p)}{\lambda} + \ell\right) - \frac{t_f}{2}\left(\frac{\ln(X_p)}{\lambda} + \ell\right)^2 (Q-2)}{A_m\,E_m}$$

$$+ \frac{\left(P - t_f\left(\frac{\ln(X_p)}{\lambda} + \ell\right)\right)\frac{(Q-2)}{\lambda}\left(\frac{1 - X_p}{1 + X_p}\right) - t_f\,\ell\left(\frac{\ln(X_p)}{\lambda} + \ell\right)}{A_m\,E_m} \tag{5.80}$$

To get the values of t_f and t_{max}, a system of three non-linear equations in three unknown has to be solved, the three unknowns being t_f, t_{max}, and X_p. The first equation is obtained by setting the right-hand side of Eq. 5.78 equal to zero. The second equation is obtained by setting the right-hand side of Eq. 5.79 equal to P_p, the maximum recorded load on the $(P\text{-}\Delta)$ curve, and the third equation consists of equating the right-hand side of Eq. 5.80 to Δ_p, the end slip corresponding to P_p.

The corresponding system of three equations in three unknowns is thus as follows:

$$\frac{t_f}{\lambda X_p} + \frac{t_{max}}{\lambda}\,\frac{\frac{-2}{Q}\,X_p^2 - 4\left(1 - \frac{1}{Q}\right)X_p - \frac{2}{Q}}{\left(\left(1 - \frac{1}{Q}\right)X_p^2 + \frac{2}{Q}\,X_p + \left(1 - \frac{1}{Q}\right)\right)^2} = 0 \tag{5.81}$$

$$\frac{t_f}{\lambda}\ln(X_p) + t_f\,\ell + \frac{t_{max}}{\lambda}\,\frac{1 - X_p^2}{\frac{2}{Q}\,X_p + \left(1 - \frac{1}{Q}\right)\left(1 + X_p^2\right)} = P_p \tag{5.82}$$

$$\frac{P_p\,(Q-1)\left(\frac{\ln(X_p)}{\lambda}+\ell\right)-\frac{t_f}{2}\left(\frac{\ln(X_p)}{\lambda}+\ell\right)^2(Q-2)-t_f\,\ell\left(\frac{\ln(X_p)}{\lambda}+\ell\right)}{A_m\,E_m}$$

$$+\frac{\left(P_p-t_f\left(\frac{\ln(X_p)}{\lambda}+\ell\right)\right)\frac{(Q-2)}{\lambda}\left(\frac{1-X_p}{1+X_p}\right)}{A_m\,E_m}=\Delta_p \qquad (5.83)$$

the value of u_p corresponding to the value found for X_p has to be between 0 and ℓ. The above three equations, when solved, lead to the values of t_f, t_{max} and X_p or equivalently u_p. The numerical solution is described in Appendix V-A.

The experimental pull-out curves developed in the course of this investigation suggested a steep initial decay in the post-peak pull-out behavior, that is when Δ is close to Δ_o. A parametric study of Eq. 5.70 indicated that the factor reflecting the rate of initial decay is η. To best simulate the real experimental curves, a good value for η was found to be near 0.2.

To evaluate the factor ξ, one point on the experimental pull-out curve is needed, say (P_x, Δ_x). Then, from Eq. 5.65, and using the values of P_x and Δ_x, δ can be solved for:

$$\delta = \frac{P_x\,\nu_f}{E_f\,\pi\,r_f}\left(1-\mathrm{Exp}\left(\frac{-2\,\nu_f\,\mu\,(\ell-\Delta_x+\Delta_o)}{E_f\,r_f\left(\frac{(1+\nu_m)}{E_m}+\frac{(1-\nu_f)}{E_f}\right)}\right)\right)^{-1} \qquad (5.84)$$

Then, substituting in Eq. 5.66, ξ can be solved for:

$$\xi = \frac{e^{-(\ell)^{0.2}}-\left(\frac{\delta}{\delta_o}\right)e^{-(\ell-\Delta_x-\Delta_o)^{0.2}}}{e^{-(\Delta_x-\Delta_o)^{0.2}}-\left(\frac{\delta}{\delta_o}\right)} \qquad (5.85)$$

where δ is as given in Eq. 5.84, and δ_o is as given in Eq. 5.67.

With the five basic parameters κ, τ_{max}, τ_f , Δ_o, and ξ known, the whole bond shear stress versus slip relationship can be constructed. Examples and correlation with experimental observations are presented in Figs. 5.12-5.18. Those examples show the application of the analytical model in solving the dual problem as explained earlier in section 5.5 of this chapter. The numerical data used in the solution is presented in Appendix V-B. Examples on the application of the proposed model in solving the primal problem i.e. predicting the pull-out curve are presented in Chapter 6 (Figs. 6.22-6.27).

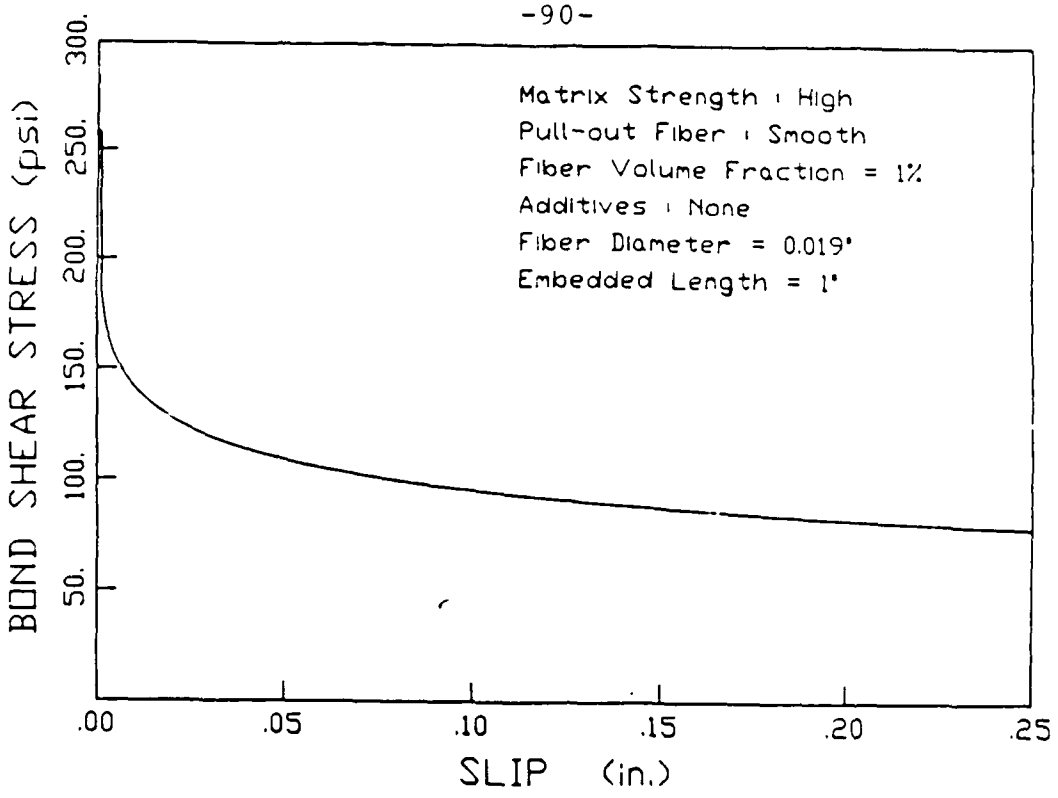

5.12a - **Bond shear stress versus slip, H1SN series, full scale.**

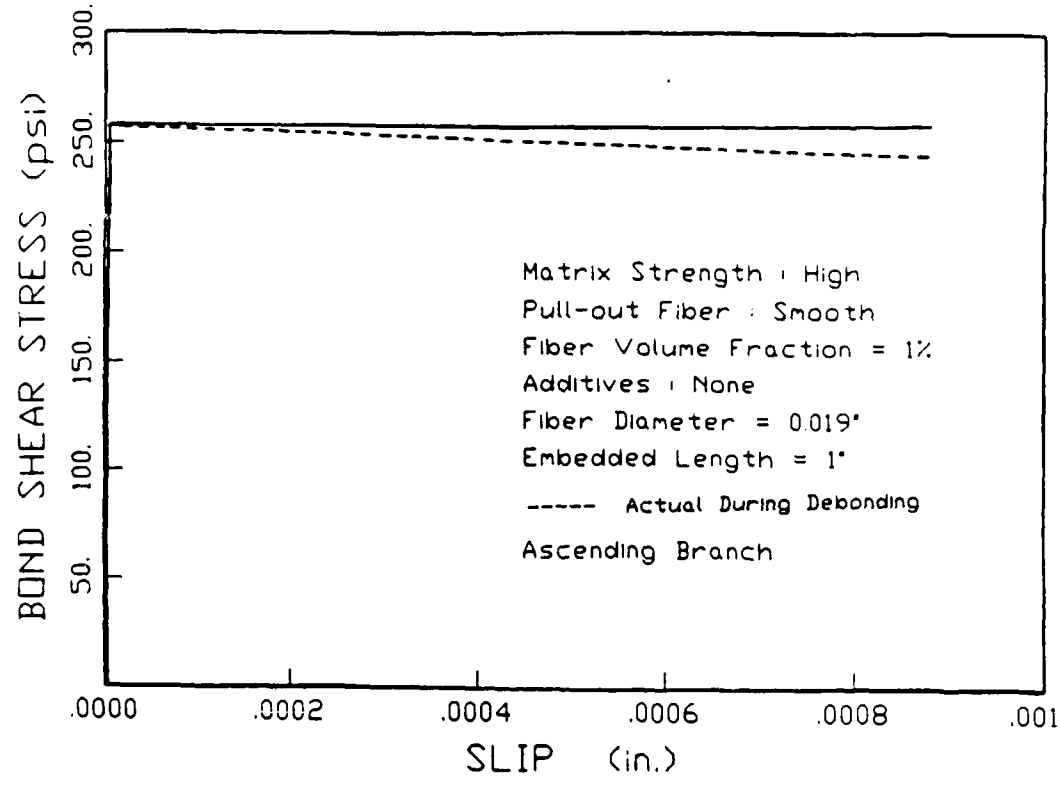

5.12b - **Bond shear stress versus slip, H1SN series, small scale.**

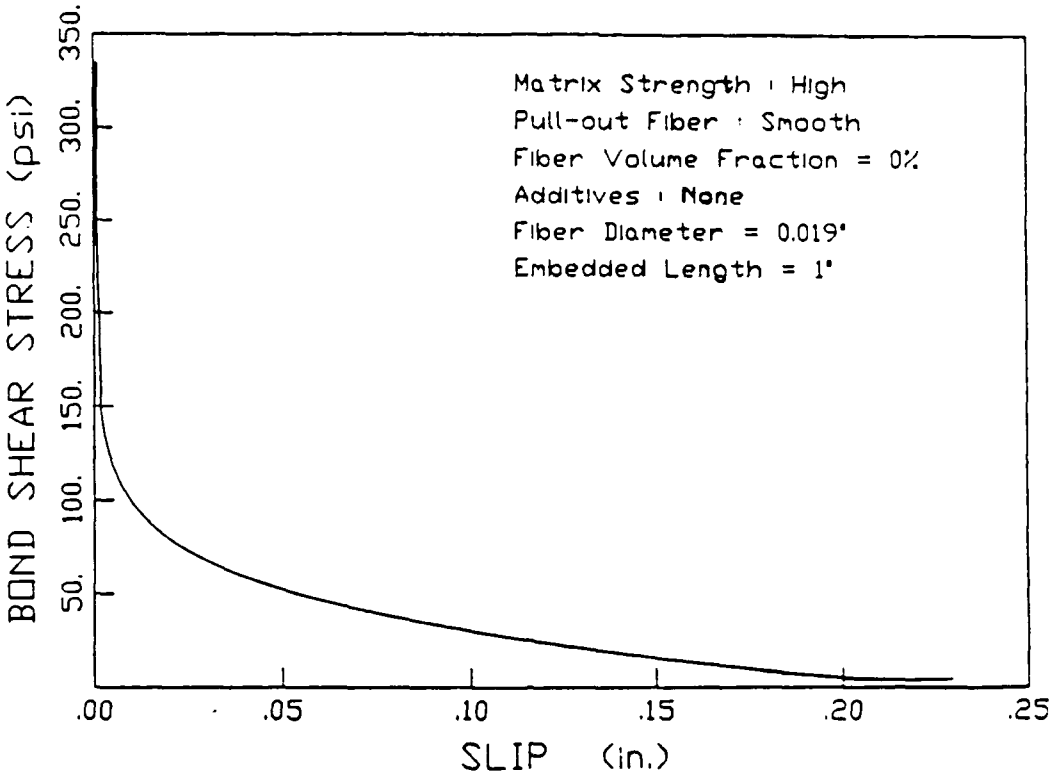

5.13a - Bond shear stress versus slip, H0SN series, full scale.

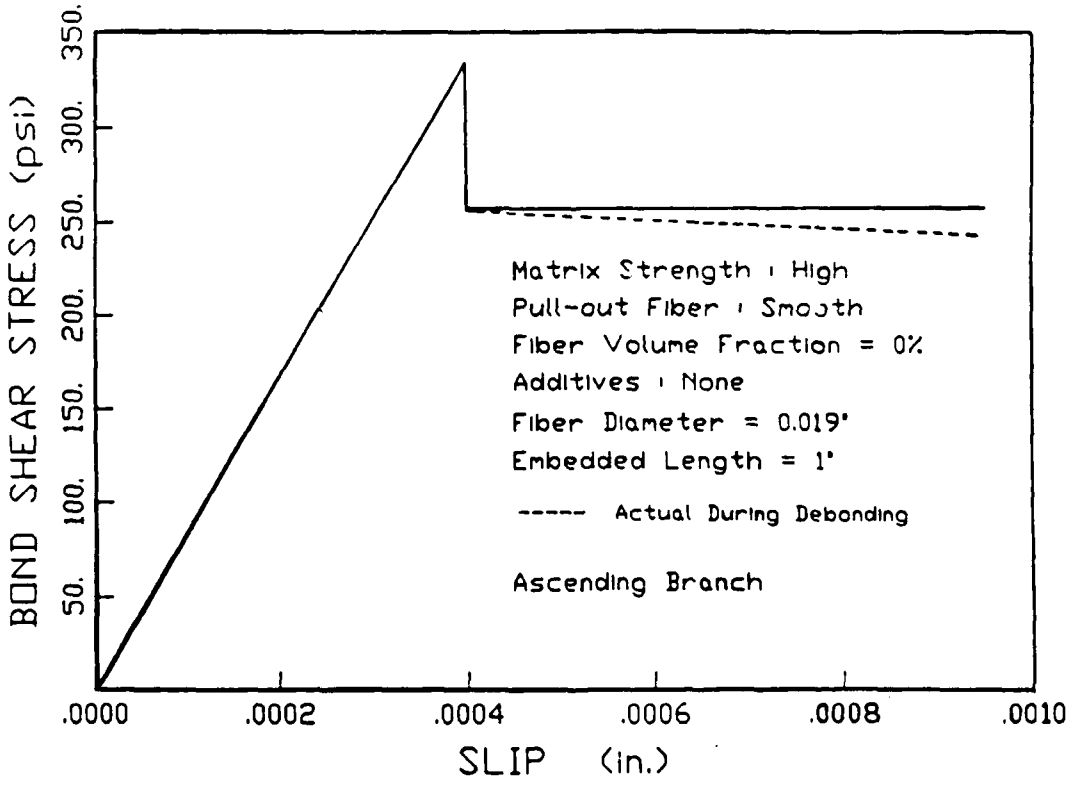

5.13b - Bond shear stress versus slip, H0SN series, small scale.

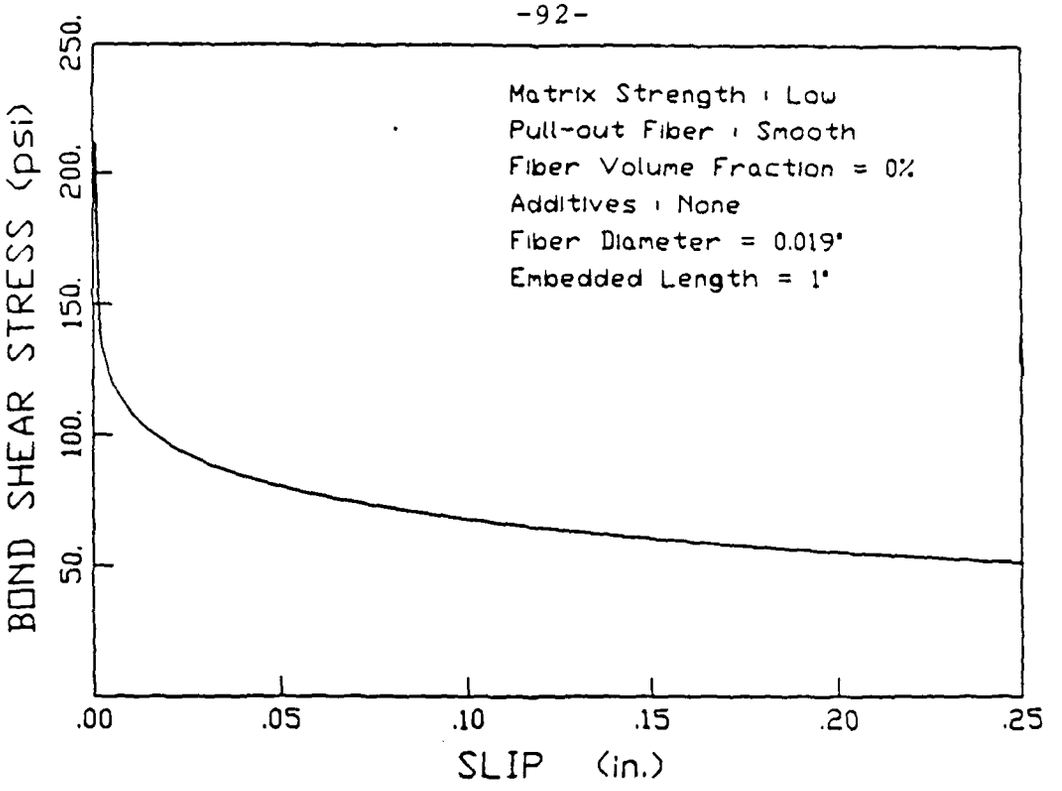

5.14a - Bond shear stress versus slip, L0SN series, full scale.

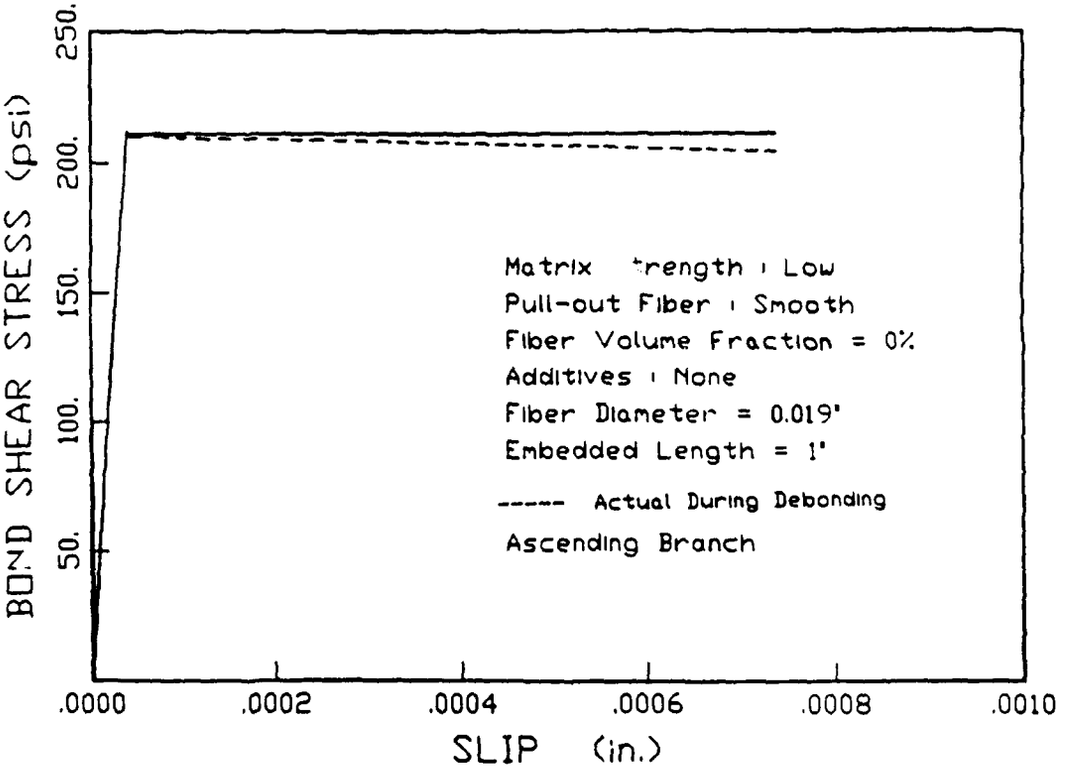

5.14b - Bond shear stress versus slip, L0SN series, small scale.

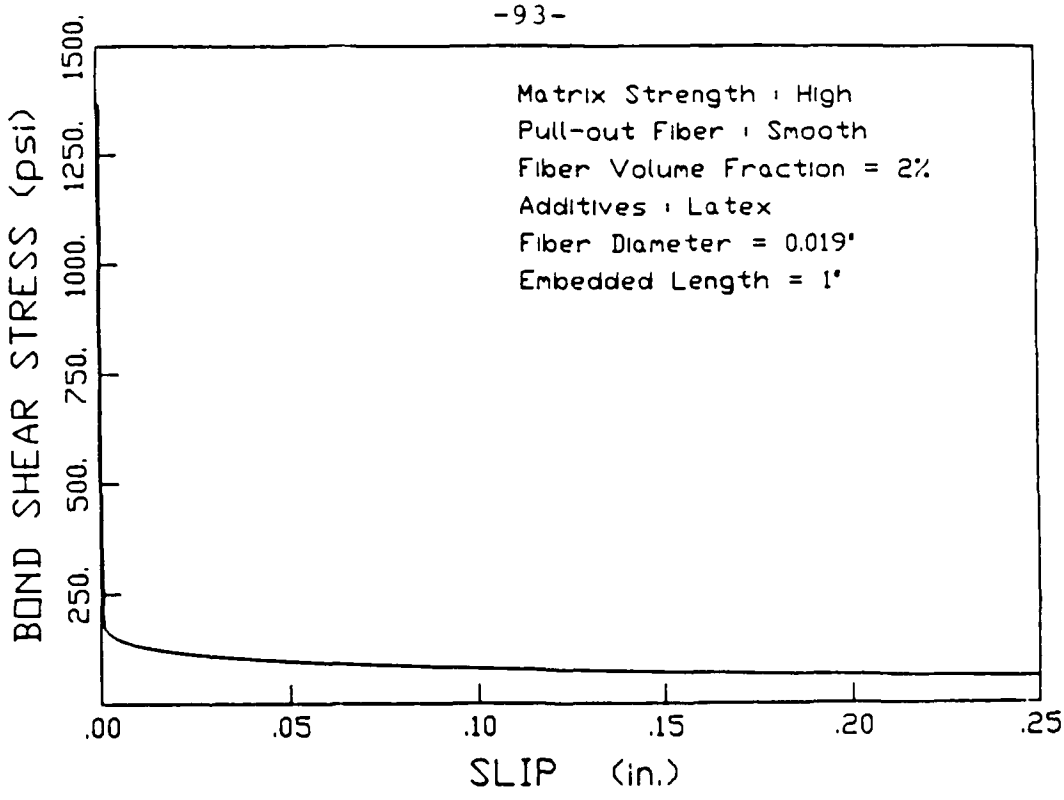

5.15a - Bond shear stress versus slip, H2SL series, full scale.

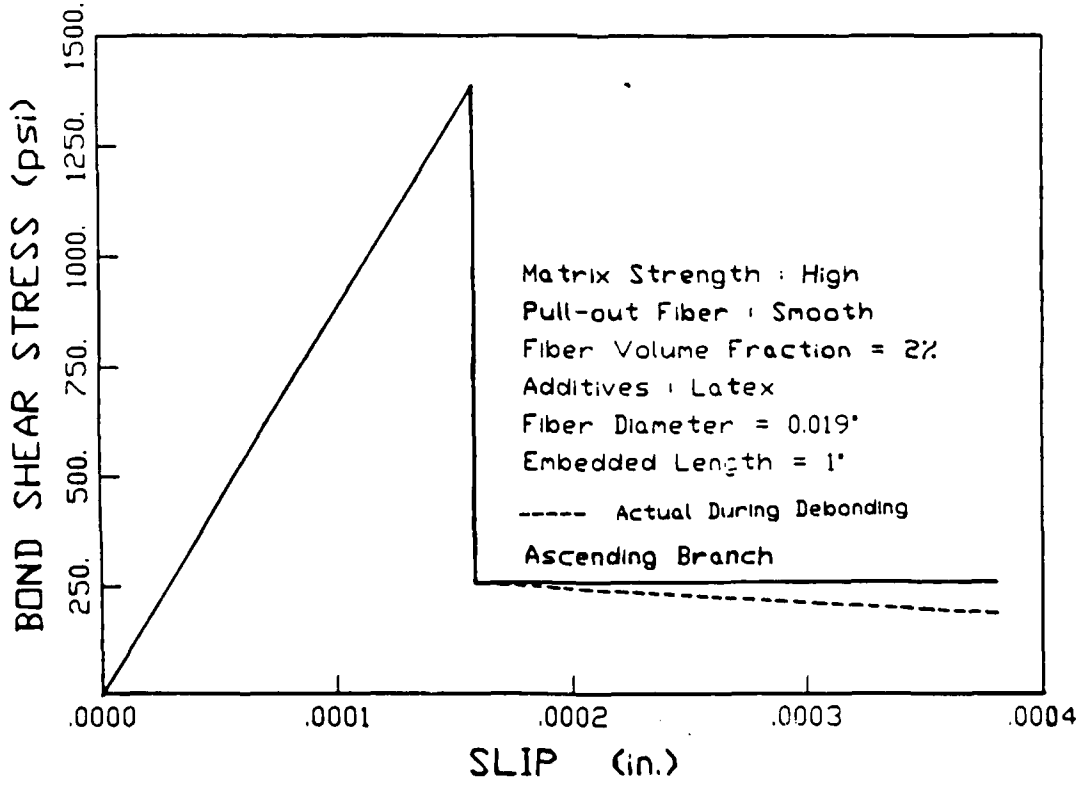

5.15b. Bond shear stress versus slip, H2SL series, small scale.

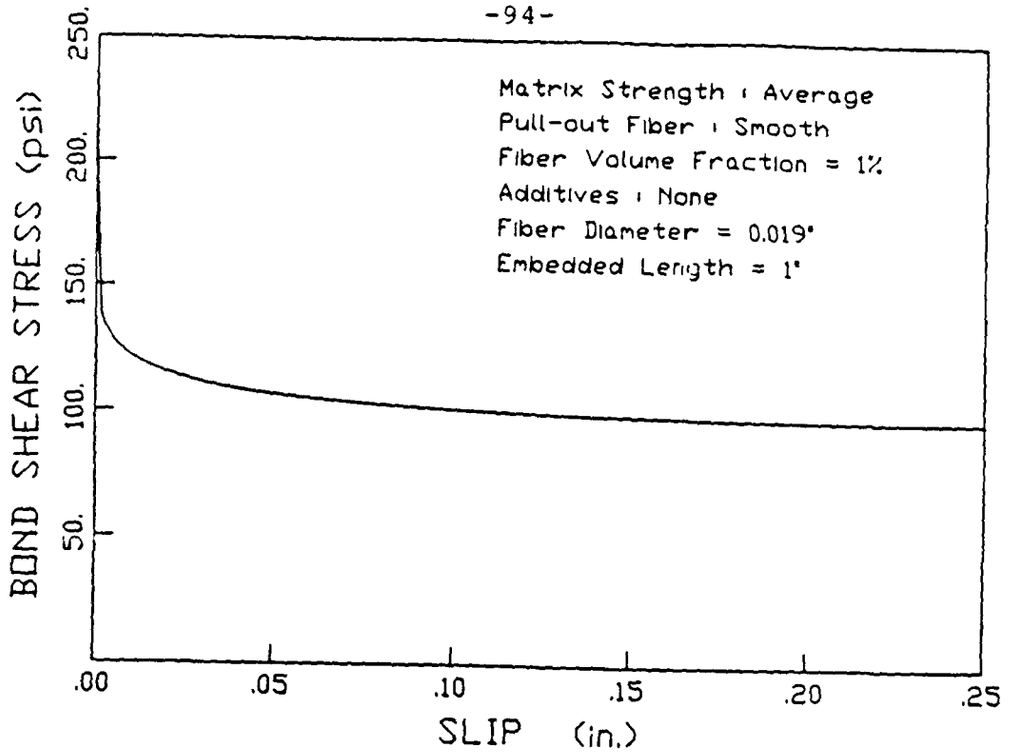

5.16a - Bond shear stress versus slip, A1SN series, full scale.

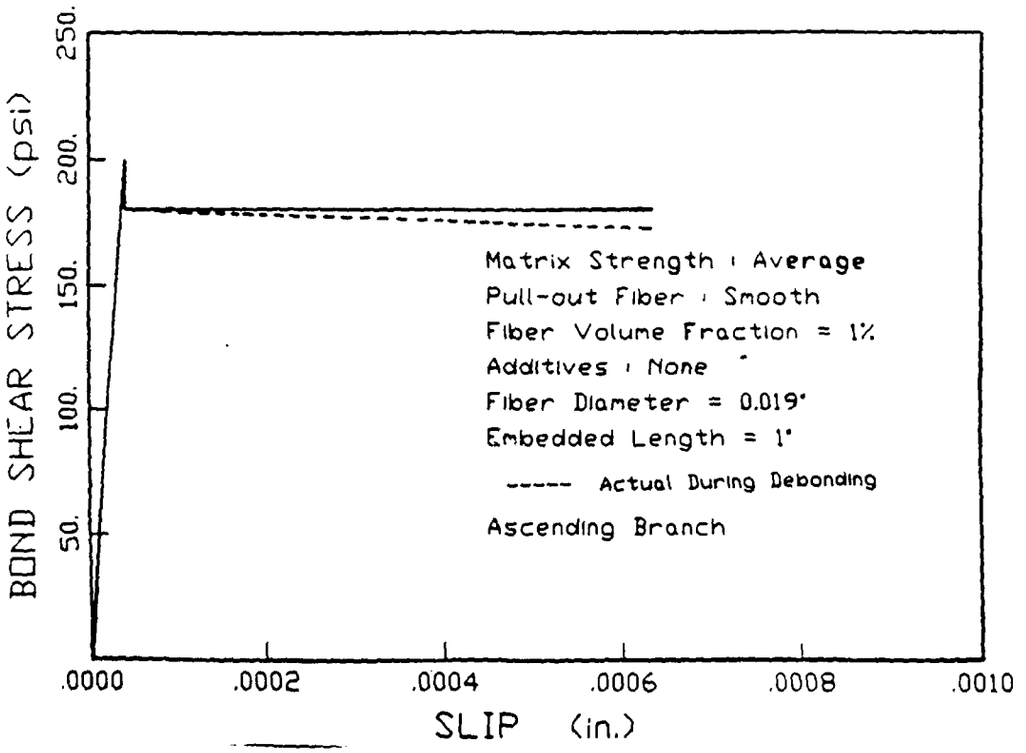

5.16b - Bond shear stress versus slip, A1SN series, small scale.

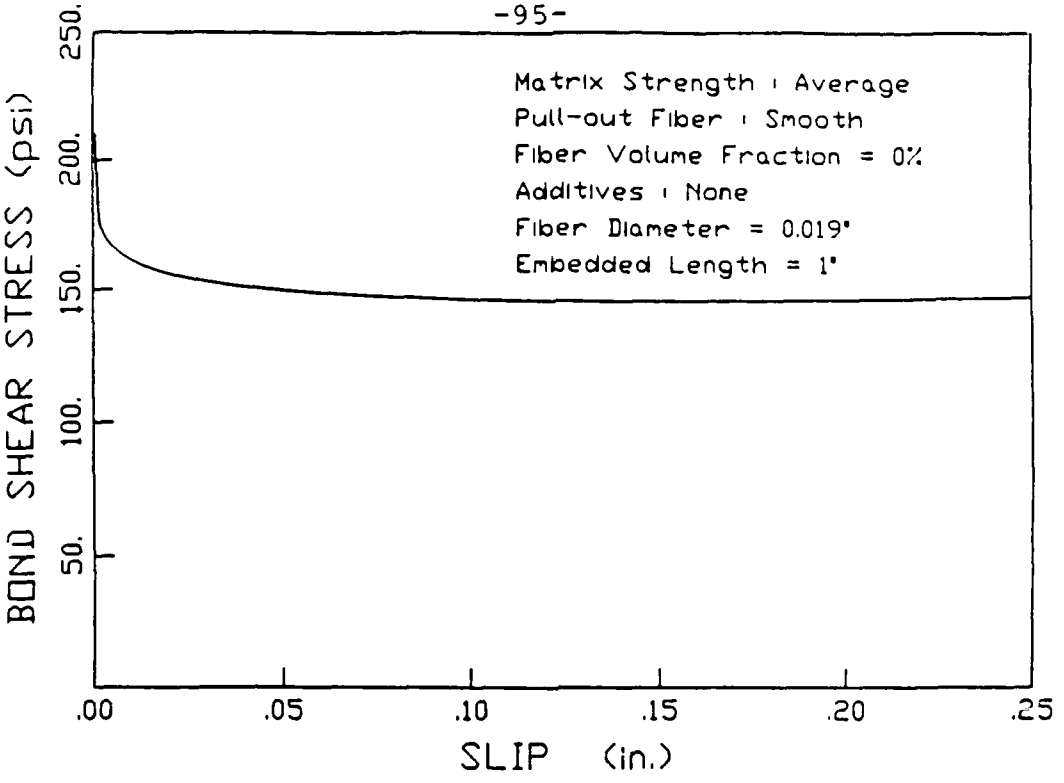

5.17a - Bond shear stress versus slip, A0SN series, full scale.

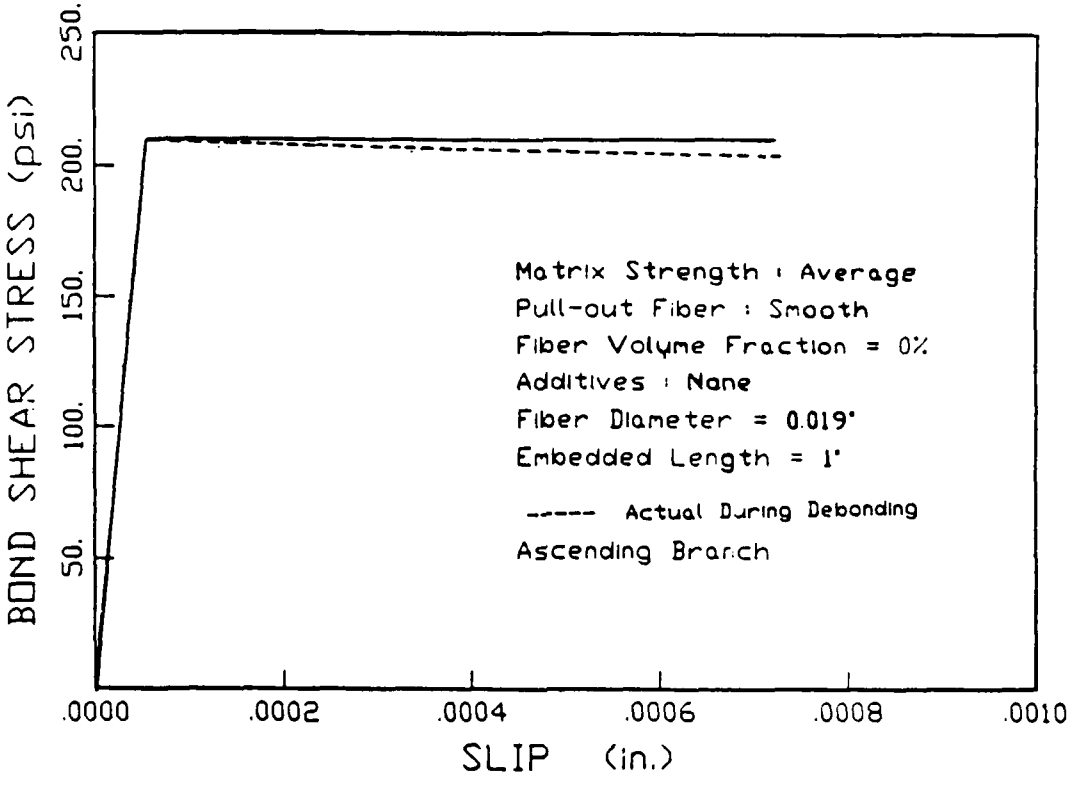

5.17b - Bond shear stress versus slip, A0SN series, small scale.

APPENDIX V-A

APPLICATION OF NEWTON'S METHOD FOR SOLVING A SYSTEM OF NON-LINEAR EQUATIONS TO THE DUAL PROBLEM OF PULL-OUT

A.1 GENERAL

A system of n non-linear equations in n unknows can be expressed as follows:

$$F(\zeta) = 0 \qquad (A.1)$$

where F is a vector of functions F_1, F_2, ...F_n, evaluated at the solution vector of the unknows z_1, z_2, ...z_n, or:

$$F = \begin{pmatrix} F_1 \\ F_2 \\ . \\ . \\ . \\ F_n \end{pmatrix}$$

and $\zeta = (z_1 \quad z_2 \quad . \quad . \quad . \quad z_n)$

hence Eq. (A.1) is equivalent to:

$$\begin{pmatrix} F_1(z_1, z_2, \ldots z_n) \\ F_2(z_1, z_2, \ldots z_n) \\ \cdot \\ \cdot \\ \cdot \\ F_n(z_1, z_2, \ldots z_n) \end{pmatrix} = \begin{pmatrix} 0 \\ 0 \\ \cdot \\ \cdot \\ \cdot \\ 0 \end{pmatrix} \qquad (A.2)$$

Newton method, discussed in the following section, converges to the exact solution vector ζ, provided the initial guess vector, say $z^{(0)}$ is close enough to ζ, and provided the Jacobian F' of F is continuous and the matrix $F'(\zeta)$ is invertible.

A.2 ALGORITHM

The algoritm to be followed in Newton's method is to start from the initial guess vector $z^{(0)}$, and successively improve it till the improvement becomes insignificant. Given a guess $z^{(m)}$, an improved solution $z^{(m+1)}$ over $z^{(m)}$ can be obtained by the following equation:

$$z^{(m+1)} = z^{(m)} - [F'(z^{(m)})]^{-1} F(z^{(m)}) \qquad (A.3)$$

or

$$F'(z^{(m)}) (\Delta z^{(m+1)}) = F(z^{(m)}) \qquad (A.4)$$

where

$$\Delta z^{(m+1)} = z^{(m+1)} - z^{(m)} \qquad (A.5)$$

F' is the Jacobian of the vector of functions $F_1, F_2, \ldots F_n$. Therefore, F' is an $n \times n$ matrix, defined by its F'_{ij} element, that is the element in the i^{th} row and the j^{th} column, as:

$$F'_{ij} = \frac{\partial F_i}{\partial z_j} \qquad (A.6)$$

Therefore, the way to solve the system of n non-linear equations in n unknowns consists of defining the vector F and the corresponding Jacobian matrix F', and then, starting with an initial guess vector $z^{(0)}$, successively improving the solution by solving Eq. A.4 for $\Delta z^{(m+1)}$, and then finding an improved solution $z^{(m+1)}$ in the following equation:

$$z^{(m+1)} = \Delta z^{(m+1)} + z^{(m)} \qquad (A.7)$$

A.3 Application of Newton's Method to the Dual Problem of Pull-out.

It can be recalled from Chap. 7 that the dual pull-out problem consists of solving three non-linear equations in t_f, t_{max}, and u. The equations in question are rewritten here:

$$\frac{t_f\, e^{\lambda(\ell - u)}}{\lambda} + \frac{t_{max}}{\lambda}\left(\frac{\frac{-2}{Q} e^{-2\lambda(\ell - u)} - 4\left(1 - \frac{1}{Q}\right) e^{-\lambda(\ell - u)} - \frac{2}{Q}}{\left(\left(1 - \frac{1}{Q}\right) e^{-2\lambda(\ell - u)} + \frac{2}{Q}\, e^{-\lambda(\ell - u)} + \left(1 - \frac{1}{Q}\right)\right)^2} \right) = 0 \qquad (A.8)$$

$$t_f u + \frac{t_{max}}{\lambda} \frac{1 - e^{-2\lambda(\ell - u)}}{\frac{2}{Q}\, e^{-\lambda(\ell - u)} + \left(1 - \frac{1}{Q}\right)\left(1 + e^{-2\lambda(\ell - u)}\right)} = P_p \qquad (A.9)$$

$$\frac{\left(P_p(Q-1)u - \frac{t_f u^2}{2}(Q-2) + \left(P_p - t_f u\right)\left(\frac{1-e^{-\lambda(\ell-u)}}{1+e^{-\lambda(\ell-u)}}\right)\frac{Q-2}{\lambda} - t_f u \ell\right)}{A_m E_m} = \Delta_p \qquad (A.10)$$

The vector of functions F is equal to:

$$F = \begin{pmatrix} F_1 \\ F_2 \\ F_3 \end{pmatrix} \tag{A.11}$$

The vector of unknowns ζ is:

$$\zeta = \begin{pmatrix} t_f \\ t_{max} \\ u \end{pmatrix} \tag{A.12}$$

The functions F_1, F_2, and F_3 are defined respectively as:

$$F_1(t_f, t_{max}, u) = \frac{t_f\, e^{\lambda(\ell - u)}}{\lambda} +$$

$$\frac{t_{max}}{\lambda}\left(\frac{\frac{-2}{Q}\, e^{-2\lambda(\ell - u)} - 4\left(1 - \frac{1}{Q}\right) e^{-\lambda(\ell - u)} - \frac{2}{Q}}{\left(\left(1 - \frac{1}{Q}\right) e^{-2\lambda(\ell - u)} + \frac{2}{Q}\, e^{-\lambda(\ell - u)} + \left(1 - \frac{1}{Q}\right)\right)^2}\right) \tag{A.13}$$

$$F_2(t_f, t_{max}, u) =$$

$$t_f\, u + \frac{t_{max}}{\lambda} \frac{1 - e^{-2\lambda(\ell - u)}}{\frac{2}{Q}\, e^{-\lambda(\ell - u)} + \left(1 - \frac{1}{Q}\right)\left(1 + e^{-2\lambda(\ell - u)}\right)} - P_p \tag{A.14}$$

$$F_3(t_f, t_{max}, u) =$$

$$\left(P_p(Q-1)u - \frac{t_f u^2}{2}(Q-2) + \left(P_p - t_f u\right)\left(\frac{1 - e^{-\lambda(\ell - u)}}{1 + e^{-\lambda(\ell - u)}}\right)\frac{Q-2}{\lambda} - t_f u \ell\right)$$

$$- A_m E_m \Delta_p \tag{A.15}$$

The Jacobian matrix F' can be written as follows:

$$F' = \begin{pmatrix} \frac{\partial F_1}{\partial t_f} & \frac{\partial F_1}{\partial t_{max}} & \frac{\partial F_1}{\partial u} \\ \frac{\partial F_2}{\partial t_f} & \frac{\partial F_2}{\partial t_{max}} & \frac{\partial F_2}{\partial u} \\ \frac{\partial F_3}{\partial t_f} & \frac{\partial F_3}{\partial t_{max}} & \frac{\partial F_3}{\partial u} \end{pmatrix} \qquad (A.16)$$

The 9 elements of the Jacobian matrix F' are given next:

$$F'_{1,1} = \frac{\partial F_1}{\partial t_f} = \frac{e^{\lambda(t - u)}}{\lambda} \qquad (A.17)$$

$$F'_{2,1} = \frac{\partial F_2}{\partial t_f} = u \qquad (A.18)$$

$$F'_{3,1} = \frac{\partial F_3}{\partial t_f} = -\left(\left(\frac{1-e^{-\lambda(t-u)}}{1+e^{-\lambda(t-u)}}\right) \frac{Q-2}{\lambda} + t \right) u - \frac{(Q - 2)}{2} u^2$$

$$F'_{1,2} = \frac{\partial F_1}{\partial t_{max}} = \frac{1}{\lambda}\left(\frac{\frac{-2}{Q} e^{-2\lambda(t - u)} - 4\left(1 - \frac{1}{Q}\right) e^{-\lambda(t - u)} - \frac{2}{Q}}{\left(\left(1 - \frac{1}{Q}\right) e^{-2\lambda(t - u)} + \frac{2}{Q} e^{-\lambda(t - u)} + \left(1 - \frac{1}{Q}\right)\right)^2} \right)$$

(A.20)

$$F'_{2,2} = \frac{\partial F_2}{\partial t_{max}}$$

$$= \frac{1}{\lambda} \frac{1 - e^{-2\lambda(t - u)}}{\frac{2}{Q} e^{-\lambda(t - u)} + \left(1 - \frac{1}{Q}\right)\left(1 + e^{-2\lambda(t - u)}\right)} \tag{A.21}$$

$$F'_{3,2} = \frac{\partial F_3}{\partial t_{max}}$$

$$= 0 \tag{A.22}$$

Since the partial derivatives involving the variable u are rather complex and involved, the functions F_1 and F_2 will be rewritten as follows first:

$$F_1(t_f, t_{max}, u) = \frac{t_f e^{\lambda(t - u)}}{\lambda} + \frac{t_{max}}{\lambda} \frac{\phi(u)}{\eta(u)} \tag{A.23}$$

in which

$$\phi(u) = \frac{-2}{Q} e^{-2\lambda(t - u)} - 4\left(1 - \frac{1}{Q}\right) e^{-\lambda(t - u)} - \frac{2}{Q} \tag{A.24}$$

and

$$\eta(u) = \left(\left(1 - \frac{1}{Q}\right) e^{-2\lambda(t - u)} + \frac{2}{Q} e^{-\lambda(t - u)} + \left(1 - \frac{1}{Q}\right)\right)^2 \tag{A.25}$$

$$F_2(t_f, t_{max}, u) = t_f u + \frac{t_{max}}{\lambda} \frac{\mu(u)}{\varpi(u)} - P_p \tag{A.26}$$

in which:

$$\mu(u) = 1 - e^{-2\lambda(t - u)} \tag{A.27}$$

and

$$\varpi(u) = \frac{2}{Q} e^{-\lambda(t - u)} + \left(1 - \frac{1}{Q}\right)\left(1 + e^{-2\lambda(t - u)}\right) \tag{A.28}$$

$$F'_{1,3} = \frac{\partial F_1}{\partial u}$$

$$= -t_f e^{\lambda(t - u)} + \frac{t_{max}}{\lambda} \frac{\phi'(u)\,\eta(u) - \phi(u)\,\eta'(u)}{\eta^2(u)} \qquad (A.29)$$

in which

$$\phi'(u) = \frac{-4\lambda}{Q} e^{-2\lambda(t - u)} - 4\lambda\left(1 - \frac{1}{Q}\right) e^{-\lambda(t - u)} \qquad (A.29)$$

and

$$\eta'(u) = 2\left(2\lambda\left(1 - \frac{1}{Q}\right) e^{-2\lambda(t - u)} + \frac{2\lambda}{Q} e^{-\lambda(t - u)}\right) *$$

$$\left(\left(1 - \frac{1}{Q}\right) e^{-2\lambda(t - u)} + \frac{2}{Q} e^{-\lambda(t - u)} + \left(1 - \frac{1}{Q}\right)\right)$$

(A.30)

$$F'_{2,3} = \frac{\partial F_2}{\partial u}$$

$$= t_f + \frac{t_{max}}{\lambda} \frac{\mu'(u)\varpi(u) - \mu(u)\varpi'(u)}{\varpi^2(u)} \qquad (A.31)$$

in which:

$$\mu'(u) = -2\lambda e^{-2\lambda(t - u)} \qquad (A.32)$$

and

$$\varpi'(u) = \frac{2\lambda}{Q} e^{-\lambda(t - u)} + 2\lambda\left(1 - \frac{1}{Q}\right) e^{-2\lambda(t - u)} \qquad (A.33)$$

$$F'_{3,3} = \frac{\partial F_3}{\partial u}$$

$$= P_p (Q - 1) - 2 t_f u (Q - 2) - t_f \ell$$

$$- \frac{2 P_p e^{-\lambda(\ell - u)} (Q - 2)}{(1 + e^{-\lambda(\ell - u)})^2} - t_f \frac{Q - 2}{\lambda} \frac{1 - e^{-\lambda(\ell - u)}}{1 + e^{-\lambda(\ell - u)}}$$

$$+ \frac{2 t_f u e^{-\lambda(\ell - u)} (Q - 2)}{(1 + e^{-\lambda(\ell - u)})^2} \qquad \text{(A.34)}$$

APPENDIX V-B

NUMERICAL DATA USED IN THE SOLUTION OF THE DUAL PROBLEM

TEST RESULTS: H1SN series

. Slope (P/Δ) : 44×10^3 lb/in

. Max. pullout load: 15.4 lb

. Slip at max load : 8.8×10^{-4} in

. Point on the descending branch (4.3 lb, 0.15 in)

. High strength concrete (8.6 ksi).

. 1% fiber by volume.

. No additives.

MEASURED PARAMETERS:

. Fiber diameter : 0.019 in.

. Fiber Embedded length : 1 in.

ASSUMED PARAMETERS:

. Fiber modulus of elasticity (E_f) : 3×10^7 psi.

. Matrix modulus of elasticity (E_m) : 3×10^6 psi.

. Effective matrix area surrounding the fiber : 1 in^2.

. Coooefficient of friction (stell-mortar) : 0.5.

. Fiber poisson's ratio : 0.2.

. Matrix poisson's ratio : 0.2.

COMPUTER PROGRAM:

Solving the three basic nonlinear equations yielded the following:

ξ = 0.786

κ = 56.9×10^6 lb/in^3

τ_m = 258 psi

τ_f = 258 psi

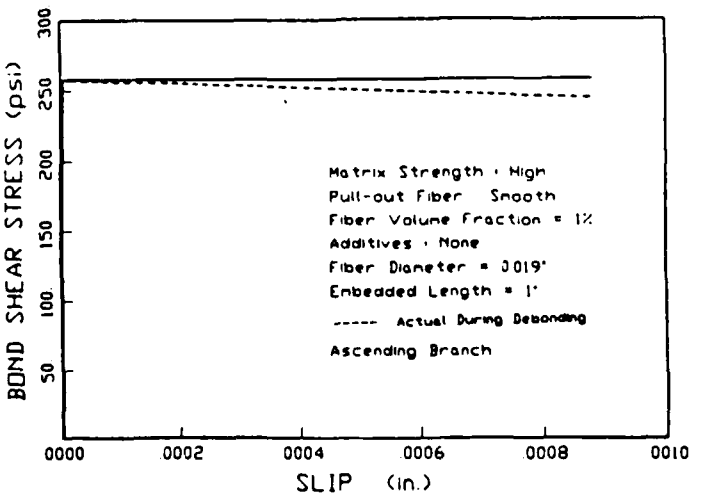

Bond shear stress versus slip, H1SN series, small scale.

TEST RESULTS: H0SN series

. Slope (P/Δ) : 25×10^3 lb/in
. Max. pullout load: 15.6 lb
. Slip at max load : 9.25×10^{-4} in
. Point on the descending branch (1.3 lb, 0.1 in)

. High strength concrete (8.6 ksi).
. 0% fiber by volume.
. No additives.

MEASURED PARAMETERS:

. Fiber diameter : 0.019 in.
. Fiber Embedded length : 1 in.

ASSUMED PARAMETERS:

. Fiber modulus of elasticity (E_f) : 3×10^7 psi.
. Matrix modulus of elasticity (E_m) : 3×10^6 psi.
. Effective matrix area surrounding the fiber : 1 in^2.
. Coooefficient of friction (stell-mortar) : 0.5.
. Fiber poisson's ratio : 0.2.
. Matrix poisson's ratio : 0.2.

COMPUTER PROGRAM:

Solving the three basic nonlinear equations yielded the following:

ξ = 1.3

κ = 0.841×10^6 lb/in^3

τ_m = 334 psi

τ_f = 257 psi

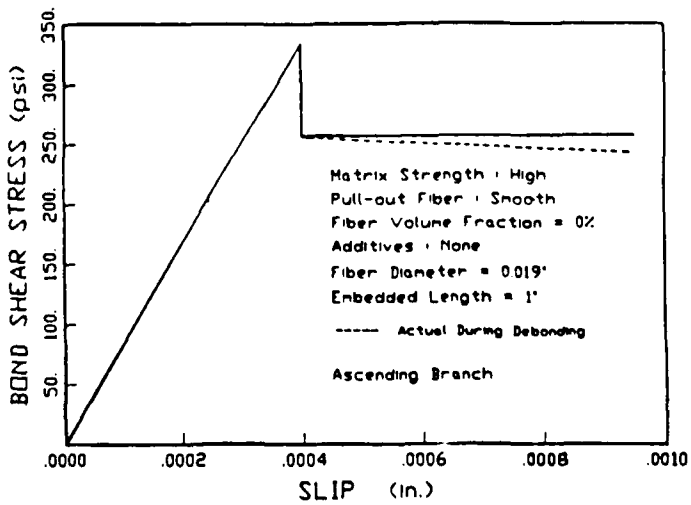

Bond shear stress versus slip, H0SN series, small scale.

TEST RESULTS: L0SN series

. Slope (P/Δ) : 52.1×10^3 lb/in
. Max. pullout load: 12..6 lb
. Slip at max load : 7.3×10^{-4} in
. Point on the descending branch

. Low strength concrete (4.8 ksi).
. 0% fiber by volume.
. No additives.
(2.97 lb, 0.15 in)

MEASURED PARAMETERS:

. Fiber diameter : 0.019 in.
. Fiber Embedded length : 1 in.

ASSUMED PARAMETERS:

. Fiber modulus of elasticity (E_f) : 3×10^7 psi.
. Matrix modulus of elasticity (E_m) : 3×10^6 psi.
. Effective matrix area surrounding the fiber : 1 in^2.
. Coooefficient of friction (stell-mortar) : 0.5.
. Fiber poisson's ratio : 0.2.
. Matrix poisson's ratio : 0.2.

COMPUTER PROGRAM:

Solving the three basic nonlinear equations yielded the following:

ξ = 0.91

κ = 5.25×10^6 lb/in^3

τ_m = 211 psi

τ_f = 211 psi

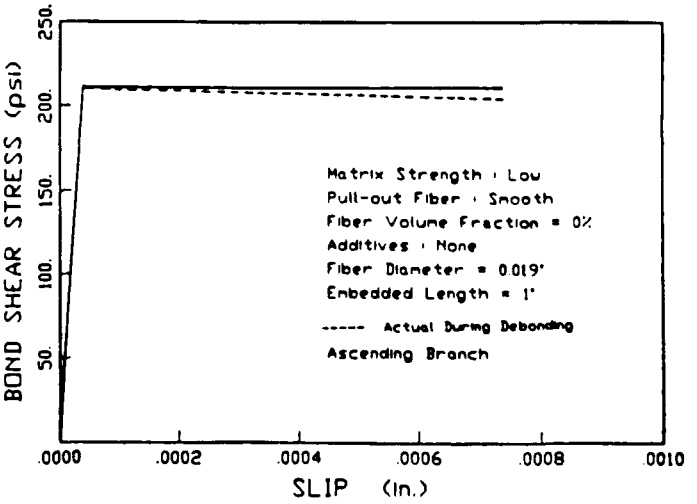

Bond shear stress versus slip, L0SN series, small scale.

TEST RESULTS: H2SL series

. Slope (P/Δ) : 67.8×10^3 lb/in
. Max. pullout load: 22.1 lb
. Slip at max load : 15.9×10^{-4} in
. Point on the descending branch (4.8 lb, 0.1 in)

. High strength concrete (8.6 ksi).
. 2% fiber by volume.
. Latex as an additive.

MEASURED PARAMETERS:

. Fiber diameter : 0.019 in.
. Fiber Embedded length : 1 in.

ASSUMED PARAMETERS:

. Fiber modulus of elasticity (E_f) : 3×10^7 psi.
. Matrix modulus of elasticity (E_m) : 3×10^6 psi.
. Effective matrix area surrounding the fiber : 1 in^2.
. Coooefficient of friction (stell-mortar) : 0.5.
. Fiber poisson's ratio : 0.2.
. Matrix poisson's ratio : 0.2.

COMPUTER PROGRAM:

Solving the three basic nonlinear equations yielded the following:

ξ = 0.938

κ = 8.79×10^6 lb/in^3

τ_m = 1390 psi

τ_f = 259 psi

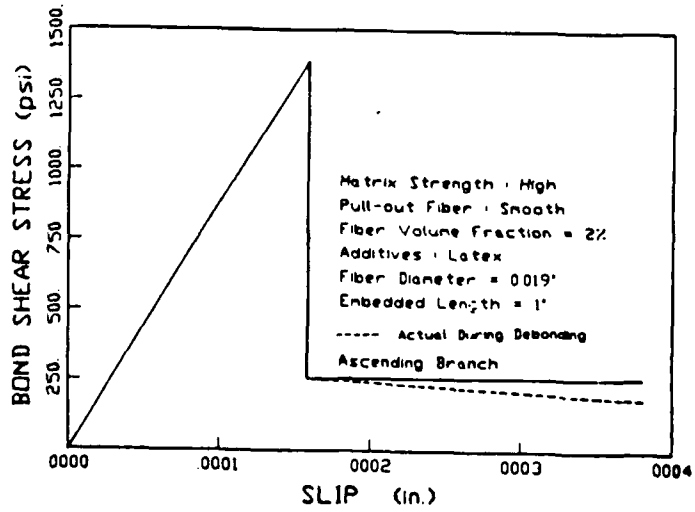

Bond shear stress versus slip, H2SL series, small scale.

TEST RESULTS: A1SN series

. Slope (P/Δ) : 55×10^3 lb/in
. Max. pullout load: 10.8 lb
. Slip at max load : 6.34×10^{-4} in
. Point on the descending branch (5 lb, 0.15 in)

. Average strength concrete (7.4 ksi).
. 1% fiber by volume.
. No additives.

MEASURED PARAMETERS:

. Fiber diameter : 0.019 in.
. Fiber Embedded length : 1 in.

ASSUMED PARAMETERS:

. Fiber modulus of elasticity (E_f) : 3×10^7 psi.
. Matrix modulus of elasticity (E_m) : 3×10^6 psi.
. Effective matrix area surrounding the fiber : 1 in^2.
. Coooefficient of friction (stell-mortar) : 0.5.
. Fiber poisson's ratio : 0.2.
. Matrix poisson's ratio : 0.2.

COMPUTER PROGRAM:

Solving the three basic nonlinear equations yielded the following:

ξ = 0.0337

κ = 5×10^6 lb/in^3

τ_m = 200 psi

τ_f = 180 psi

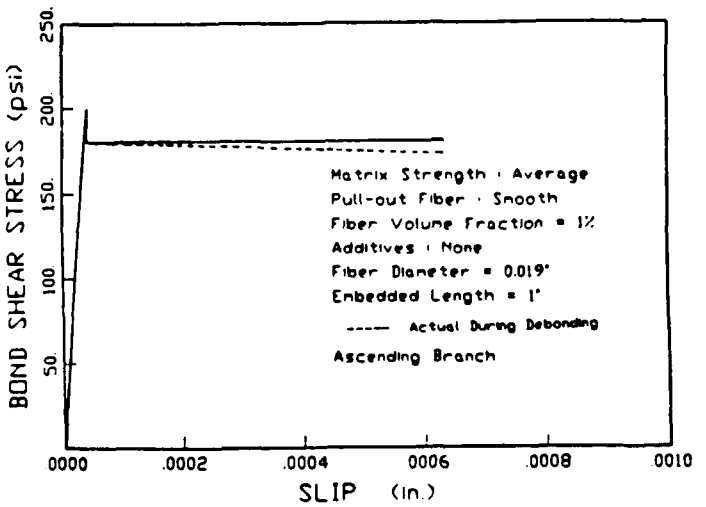

Bond shear stress versus slip, A1SN series, small scale.

TEST RESULTS: A0SN series

. Slope (P/Δ) : 45×10^3 lb/in
. Max. pullout load: 12.6 lb
. Slip at max load : 7.18×10^{-4} in
. Point on the descending branch (4.9 lb, 0.1 in)

. Average strength concrete (7.4 ksi).
. 0% fiber by volume.
. No additives.

MEASURED PARAMETERS:

. Fiber diameter : 0.019 in.
. Fiber Embedded length : 1 in.

ASSUMED PARAMETERS:

. Fiber modulus of elasticity (E_f) : 3×10^7 psi.
. Matrix modulus of elasticity (E_m) : 3×10^6 psi.
. Effective matrix area surrounding the fiber : 1 in^2.
. Coooefficient of friction (stell-mortar) : 0.5.
. Fiber poisson's ratio : 0.2.
. Matrix poisson's ratio : 0.2.

COMPUTER PROGRAM:

Solving the three basic nonlinear equations yielded the following:

ξ = -1

κ = 3.87×10^6 lb/in^3

τ_m = 210 psi

τ_f = 210 psi

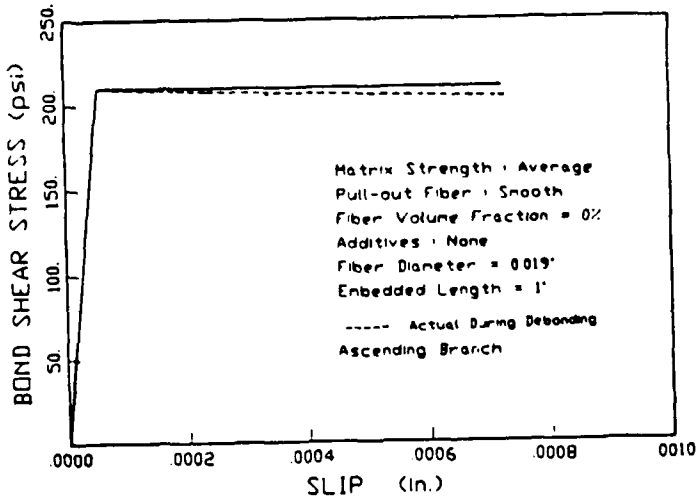

Bond shear stress versus slip, A0SN series, small scale.

CHAPTER VI

EXPERIMENTAL INVESTIGATION AND RESULTS

6.1 EXPERIMENTAL PROGRAM

Table 6.1 summerizes the experimental program carried out in this study. A total of fifty-two series, four fibers each, were tested. The program was designed in such a way so as to investigate the effects of the fiber type, matrix strength, fiber reinforcement ratio, fiber diameter, fiber embedment length ,and additives on the interfacial bond in cementitious composites. Test series were given names that would indicate the mix and fiber type as well. A typical code name would consist of four alphanumeric characters. The first character is a letter that indicates the matrix strength: H for high strength, A for average strength, and L for low strength. The second character is a numeral that indicates the fiber volume fraction in the matrix, such as 0, 1, 2, or 3. The third character is a letter that indicates the fiber type: S for smooth, D for deformed, and H for hooked. Finally, the fourth and last character indicates the additive used: F for fly ash, L for latex, M for microsilica, and N for no additives. A typical code name for a specimen could be: L0SN for a Low strength matrix with 0% fiber reinforcement, in which the pull-out fiber is Smooth, and where No additives are used. When a different diameter or embedded length is used a remark is added near the specimen code.

Table 6.1 - Experimental Program

Matrix Strength	V_f	Fiber Type	Additives	Code
High	0	Smooth	None	H0SN
High	0	Smooth	None	H0SN, L=0.5"
High	0	Smooth	Latex	H0SL
High	0	Hooked	None	H0HN
High	0	Hooked	None	H0HN L=0.5"
High	0	Deformed	None	H0DN
High	1	Smooth	None	H1SN
High	1	Deformed	None	H1DN
High	2	Smooth	None	H2SN
High	2	Smooth	Latex	H2SL
High	2	Smooth	Microsilica	H2SM
High	0	Smooth	Microsilica	H0SM
High	2	Smooth	Fly Ash	H2SF
High	2	Deformed	None	H2DN
High	3	Smooth	None	H3SN
High	3	Deformed	None	H3DN
Average	0	Smooth	None	A0SN
Average	0	Smooth	Latex	A0SL
Average	0	Smooth	Fly Ash	A0SF
Average	0	Smooth	None	A0SN, L=0.5"
Average	0	Smooth	None	A0SN, L=1.5"
Average	0	Smooth	None	A0SN,D=0.01"
Average	0	Smooth	None	A0SN,D=0.03"
Average	0	Smooth	None	A0SN,D=0.04"
Average	0	Hooked	None	A0HN
Average	1	Hooked	None	A1HN
Average	0	Hooked	None	A0HN L=0.5"
Average	0	Deformed	None	A0DN
Average	0	Deformed	None	A0DN,L=0.5"

Average	1	Smooth	None	A1SN
Average	2	Smooth	None	A2SN
Average	3	Smooth	None	A3SN
Average	1	Deformed	None	A1DN
Average	1	Deformed	None	A1DN,L=0.5"
Average	2	Deformed	None	A2DN
Low	0	Smooth	None	L0SN
Low	0	Hooked	None	L0HN
Low	1	Hooked	None	L1HN
Low	3	Hooked	None	L3HN
Low	0	Deformed	None	L0DN
Low	0	Deformed	Latex	L0DL
Low	0	Deformed	Microsilica	L0DM
Low	1	Smooth	None	L1SN
Low	2	Smooth	None	L2SN
Low	2	Deformed	None	L2DN
Low	3	Deformed	None	L3DN
SIFCON	12	Smooth	None	L=1",D=0.01"
SIFCON	12	Smooth	None	L=1,D=0.019"
SIFCON	12	Smooth	None	L=1",D=0.03"
SIFCON	12	Smooth	None	L=1",D=0.04"
Average	0	Deformed	None	A0DN *
Average	0	Hooked	None	H0HN *

* [Pull-out Fiber was greased on the surface].

6.2 TEST SET-UP

Each test series consists of a block of matrix 7"x4"x1" crossed by four pull-out or pull-through fibers (Fig. 6.1). Hence a series represents four tests. The test set-up used in this study is illustrated in Fig. 6.2. As can be seen in the figure, the top end of the fiber is held by a specially designed grip attached to the load cell of an INSTRON machine, while the bottom end of the same fiber is attached to a miniature LVDT, connected to the bench of the machine. Also, the displacement of the top end of the

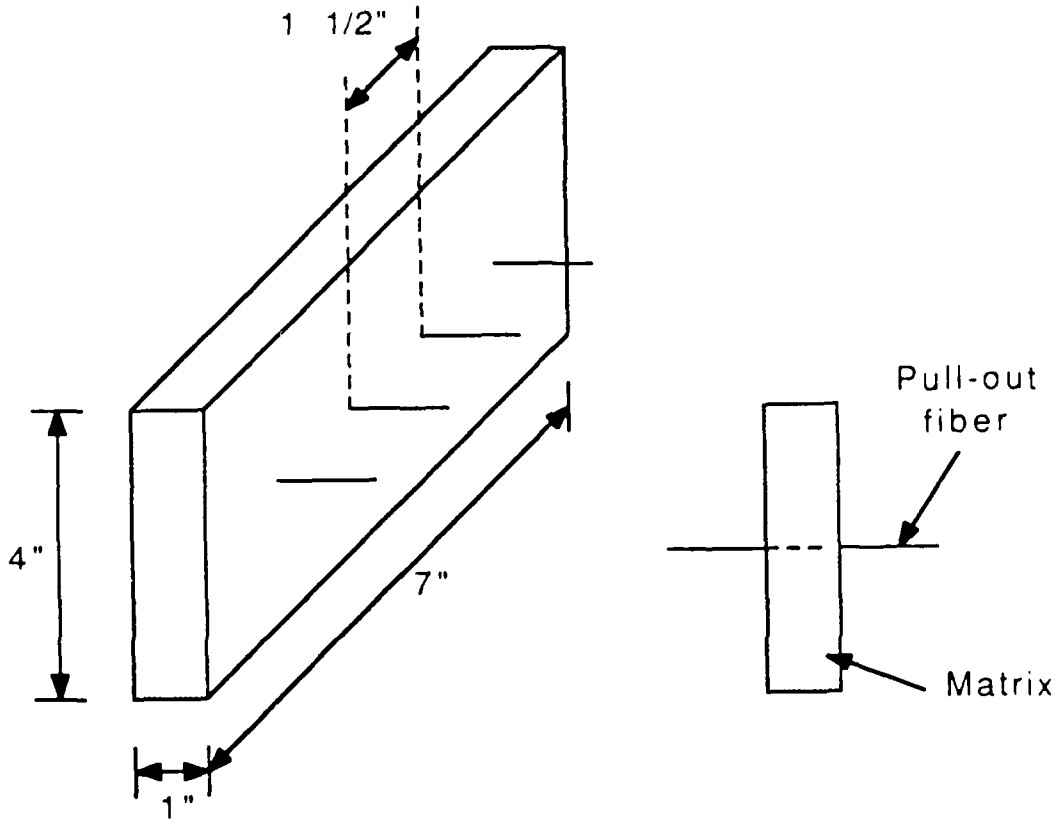

Fig. 6.1 - View of specimen showing block matrix and pull-out fibers .

TEST SET-UP

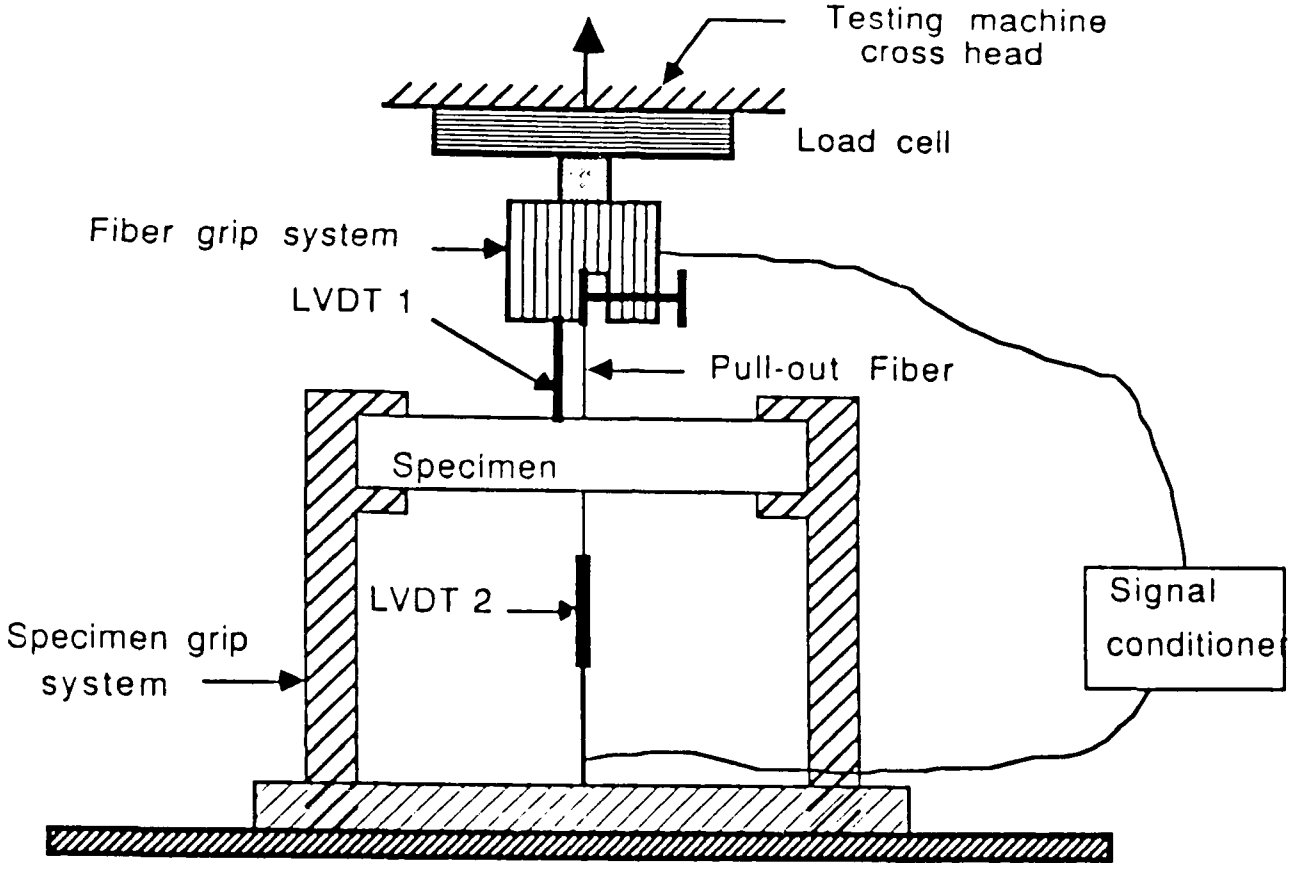

Fig. 6.2 - Test - setup* .

*For pull-out tests, the same setup was used with only one LVDT at the top.

fiber is monitored by means of another miniature LVDT installed inside the grip. The end of the core of this LVDT touches the top surface of the specimen. The upward movement of the crosshead of the testing machine applies a pull-out force on the top end of the fiber. The value of the force, as well as the movements at both ends of the fiber are recorded by a Data Acquisition System, and stored on a disk. Although only the readings of the top LVDT are needed to obtain the ascending branch of the full pull-out curve, and hence the bond shear stress-slip relationship, the reading of the bottom LVDT is useful in determining the load at which full debonding occurs. The LVDTs used are Schaevitz, 250 MHR, with a stroke of ±0.25 in, and a sensitivity of 1×10^{-4} in.

When the smooth or deformed fibers were used (0.3 and 0.5 mm in diameter respectively), a 100 lb. load cell was used. The hooked fibers necessitated the use of a 1,000 lb. load cell.

The tests were all crosshead movement-controlled. The speed of the crosshead movement, and hence of the test was varied during the test. A typical test started off rather slow (0.002 in./min) for the ascending branch, and ended at a much higher rate (0.1 in/min) for the steady portion of the descending branch .

6.3 VARIABLES INVESTIGATED

6.3.1 Fiber Parameters

6.3.1.1 Pull-out Fiber Type. Three different types of fibers were pulled out, namely: smooth, deformed, and hooked. While the actual length of the fibers may differ, the embedment length was kept equal to 1" for most of the specimens. As seen in Table 6.1, two other embedment lengths (0.5" and 1.5") were selectively used. The information about most of the pull-out fibers used is summarized in Table 6.2. Fig. 6.3 shows the shapes of these fibers .

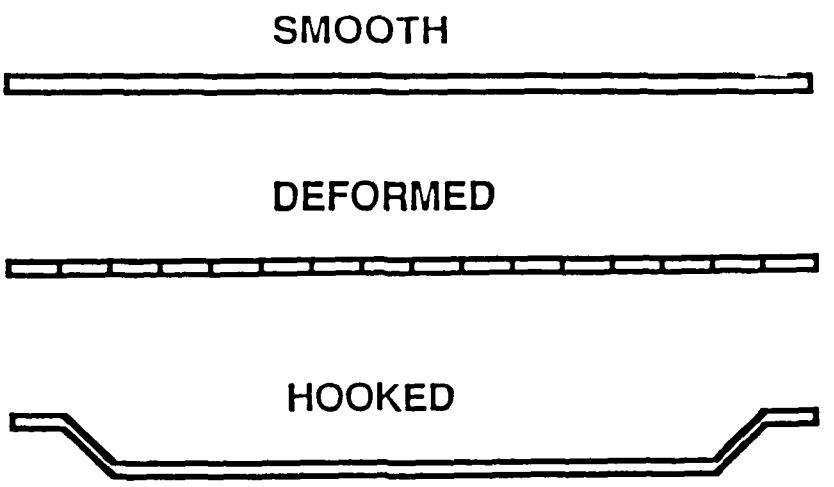

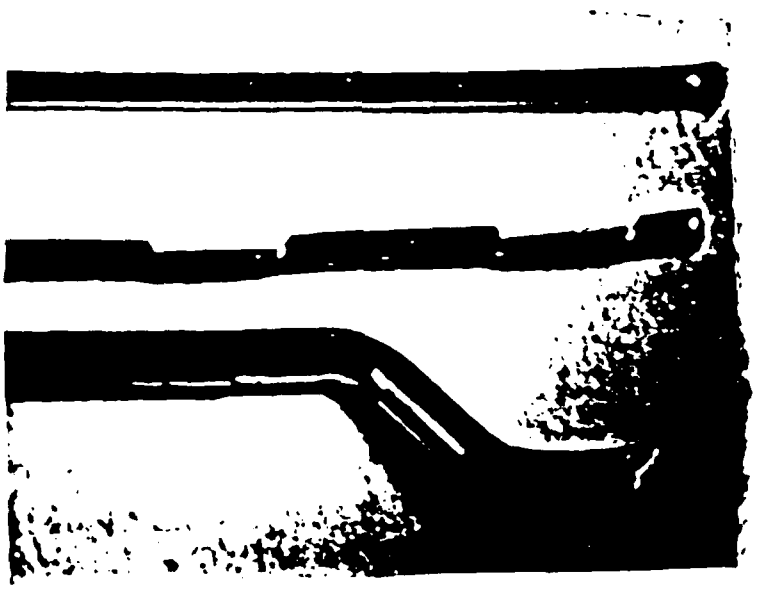

Fig. 6.3 - Types of pull-out fibers used .

Table 6.2 - Fiber Specifications.

Fiber Type	Code	Diameter (in.)
Smooth	S	0.019
Deformed	D	0.018
Hooked	H	0.03

6.3.1.2 Fiber Diameter. For smooth fibers, four different fiber diameters were used , 0.01 ", 0.019" [control diameter] , 0.03 ", and 0.04 " . In most cases the embedment length was 1" , and the matrix was plain of average strength .

6.3.1.3 Fiber Embedment Length. Three different embedment lengths were investigated , namely , 0.5 ", 1"[control length] , and 1.5". For the 0.5" and 1.5" cases, the matrix was plain mortar of average strength and the diameter was 0.019 " for smooth fibers, 0.018" for deformed fibers,and 0.03" for hooked fibers.

6.3.2 Matrix Parameters

6.3.2.1 Matrix Strength. Three different mix proportions were used to create low strength, average strength, and high strength matrices. The sand-cement ratio was kept constant at 2.0, while the water-cement ratio used was 0.40, 0.50, and 0.60 for the high strength, average strength, and low strength mixes respectively. Type I cement and silica sand - ASTM C109 were used. For the SIFCON matrix, a very fine silica sand (type 400) was used. The mix proportions are summarized in Table 6.3.

Table 6.3 - Mix Proportions

Matrix Strength	Code	w/c ratio	Cement	Sand	f'_c (psi)*
High	H	0.4	1	2	8650
Average	A	0.5	1	2	7400
Low	L	0.6	1	2	4850
SIFCON	-	0.52	1	1	6000

* from average tests on 3"x6" cylinders.

6.3.2.2 Additives. Three different additives were used in some mixes to see whether or not their use would affect the bond properties of the interface. The additives used were Latex, Microsilica, and Fly Ash. No two additives were used simultaneously in the same mix. Information on the proportion of each additive is summarized in Table 6.4.

Table 6.4 - Additives.

Additive	Symbol	% of cement weight	% of solids in Additive
Latex	L	20	50
Fly Ash	F	20	100
Microsilica	M	20	50

6.3.2.3 Fiber volume fraction. Four different volume fractions of fibers were used in the specimens: 0% fiber volume fraction (control unreinforced mortar), 1%, 2%, and 3%.

In addition, four Slurry Infiltrated Fiber Concrete (SIFCON) specimens were tested to study the effect of fiber entanglement. The fiber volume fraction in SIFCON ($V_f \approx 11\%$) is usually significantly higher than that in normal fiber-reinforced concrete (up to 3%). In all cases of reinforced matrices, the same type of fibers (hooked, 30/50) were used in the mix .

6.4 TESTING PROCEDURE

Typical pull-out tests were performed on 52 series of four pull-out fibers each. As was mentioned in §6.2, different combinations of fibers, matrices, and additives were used. During these pull-out tests, the pull-out force, the end slip, as well as the movement of the bottom end (free end) of the pull-out fiber [for pull-through tests only] were monitored. The pull-out force and the displacement at the top end of the fiber were used to develop pull-out curves, i.e. pull-out force versus end slip curves. Typically, for each series, four different pull-out curves were obtained. For smooth fibers pull-out and pull-through tests were conducted at a crosshead speed of 0.002 in/min up to the peak load. For deformed and

hooked fibers the crosshead speed ranged from 0.002 to 0.02 in/min up to the peak load. The speed was then increased up to 0.1 in/min in the steady portion of the descending branch.

For any given pull-out test, both the pull-out load P (lbs.) and the end slip Δ (in.) at the section where the fiber enters the matrix were recorded by a data acquisition system and stored in a data file on IBM-Diskettes. The data were processed as described in Fig. 6.4 . The pull-out load versus end slip relationship was then developed and plotted using such data files. Plots with different vertical and horizontal scales were used depending on the specimen type.

6.5 CURVE AVERAGING PROCEDURE

One representative curve was needed for each of the series tested. The criterion used to chose the proper averaging method was that the average curve has a peak pull-out load P_p equal to the average of the peak pull-out loads recorded for the individual pull-out tests. Furthermore, the average curve was to have a corresponding end slip at peak Δ_p equal to the average end slips at peak for the individual tests. Finally, equal weights were to be assigned to all curves used in averaging.

The average curves were obtained using a computer program written by D. E. Otter [47]. The method used to obtain these curves was as follows: the peak pull-out loads for all tests in the series were first determined and averaged, and so were their corresponding end slips. The average peak pull-out load, as well as its corresponding end slip were hence determined. The pull-out loads on the ascending (pre-peak) branch of each pull-out curve were evaluated at 50 equal end slip intervals. The interval was selected in terms in each curve's own peak displacement . The average of these loads at each interval was evaluated, and taken as the average load at the corresponding end slip interval based on the peak point of the average curve. The same interval was used for the descending (post-peak) branch of the average curve. Examples of series of four pull-out tests and their average curve (in dotted line) are shown in Fig. 6.5.

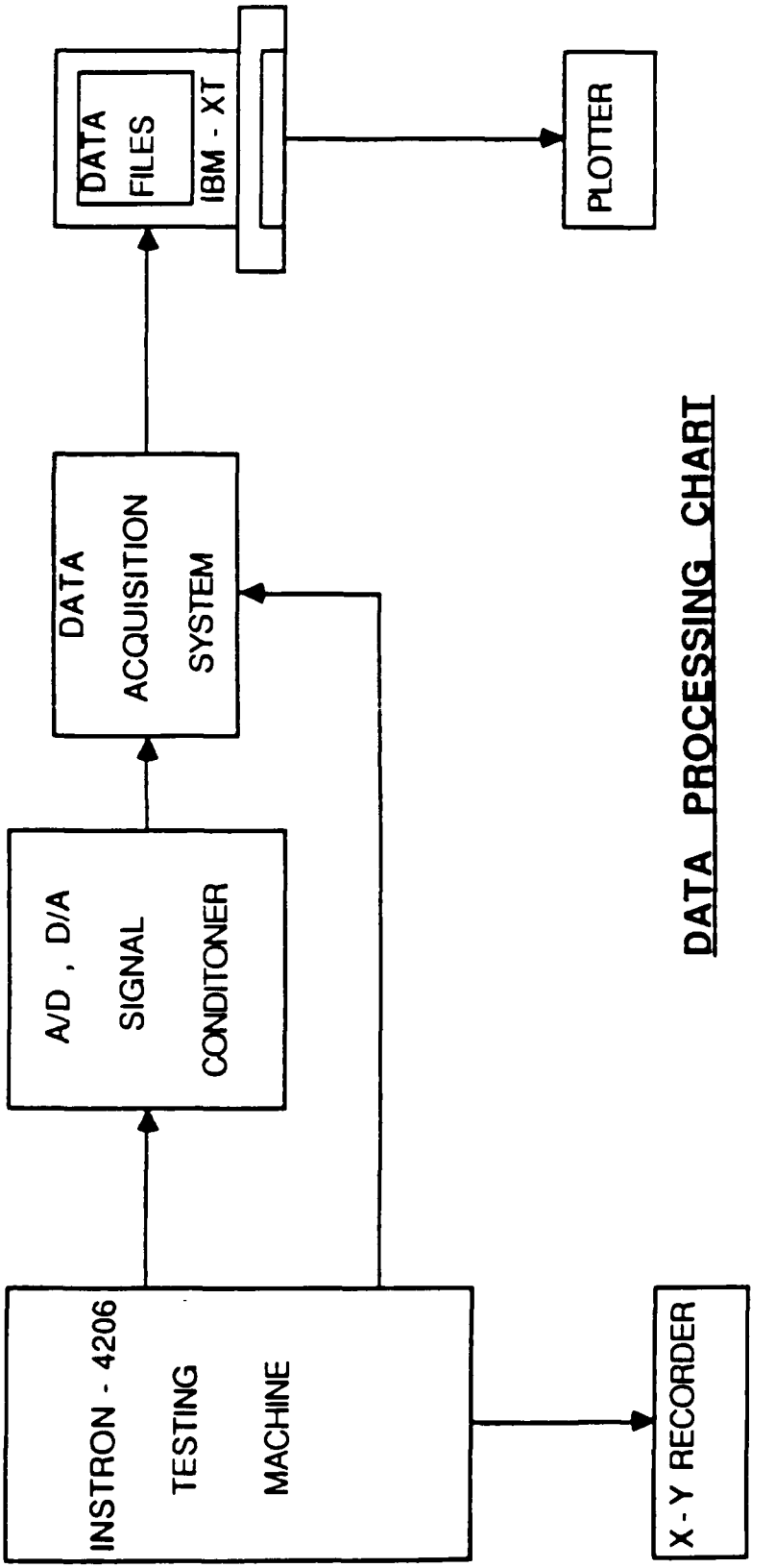

Fig. 6.4 - Data processing chart.

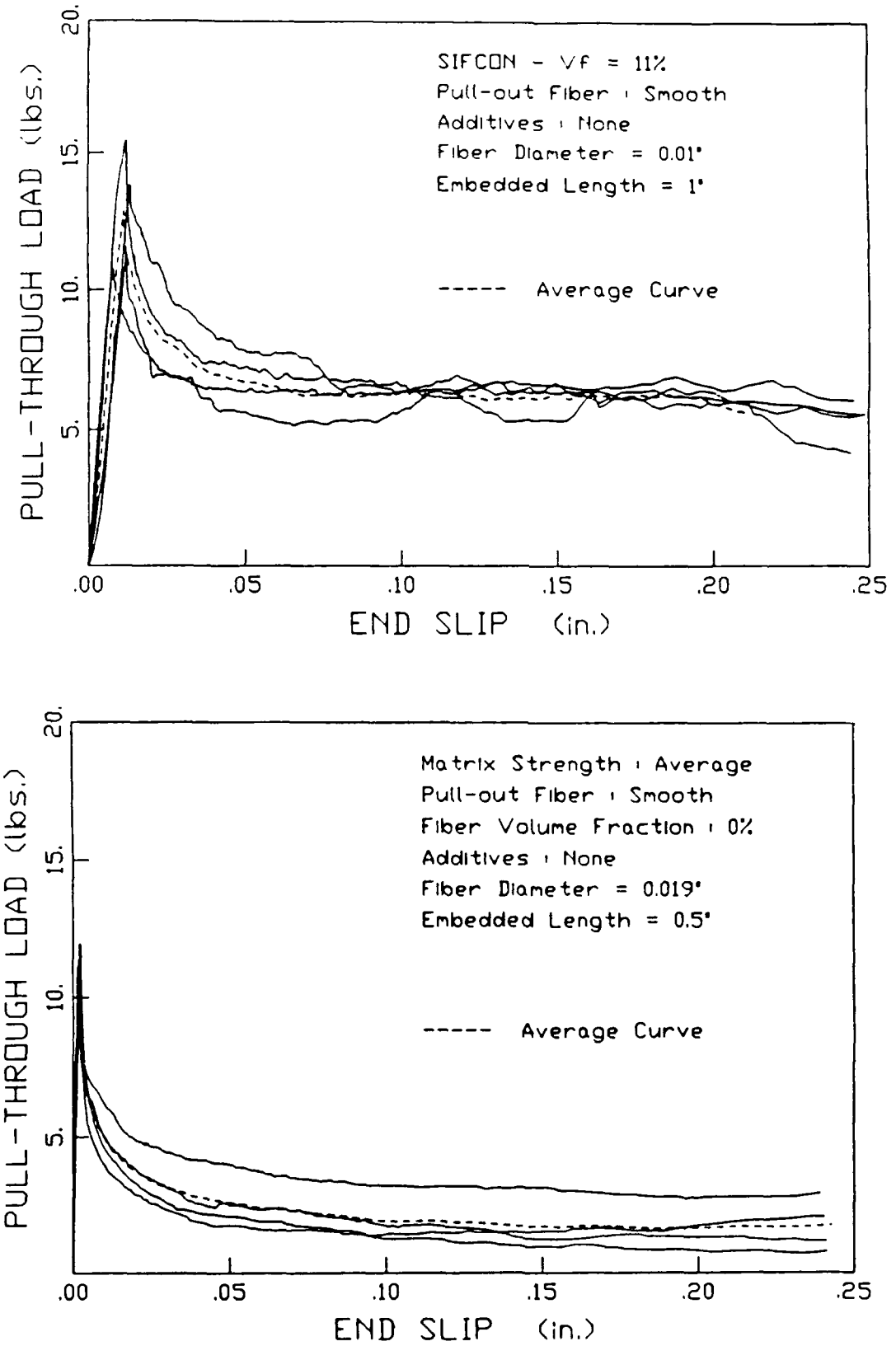

Fig. 6.5 - Pull-out tests of the four fibers and the average curve .

6.6 PULL-THROUGH VERSUS PULL-OUT TESTS

In the pull-through tests the fiber extends below the bottom surface of the specimen so that the embedment length remains constant during the pull-out process. For the pull-out tests, the fiber does not extend below the bottom surface of the specimen and thus the emdedment length decreases during pull-out .

The differences in loads measured in the pull-out and pull-through tests for 1" embedment length were not significant for end slips less than about 0.2" . To show the difference between these two types of tests at larger slips, pull-out and pull-through loads were plotted versus the end slip for the entire embedment length , i.e. up to 1" embedment length . Figs. 6.6 and 6.7 show some typical results. It can be observed that there is some decay in the response, even when the embedded length remains constant.

6.7 PULL-OUT LOAD VERSUS END SLIP RELATIONSHIPS

6.7.1 Smooth Fibers

For smooth fibers the load was generally linear up to a load termed P_{crit} in Chapter V. The value of P_{crit} however was close to P_p, the peak load. After P_p, the load dropped quickly, the higher the matrix strength, the faster the drop (up to 60% drop in the peak load at full debonding in some series). As shown in Fig. 6.8a, the descending branch of the curve indicates that debonding in smooth fibers is faster than for other types of fibers. The rate of debonding is negative (positive curvature), meaning that as the slip increases, the bond decreases drastically.

In the case of pull-through tests, after full debonding has occurred, the load approaches a constant value at small slips. However large slips tend to induce decay at the interface between the fiber and the matrix and the concrete tunnel around the fiber surface is damaged. In the case of pull-out tests, frictional forces decrease not only because of decay but also because the embedment length decreases.

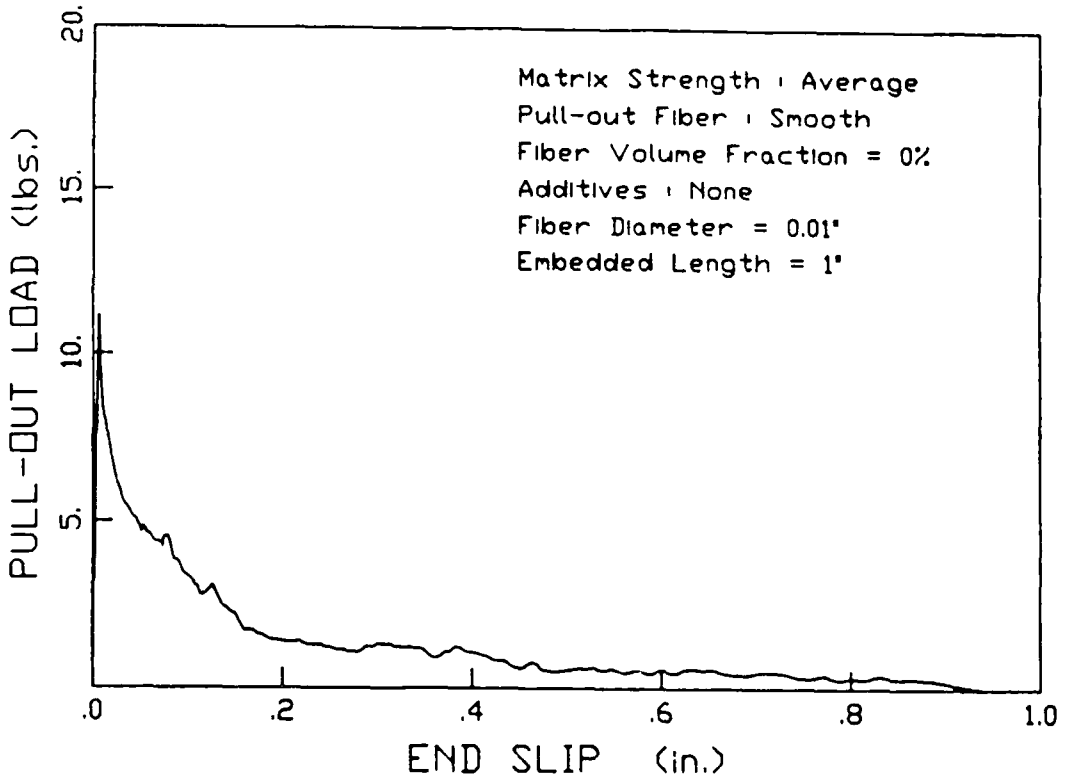

Fig. 6.6 - Pull - out test of a smooth fiber up to 1" end slip .

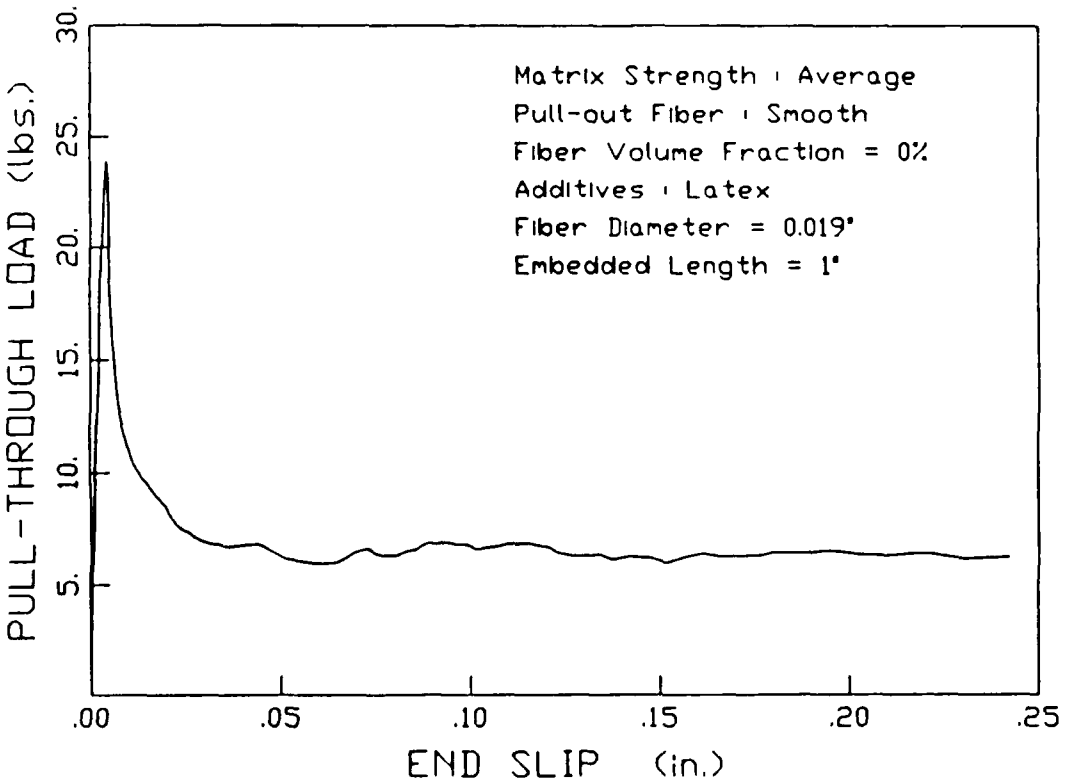

Fig. 6.7 - Pull-through test of a smooth fiber up to 1" end slip .

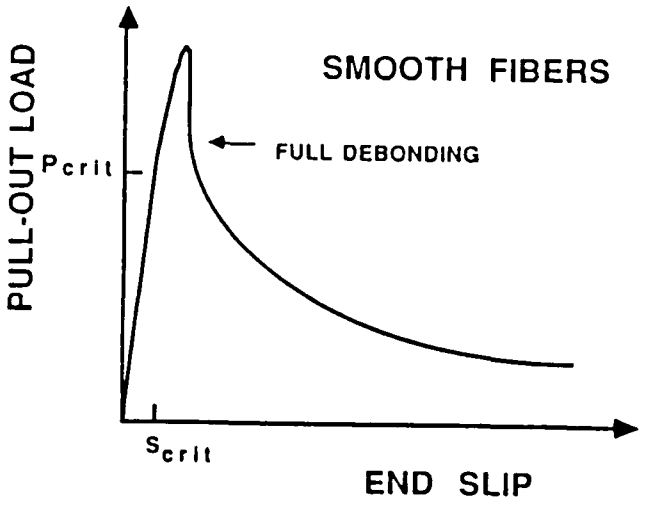

Fig. 6.8a - Typical pull-out load versus slip relationship of smooth fiber .

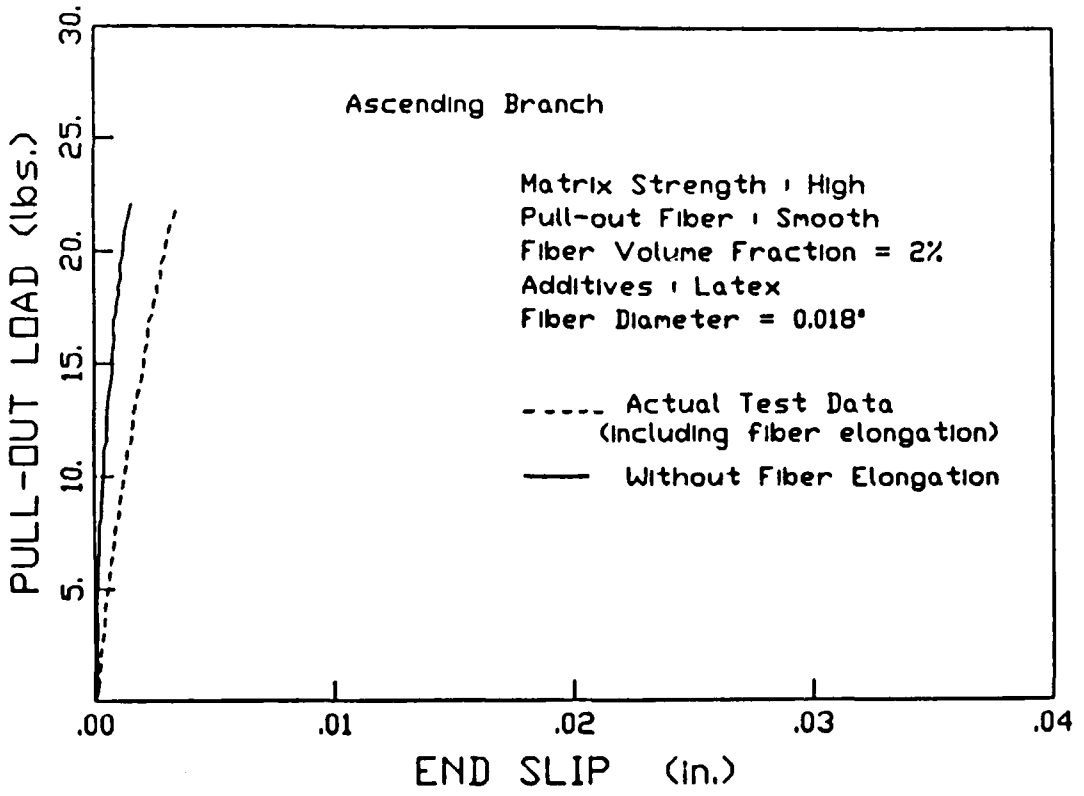

Fig. 6.8b - Ascending branch of pull-out curve of smooth fiber with and without elastic strains.

In the ascending branch it is observed that the elastic strain contribution to the measured slip was significant especially for small fiber diameters (0.01") . This contribution decreased when larger diameters were used although the pull-out load increased . Fig. 6.8b illustrates the pull-through curve when elastic strains are accounted for , i.e, the elastic elongation at the free end is substracted from the observed slip.

Another source of error is due to the fact that the smooth fibers, being cut from spring-type steel wire, were not perfectly straight , i.e. (had some curvature). Such imperfections in straightness or at the fiber tip which becomes flat due to cutting did influence the pull-out load versus slip measurements especially at large slips .

Table 6.5 shows some values of (P/Δ), the initial slope of the load-slip curve for different types of specimens in which the pull-out fibers were smooth. These values range from 25,000 lb/in to 68,000 lb/in, depending on the type of specimen. In these results, the value of Δ is corrected to account for the elastic strain contribution.

Table 6.5 - Pull-out Data

Series	$\left(\frac{P}{\Delta}\right)$ (10^3 lbs/in)	P_p (lbs.)	Δ_p (10^{-4} in.)
H2SF	44.0	13.4	7.80
L0SN	52.1	12.6	7.30
A1SN	55.0	10.8	6.34
H2SL	67.8	22.1	15.9
H2SM	30.0	16.8	9.48
H0SN	25.0	15.6	9.25
L2SN	31.0	10.3	6.01
A0SN	45.0	12.6	7.18
H0SL	40.8	12.1	7.12
H3SN	35.0	17.2	4.33
A2SM	28.0	12.5	2.72
H2SN	40.0	18.9	18.2

The readings of the bottom LVDT showed that the load at which the fiber starts to pull out is, in general, slightly less than the maximum observed load. Table 6.6 summerizes the values of the peak load and the load at which the second LVDT starts to move with their corresponding displacements as obtained from tests not including the effect of fiber elongation. In Table 6.6, Δ_2 is the end slip of the first LVDT for the load P_2 described in column 4. Fig. 6.9 shows the ascending branch up to the peak load on a larger scale for smooth fibers as obtained from tests without accounting for fiber elongation.

Table 6.6 - Loads and displacements of smooth fibers.

Series	P_{max}(lbs.)	Δ_{max} (in.)	P_2 (lbs.)	Δ_2 (in.)
A0SL	21.7	0.00382	19.3	0.00419
A0SN	13.4	0.00294	13.0	0.00310
A0SN D=0.03	20.6	0.00260	-	-
A2SN	16.7	0.00291	-	-
A3SN	18.8	0.00275	15.9	0.00322
A0SN D=0.01	10.6	0.00717	10.2	0.00754
A0SN L=0.5"	10.5	0.00226	9.8	0.00226
H0SM	14.6	0.0030	13.7	0.00322
Sifcon D=0.01	12.3	0.00921	11.5	0.00921
sifconD=0.019	22.0	0.00464	16.0	0.00515
Sifcon D=0.03	30.2	0.00159	28.5	0.00196

To account for fiber elongation during pull-out, the elastic elongation $\Delta_e = (P*L)/(Af*Es)$ should be substracted from the values of Δ_{max} and Δ_2. For example , for series A0SL, P=21.7 lbs., L= 0.5", Af= 0.000283 in2, Es = 29000 ksi $\Rightarrow$ Δ_e = 0.00132 in, thus the corrected value of Δ_{max} is 0.00382 - 0.00132 = 0.0025 in. It should be noted here that the values of Δ given in Tables 6.7 and 6.8 do not include the effect of fiber elongation.

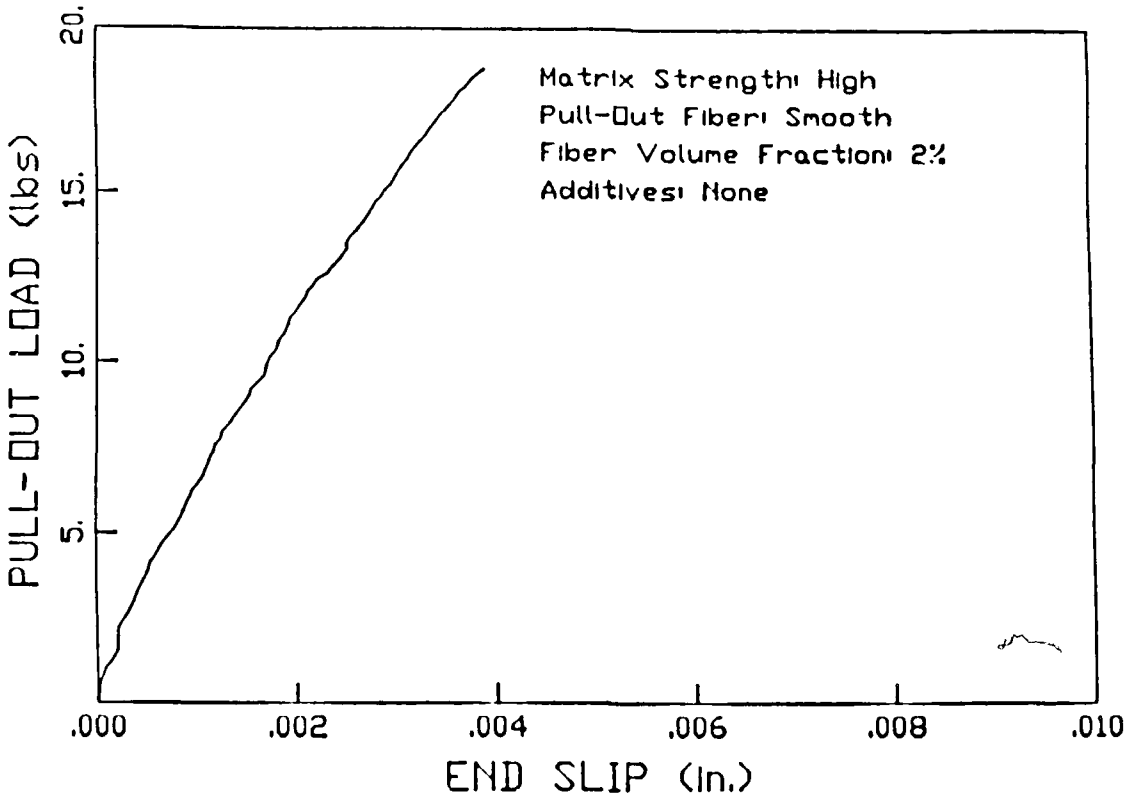

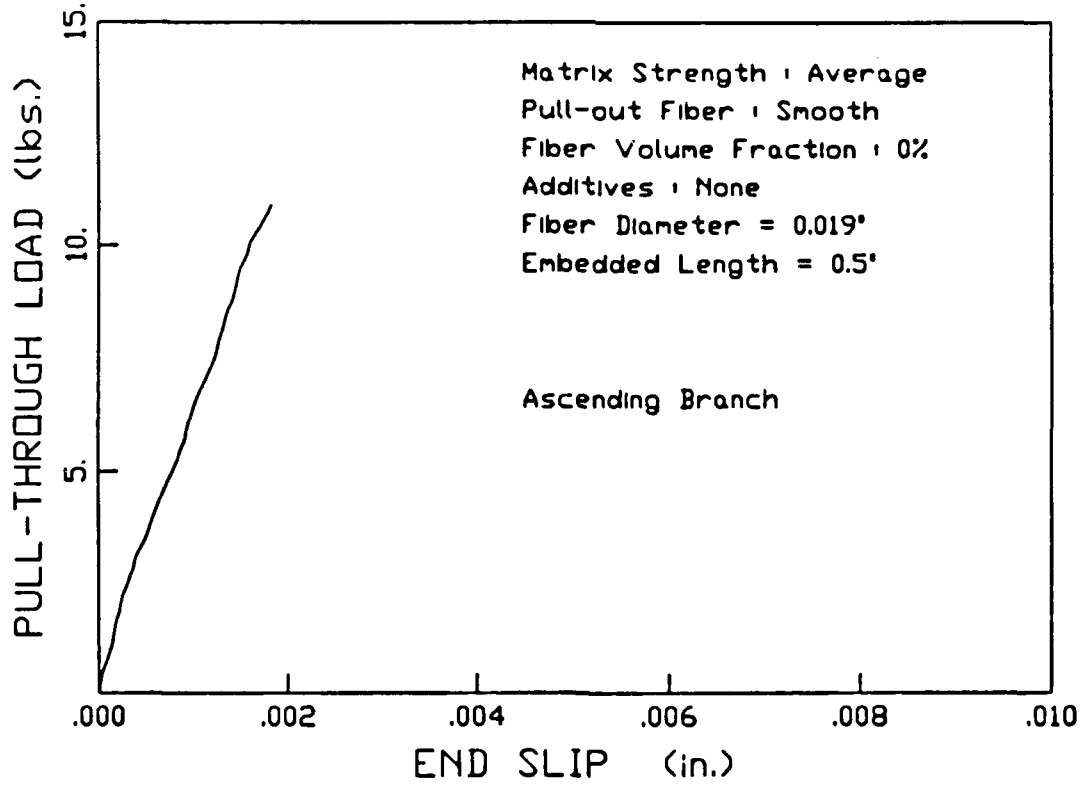

Fig. 6.9 - Experimental pull-out curves of smooth fibers up to the peak load .

6.7.2 Deformed Fibers

Typical pull-out load versus end slip curves of deformed fibers are shown in Fig. 6.10. It can be observed that the ascending branch is made out of two parts. The first part is linear and the second part is highly nonlinear. It is observed that for the second part, the resistance to pull-out is due not only to the interfacial bond between the fiber and the matrix (similar in nature to that found in the case of smooth fibers), but due to an additional resisting force provided by the mechanical deformations on the fiber surface. Fig. 6.11 shows the ascending part of a pull-out curve on a larger scale for a typical deformed fiber, while Fig. 6.12, shows the pull-out curve for a deformed fiber up to an end slip of 0.25" . Following the peak load, the pull-out load starts to drop. However, in this case the drop is different from that seen in the case of smooth fibers. This difference is due to the fact that for deformed fibers, as the slip increases, the smooth portion of fiber surface tends to debond fast (as in the case of smooth fibers) while the mechanical indentations on the fiber surface try to displace the concrete encasing these deformations. When that concrete is displaced or crushed, the load drops drastically to values close to zero. This can be explained by the fact that when the concrete in contact with the fiber surface has been highly disturbed, it could no longer provide the frictional resistance, as the one observed in the case of smooth fibers. However as soon as the deformations enter another section of the tunnel (of different cross section), the load picks up again and a cyclic response is observed. This is illustrated in Figs. 6.13 and 6.14.

Pull-out tests performed on deformed fibers showed that these fibers would reach ultimate strains and fail at loads around 45 lbs. Many fibers failed when such load levels were reached or exceeded. Deformed fibers whose diameter is 0.018", exhibit very high stresses before debonding and, as a result, failure may occur before full debonding or the start of pull-out. An optimum case will be when the fiber debonds completely and starts pulling-out just before the ultimate strength of the fiber is reached. Data from tests on deformed fibers [not including the effect of fiber elongation] showed that the displacements at maximum loads were 15 to 20 times those of smooth fibers. If fiber elongation is accounted for, this value could

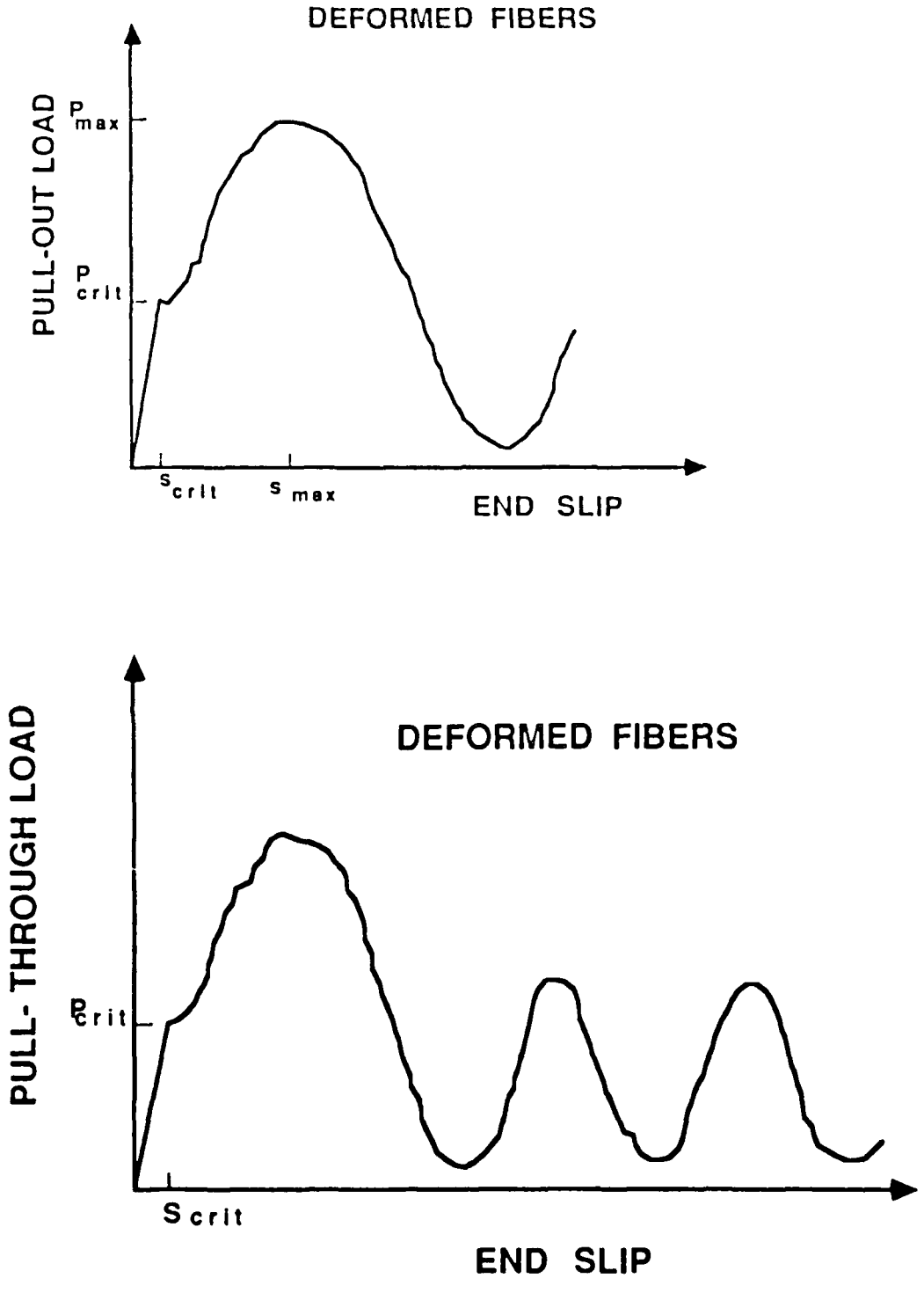

Fig. 6.10 - Typical pull-out load versus end slip of deformed fibers .

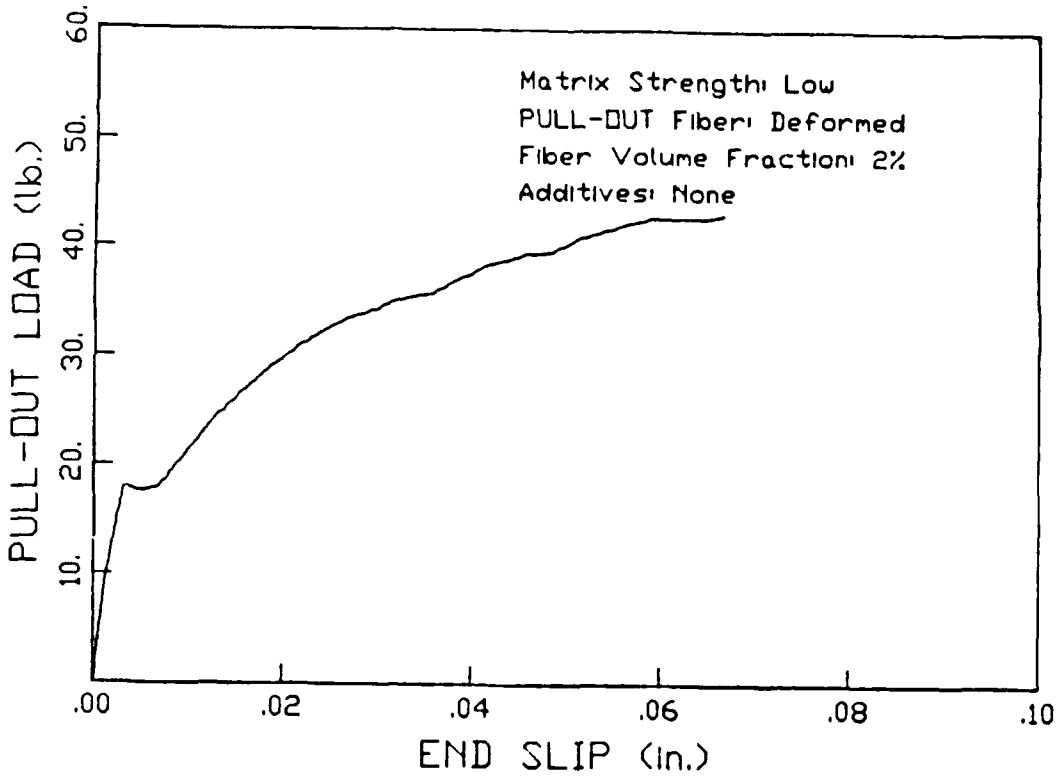

Fig. 6.11 - Pull-out curve of deformed fiber up to the peak load .

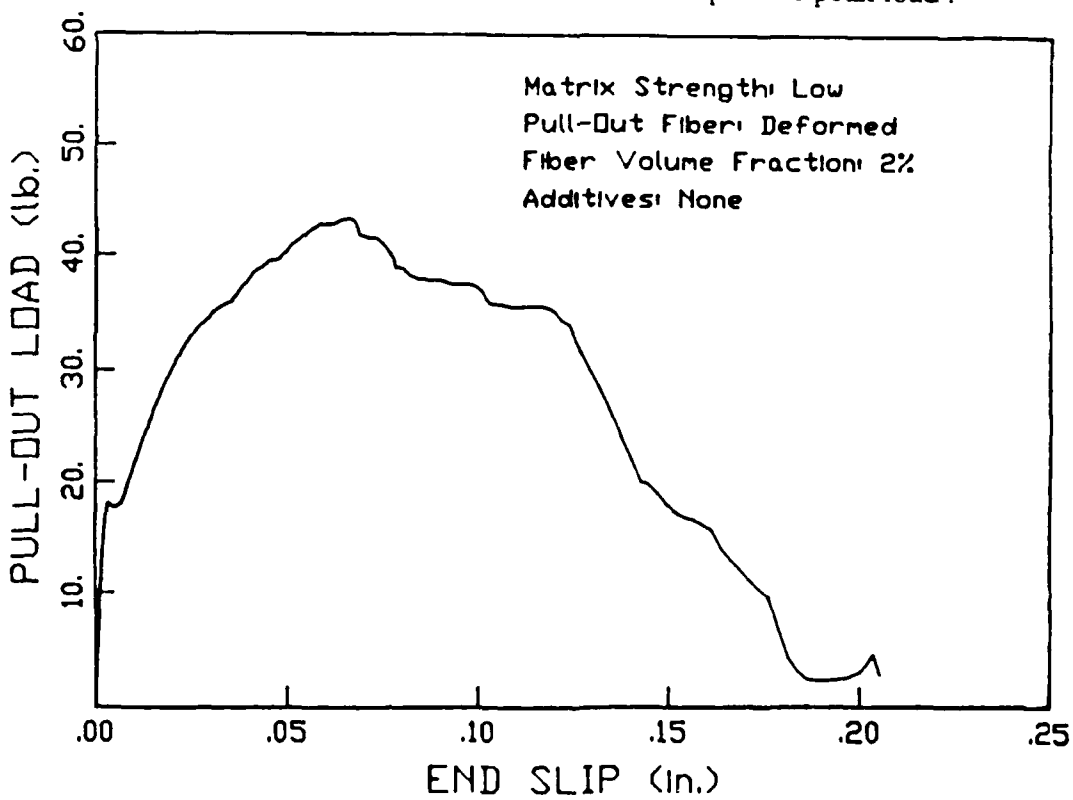

Fig. 6.12 - Pull-out load versus end slip of deformed fibers .

exceed 50 . Table 6.7 shows values of loads and displacements of deformed fibers at peak load and the load at which the second LVDT (attached to the free end) starts to move.

Table 6.7 - Loads and displacements of deformed fibers.

Series	P2 (lbs.)	$\Delta_{2(in.)}$	Pmax (lbs.)	Δ_{max} (in.)
A0DN	11.5	0.00975	35.4	0.0511
A1DN	16	0.00341	33.8	0.0822
L2DN	18	0.00335	43.3	0.0660
L3DN	12	0.00792	40.0	0.0423
L0DM	6.5	0.00171	21.6	0.0674

The pull-out behavior of deformed fibers for large slips is shown in Figs. 6.13 and 6.14. In Fig. 6.14, which shows a pull-through curve, it is observed that the curve repeats itself every 0.2" over the descending branch. This corresponds to the size of the deformed portion (indentation) of each segment of the fiber. The load cycles reach about the same peak value and have the same shape. This can be explained as follows: as slip increases, the already disturbed concrete by the previous indentation is again disturbed by the following indentation. The total resisting force is thus approximately the same.

Fig. 6.13 shows a pull-out test, where the repeated curves are decreasing in amplitude. This decrease is due to the fact that the number of deformations decreases with a decrease in the embedment length during pull-out .

A final observation on deformed fibers, is that the deformations (or indentations) on the fiber surface were not exactly uniform for all batches of fibers used. For some fibers surface deformations were not deep

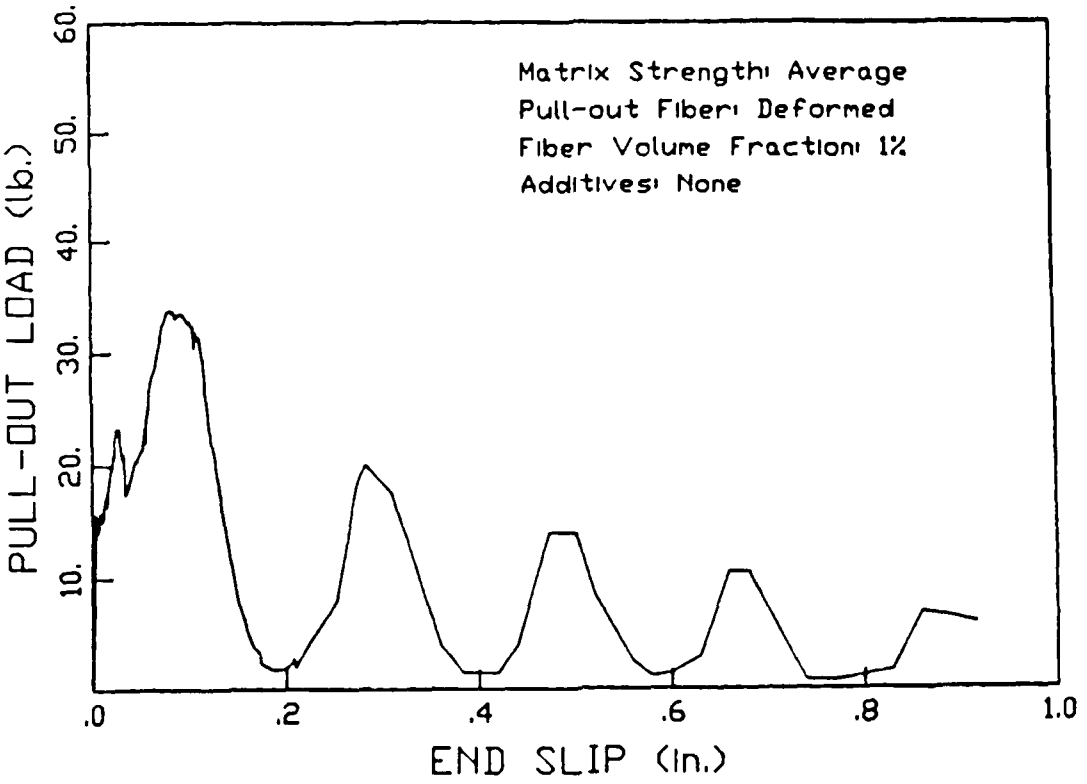

Fig. 6.13 - Pull-out test of deformed fibers up to 1" end slip .

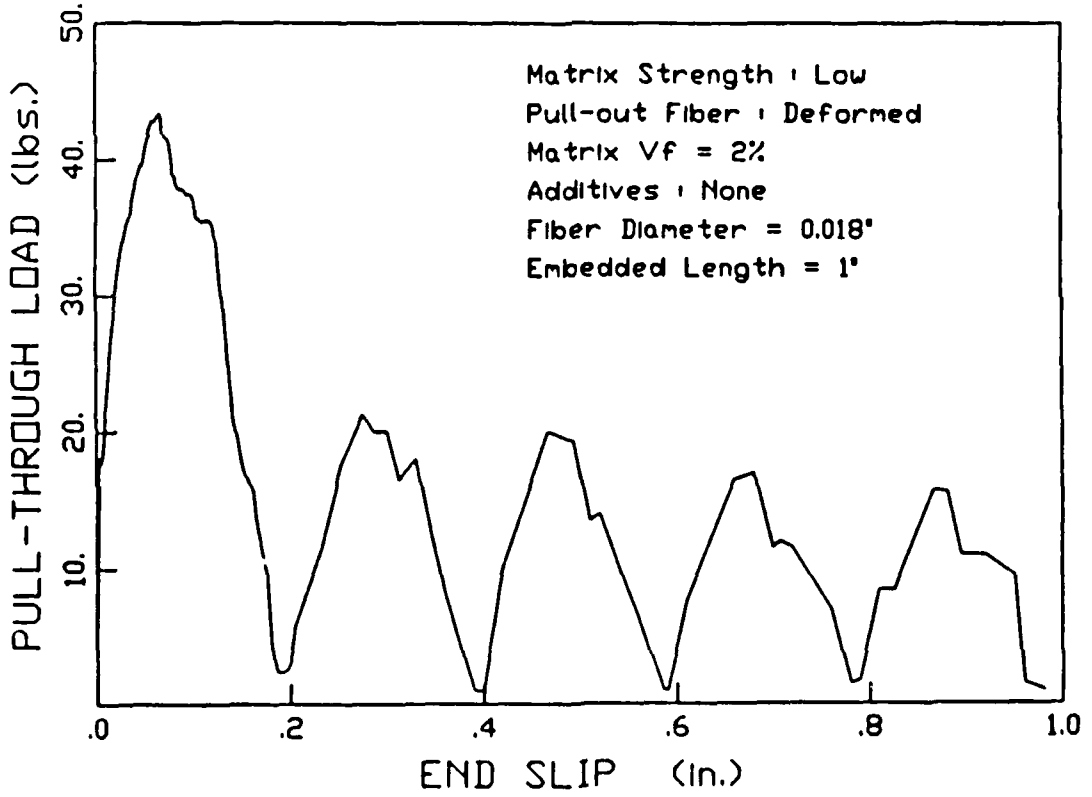

Fig. 6.14 - Pull-through test of deformed fibers up to 1" end slip .

enough . As a result of this, these fibers were pulled out rather easily from the matrix .

6.7.3 Hooked Fibers

A typical pull-out load versus end slip curve for hooked fibers is shown in Fig. 6.15. As was the case for deformed fibers, the ascending branch is made up of a linear and a non-linear part. Figs. 6.16, 6.17, and 6.18 show actual pull-out load versus slip behavior of hooked fibers respectively up to the peak load, up to 0.25 " end slip ,and up to 0.5 " end slip . Fig. 6.19 shows a typical pull-out load versus end slip curve up to 1" end slip.

Although hooked fibers used in the tests have a different diameter than either smooth or deformed fibers, it is still possible to compare their behavior with the smooth or the deformed fibers. The ascending branch had generally a steeper slope, due to the presence of the hook, which provides a considerable resisting force to pull-out. As the hook is being pulled out from the matrix, it pushes on the surrounding concrete and tends to straighten up, hence causing the slope of the ascending branch to start decreasing. When the hook has been partially straightened and debonding has occurred, the pull-out load starts to drop. As the slip increases, the load continues to drop as the partially straightened fiber tries to slip further in the surrounding concrete tunnel. Therefore, the shape of a portion of the descending branch reflects the case of a partially straightened fiber trying to pull out, hence inducing frictional forces along its surface. When the hook becomes straight, the descending branch drops fast and the last lower portion of the curve reflects mainly the frictional forces between the fiber surface and the matrix.

The maximum pull-out load for hooked fibers varied from 50 lbs. to 105 lbs. depending on the matrix strength. Displacements at peak loads were 10 to 15 times those of smooth fibers, not including the effect of fiber elongation. If fiber elongation is accounted for,this value could exceed 30. On the other hand, displacements at peak loads of hooked fibers were less than those of deformed fibers . Table 6.8 shows the peak loads and the corresponding displacements of hooked fibers.

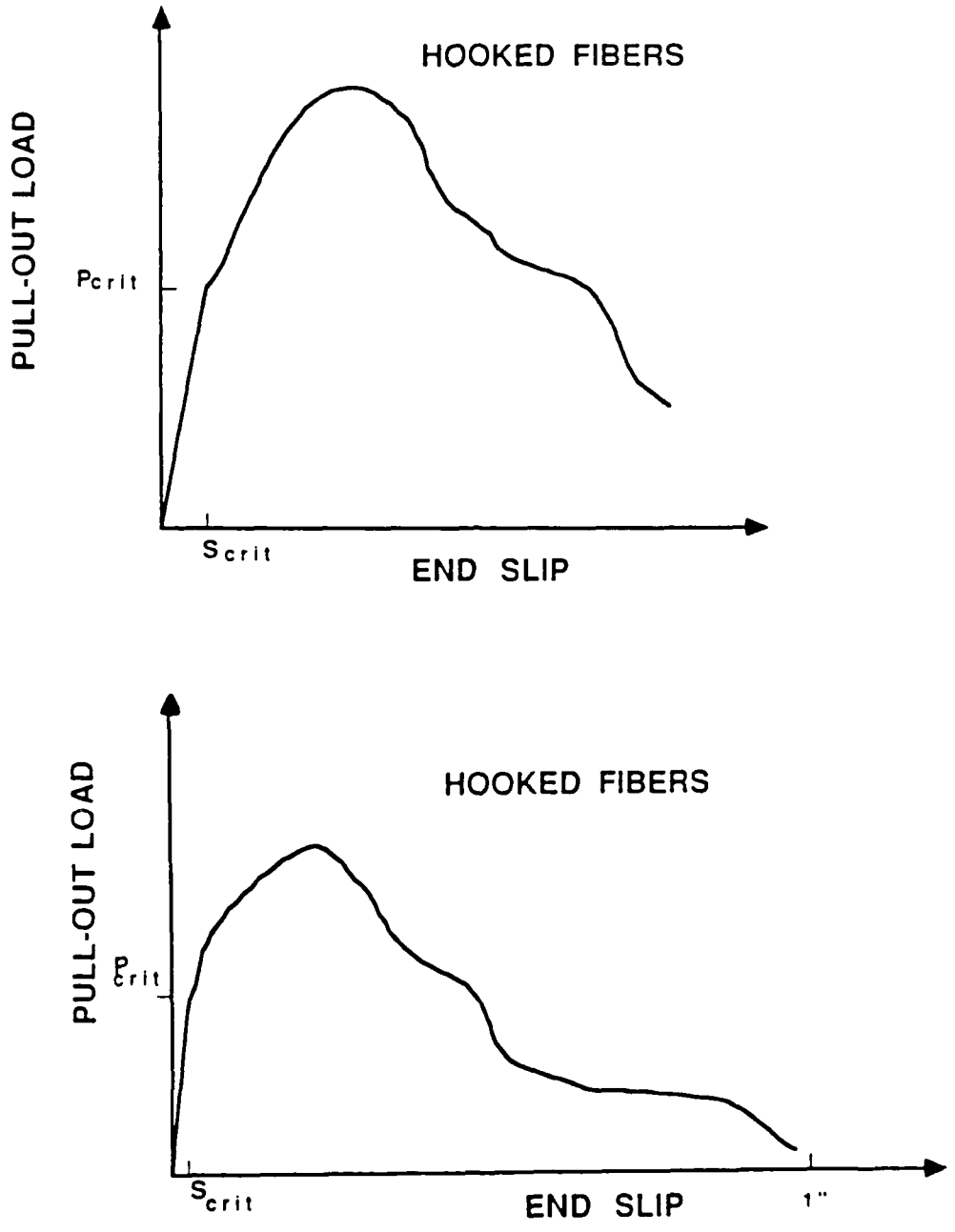

Fig. 6.15 - Typical pull-out load versus end slip relationship of hooked fibers .

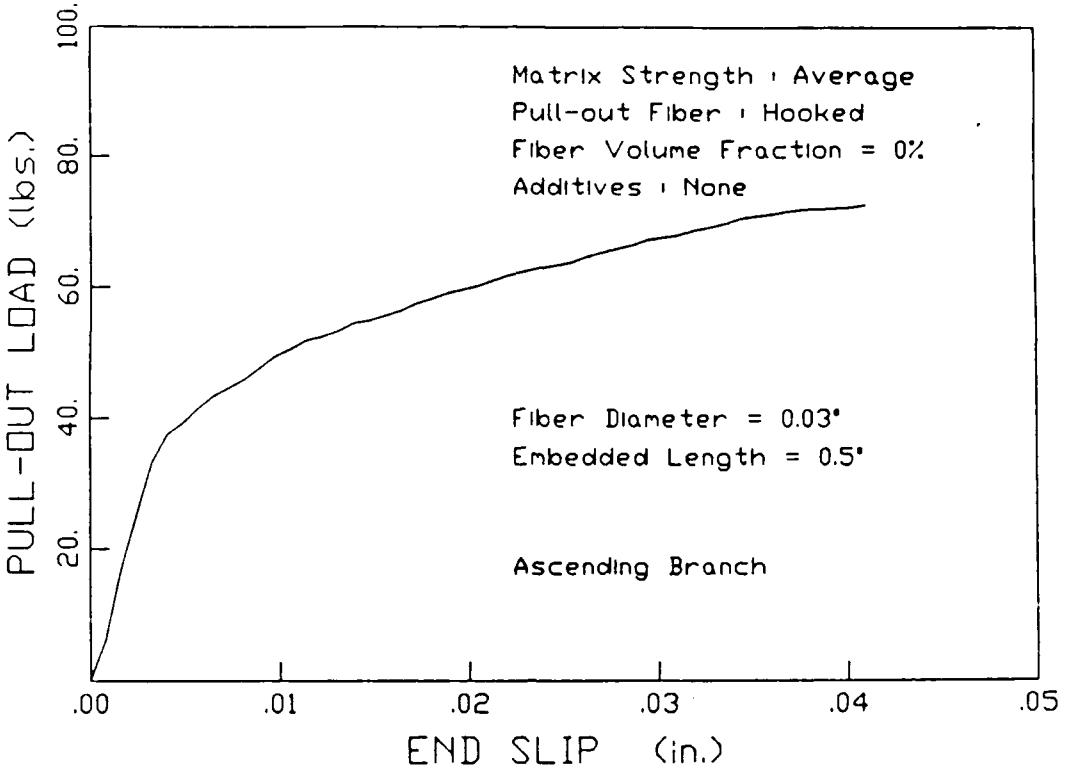

Fig. 6.16 - Pull-out curve of hooked fibers up to the peak load .

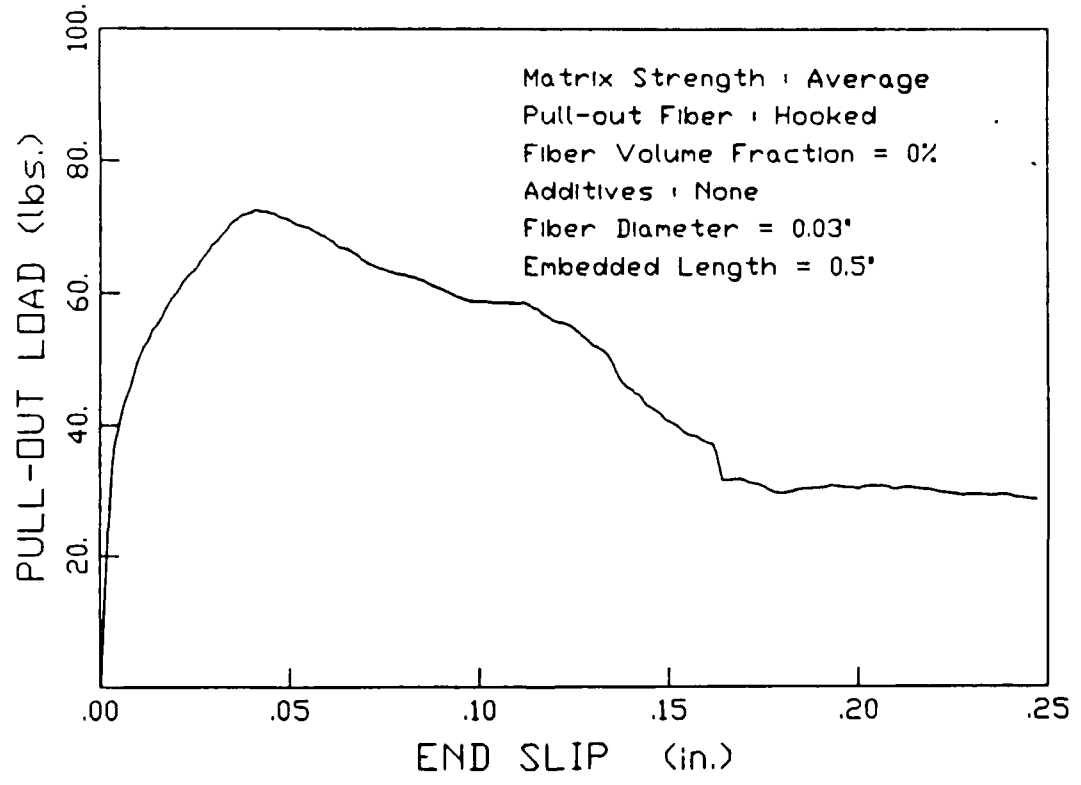

Fig. 6.17 - Pull-out curve of hooked fibers up to 0.25 " end slip .

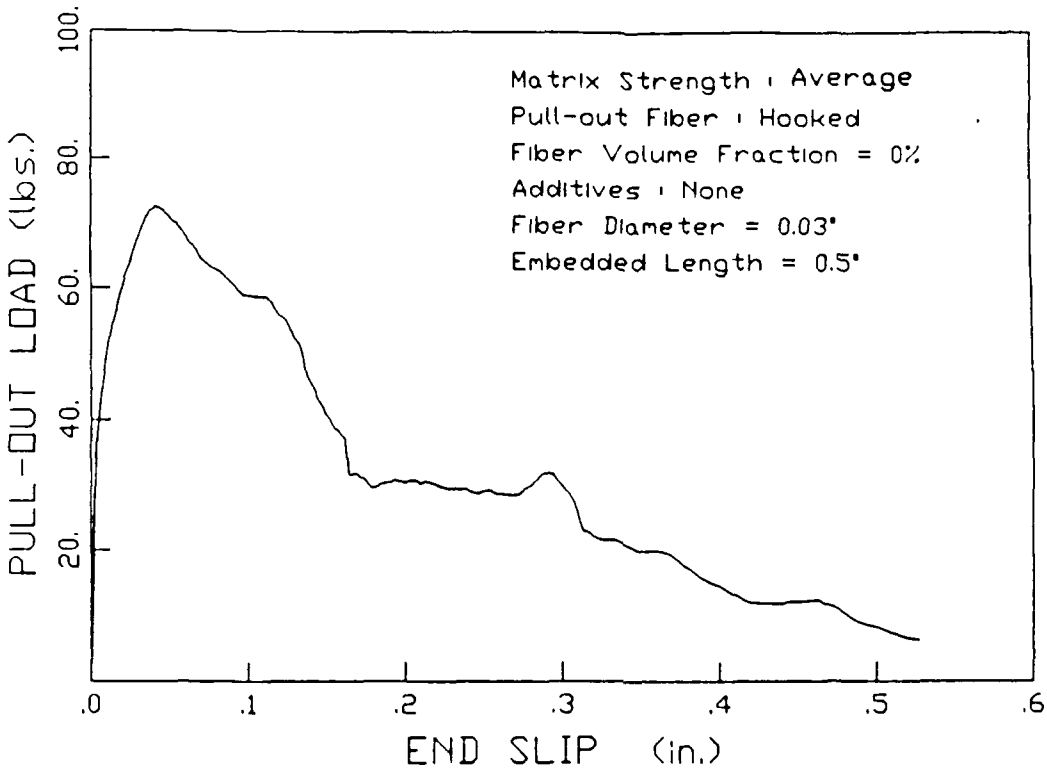

Fig. 6.18 - Pull-out curve of hooked fibers up to 0.5" end slip .

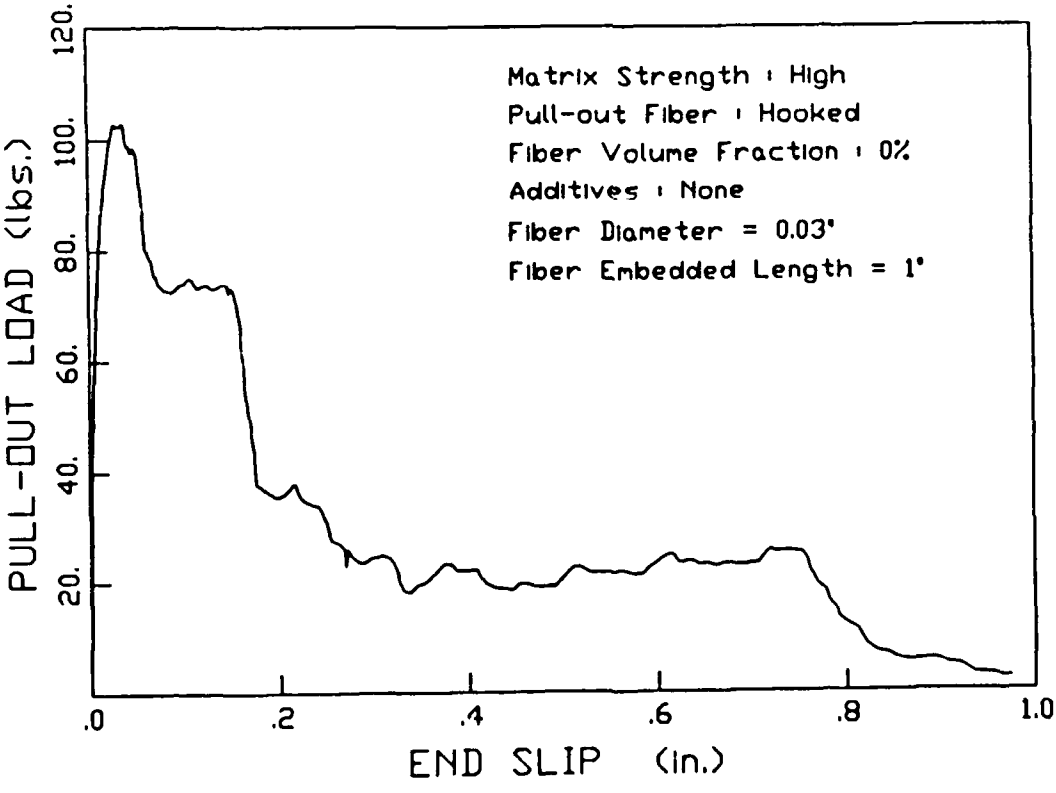

Fig. 6.19 - Pull-out curve of hooked fibers up to 1" end slip .

Table 6.8 - Loads and displacements of hooked fibers.

Series	Pmax (lbs.)	Δmax (in.)
H0HN	102.8	0.0288
A0HN	80.3	0.0354
L0HN	58.9	0.030
A1HN	91.7	0.0478
L1HN	48.8	0.0437
L3HN	66.1	0.0354
H0HN L=0.5"	89.2	0.0332
A0HN L=0.5"	72.6	0.0411

It was observed in some experiments that the hook had broken inside the matrix before straightening .When the hook breaks the load drops faster and the pull-out behavior afterwards resembles that of a smooth fiber. Fig. 6.20 shows end hooks before and after pull-out. Fig. 6.21(a) shows three pull-out tests of hooked fibers up to 1" end slip while figure 6.21 (b) shows the pull-out load versus end slip of hooked fibers where two fibers had broken inside the matrix.

6.8 PULL-OUT WORK

The pull-out work, or the dissipated bond energy is defined as the area under the pull-out curve. This area was found to be much smaller in the case of smooth fibers, than for deformed or hooked fibers.

Typical Pull-out work values calculated for the three types of fibers from test data are shown in Table 6.9 . The table shows pull-out work values for pull-out and pull-through tests at peak loads, at 0.2" end slip, and at 1" end slip.

(a) Hook before pull-out.

(b) Straightened hook.

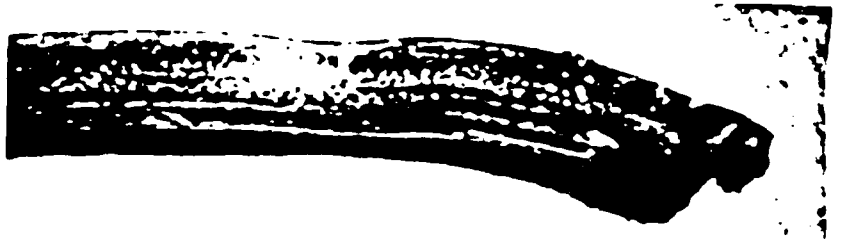

(c) Broken hook.

Fig. 6.20 - End hooks before and after pull-out.

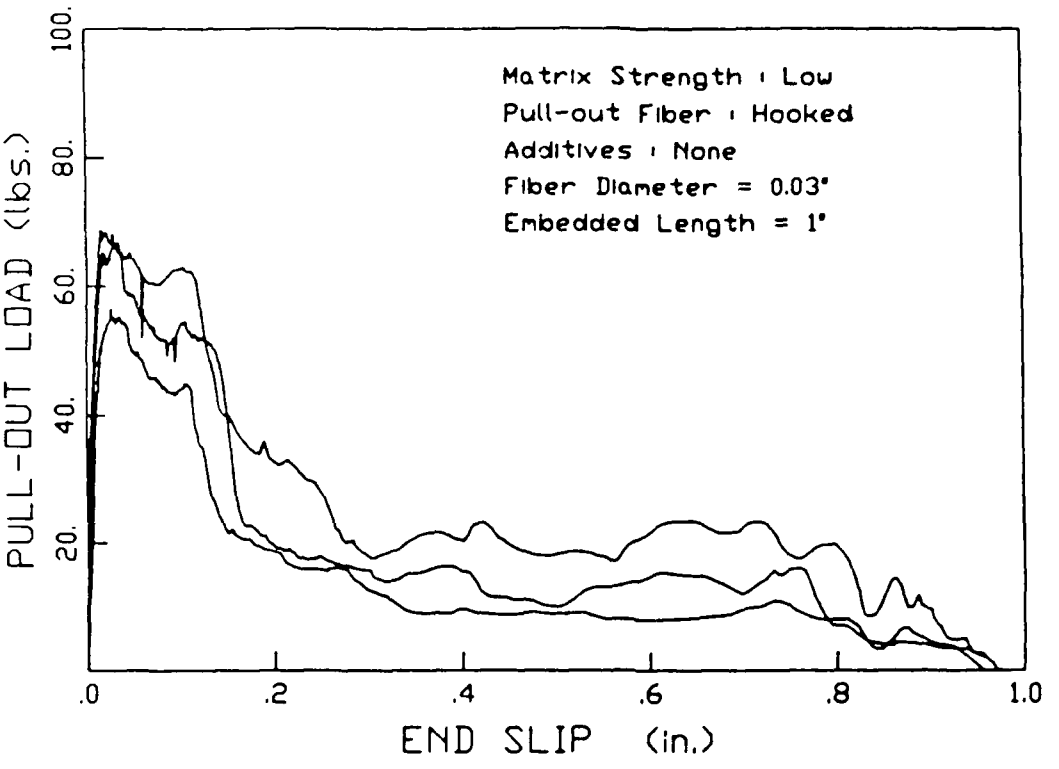

(a)

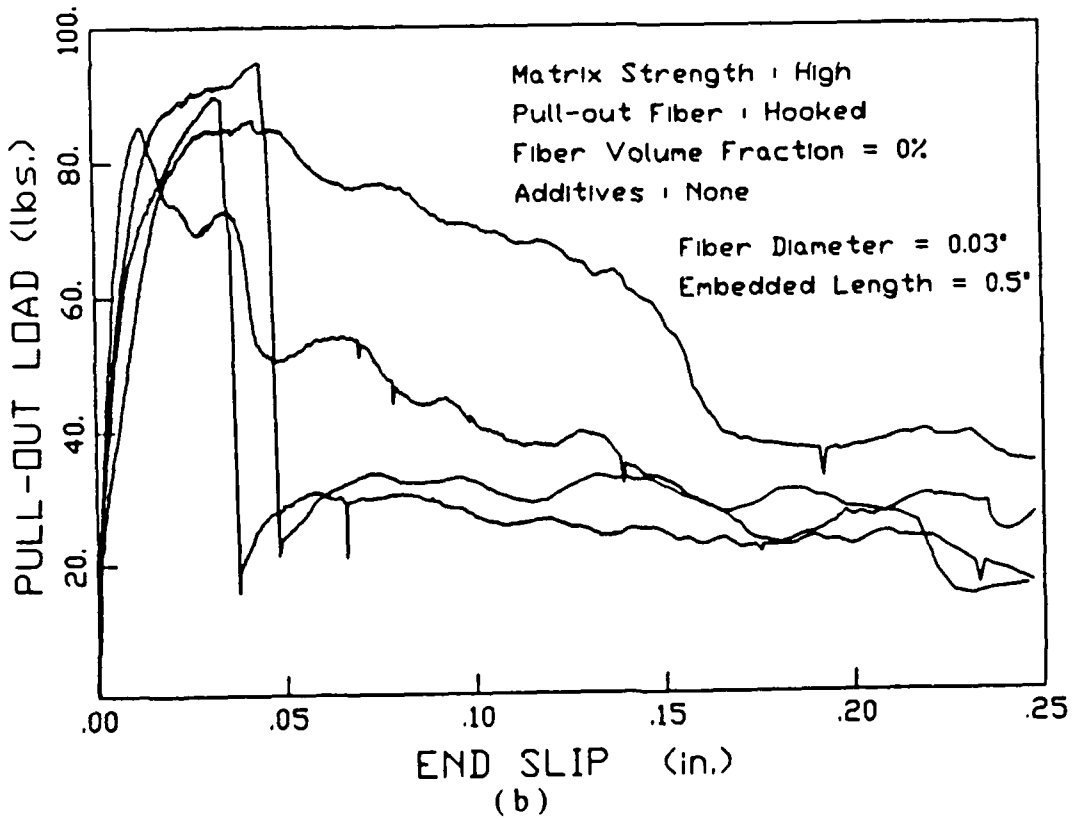

(b)

Fig. 6.21 - Pull-out load versus end slip of hooked fibers

Table 6.9 - Pull-out work for different types of fibers .

Series	Test	Wmax(lb-in)	W 0.2" (lb-in)	W 1"(lb-in)
H3SN	Pull-through	0.0239	1.25	-
H2SN	Pull-through	0.0481	1.21	-
H2SM	Pull-out	0.0473	0.925	-
L0SN	Pull-through	0.0178	0.761	-
H1SN	Pull-through	0.0243	1.21	4.29
A0SN	Pull-out	0.0336	1.29	4.06
A0SL	Pull-out	0.0694	0.967	4.40
A0SN D=0.01"	Pull-out	0.0436	0.761	1.37
Sifcon D=0.01	Pull-through	0.0736	1.32	6.12
A0SN D=0.03"	Pull-through	0.0342	1.41	-
H1DN	Pull-through	3.76	5.13	13.4
A0DN	Pull-through	4.35	6.03	16.9
L2DN	Pull-hrough	2.19	5.47	14.8
L0HN	Pull-out	1.21	8.81	18.7
L1HN	Pull-out	1.69	6.93	-
L3HN	Pull-out	1.78	8.56	-
A0HN	Pull-out	2.33	10.9	23.9
A1HN	Pull-out	3.41	-	-
A0HN L=0.5"	Pull-out	2.29	10.5	16.8
H0HN	Pull-out	3.06	14.5	29.2

To compare pull-out work of different types of fibers, pull-out work values of some series of deformed and hooked fibers were normalized with respect to the pull-out work values of smooth fibers at peak load, at 0.2" end slip, and at 1" end slip . Normalization was done by dividing the pull-out work of deformed and hooked fibers by the pull-out work of smooth fibers. Table 6.10 shows these values.

Table 6.10 - Pull-out work ratios

Series	Wmax/WmaxS	W0.2"/W0.2"S	W1"/W1"S
L2DN	123	6.82	4.03
A0DN	129	4.67	4.16
L0HN	67	7.33	4.1
A0HN	69	7.73	4.2

It is observed in Table 6.10 that the pull-out work to the peak, W_{max} for smooth fibers is about 0.7% to 1.5% of the work to the peak of deformed or hooked fibers. This value increases to about 15% to 20% at 0.2 " end slip and to about 25% at 1" end slip.

6.9 DEVELOPMENT OF BOND SHEAR STRESS VERSUS SLIP RELATIONSHIP CURVES

The procedure described in Chapter V was used to predict bond shear stress versus slip relationships from the average pull-out curves. Since the development of the theory in Chapter V was based on the assumption that the bond shear stress versus slip curve is elastic with an exponentially decaying frictional zone, the $(\tau\text{-}S)$ curves predicted had the same characteristic shape. Since only selected pull-out curves were used to predict the $(\tau\text{-}S)$ curves, the bond-slip curves obtained are representative but not exact for all cases. A more accurate way of getting the bond slip curve for a given matrix-fiber combination would be to perform a point by point analysis of the pull-out curve, and for each point on the curve, get a corresponding point on the $(\tau\text{-}S)$ curve. Such a method would be substantially more complicated and numerically involved. The main parameters found for individual series using the procedure described in Chapter V, namely κ, τ_{max}, τ_f, and ξ are given in Table 6.11.

Using the parameters of Table 6.11, it is possible to predict the pull-out load versus end slip as described in Chapter V. The predicted curve can then be compared to the experimentally observed curve. Such comparisons are shown in Figs. 6.22 to 6.28. Figs. 6.28 (b), (c), and (d) show a magnified scale of the ascending branch only. It can be observed that the predicted curves are in reasonably good agreement with the experimental curves.

Table 6.11 - Pull-out Data

Series	κ (10^6 lb/in^3)	τ_{max} (psi)	τ_f (psi)	ξ
H2SF	3.69	255	223	0.053
L0SN	5.25	211	211	0.910
A1SN	5.00	200	180	0.0337
H2SL	8.79	1390	259	0.938
H2SM	1.51	285	275	1.03
H0SN	0.841	334	257	1.30
L2SN	1.65	176	172	-6.50
A0SN	3.87	210	210	-1.00
H0SL	3.13	207	202	1.06
H3SN	2.21	289	289	0.523
A2SM	1.24	209	209	5.73
H2SN	3.00	300	280	2.28

6.10 EFFECT OF FIBER AND MATRIX PARAMETERS ON THE LOAD-SLIP RELATIONSHIP

6.10.1 Effect of Matrix Strength

As shown in Fig. 6.29, for the case of hooked fibers with different matrix strength, the pull-out load increases with increasing matrix strength. For smootn fibers this increase was mostly noticeable in the ascending branch.

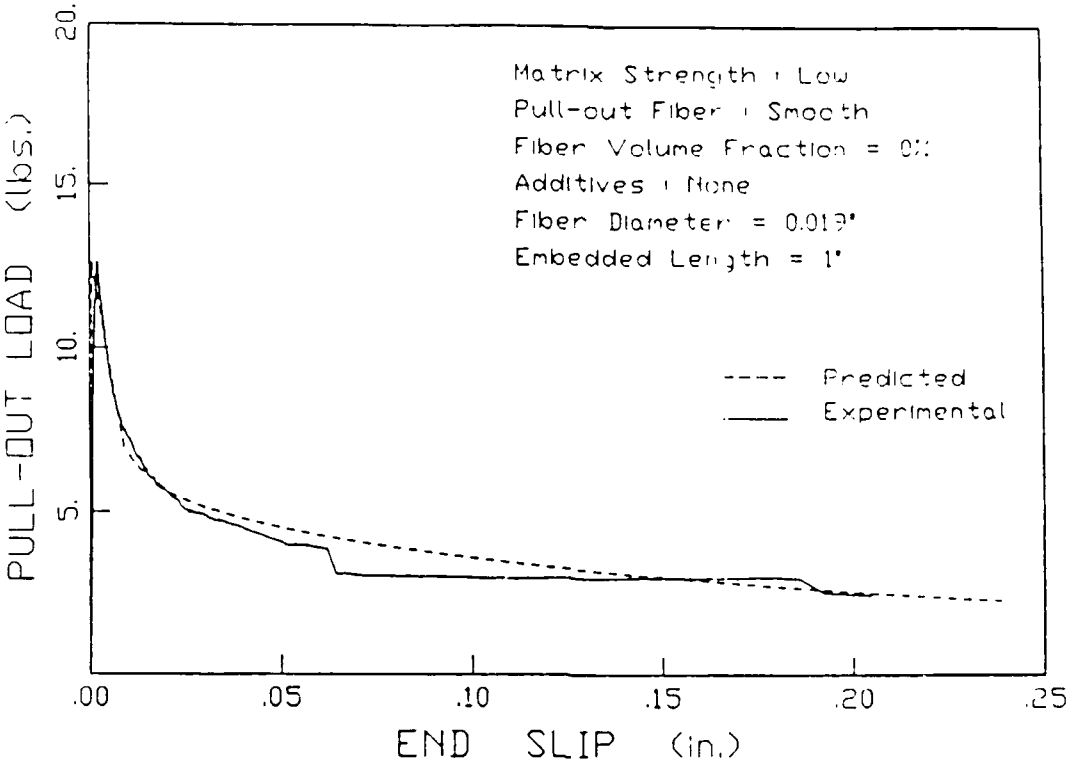

Fig. 6.22 - Experimental pull-out curve versus analytical prediction of pull-out curve of smooth fibers.

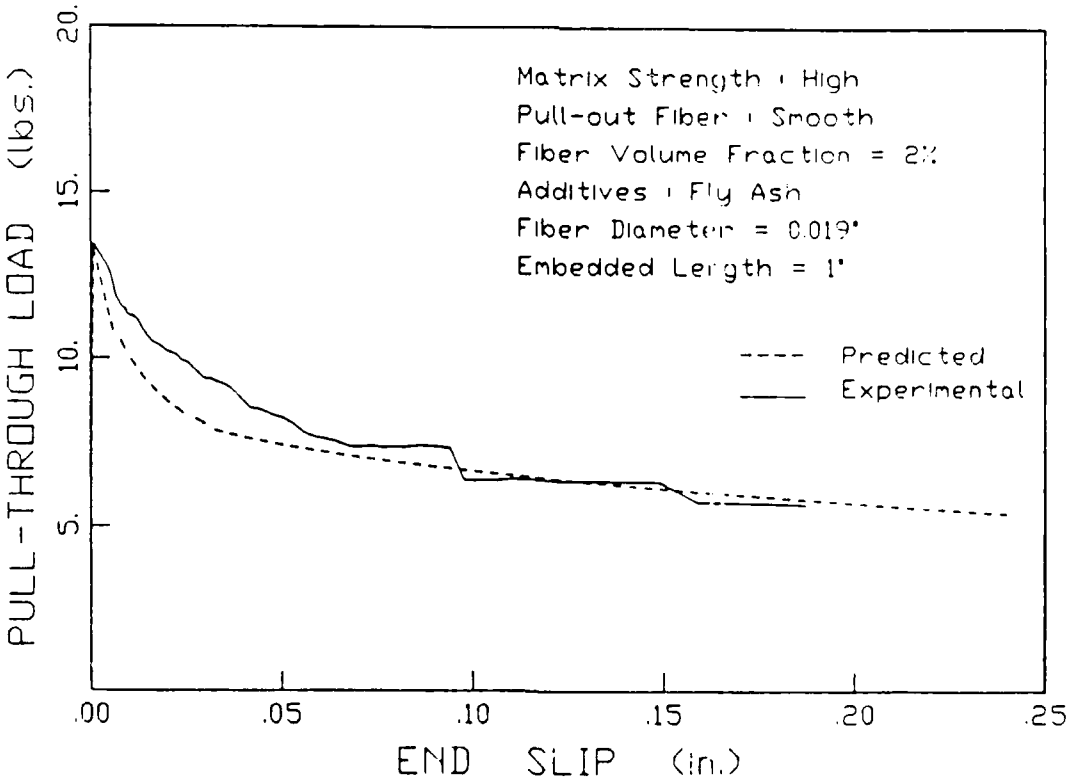

Fig. 6.23 - Experimental pull-out curve versus analytical prediction of pull-out curve of smooth fibers.

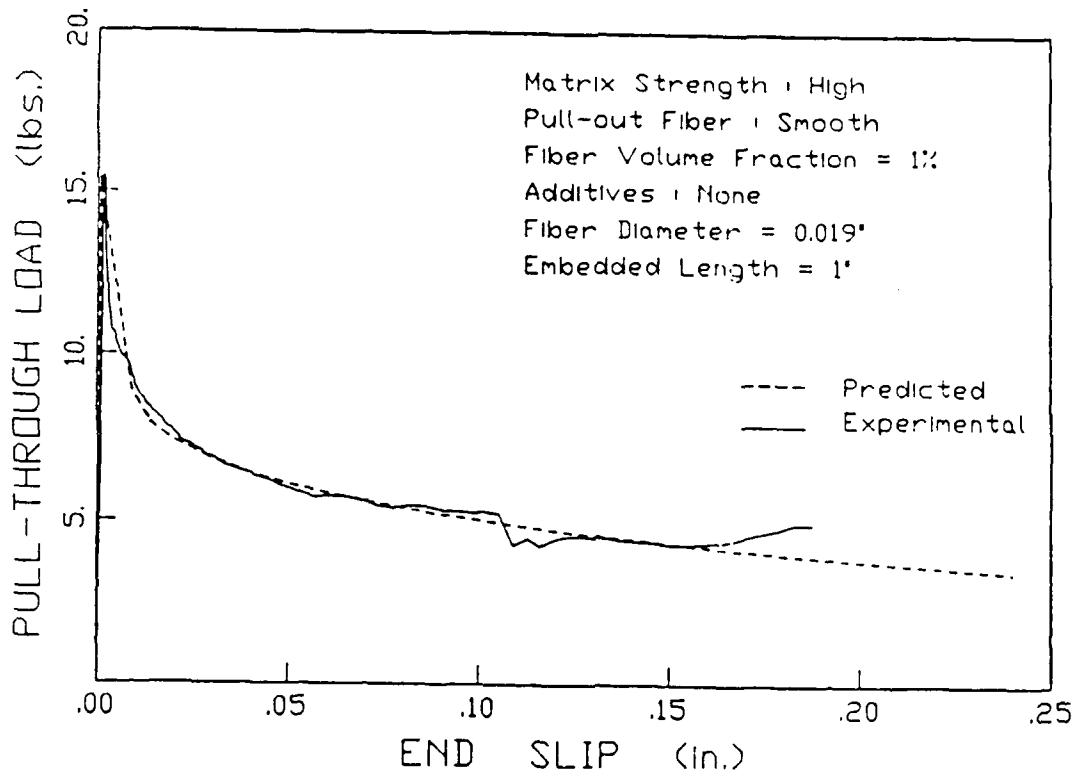

Fig. 6.24 - Experimental pull-out curve versus analytical prediction of pull-out curve of smooth fibers .

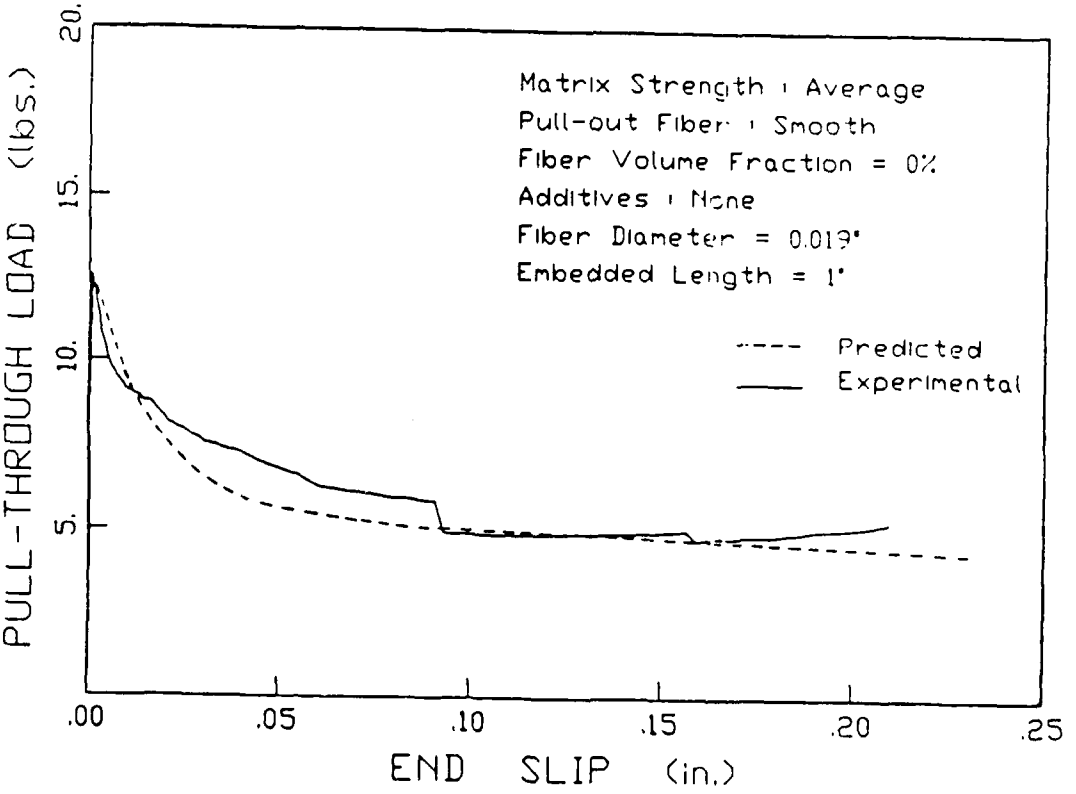

Fig. 6.25 - Experimental pull-out curve versus analytical prediction of pull-out curve of smooth fibers .

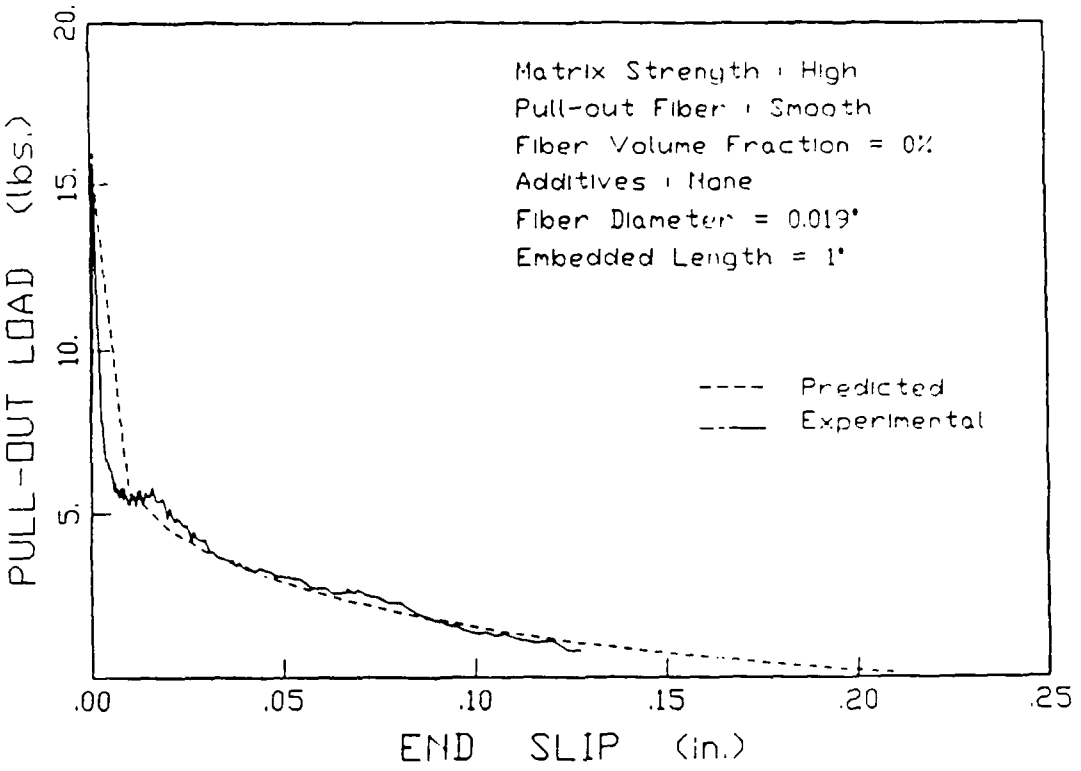

Fig. 6.26 - Experimental pull-out curve versus analytical prediction of pull-out curve of smooth fibers .

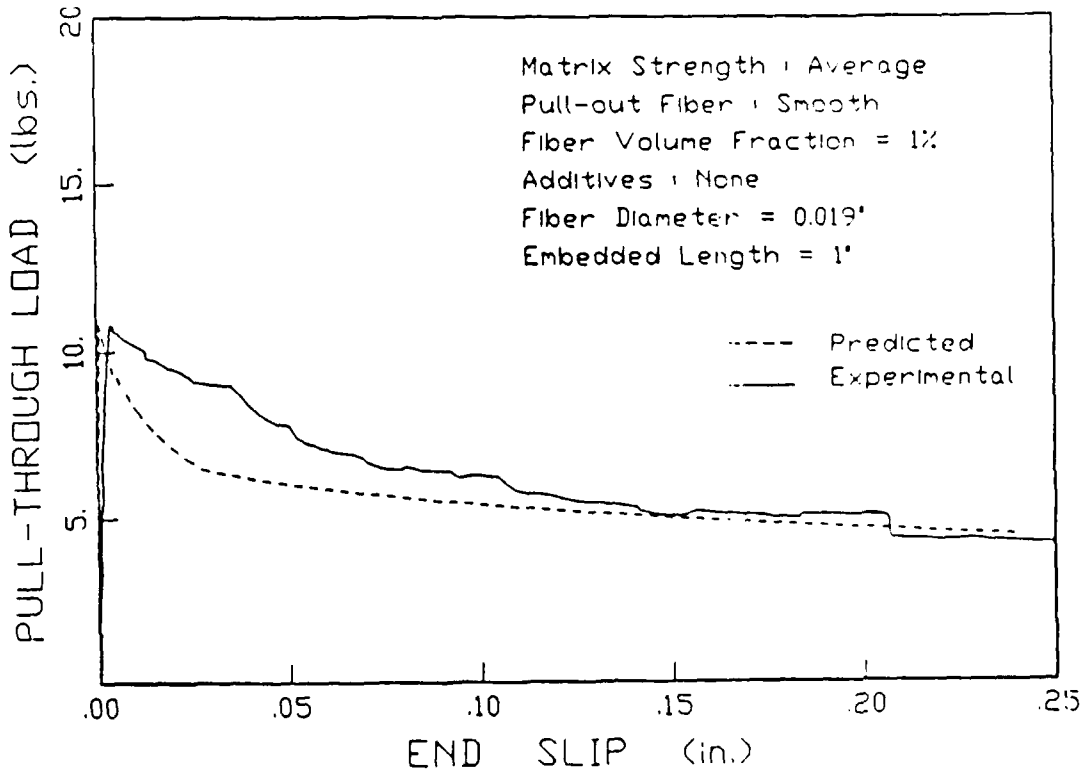

Fig. 6.27 - Experimental pull-out curve versus analytical prediction of pull-out curve of smooth fibers .

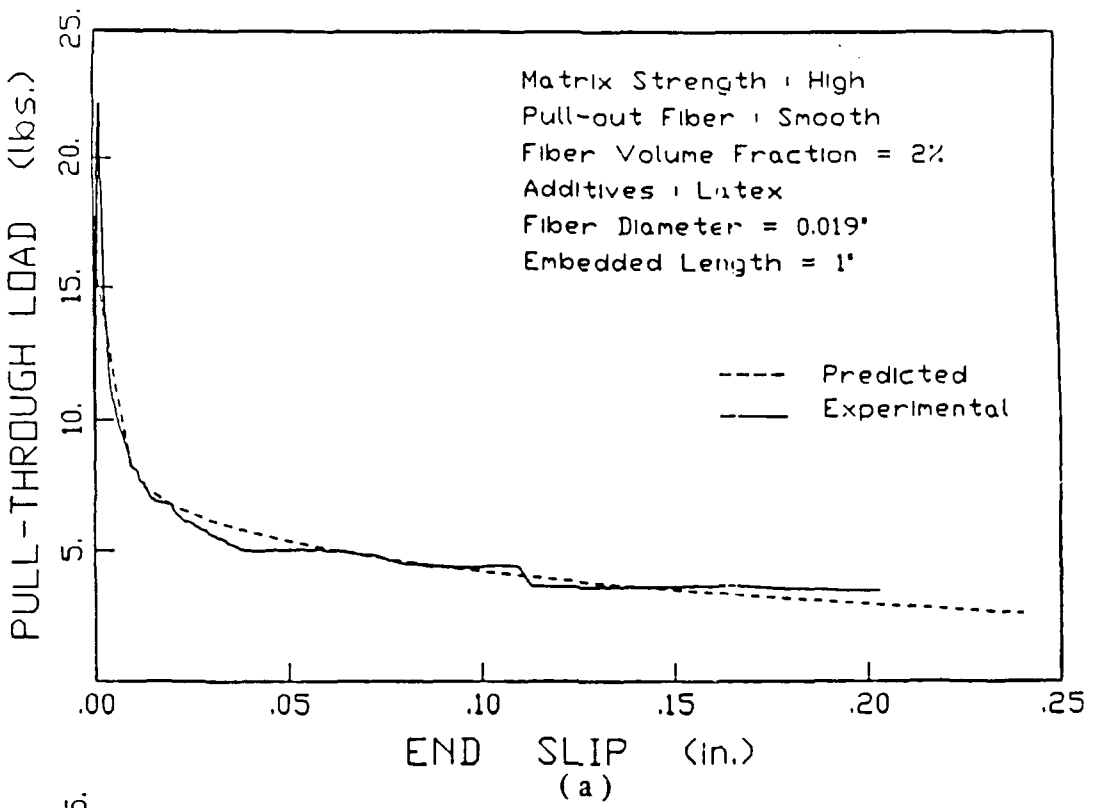

(a)

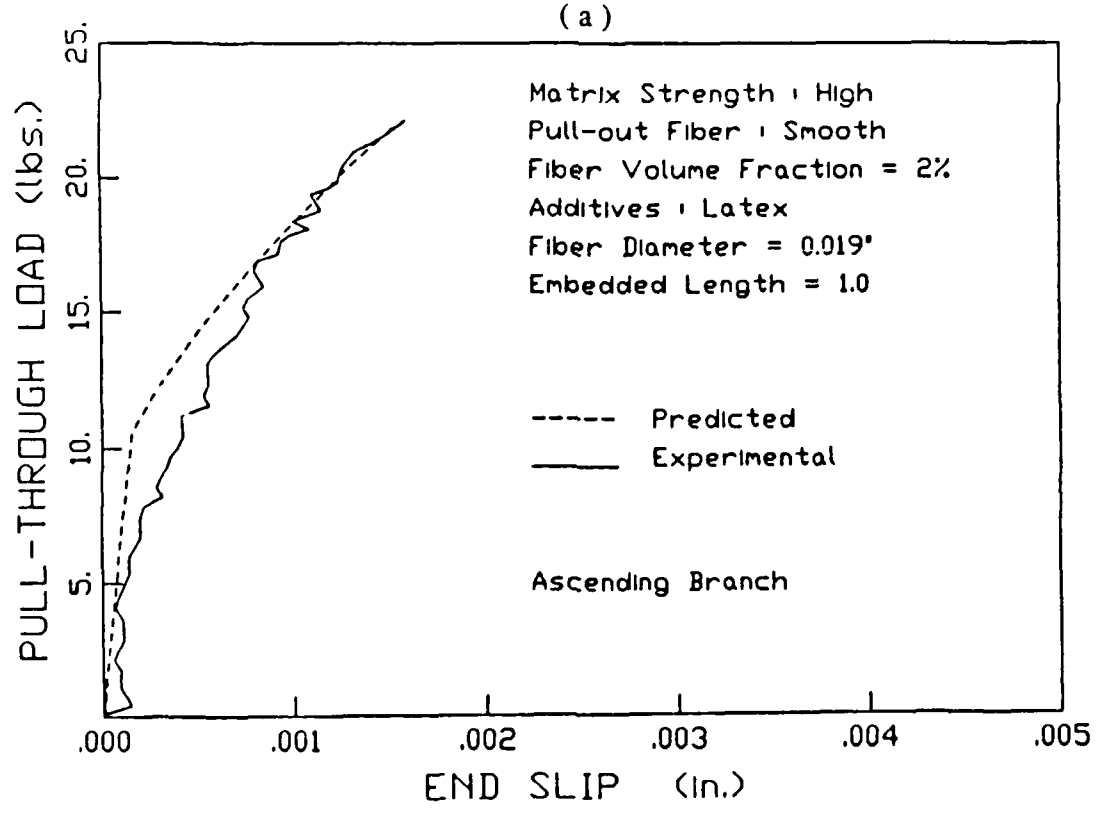

(b)

Fig. 6.28 - Experimental pull-out curve versus analytical prediction of pull-out curve of smooth fibers .

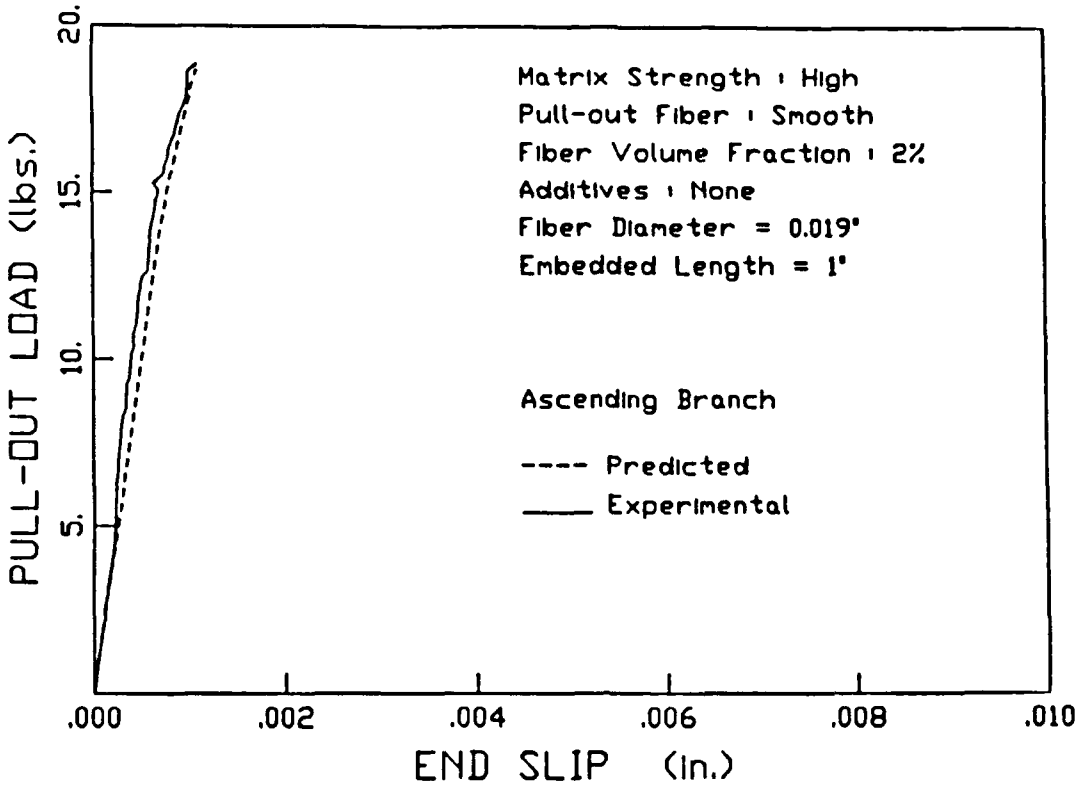

(c)

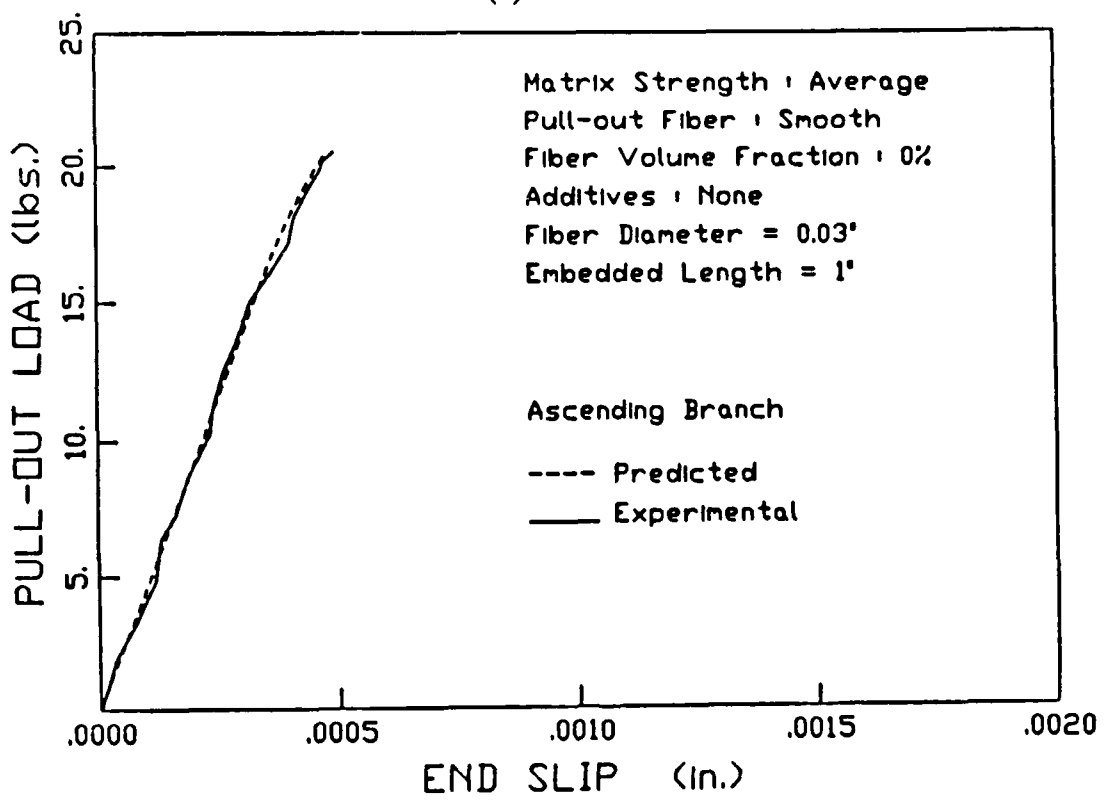

(d)

Fig. 6.28 - Experimental pull-out curve versus analytical prediction of pull-out curve of smooth fibers up to the peak load

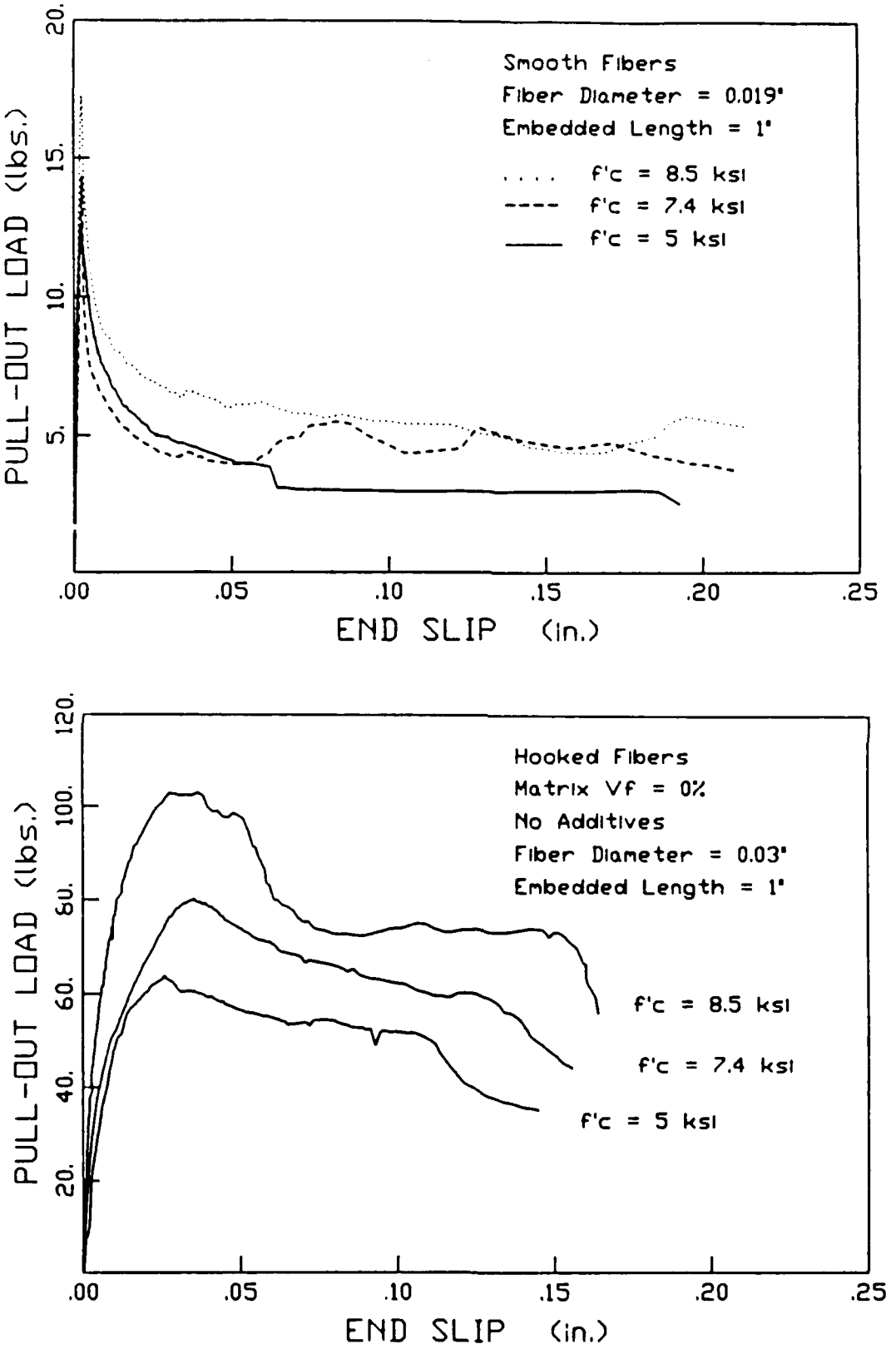

Fig 6.29 - Effect of matrix strength on pull-out load end slip relationship.

6.10.2 Effect of Fiber Volume Fraction

The effect of fiber volume fraction is shown in Fig. 6.30 . This effect seems to be rather insignificant. It can be observed that an increase up to 3% in fiber volume fraction increases the pull-out load by about 10%, while it leads in the post-peak range to a slight increase in the fiber resistance to pull-out. This trend was not clear when compared to the variability of results observed. It seems that the pull-out fibers, being much smaller in diameter than ordinary reinforcement, probably do not cause appreciable damage to the surrounding concrete upon pull-out; thus adding some fibers to the matrix may not add much to the interfacial bond strength between the fiber and the matrix .

When SIFCON matrices were used [Vf = 11%], considerable improvement in the interfacial bond strength between the fiber and the matrix was observed, both before debonding and after debonding . An increase of 20% to 25% in the pull-out load was observed before debonding and 75% to 80% increase was observed after debonding . The presence of fibers in the matrix in such high percentages seems to provide an additional bond component, namely fiber interlock. Such an arrangement provides excellent confinement to the mortar which considerably increases the interfacial bond strength and the pull-out work. Also it helps reduce frictional decay in the descending branch of the curve. Fig. 6.31 shows a typical pull-out load versus end slip curve using plain and SIFCON matrices .

6.10.3 Effect of Additives

The effect of additives is presented in Fig. 6.32. In terms of maximum pull-out load values, Latex was found to yield the highest values, followed by Fly ash . Microsilica did not seem to improve the interfacial bond strength and the test series was repeated twice to ascertain this result. With Latex a 50% to 60% increase in the pull-out load was observed over plain matrix; this remarkable increase in pull-out load leads to a rapid drop in the load at debonding as was observed with high strength matrices . After complete debonding, the load remains almost constant in the

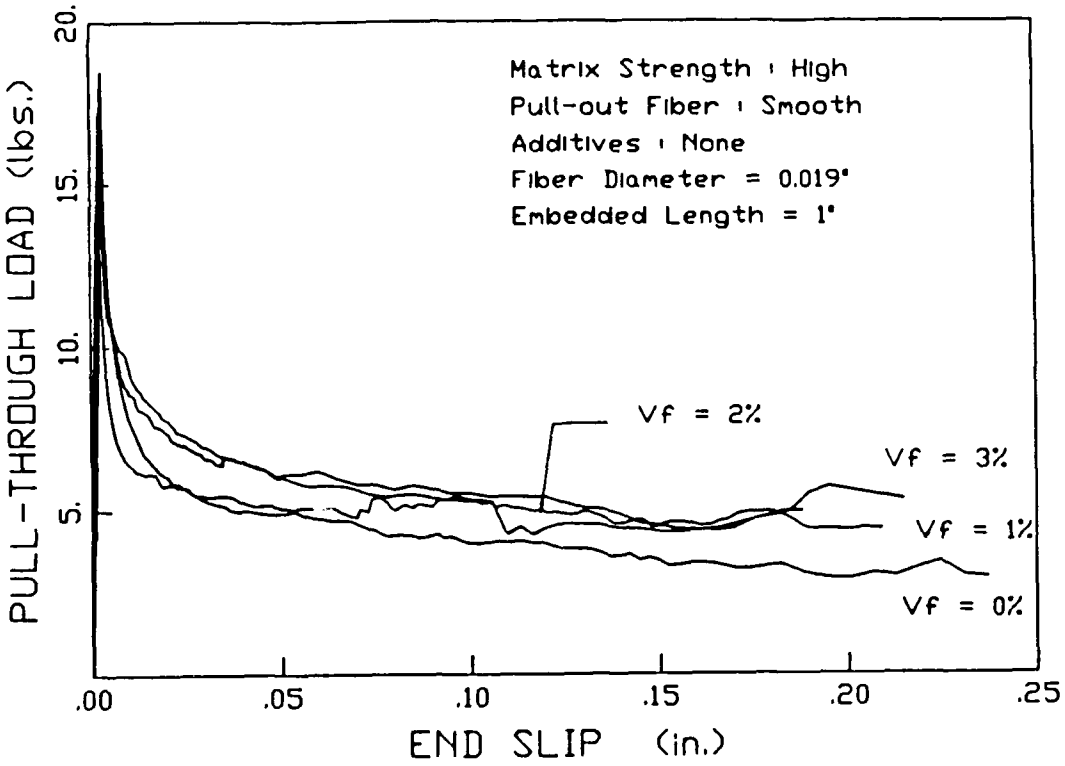

Fig. 6.30 - Effect of fiber volume fraction on pull-out load slip relationship of smooth fibers .

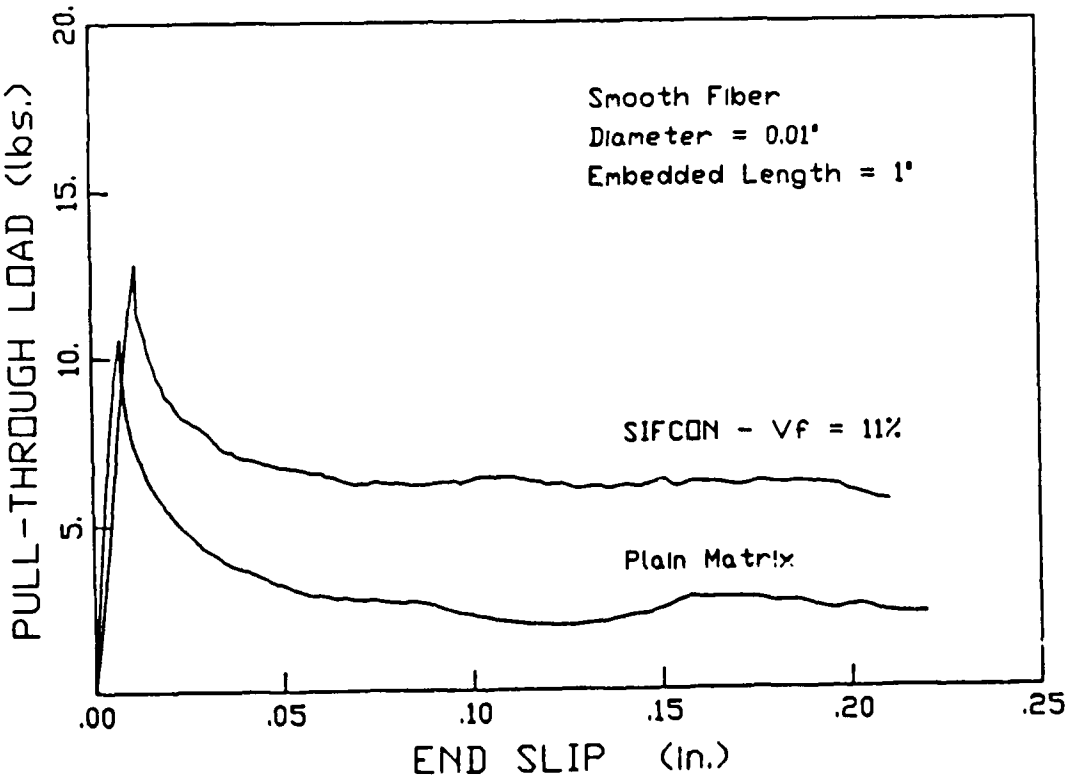

Fig. 6.31 - Effect of SIFCON matrix on pull-out load slip behaviour of smooth fibers .

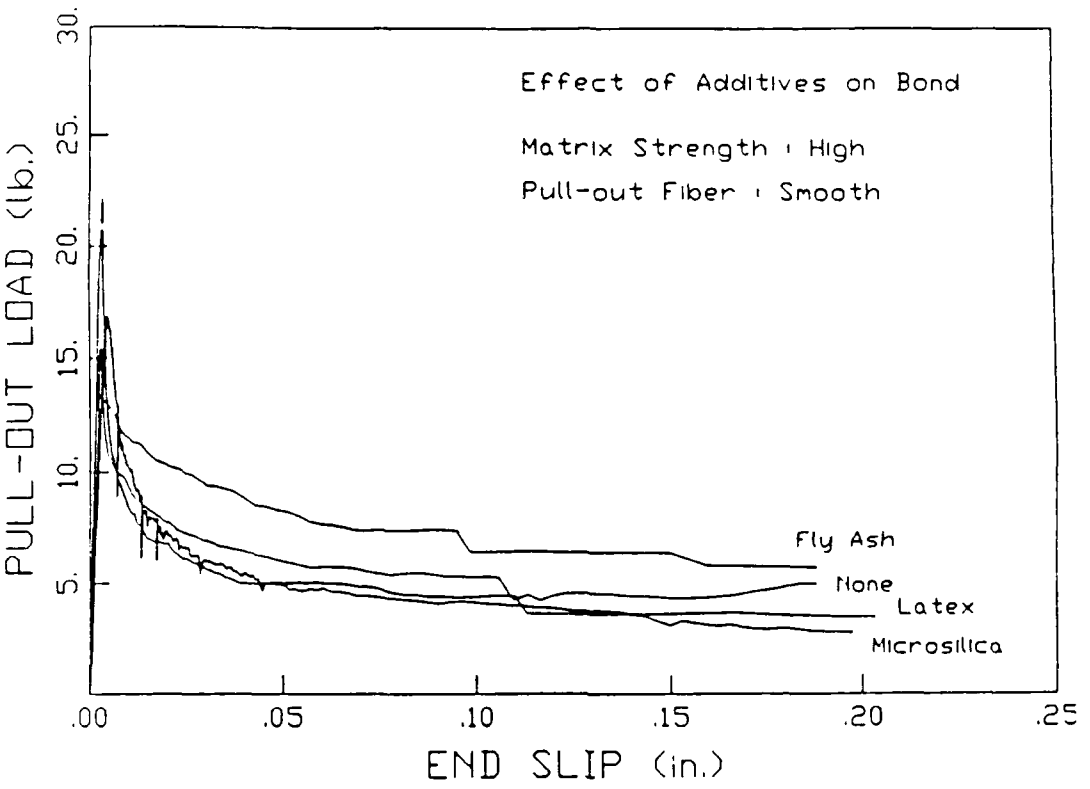

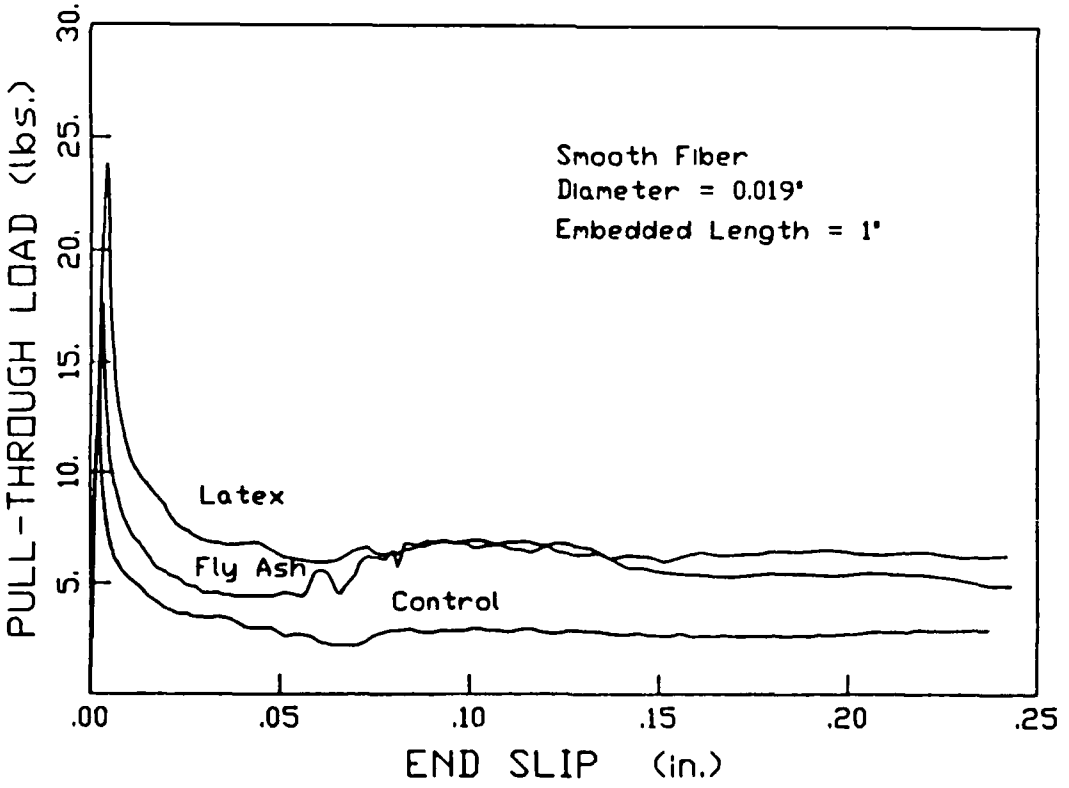

Fig. 6.32 - Effect of additives on pull-out slip relationship of smooth fibers .

frictional phase. Fly ash increased the maximum pull-out load by 10% to 20% and was more effective than Latex in improving friction forces.

6.10.4 Effect of Fiber Diameter

Pull-out load versus end slip curves for fibers of different diameters are shown in Fig. 6.33 . A change in fiber diameter did not affect the pul-out load -end slip behavior of smooth fibers. Elastic strains in the free portion of the fiber decreased as fiber diameter was increased although the pull-out load increased . It was observed that the load-slip measurements became more sensitive to fiber curvature as the diameter increases.

6.10.5 Effect of Fiber Embedment Length

The effect of fiber embedment length on bond strength is shown in Figs. 6.34 , 6.35, and 6.36. It was observed that the ascending branch of the curve is less sensitive to the fiber embedment length than the descending branch for smooth fibers. The pull-out load end slip relationship exhibited the same behaviour in both cases for the three different types of fibers. In hooked fibers, since the hook contributed most to the pull-out load, changing the embedment length from 0.5" to 1" did little to the ascending portion of the curve. However, in deformed fibers , since the number of surface indentations increase with the increase in embedment length, changing the embedment length from 0.5" to 1" approximately doubled the value of loads in the ascending branch.

6.10.6 Contribution of Surface Indentations and End Hooks

6.10.6.1 Surface Indentations. In one series of deformed fibers, the pull-out fibers were greased on the surface to isolate the effect of surface indentations. The average pull-out curve versus end slip of this series was then superimposed on the pull-out curve versus end slip of a smooth fiber of same diameter. The resulting pull-out curve versus end slip curve was compared to the experimentally observed curve of deformed fibers. Such a comparison is shown in Fig. 6.37. It is observed that the two curves are quite similar . The difference between the two curves can be attributed to

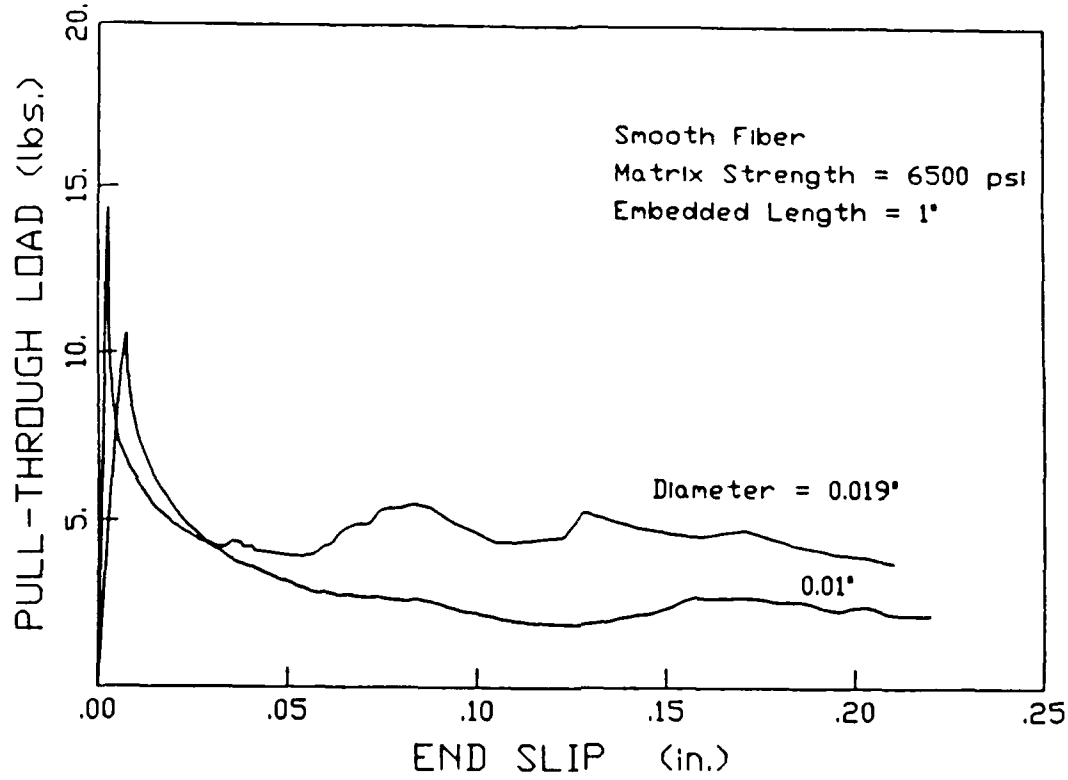

Fig. 6.33 - Effect of fiber diameter on pull-out slip relationship of smooth fibers .

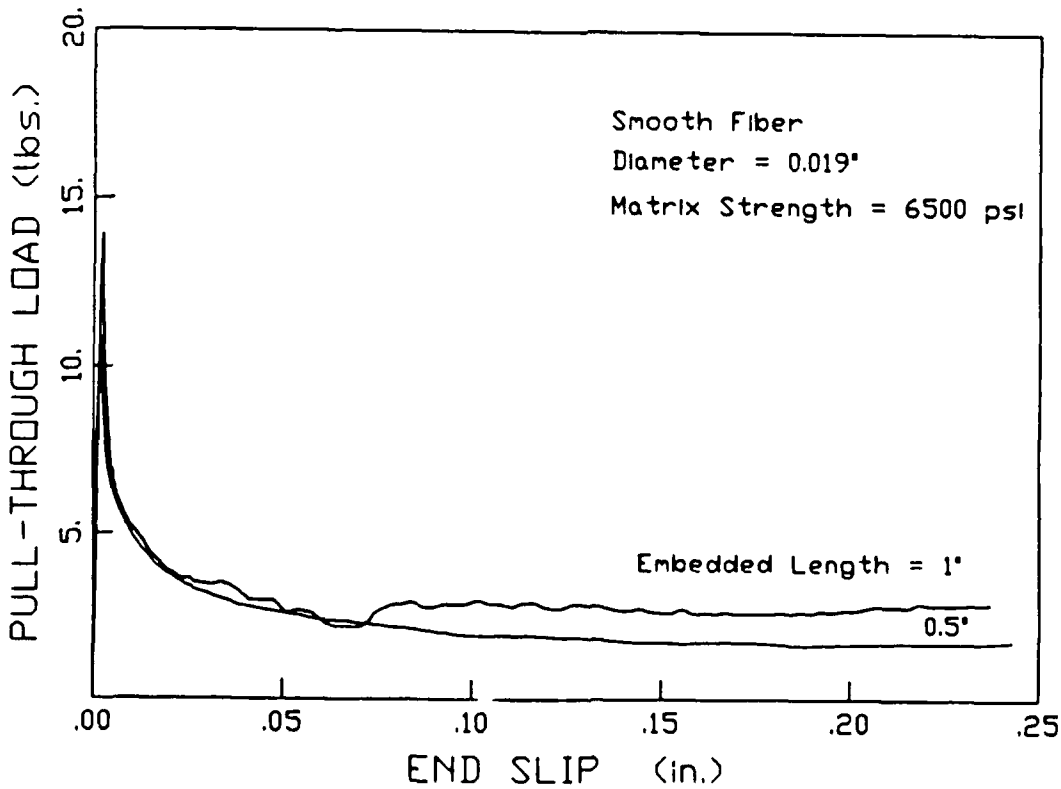

Fig. 6.34 - Effect of fiber embeddment length on pull-out load slip behaviour of smooth fibers .

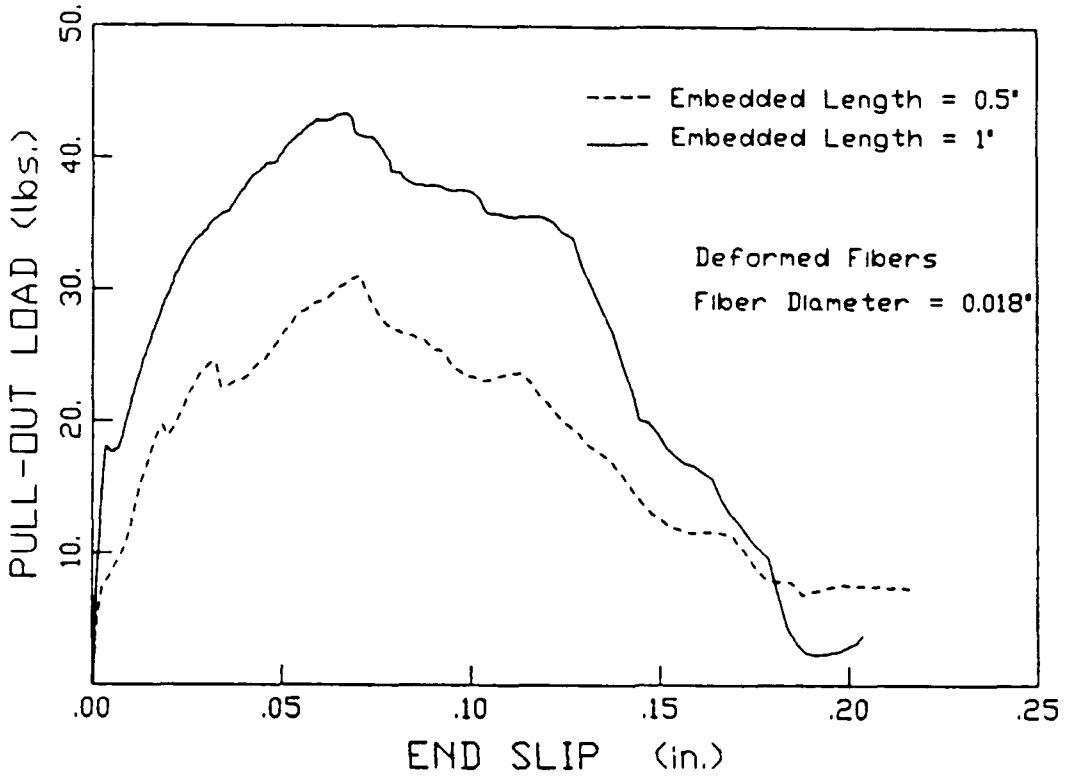

Fig. 6.35 - Effect of fiber embeddment length on pull-out load slip behaviour of deformed fibers .

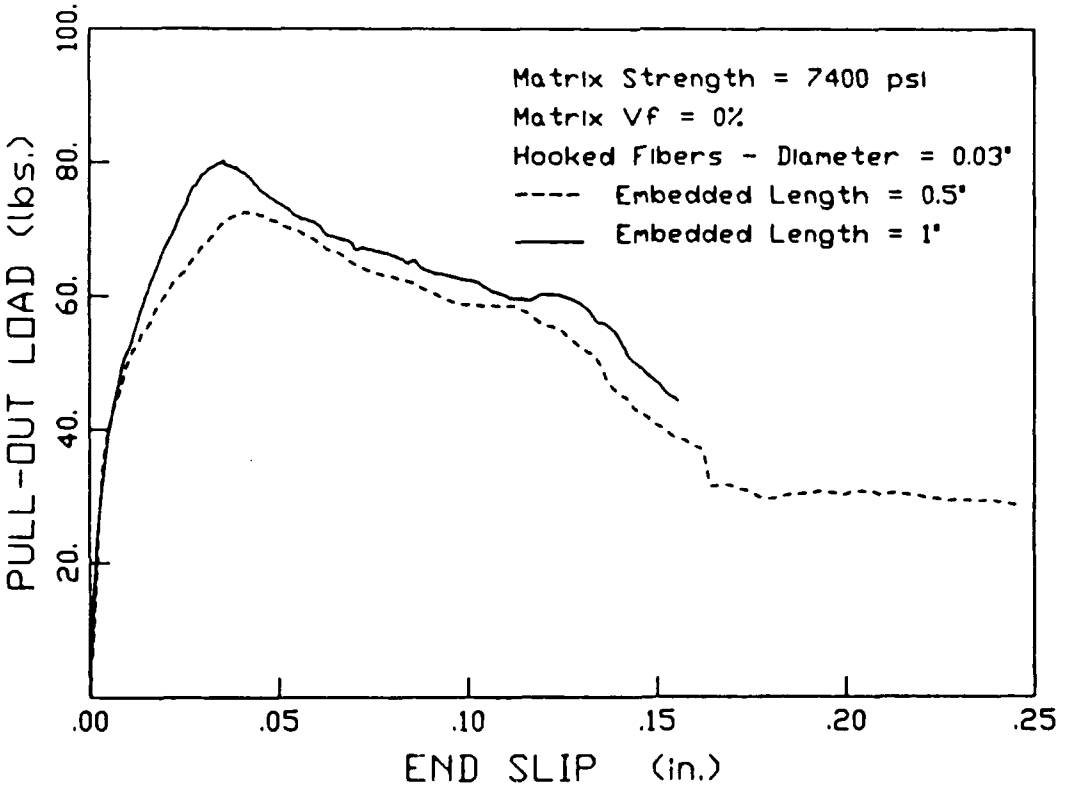

Fig. 6.36 - Effect of fiber embeddment length on pull-out load slip behaviour of hooked fibers .

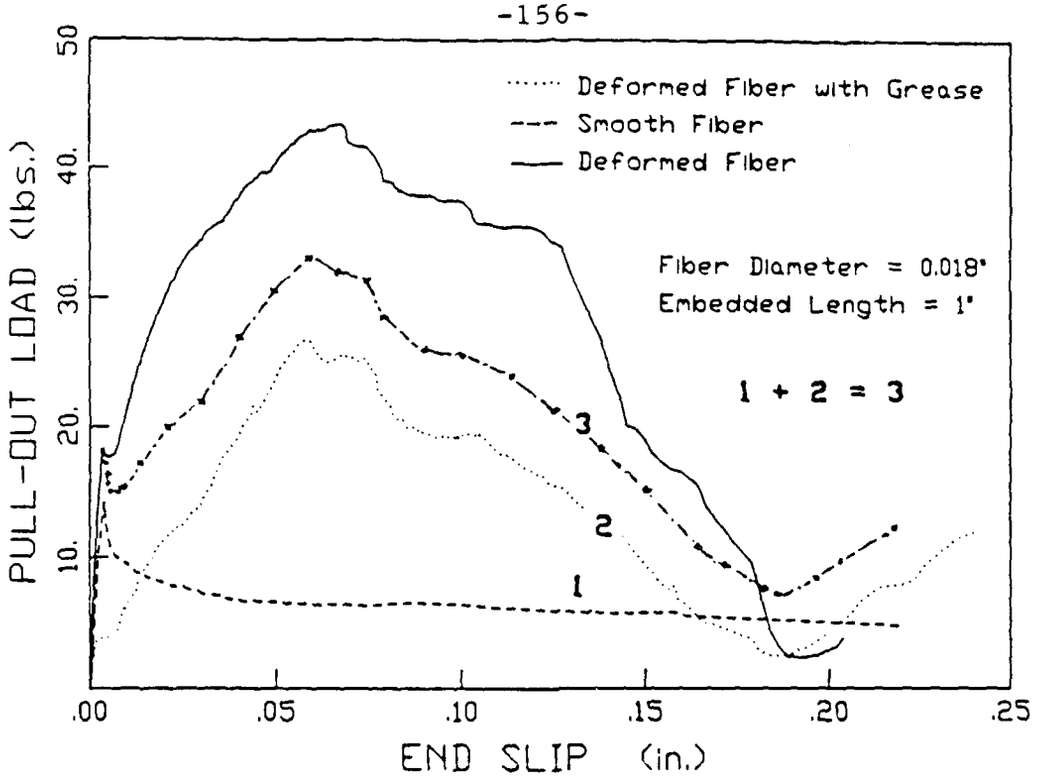

Fig. 6.37 - Experimental pull-out curve versus superposition pull-out curve of deformed fibers.

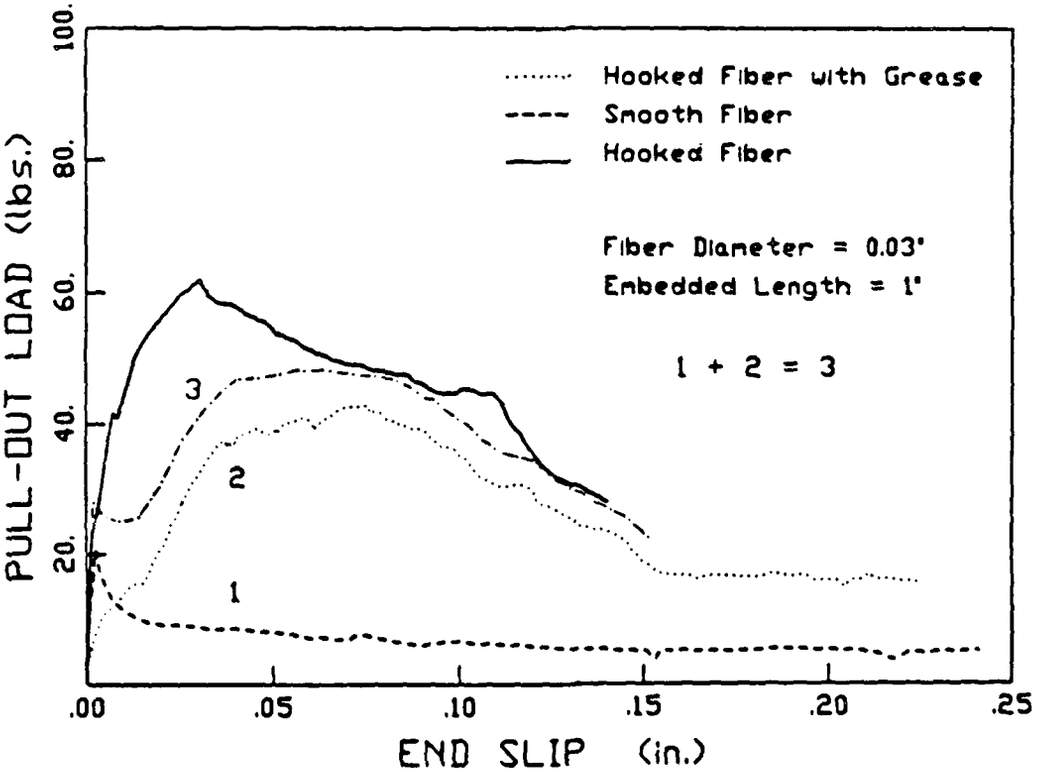

Fig. 6.38 - Experimental pull-out curve versus superposition pull-out curve of hooked fibers.

the variability in experimental data and to the non- uniformity of grease distribution on the fiber surface.

6.10.6.2 End Hooks. In one series of hooked fibers, the pull-out fibers were greased on the surface to isolate the contribution of the end hook to the pull-out load. The average pull-out load versus end slip of this series was then superimposed on the pull-out load versus end slip curve of a smooth fiber of same diameter. Similar to deformed fibers, the resulting curve was compared to the experimentally observed curve. Such comparison is shown in Fig. 6.38. Here also, the two curves are in reasonably good agreement.

6.10.7 Stress Levels in Pull-out Fibers

The pull-out load of the average curve of one series of smooth, deformed, and hooked fibers was divided by the corresponding fiber area [$(\Pi*d*d)/4$] to obtain the fiber axial stress. Fig. 6.39 shows the values of fiber stresses versus slip for the three types of fibers. It is observed that the stress levels in smooth fibers are much smaller than those of deformed or hooked fibers. Many deformed fibers failed during pull-out because stress levels were close to the failure stress of the fiber ($\sigma \sim \sigma_u$ = 170 ksi). For hooked fibers , the fiber stress varied from 100 to 150 ksi approximately.

6.11 GENERAL OBSERVATIONS AND CONCLUSIONS

From the results of this limited experimental study, the following conclusions can be drawn:

1. Hooked fibers and deformed fibers have higher resistance to pull-out than smooth fibers because of the mechanical contribution of end hook and surface deformations respectively. At larger slips, deformed fibers provide oscillatory resistance to pull-out , while the resistance of hooked fibers continues to decrease as the end hook straightens out . Smooth fiber resistance to pull-out also decreases but at a faster rate than deformed or hooked fibers .

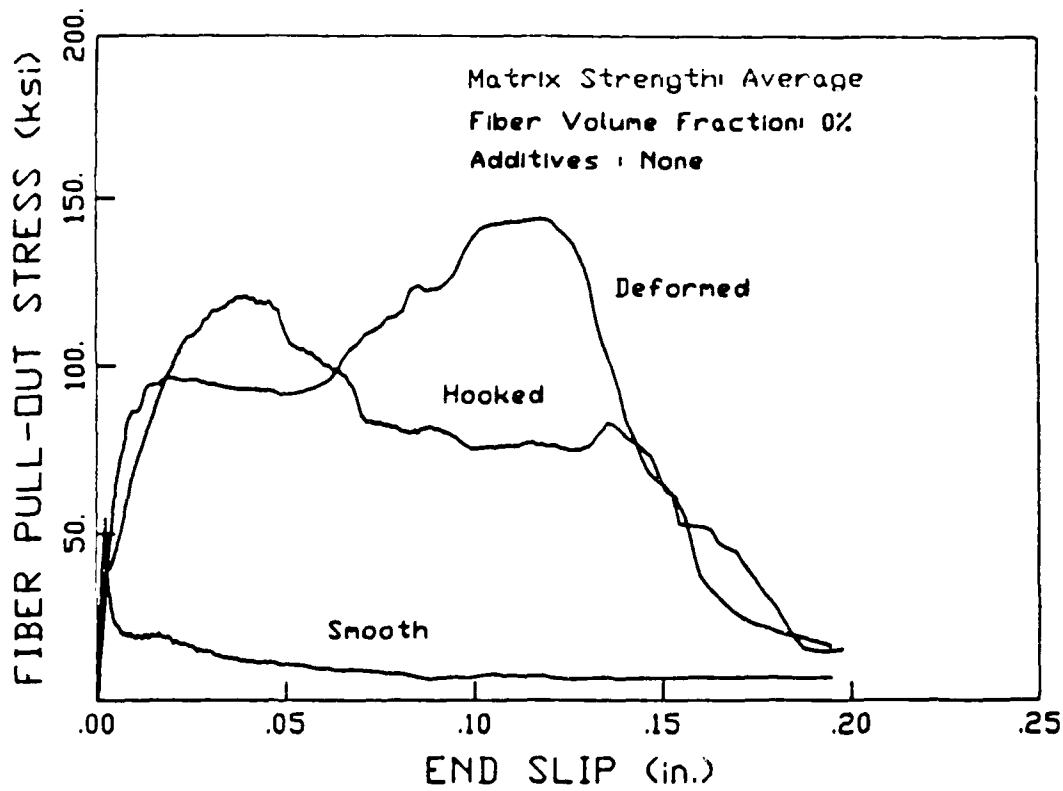

Fig. 6.39 - Stress levels in pull-out fibers.

2. As matrix strength increases, the bond between the fiber and the matrix increases. However, debonding following the peak load is much faster for high strength matrices .

3. Fiber volume fraction in the matrix has little effect on the bond between the fiber and the matrix . An increase of 10% to 15% in the maximum pull-out load was observed as the fiber volume fraction increases from 0% to 3% . A similar trend was observed in the post peak range.

4. The presence of latex emulsion and fly ash in the matrix, was found to improve the bond at the fiber matrix interface. However, latex was much more effective than fly ash. The addition of microsilica did not lead to any noticeable improvement in the bond strength at the interface .

5. The pull-out work of smooth fibers is significantly smaller than that of deformed or hooked fibers. It was also observed that, in the case of smooth fibers, the amount of pull-out work to the peak load was a small fraction of the total pull-out work. This means that, in the case of smooth fibers, the work provided by frictional forces is larger than that provided by the forces of initial adhesion. For hooked or deformed fibers on the other hand, the fraction of the pull-out work to the peak load was larger than for smooth fibers, and the work contributed by the mechanical forces was dominant. Everything else being equal, the pull-out work up to the complete pull-out of smooth fibers is only about 15% to 20% of that of hooked or deformed fibers.

6. Bond shear stresses increase with an increase in matrix strength, and are affected by the type of pull-out fiber used. For smooth fibers, maximum bond stresses were found to range from 176 to 334 psi, and frictional stresses ranged from 172 to 289 psi. A maximum bond stress of up to 1390 psi was observed when latex was used.

7. The fiber diameter and fiber embedment length did not affect the characteristics of the pull-out load versus end slip relationship.

8 The bond shear stress slip relationship of hooked and deformed fibers can be decomposed into two parts: one due to the interfacial bond of the smooth surface of the fiber, and the other is provided by the end hooks in case of hooked fibers or by surface indentations in the case of deformed fibers.

Appendix VI A

"Additional Experimental Load-Slip Curves"

Notes

1- For all Smooth Fibers, the Diameter is 0.019" and the Embedded Length is 1" except where indicated otherwise.
2- For all Deformed Fibers, the Diameter is 0.018" and the Embedded Length is 1" except where indicated otherwise.
3- For all Hooked Fibers, the Diameter is 0.03" and the Embedded Length is 1" except where indicated otherw

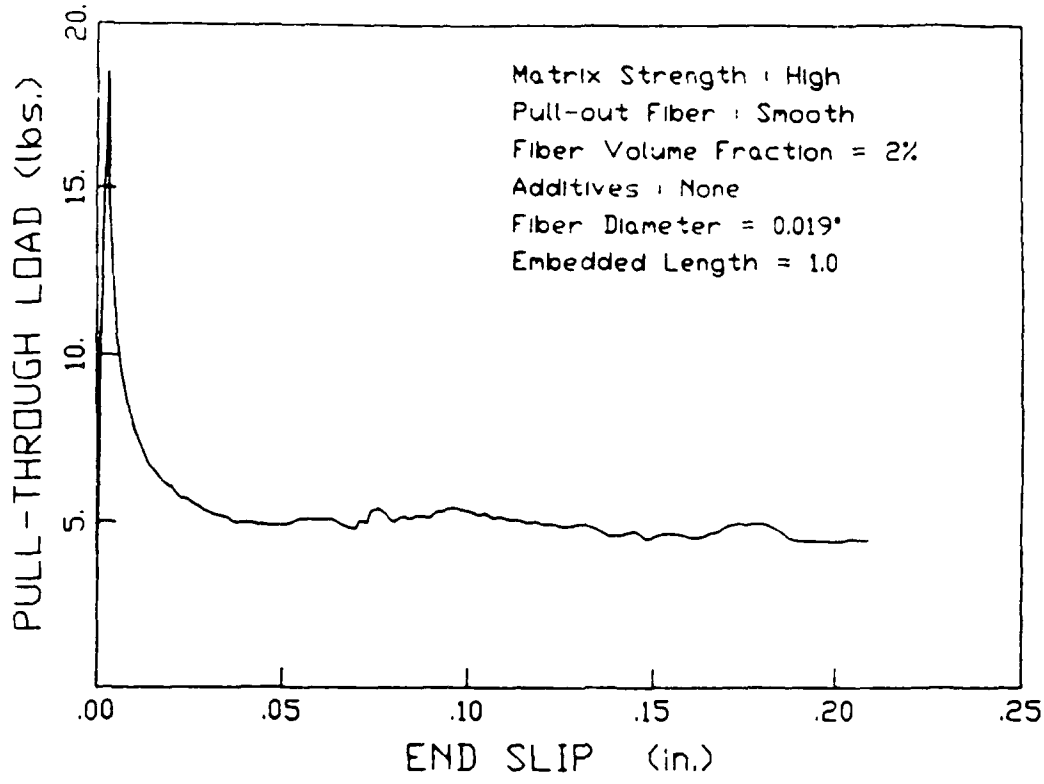
Matrix Strength : High
Pull-out Fiber : Smooth
Fiber Volume Fraction = 2%
Additives : None
Fiber Diameter = 0.019"
Embedded Length = 1.0
PULL-THROUGH LOAD (lbs.)
20.
15.
10.
5.
.00
.05
.10
.15
.20
.25
END SLIP (in.)

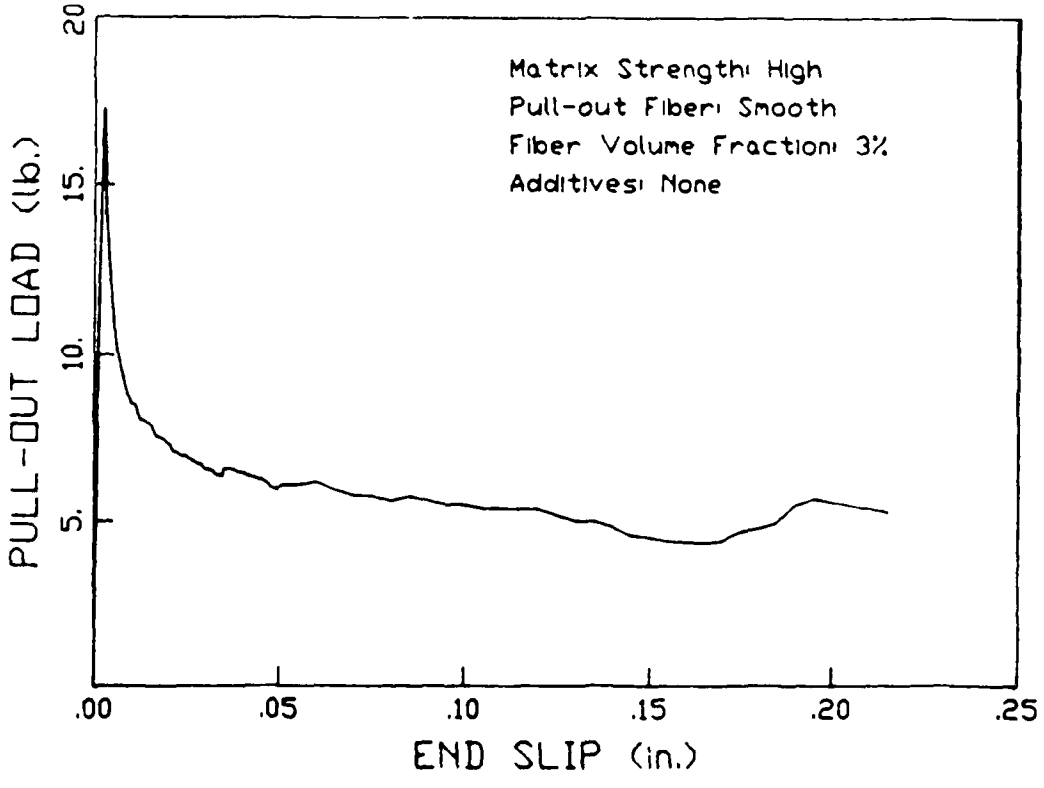
Matrix Strength: High
Pull-out Fiber: Smooth
Fiber Volume Fraction: 3%
Additives: None
PULL-OUT LOAD (lb.)
20
15.
10.
5.
.00
.05
.10
.15
.20
.25
END SLIP (in.)

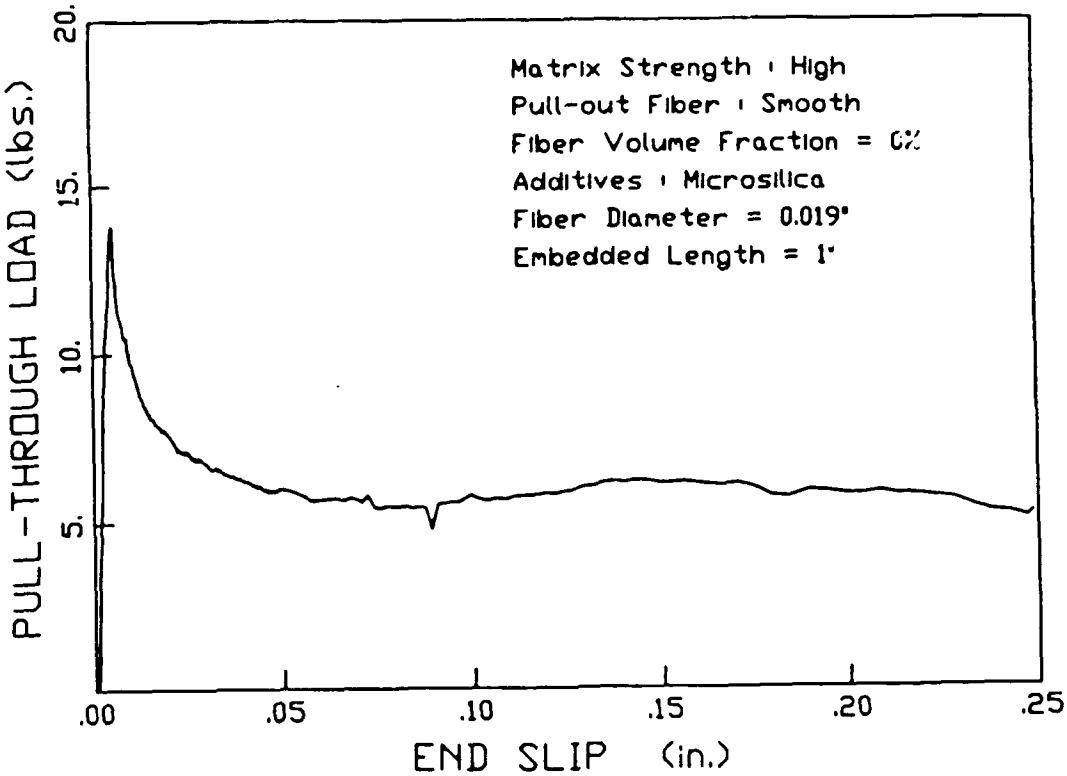
Matrix Strength : High
Pull-out Fiber : Smooth
Fiber Volume Fraction = 0%
Additives : Microsilica
Fiber Diameter = 0.019"
Embedded Length = 1"
PULL-THROUGH LOAD (lbs.)
20.
15.
10.
5.
.00
.05
.10
.15
.20
.25
END SLIP (in.)

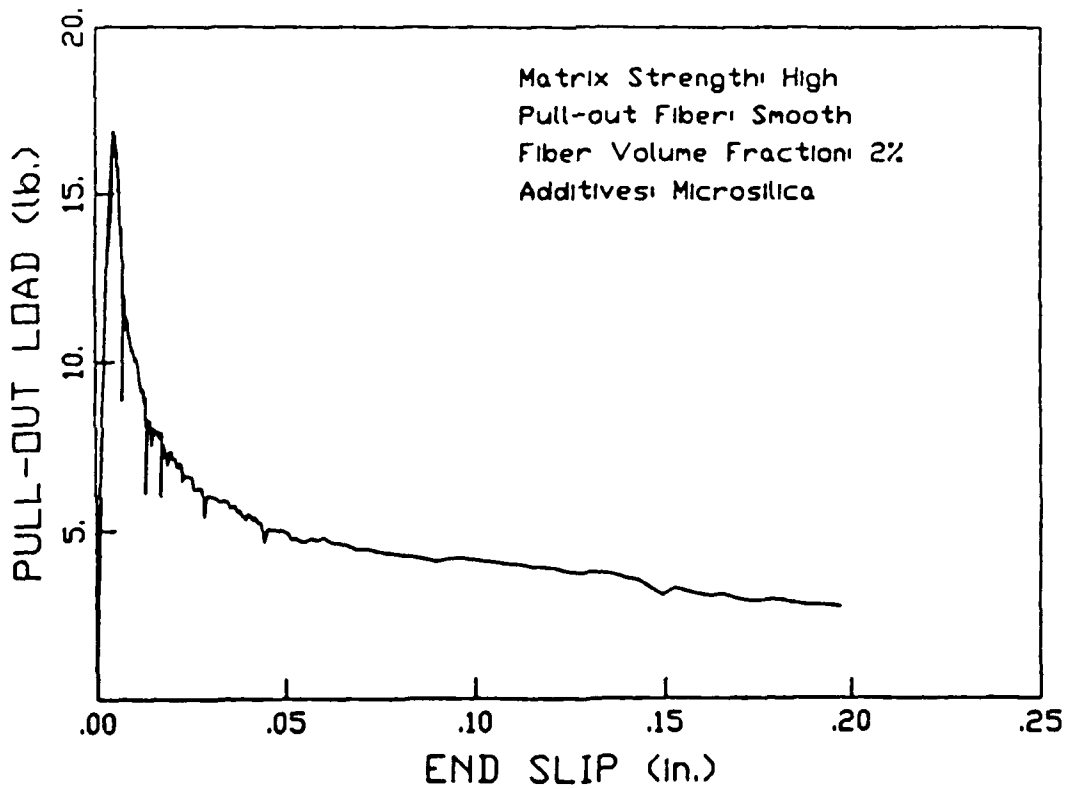
Matrix Strength: High
Pull-out Fiber: Smooth
Fiber Volume Fraction: 2%
Additives: Microsilica
PULL-OUT LOAD (lb.)
20.
15.
10.
5.
.00
.05
.10
.15
.20
.25
END SLIP (in.)

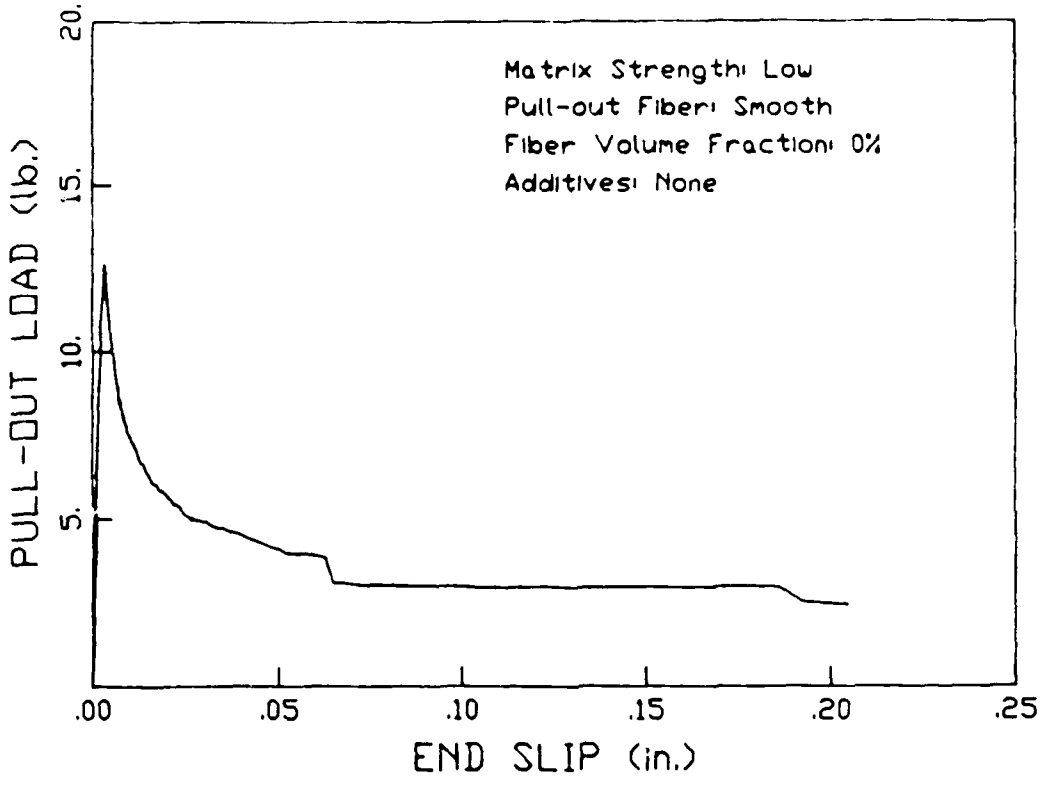
Matrix Strength: Low
Pull-out Fiber: Smooth
Fiber Volume Fraction: 0%
Additives: None
PULL-OUT LOAD (lb.)
20.
15.
10.
5.
.00
.05
.10
.15
.20
.25
END SLIP (in.)

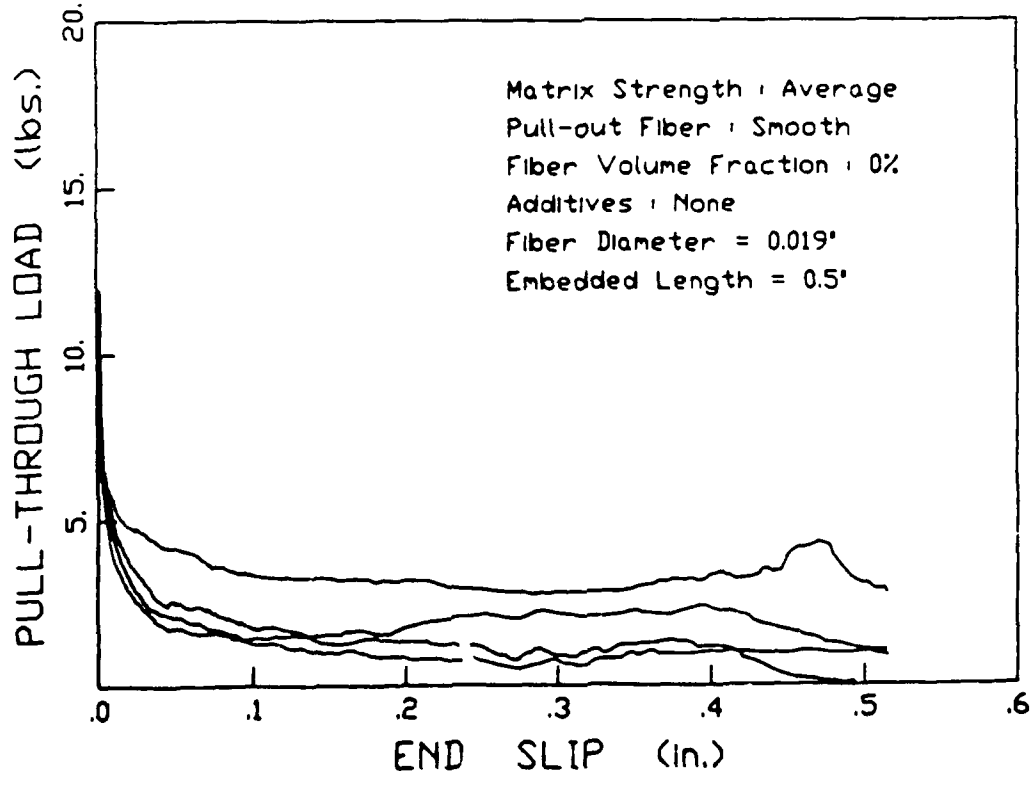
Matrix Strength : Average
Pull-out Fiber : Smooth
Fiber Volume Fraction : 0%
Additives : None
Fiber Diameter = 0.019"
Embedded Length = 0.5"
PULL-THROUGH LOAD (lbs.)
20.
15.
10.
5.
.0
.1
.2
.3
.4
.5
.6
END SLIP (in.)

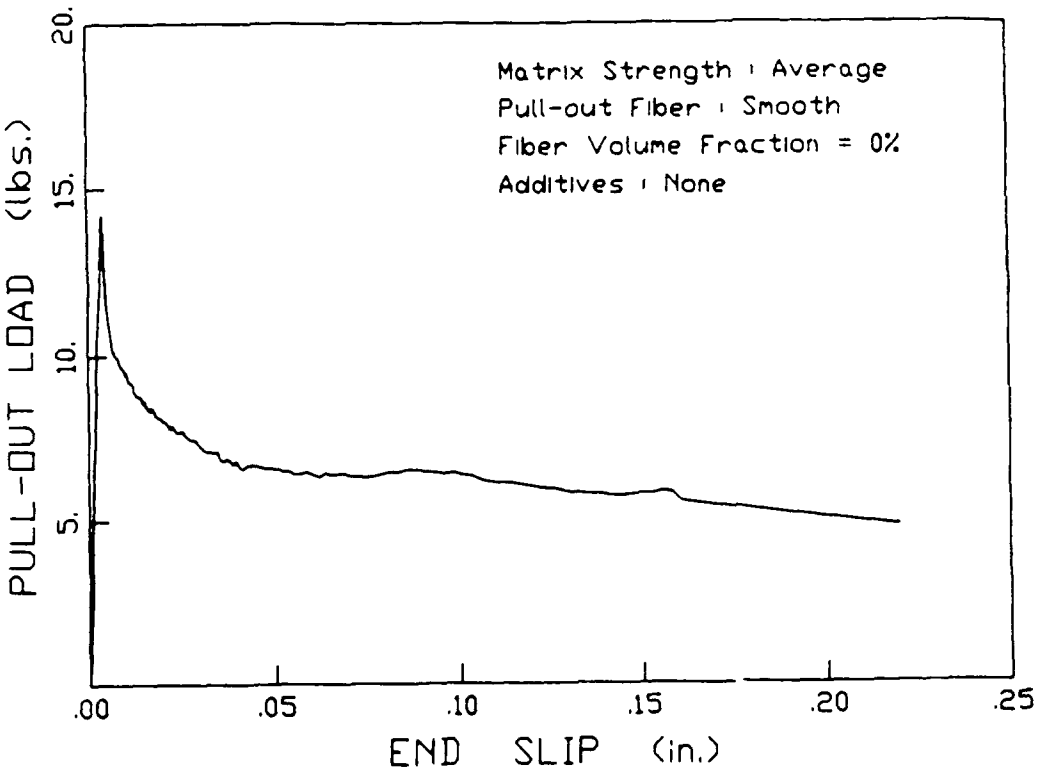
Matrix Strength : Average
Pull-out Fiber : Smooth
Fiber Volume Fraction = 0%
Additives : None
PULL-OUT LOAD (lbs.)
20.
15.
10.
5.
.00
.05
.10
.15
.20
.25
END SLIP (in.)

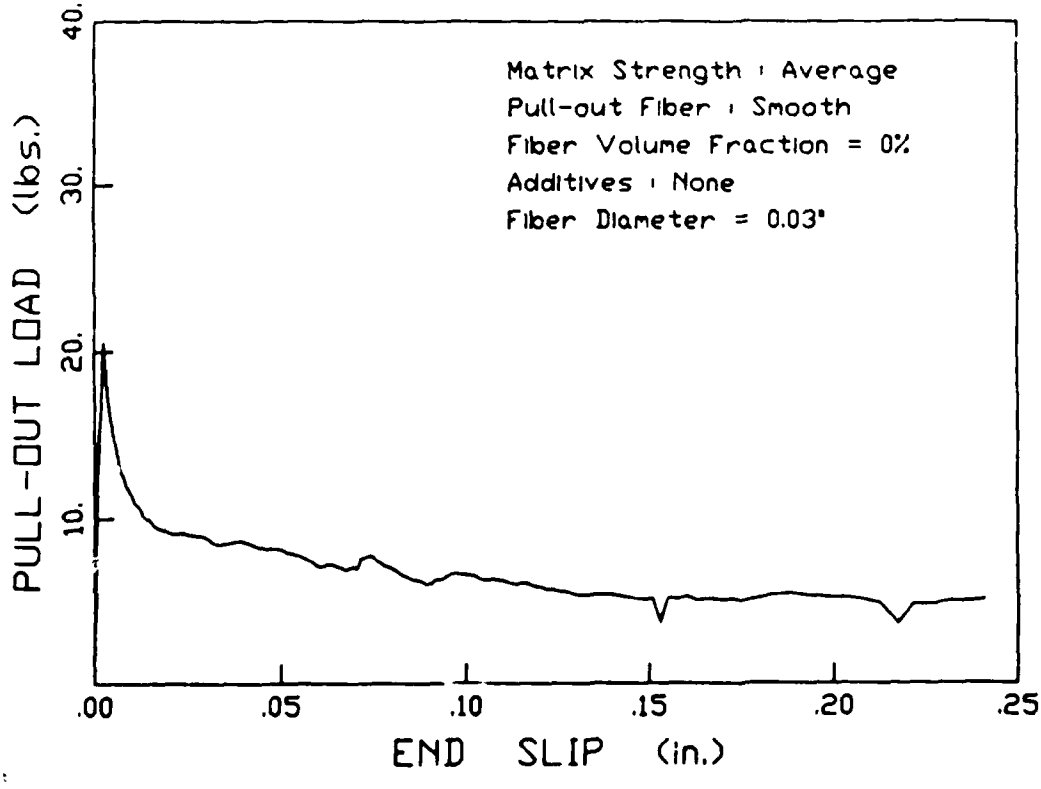
Matrix Strength : Average
Pull-out Fiber : Smooth
Fiber Volume Fraction = 0%
Additives : None
Fiber Diameter = 0.03"
PULL-OUT LOAD (lbs.)
40.
30.
20.
10.
.00
.05
.10
.15
.20
.25
END SLIP (in.)

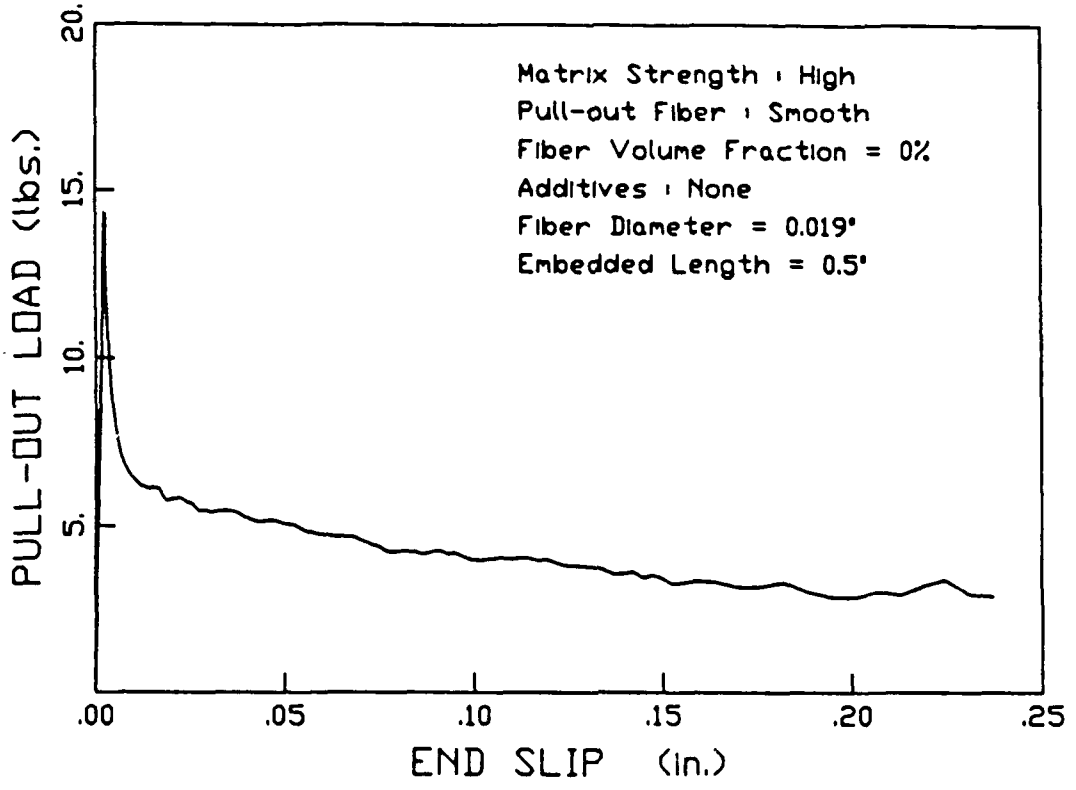
Matrix Strength : High
Pull-out Fiber : Smooth
Fiber Volume Fraction = 0%
Additives : None
Fiber Diameter = 0.019"
Embedded Length = 0.5"
PULL-OUT LOAD (lbs.)
20.
15.
10.
5.
.00
.05
.10
.15
.20
.25
END SLIP (in.)

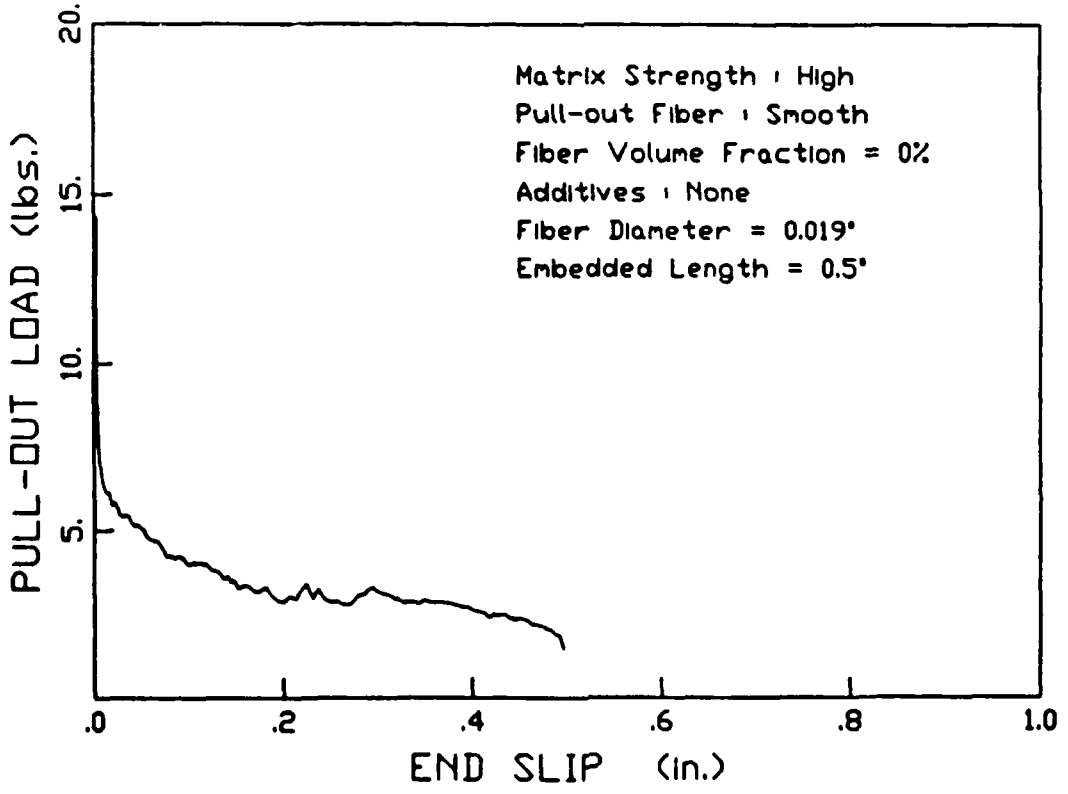
Matrix Strength : High
Pull-out Fiber : Smooth
Fiber Volume Fraction = 0%
Additives : None
Fiber Diameter = 0.019"
Embedded Length = 0.5"
PULL-OUT LOAD (lbs.)
20.
15.
10.
5.
.0
.2
.4
.6
.8
1.0
END SLIP (in.)

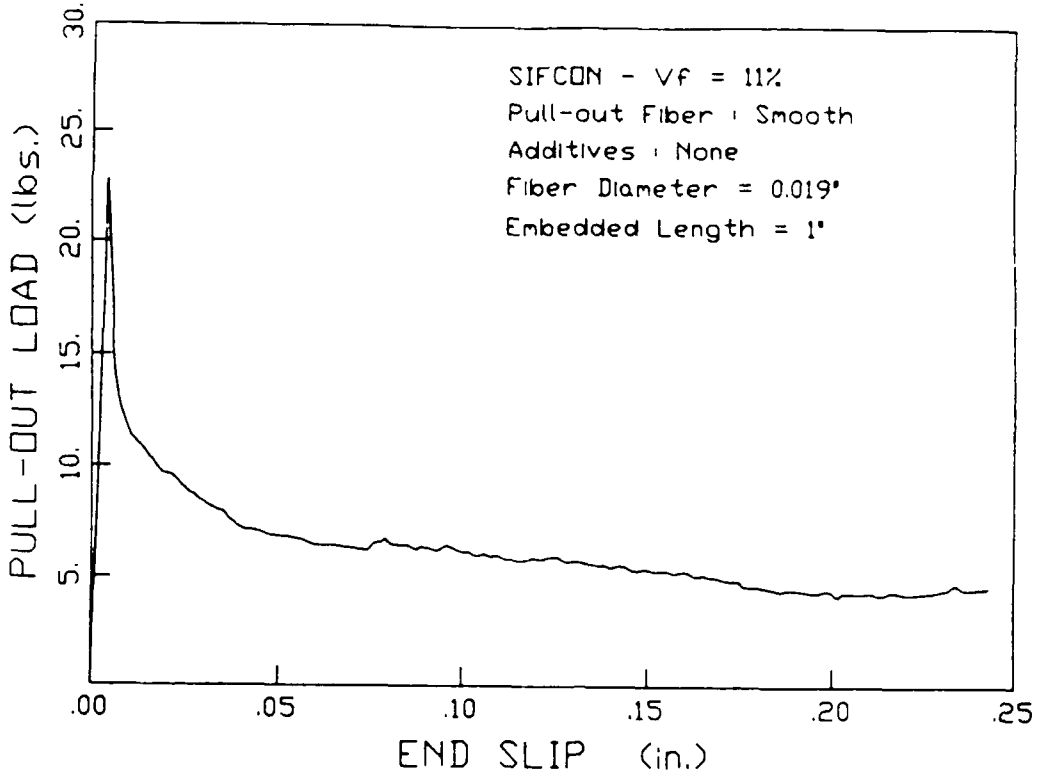
SIFCON - Vf = 11%
Pull-out Fiber : Smooth
Additives : None
Fiber Diameter = 0.019"
Embedded Length = 1"
PULL-OUT LOAD (lbs.)
5.
10.
15.
20.
25.
30.
.00
.05
.10
.15
.20
.25
END SLIP (in.)

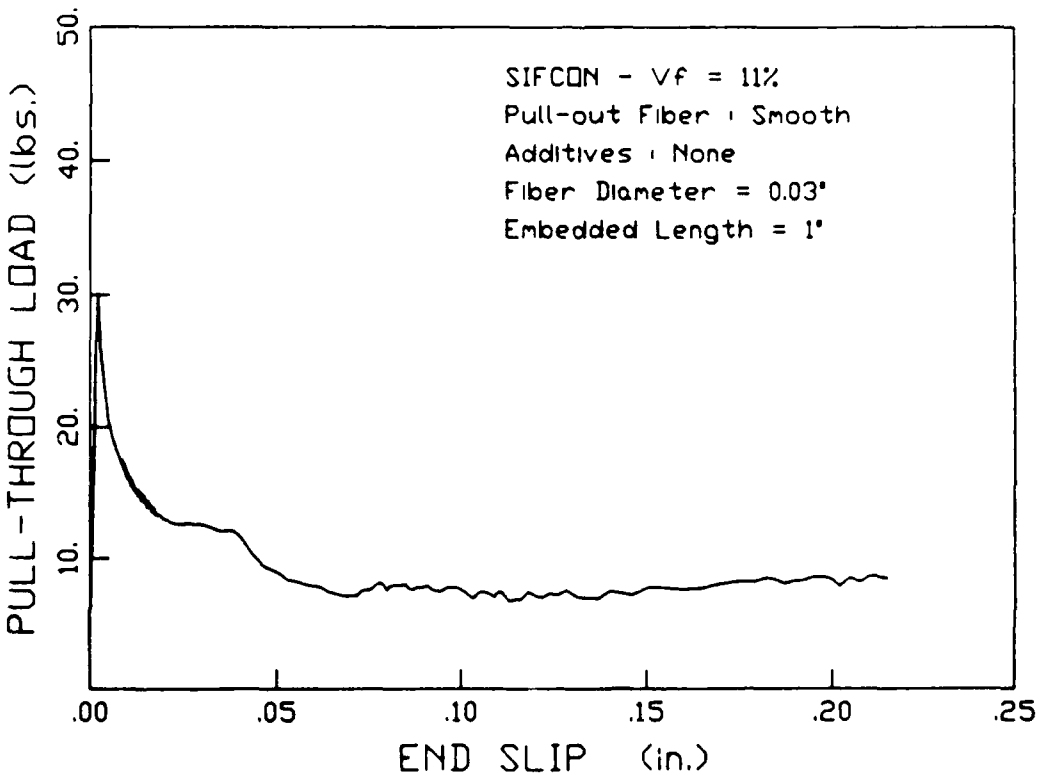
SIFCON - Vf = 11%
Pull-out Fiber : Smooth
Additives : None
Fiber Diameter = 0.03"
Embedded Length = 1"
PULL-THROUGH LOAD (lbs.)
10.
20.
30.
40.
50.
.00
.05
.10
.15
.20
.25
END SLIP (in.)

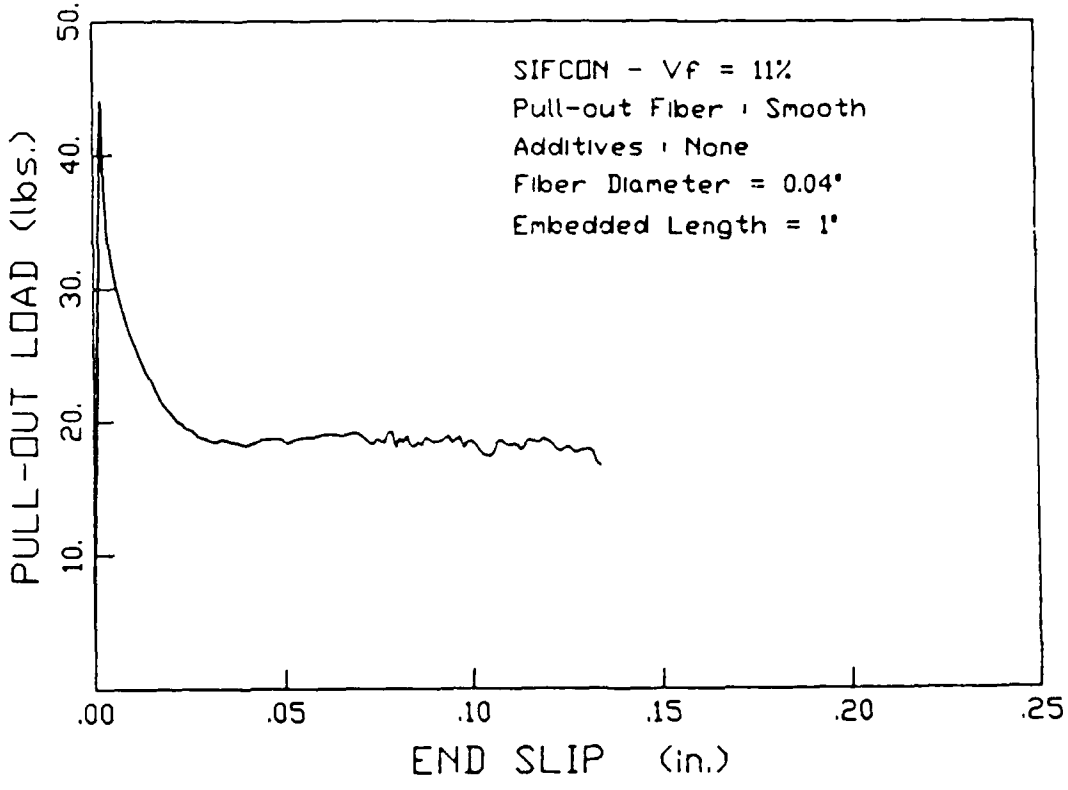
SIFCON - Vf = 11%
Pull-out Fiber : Smooth
Additives : None
Fiber Diameter = 0.04"
Embedded Length = 1"
PULL-OUT LOAD (lbs.)
50.
40.
30.
20.
10.
.00
.05
.10
.15
.20
.25
END SLIP (in.)

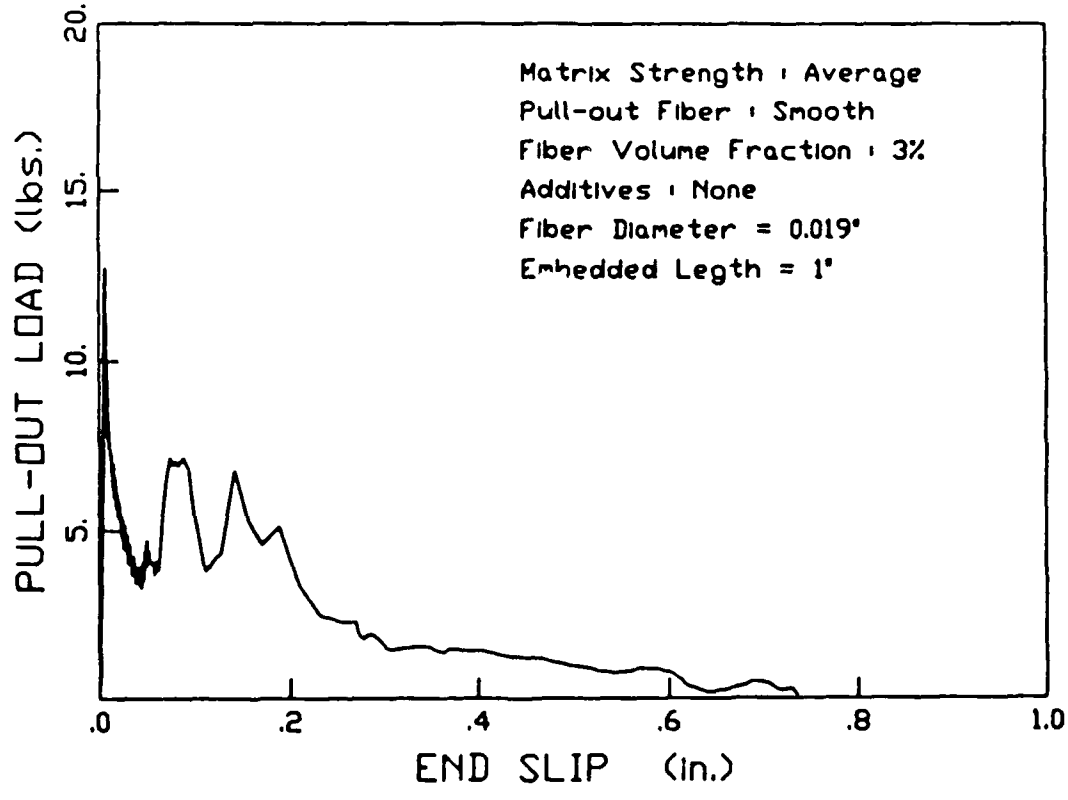
Matrix Strength : Average
Pull-out Fiber : Smooth
Fiber Volume Fraction : 3%
Additives : None
Fiber Diameter = 0.019"
Embedded Legth = 1"
PULL-OUT LOAD (lbs.)
20.
15.
10.
5.
.0
.2
.4
.6
.8
1.0
END SLIP (in.)

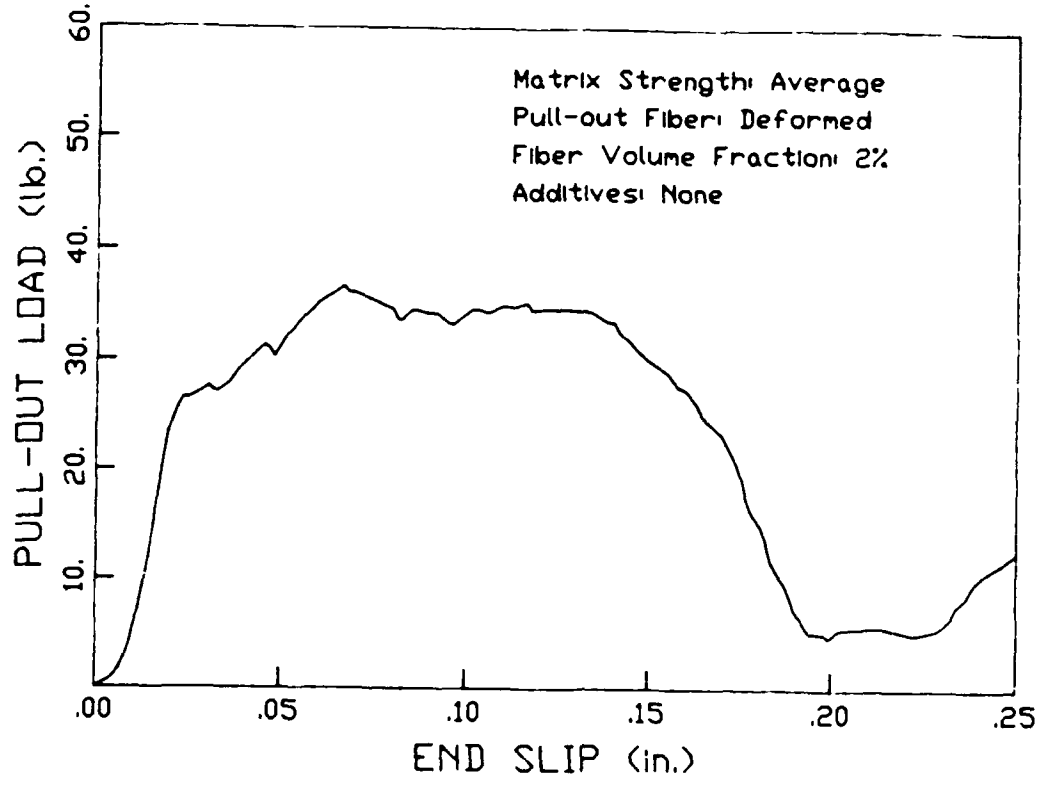
Matrix Strength: Average
Pull-out Fiber: Deformed
Fiber Volume Fraction: 2%
Additives: None
PULL-OUT LOAD (lb.)
10.
20.
30.
40.
50.
60.
.00
.05
.10
.15
.20
.25
END SLIP (in.)

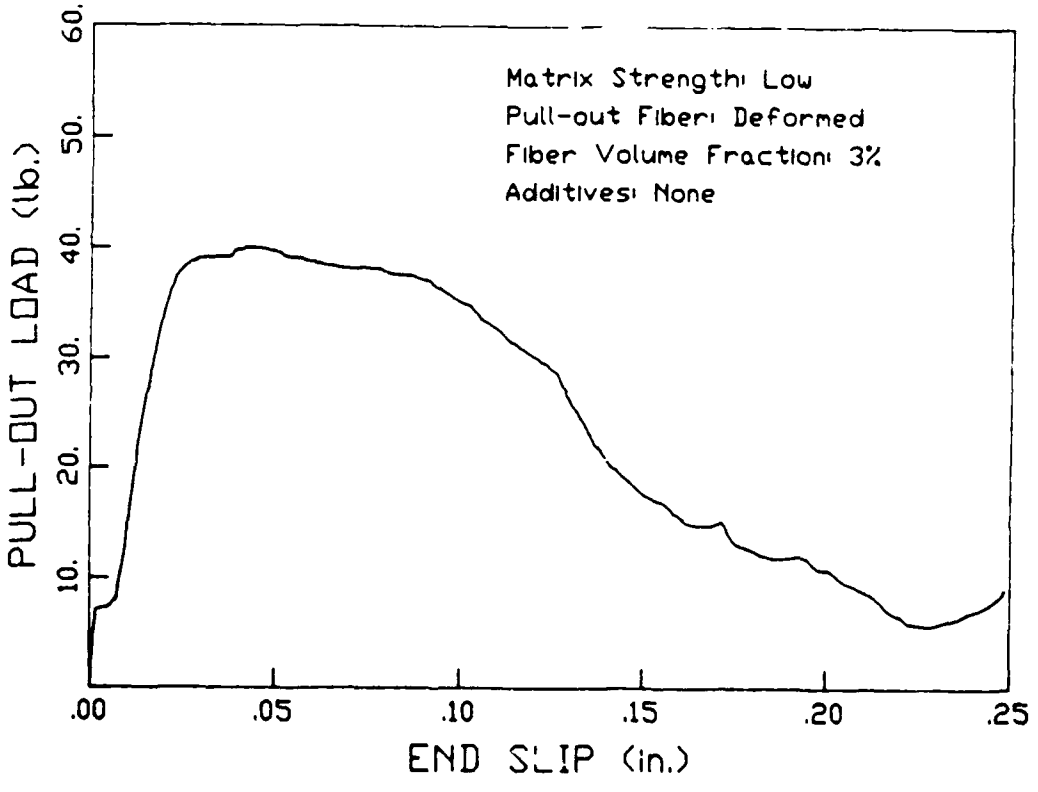
Matrix Strength: Low
Pull-out Fiber: Deformed
Fiber Volume Fraction: 3%
Additives: None
PULL-OUT LOAD (lb.)
10.
20.
30.
40.
50.
60.
.00
.05
.10
.15
.20
.25
END SLIP (in.)

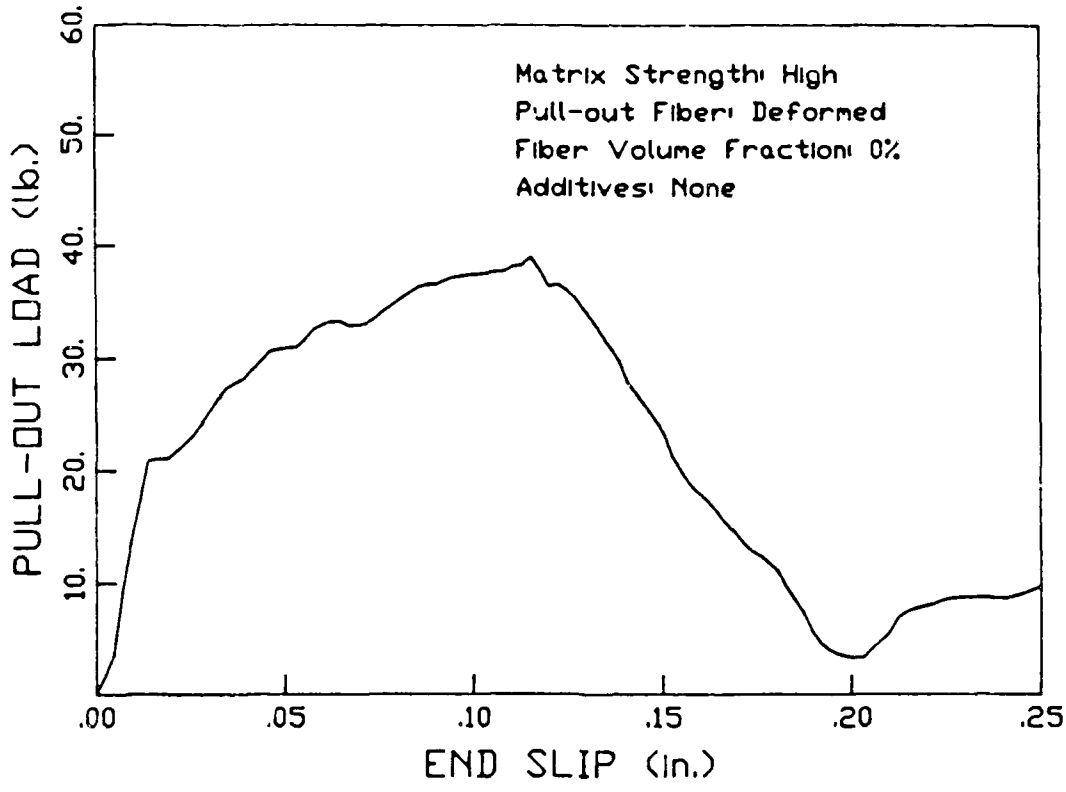
Matrix Strength: High
Pull-out Fiber: Deformed
Fiber Volume Fraction: 0%
Additives: None
PULL-OUT LOAD (lb.)
10.
20.
30.
40.
50.
60.
.00
.05
.10
.15
.20
.25
END SLIP (in.)

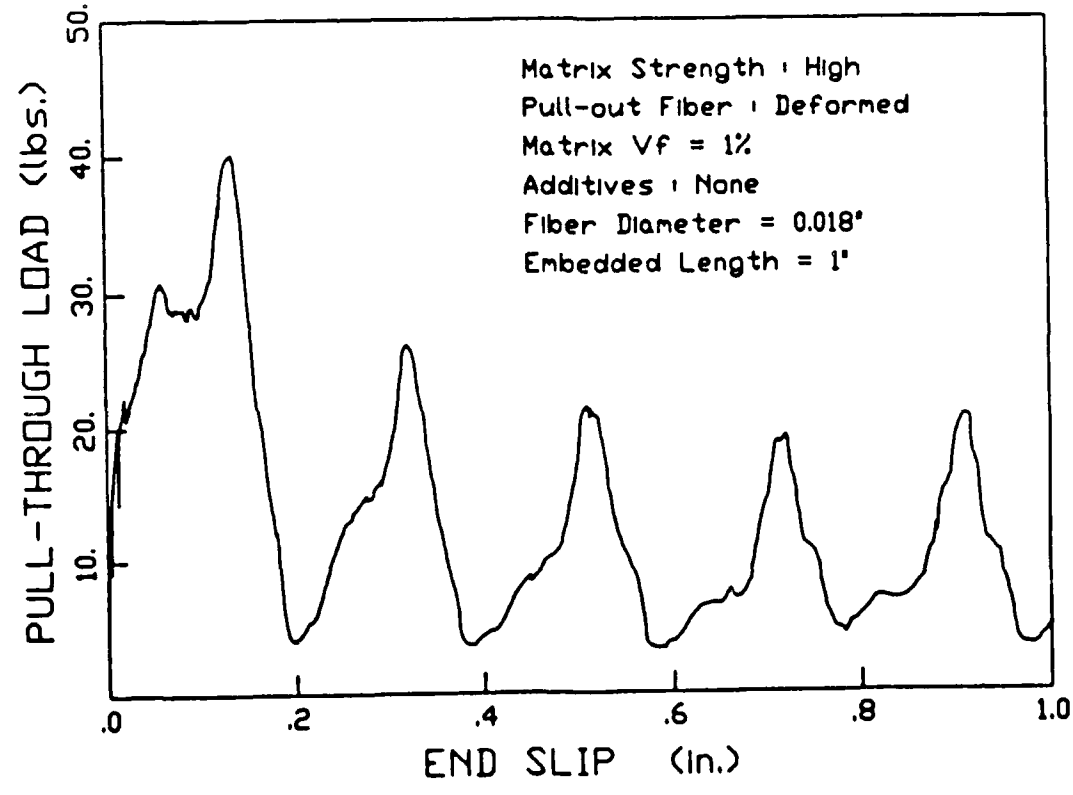
Matrix Strength : High
Pull-out Fiber : Deformed
Matrix Vf = 1%
Additives : None
Fiber Diameter = 0.018"
Embedded Length = 1"
PULL-THROUGH LOAD (lbs.)
10.
20.
30.
40.
50.
.0
.2
.4
.6
.8
1.0
END SLIP (in.)

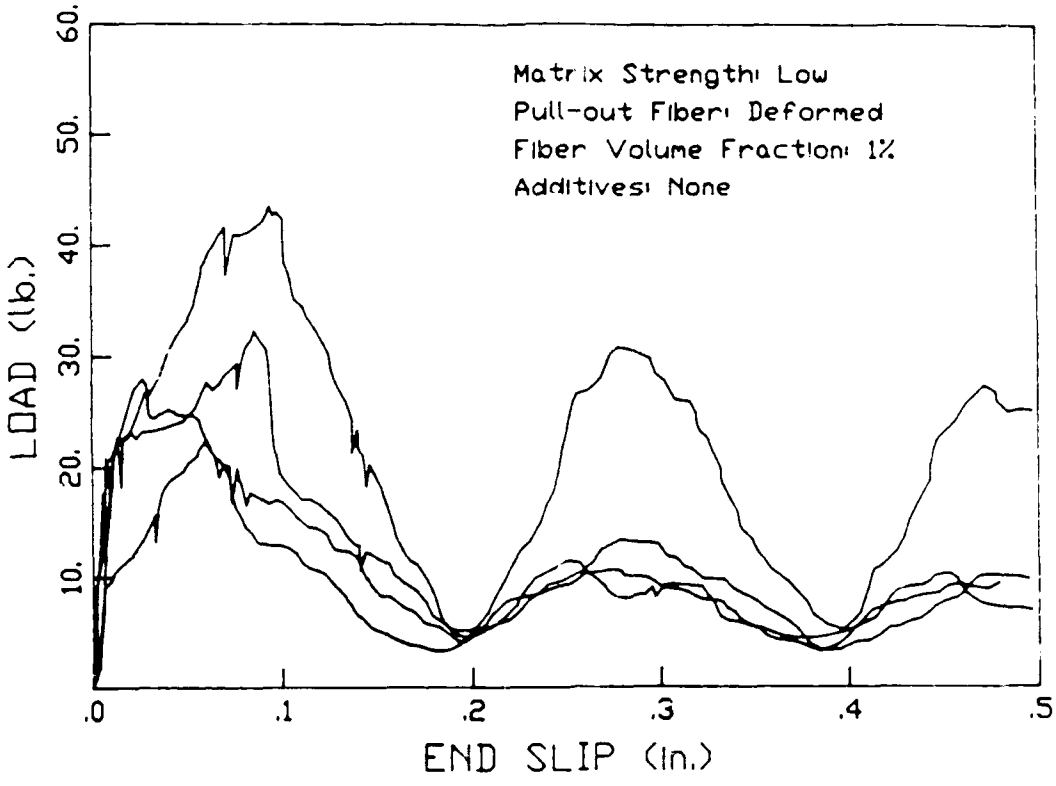
Matrix Strength: Low
Pull-out Fiber: Deformed
Fiber Volume Fraction: 1%
Additives: None
LOAD (lb.)
10.
20.
30.
40.
50.
60.
.0
.1
.2
.3
.4
.5
END SLIP (in.)

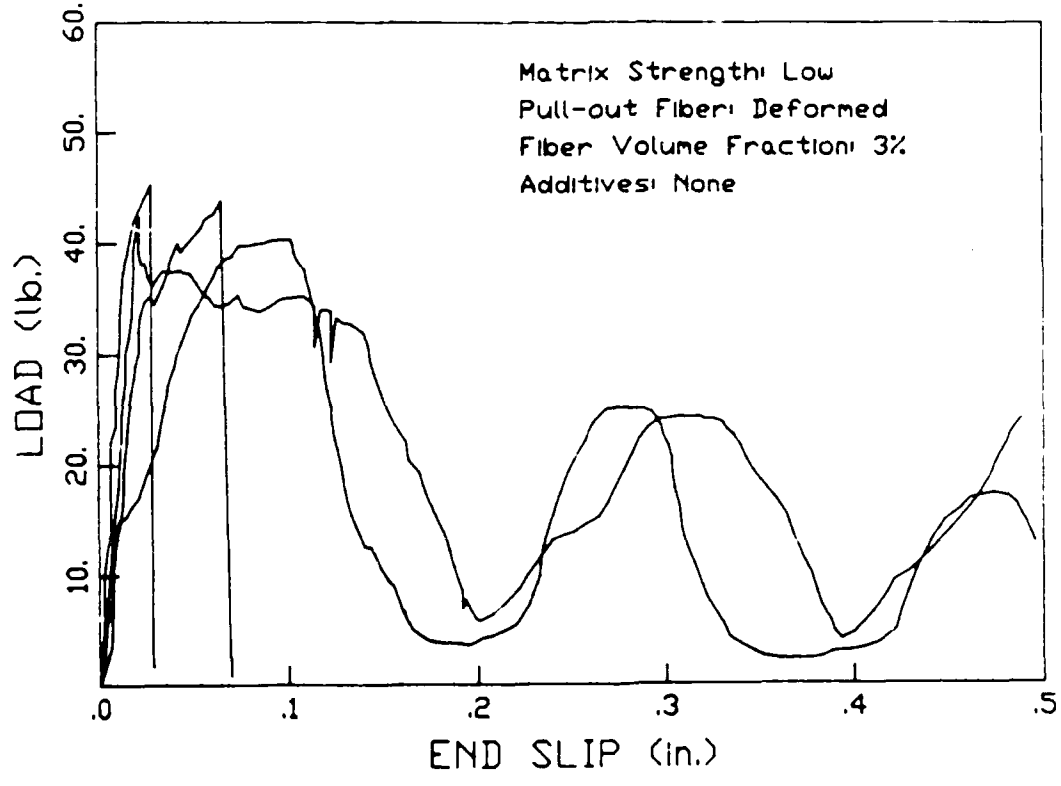
Matrix Strength: Low
Pull-out Fiber: Deformed
Fiber Volume Fraction: 3%
Additives: None
LOAD (lb.)
10.
20.
30.
40.
50.
60.
.0
.1
.2
.3
.4
.5
END SLIP (in.)

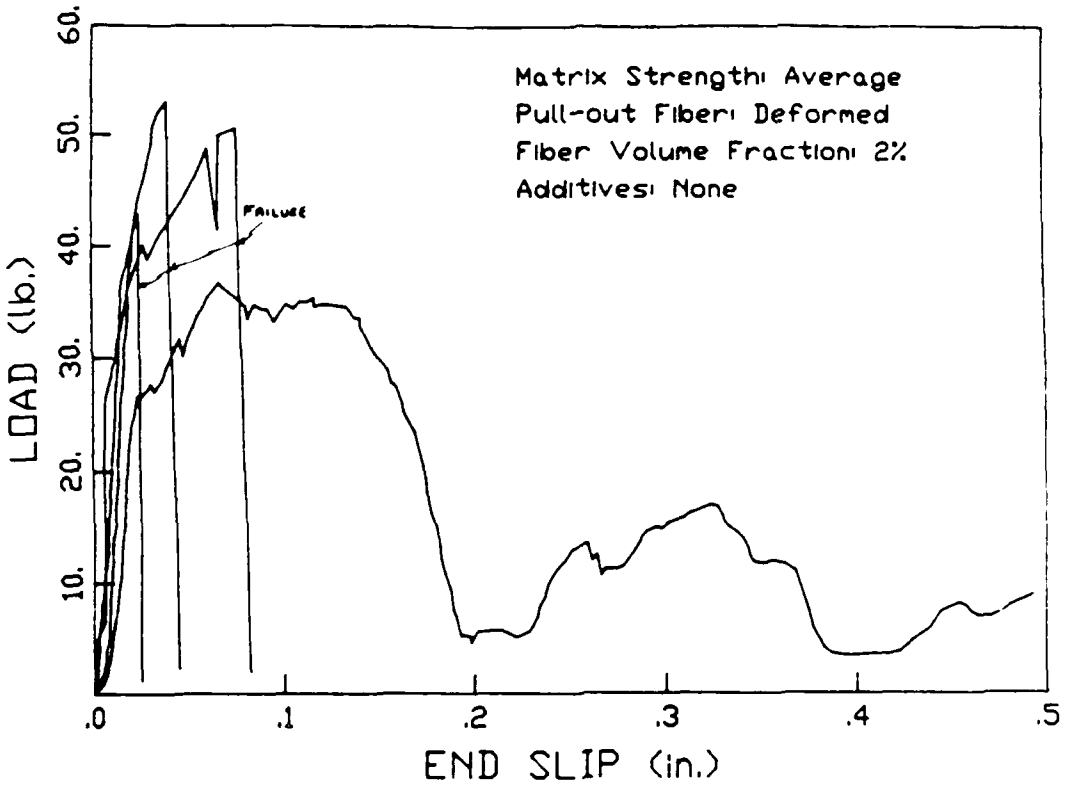
Matrix Strength: Average
Pull-out Fiber: Deformed
Fiber Volume Fraction: 2%
Additives: None
FAILURE
LOAD (lb.)
10.
20.
30.
40.
50.
60.
.0
.1
.2
.3
.4
.5
END SLIP (in.)

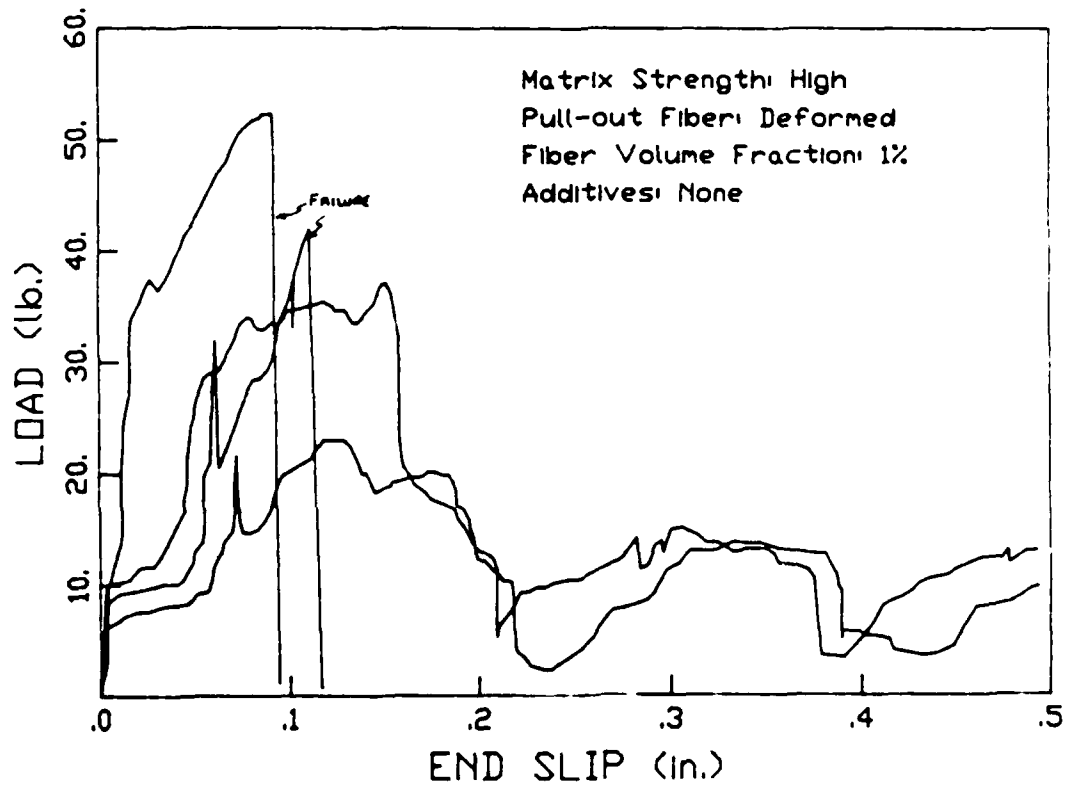
Matrix Strength: High
Pull-out Fiber: Deformed
Fiber Volume Fraction: 1%
Additives: None
FAILURE
LOAD (lb.)
10.
20.
30.
40.
50.
60.
.0
.1
.2
.3
.4
.5
END SLIP (in.)

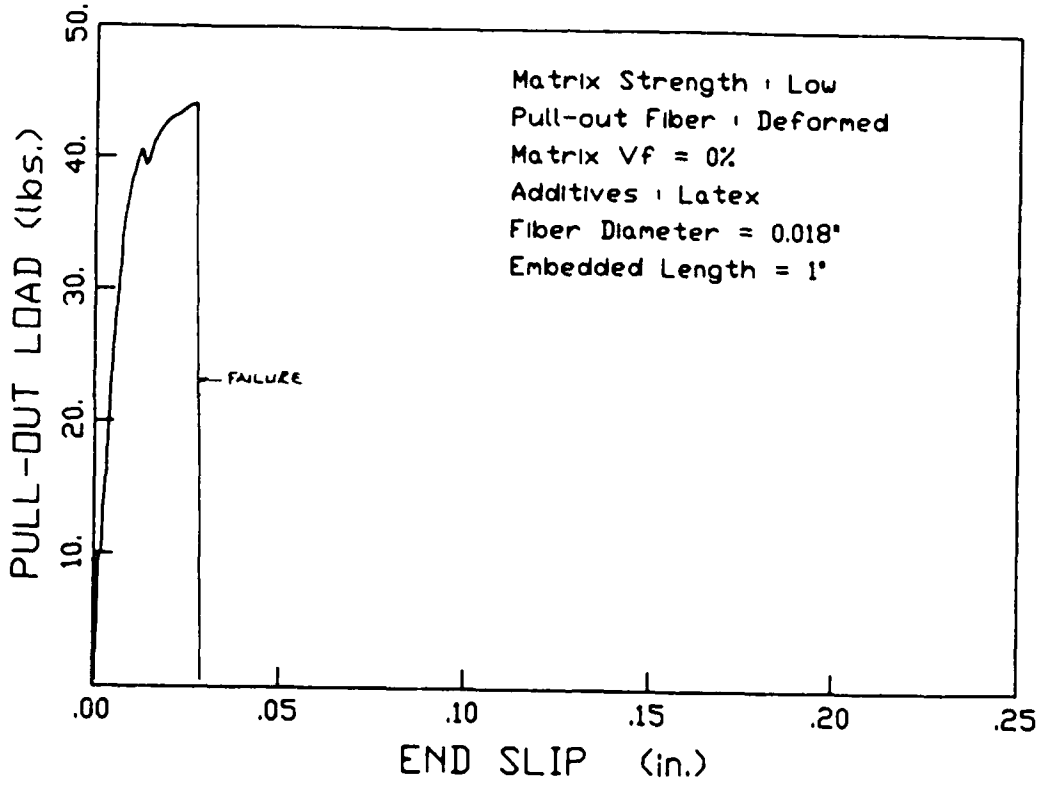
Matrix Strength : Low
Pull-out Fiber : Deformed
Matrix Vf = 0%
Additives : Latex
Fiber Diameter = 0.018"
Embedded Length = 1"
FAILURE
PULL-OUT LOAD (lbs.)
10.
20.
30.
40.
50.
.00
.05
.10
.15
.20
.25
END SLIP (in.)

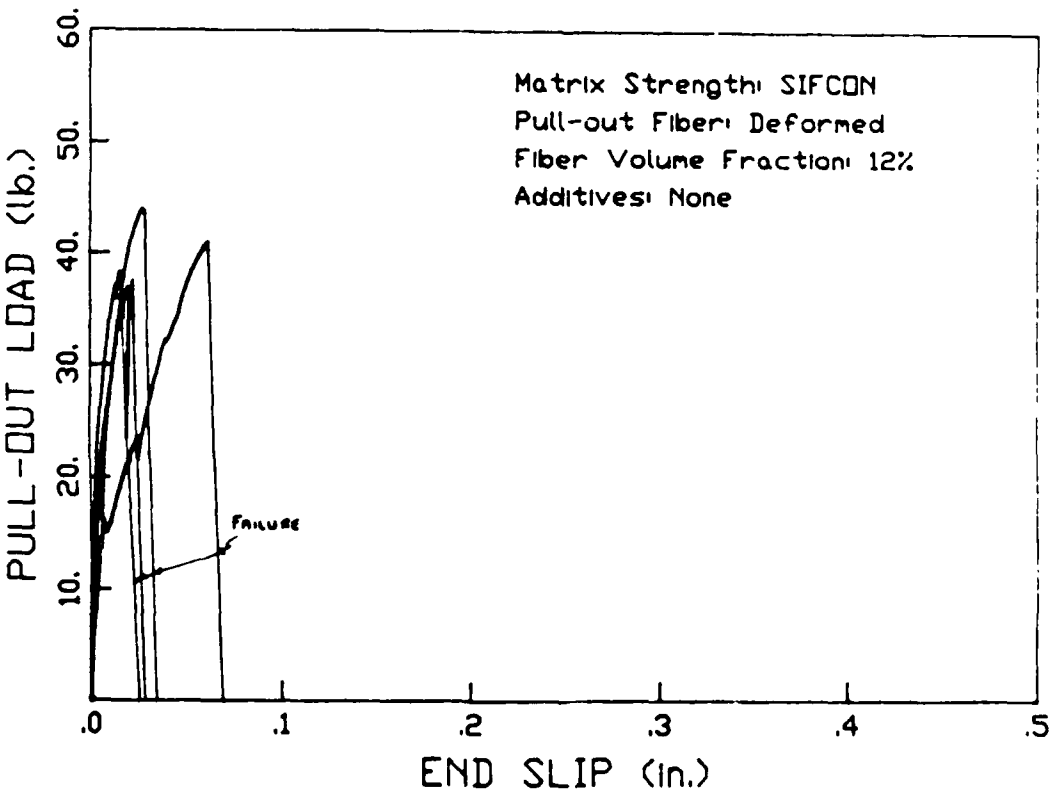
Matrix Strength: SIFCON
Pull-out Fiber: Deformed
Fiber Volume Fraction: 12%
Additives: None
FAILURE
PULL-OUT LOAD (lb.)
10.
20.
30.
40.
50.
60.
.0
.1
.2
.3
.4
.5
END SLIP (in.)

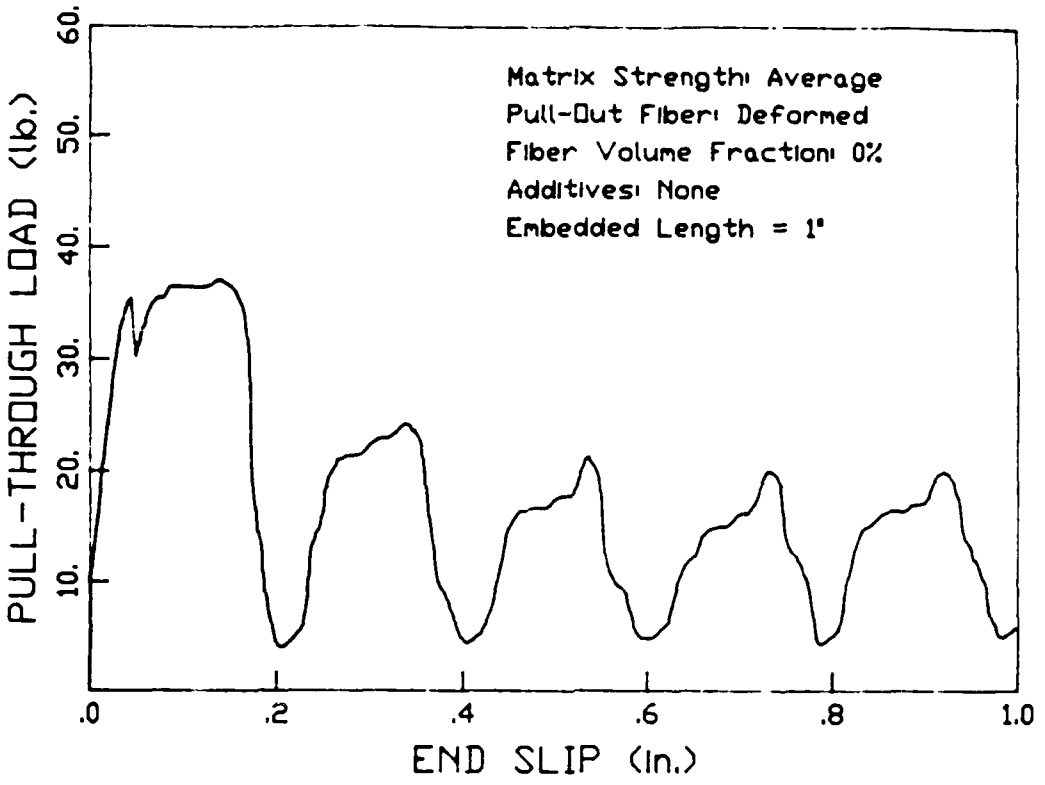
Matrix Strength: Average
Pull-Out Fiber: Deformed
Fiber Volume Fraction: 0%
Additives: None
Embedded Length = 1"
PULL-THROUGH LOAD (lb.)
10.
20.
30.
40.
50.
60.
.0
.2
.4
.6
.8
1.0
END SLIP (in.)

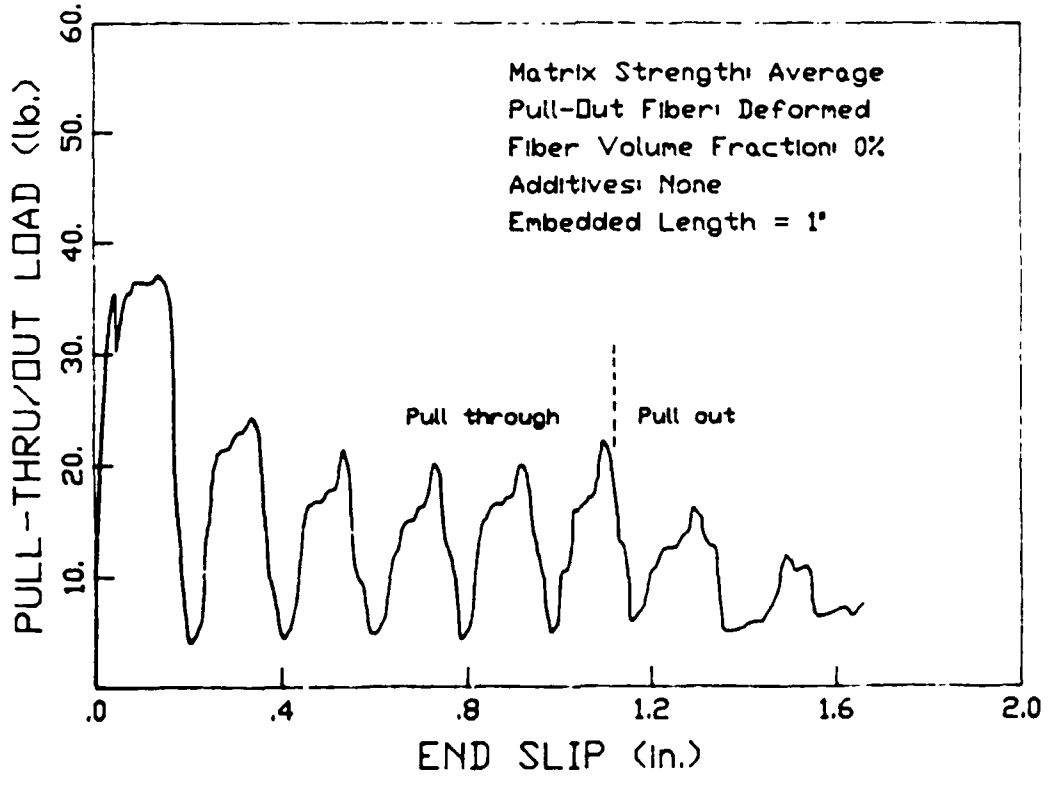
Matrix Strength: Average
Pull-Out Fiber: Deformed
Fiber Volume Fraction: 0%
Additives: None
Embedded Length = 1"
Pull through
Pull out
PULL-THRU/OUT LOAD (lb.)
10.
20.
30.
40.
50.
60.
.0
.4
.8
1.2
1.6
2.0
END SLIP (in.)

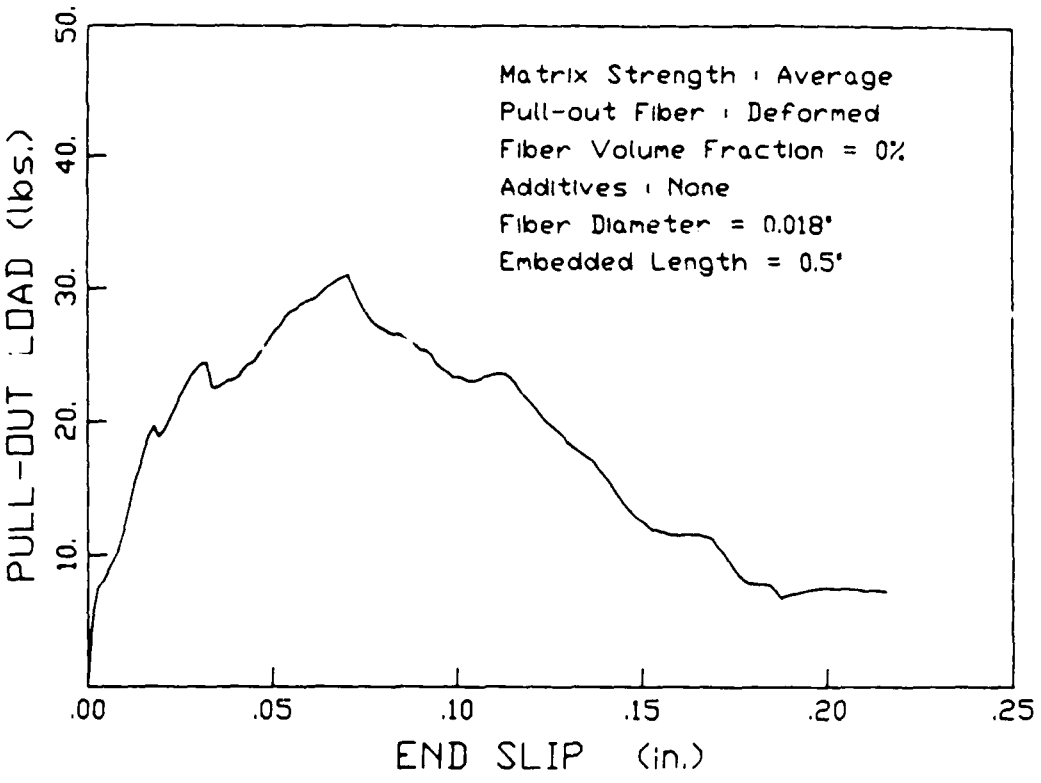
Matrix Strength : Average
Pull-out Fiber : Deformed
Fiber Volume Fraction = 0%
Additives : None
Fiber Diameter = 0.018"
Embedded Length = 0.5"
PULL-OUT LOAD (lbs.)
10.
20.
30.
40.
50.
.00
.05
.10
.15
.20
.25
END SLIP (in.)

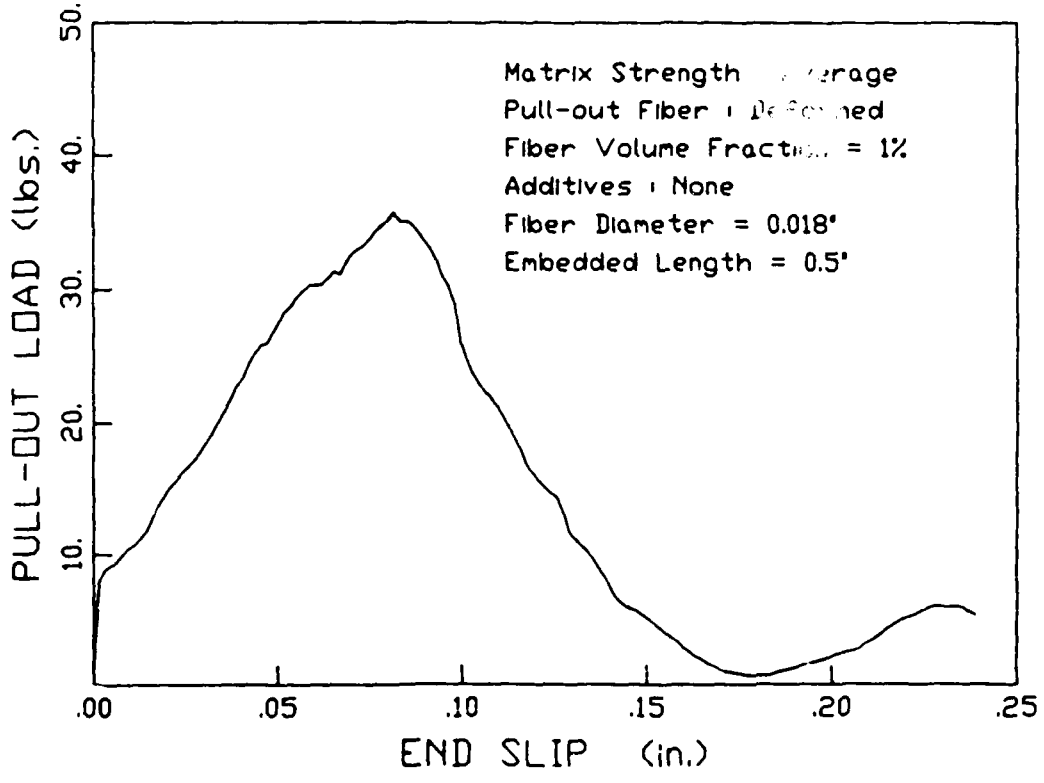
Matrix Strength : Average
Pull-out Fiber : Deformed
Fiber Volume Fraction = 1%
Additives : None
Fiber Diameter = 0.018"
Embedded Length = 0.5"
PULL-OUT LOAD (lbs.)
10.
20.
30.
40.
50.
.00
.05
.10
.15
.20
.25
END SLIP (in.)

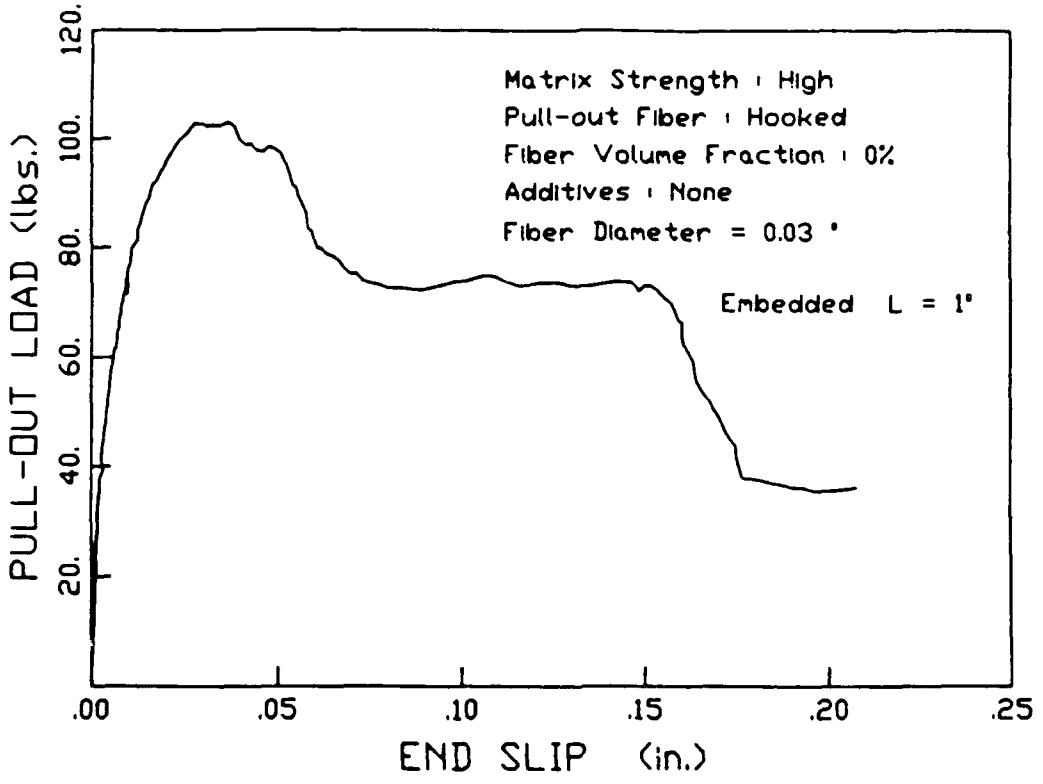
Matrix Strength : High
Pull-out Fiber : Hooked
Fiber Volume Fraction : 0%
Additives : None
Fiber Diameter = 0.03 "
Embedded L = 1"
PULL-OUT LOAD (lbs.)
20.
40.
60.
80.
100.
120.
.00
.05
.10
.15
.20
.25
END SLIP (in.)

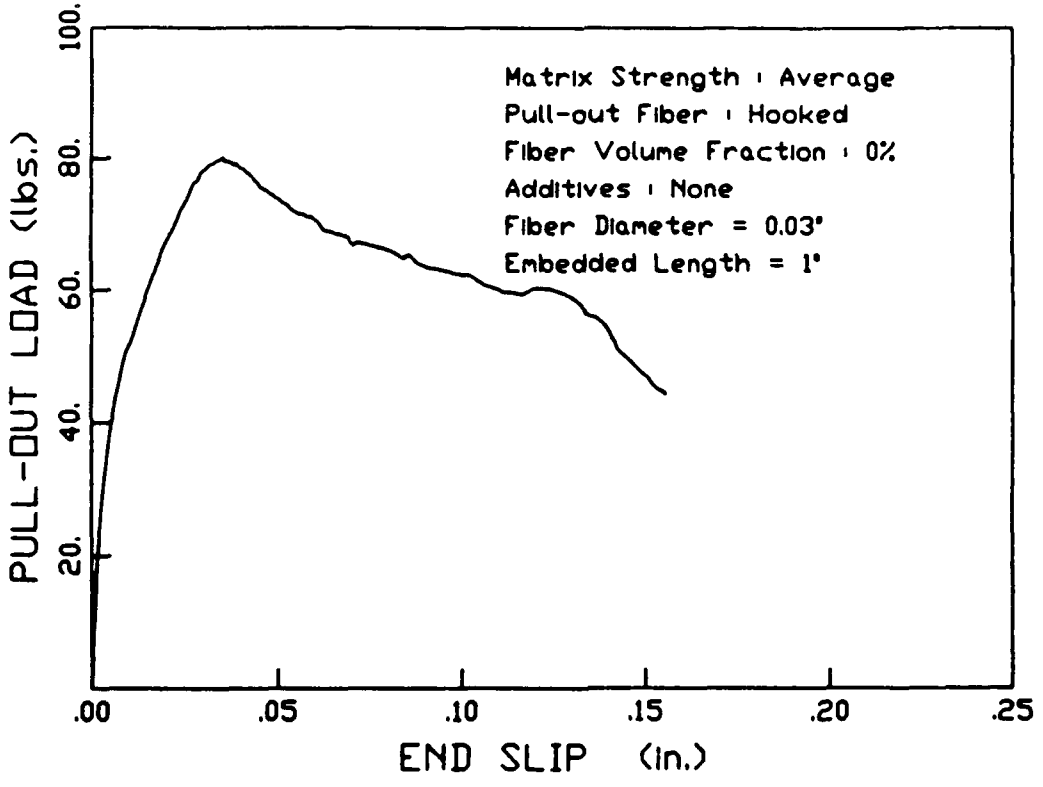
Matrix Strength : Average
Pull-out Fiber : Hooked
Fiber Volume Fraction : 0%
Additives : None
Fiber Diameter = 0.03"
Embedded Length = 1"
PULL-OUT LOAD (lbs.)
20.
40.
60.
80.
100.
.00
.05
.10
.15
.20
.25
END SLIP (in.)

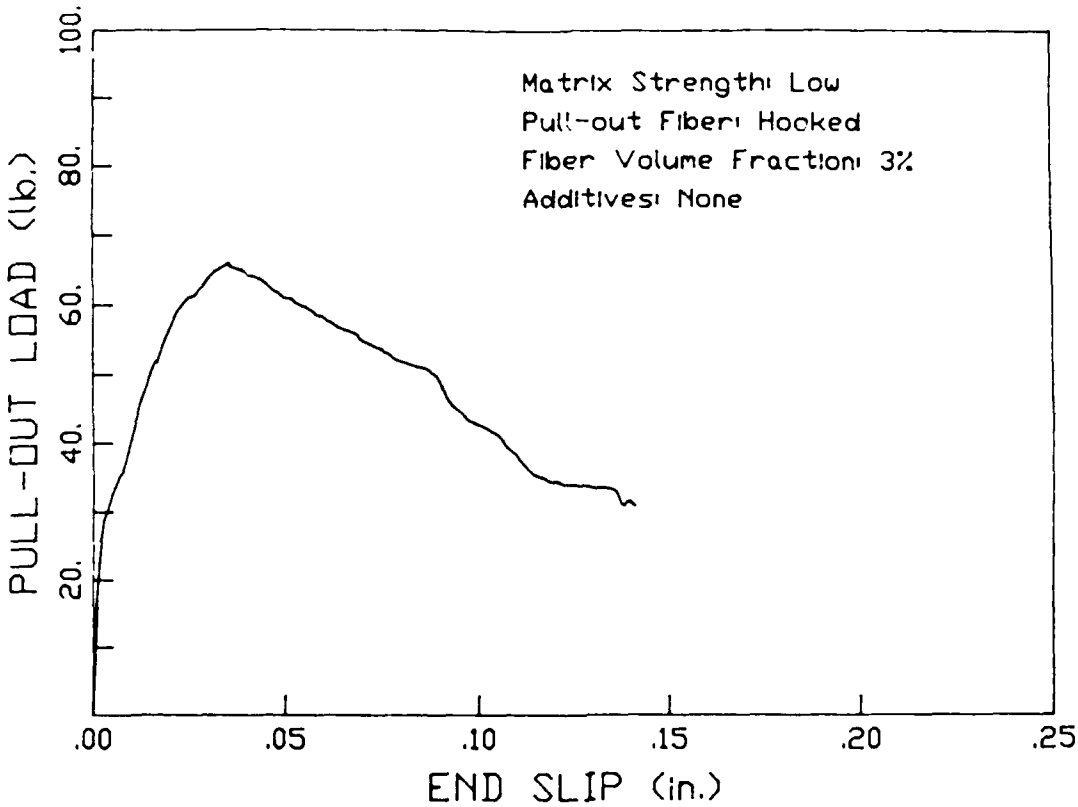
Matrix Strength: Low
Pull-out Fiber: Hooked
Fiber Volume Fraction: 3%
Additives: None
PULL-OUT LOAD (lb.)
100.
80.
60.
40.
20.
.00
.05
.10
.15
.20
.25
END SLIP (in.)

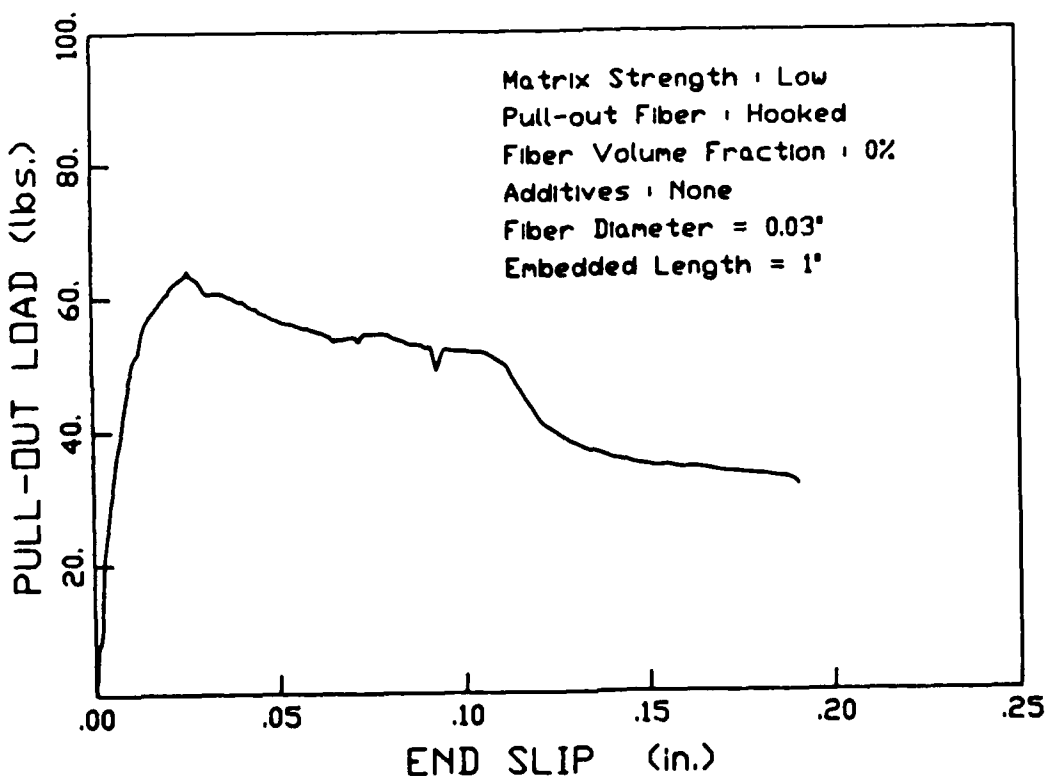
Matrix Strength : Low
Pull-out Fiber : Hooked
Fiber Volume Fraction : 0%
Additives : None
Fiber Diameter = 0.03"
Embedded Length = 1"
PULL-OUT LOAD (lbs.)
100.
80.
60.
40.
20.
.00
.05
.10
.15
.20
.25
END SLIP (in.)

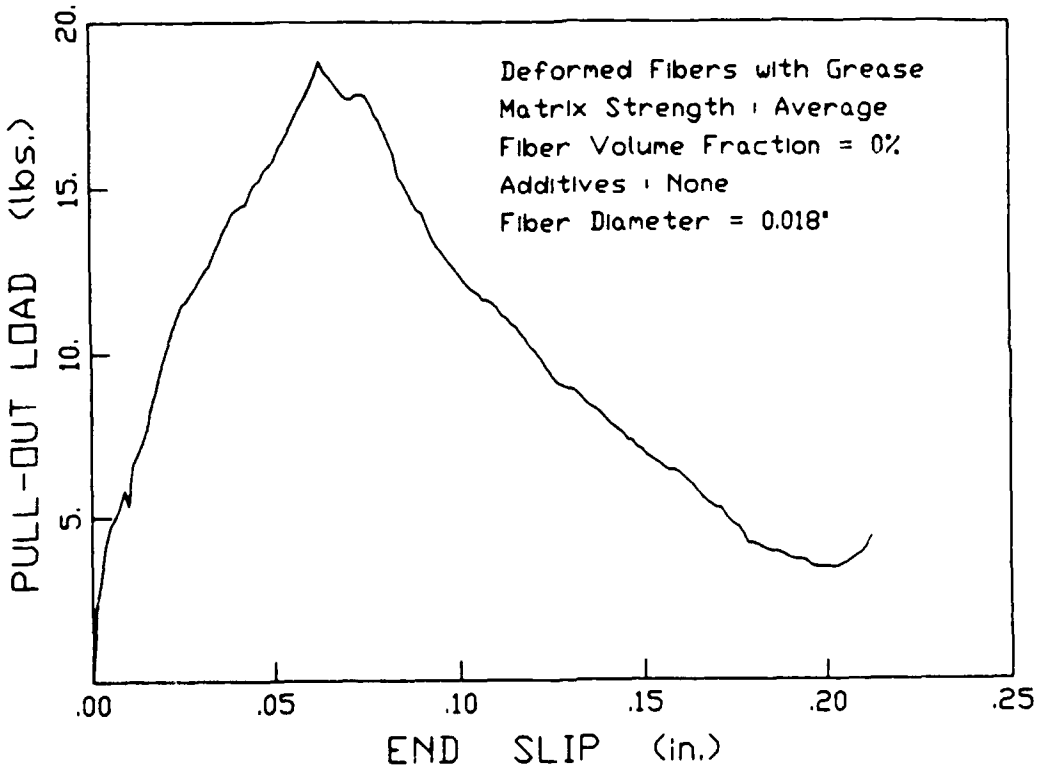
Deformed Fibers with Grease
Matrix Strength : Average
Fiber Volume Fraction = 0%
Additives : None
Fiber Diameter = 0.018"
PULL-OUT LOAD (lbs.)
5.
10.
15.
20.
.00
.05
.10
.15
.20
.25
END SLIP (in.)

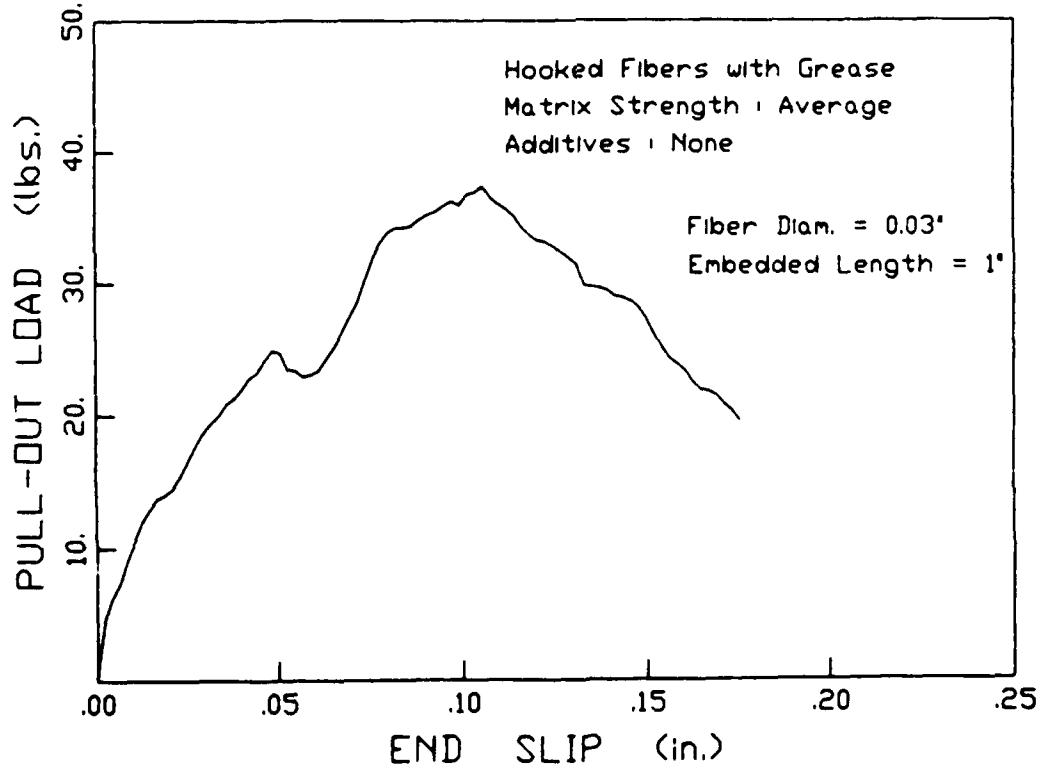
Hooked Fibers with Grease
Matrix Strength : Average
Additives : None
Fiber Diam. = 0.03"
Embedded Length = 1"
PULL-OUT LOAD (lbs.)
10.
20.
30.
40.
50.
.00
.05
.10
.15
.20
.25
END SLIP (in.)

CHAPTER VII

BOND STRESS MODEL FOR FIBER-REINFORCED CONCRETE BASED ON BOND STRESS-SLIP RELATIONSHIP

7.1 INTRODUCTION

There is a basic need for the study of bond in fiber-reinforced cementitious composites. Materials scientists and engineers have been aware of the importance of bond; the problem has indeed been addressed before. However, few thorough studies have been conducted to date, and to the best of the authors' knowledge, no complete analytical model of bond in cementitious composites has been developed.

Existing studies are incomplete, in a sense that all the aspects of bond were not investigated. Some authors assumed non-linear elastic shear bond without debonding [27, 42, 48, 54], hence ignoring the frictional bond stresses that develop after debonding occurs. Aveston et al. [3] assumed frictional shear bond with no debonding, hence ignoring the elastic bond that develops for shear stresses not exceeding the bond capacity of the interface.

To incorporate both the adhesion and the mechanical components of bond introduced crimped or deformed fibers requires a more comprehensive study of bond. Bond studies undertaken on reinforced concrete cannot be directly applied to fiber-reinforced cementitious composites. The mechanical and adhesive bond have the effect of changing both the distribution and the average value of the shear bond at the interface. Everything else being equal, a crimped fiber for example can develop more bond stresses at the interface than a smooth fiber. Likewise, a matrix con-

taining latex could develop more adhesion to the fiber, and thus induce more bond shear stresses. The matrix composition is expected to affect the bond properties of fiber-reinforced cementitious composites.

Two different analytical models of interfacial bond are derived in Chapters 7 and 8. The model presented in this chapter is based on an assumed known bond shear stress-slip relationship, which is used to analytically predict the interfacial bond shear stress, as well as the normal stress distributions in both the fiber and the matrix, when a fiber-reinforced concrete specimen is subjected to tensile stresses. The model assumes perfect alignment of the fibers, as well as a square packing. The solution applies to the case where a crack doesnot occur along the fiber or prism considered.

7.2 BASIC ASSUMPTIONS

a) The main assumption needed for the development of the model is the shear stress-slip relationship. As can be seen in Fig. 7.1, the assumed relationship is bi-linear or elastic-perfectly frictional. A region of linear elastic shear bond prevails until debonding occurs when the shear stress reaches the maximum shear capacity of the interface τ_{max}, at which point the stresses developed are of frictional nature, i.e. are independent of the amount of slip.

b) It is also assumed that the fibers are aligned within the specimen, and that they are squarely packed. A square packing means that at any given section perpendicular to the line of stress, the existing amount of fibers is the same. Also, within a given section, the spatial distribution of the fibers is uniform. Fig. 7.2 shows a square packing case.

c) Furthermore, it is assumed that each individual fiber, along with its share of matrix act and behave independently of other fibers and the rest of the matrix body. This assumption is essential to simplify the analysis of the whole composite down to that of a representative unit. The representative unit, which is a square

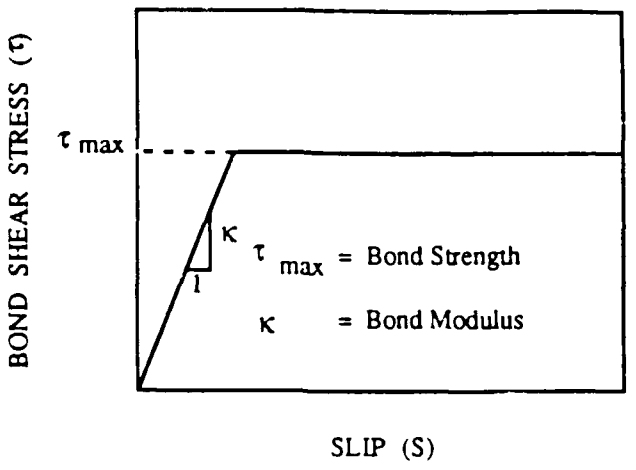

Fig. 7.1 - Bilinear bond-slip relationship.

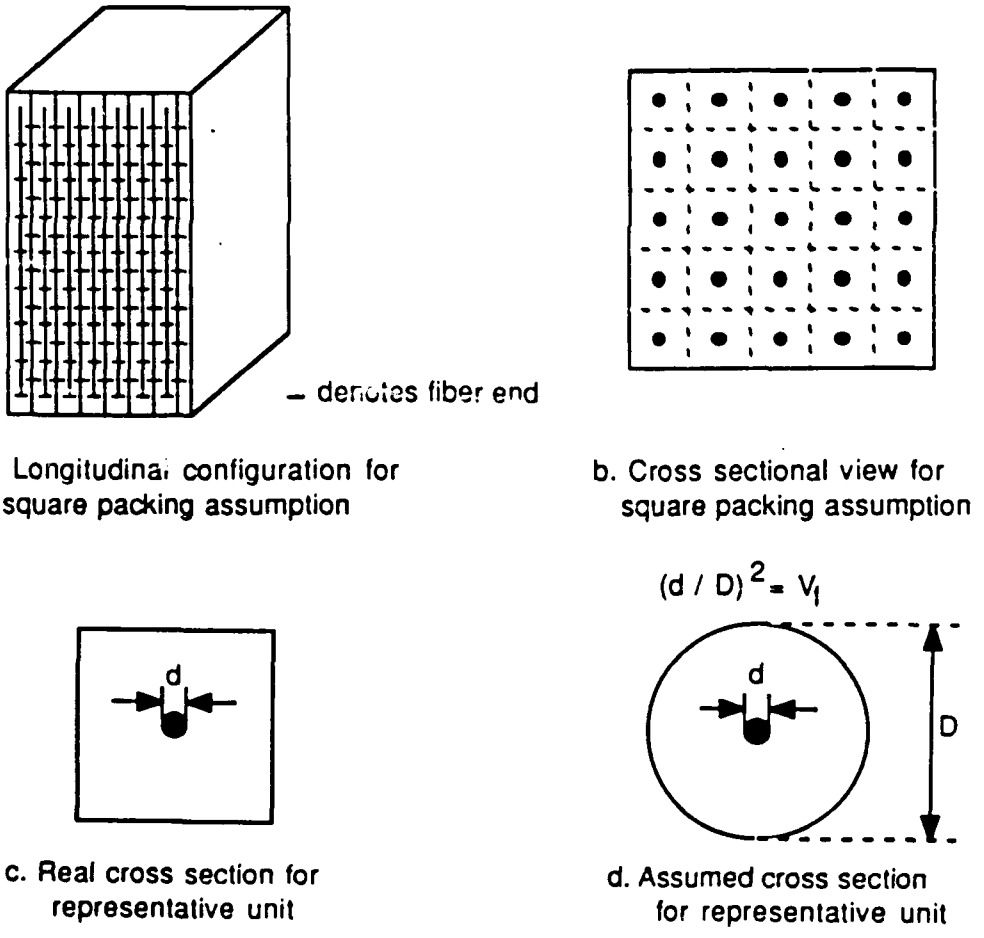

Fig. 7.2 - Square packing configuration.

prism with a fiber along its axis, is further simplified to a cylinder of matrix encasing one fiber (see Fig. 7.3).

d) Finally, the tensile load acting on the representative unit is assumed shared by the fiber and the surrounding matrix.

7.3 MATHEMATICAL DERIVATION OF THE SHEAR STRESS DISTRIBUTION

Using the bond stress-slip relationship assumed previously (see Fig. 7.1), the following equation holds for the elastic bond range:

$$\tau(x) = \kappa\, S(x) \tag{7.1}$$

The variation of slip S is equal to the difference between the strain in the fiber and the strain in the matrix. Hence:

$$\frac{dS}{dx} = \varepsilon_f(x) - \varepsilon_m(x) \tag{7.2}$$

$$= \frac{f_f(x)}{E_f} - \frac{f_m(x)}{E_m} \tag{7.3}$$

$$= \frac{F(x)}{A_f\, E_f} - \frac{T(x)}{A_m\, E_m} \tag{7.4}$$

where:

$f_f(x)$ = local stress in fiber

$f_m(x)$ = local stress in the matrix

$F(x)$ = local force in fiber

$T(x)$ = local force in the matrix

E_f = modulus of elasticity of the fiber

E_m = modulus of elasticity of the matrix in tension

A_f = area of one fiber

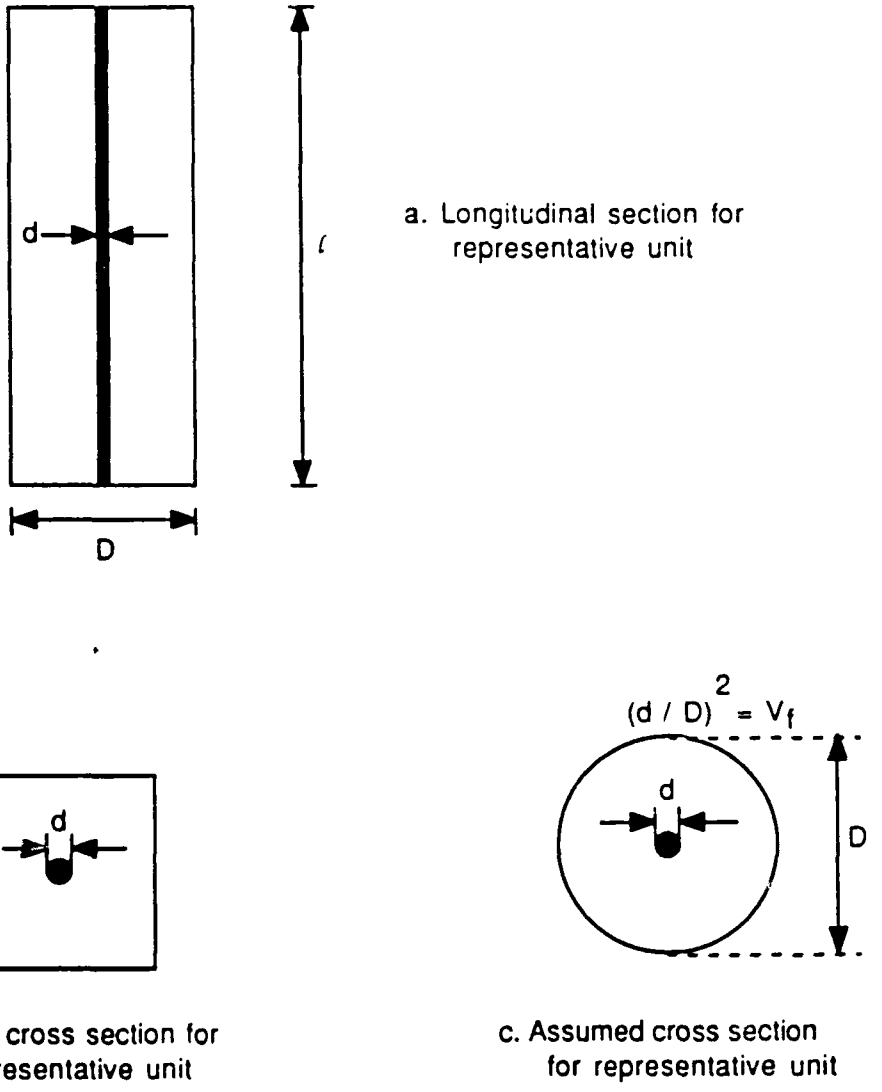

Fig. 7.3 - Typical representative unit.

A_m = area of the matrix within the representative unit

Assuming that the representative unit is subjected to a tensile force F_o, then:

$$T(x) = F_o - F(x) \tag{7.5}$$

therefore:

$$\frac{dS}{dx} = \frac{F(x)}{A_f E_f} - \frac{[F_o - F(x)]}{A_m E_m} \tag{7.6}$$

$$= \left(\frac{1}{A_f E_f} + \frac{1}{A_m E_m} \right) F(x) - \frac{F_o}{A_m E_m} \tag{7.7}$$

Since a square packing is assumed, the following relationship is true:

$$V_f = \frac{A_f}{A_f + A_m} \tag{7.8}$$

where V_f is the fiber volume fraction in the composite.

It can be shown that Eq. 7.8 can be rewritten as:

$$\frac{dS}{dx} = \frac{F(x)}{A_f E_f} \left(1 + n \frac{V_f}{1 - V_f} \right) - \frac{n F_o}{A_f E_f} \frac{V_f}{1 - V_f} \tag{7.9}$$

where n is the modular ratio, or:

$$n \quad \frac{E_f}{E_m}$$

Eq. 7.9 can be written as a function of the stress in the fiber f_f:

$$\frac{dS}{dx} = \frac{f_f(x)}{E_f} \left(1 + n \frac{V_f}{1 - V_f} \right) - \frac{n F_o}{A_f E_f} \frac{V_f}{1 - V_f} \tag{7.10}$$

Differentiating both sides of Eq. 7.10 leads to:

$$\frac{d^2S}{dx^2} = \frac{1}{E_f} \left(1 + n \frac{V_f}{1 - V_f} \right) \frac{df_f(x)}{dx} \tag{7.11}$$

but $$\frac{df_f(x)}{dx} = \frac{\tau(x)\ \psi}{A_f} \qquad (7.12)$$

where

ψ = fiber perimeter

$\tau(x)$ = local bond shear stress

thus:

$$\frac{d^2S}{dx^2} = \frac{1}{E_f}\left(1 + n\frac{V_f}{1 - V_f}\right)\frac{\tau(x)\ \psi}{A_f} \qquad (7.13)$$

Recalling Eq. 5.1, Eq. 5.13 can be rewritten as:

$$\frac{d^2S}{dx^2} = \frac{4}{d\ E_f}\left(1 + n\frac{V_f}{1 - V_f}\right) \kappa\ S(x) \qquad (7.14)$$

where d is the fiber diameter.

This differential equation is of the form:

$$S'' - K^2 S = 0 \qquad (7.15)$$

where:

$$K^2 = \frac{4}{E_f}\left(1 + n\frac{V_f}{1 - V_f}\right)\frac{\kappa}{d} \qquad (7.16)$$

The solution to this differential equation is of the form:

$$S(x) = A \sinh(Kx) + B \cosh(Kx) \qquad (7.17)$$

The constants are determined from the boundary conditions. If the origin is to be taken at the center of the fiber, then:

1. @ $x = 0$, $S = 0$, hence $B = 0$

2. @ $x = \frac{\ell}{2}$, $F = \chi F_o$

where χ is the fraction of the total force acting on the representative unit that is taken by the fiber tips.

The factor χ is reflective of the way the force F_o is applied onto the representative unit. A critical value for χ, χ_{crit}, would be the one for which the force distributions in the fiber and the matrix are constant, i.e. under equal strain conditions. If the force in the fiber is to be maximum at the tips and minimum at mid-length, χ is to be larger than χ_{crit}, but always less than 1, or $\chi_{crit} \leq \chi \leq 1$.

$$\chi_{crit} = \frac{n \ V_f}{1 + (n - 1) \ V_f} \tag{7.18}$$

$$\text{Since } \tau(x) = \kappa \, S(x)$$

$$= A \, \tau \sinh (Kx) \tag{7.19}$$

$$\text{but } \frac{df_f(x)}{dx} = \frac{\tau(x) \ \psi}{A_f}$$

therefore:

$$\frac{df_f(x)}{dx} = \frac{4}{d} \ A \, \kappa \sinh (Kx) \tag{7.20}$$

hence:

$$f_f(x) = \frac{4}{Kd} \ A \, \kappa \cosh (Kx) \tag{7.21}$$

$$F(x) = \frac{\pi \ d}{K} \ A \, \kappa \cosh (Kx) \tag{7.22}$$

$$F(\tfrac{\ell}{2}) = \frac{\pi \ d}{K} \ A \, \kappa \cosh (K\tfrac{\ell}{2}) \tag{7.23}$$

$$\text{but } F(\tfrac{\ell}{2}) = \chi \, F_o$$

$$\text{thus: } A = \frac{\chi F_o K}{\pi d \kappa \cosh(K\frac{\ell}{2})} \tag{7.24}$$

Therefore:

$$\tau(x) = \left(\frac{\chi F_o K}{\pi d \cosh(K\frac{\ell}{2})} \right) \sinh (K x) \tag{7.25}$$

$$F(x) = \left(\frac{\chi F_o}{\cosh(K\frac{\ell}{2})} \right) \cosh (K x) \tag{7.26}$$

$$\text{and } T(x) = F_o - F(x)$$

$$= F_o \left(1 - \frac{\chi}{\cosh(K\frac{\ell}{2})} \cosh (Kx) \right) \tag{7.27}$$

Eq. 7.25 is valid so long as the bond stress does not exceed the bond capacity of the interface, τ_{max} (the bond strength), also assumed to be the frictional strength between the matrix and the fiber. Fig. 7.4 shows typical force distributions within the fiber and the matrix, while Fig. 7.5 represents the variation of the bond distribution with increasing applied stresses up to, and then past the stress that would create a shear stress equal to τ_{max}. It also shows how debonding occurs in similar cases. If for a given tensile force, the maximum theoretical shear stress in a fiber is referred to as τ_1, then:

$$\tau_1 = \left(\frac{\chi F_o K}{\pi d} \right) \tanh (K\frac{\ell}{2}) \tag{7.28}$$

If τ_1 is larger than τ_{max}, then debonding occurs, at a distance ℓ_t from the center of the fiber on each side (Fig. 7.5). Over the still bonded region, Eq. 7.25 applies with two modifications, namely that the length is $2\ell_t$ instead of ℓ, and the force is $(\chi F_o - \tau_{max} \psi \ell_d)$ instead (χF_o), hence:

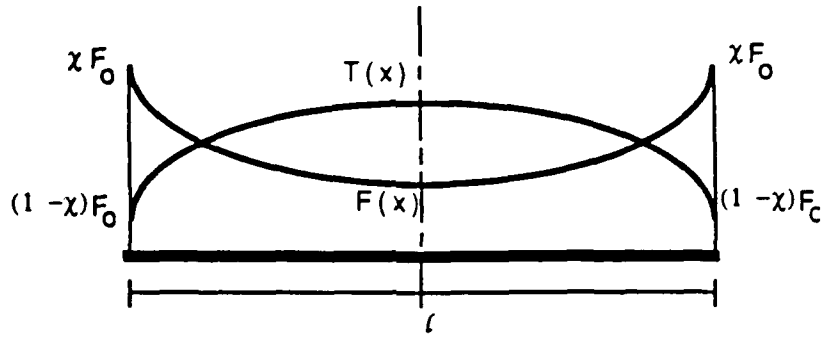

Fig. 7.4 - Typical force distributions within the fiber F(x) and within the matrix T(x).

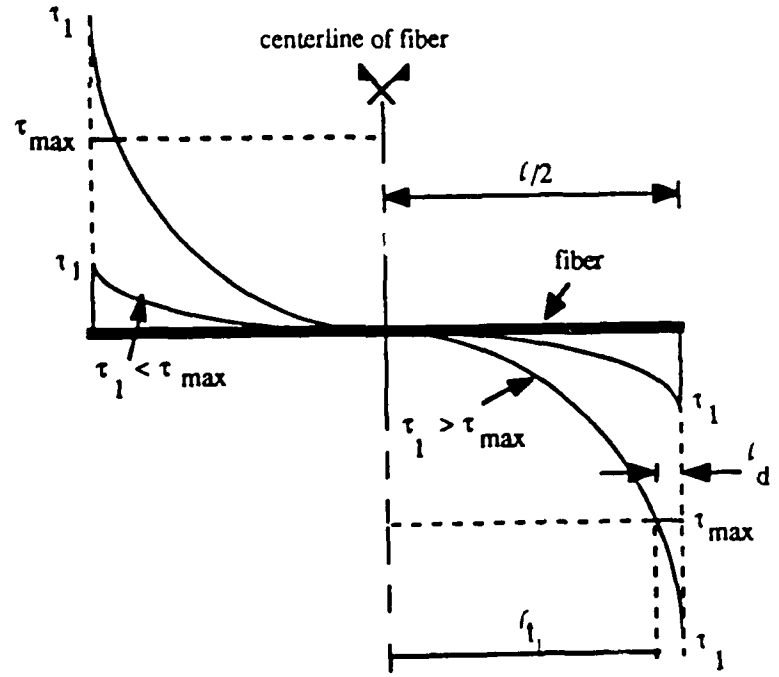

Fig. 7.5 - Typical shear stress distributions at the interface between the fiber and the matrix, before and after debonding.

$$\tau(x) = \frac{(\chi F_o - \tau_{max} \psi \ell_d) K}{\pi d \cosh(K \ell_t)} \sinh(K x) \qquad (7.29)$$

The value of ℓ_t can be found by solving the following non-linear equation in ℓ_t, or:

$$\tau(\ell_t) = \tau_{max}$$

or

$$\tau_{max} = \frac{\chi F_o - \tau_{max} \psi \left(\frac{\ell}{2} - \ell_t\right)}{\pi d} K \tanh(K \ell_t) \qquad (7.30)$$

ℓ_d, (Fig. 7.5), defined as half the debonded length is then equal to:

$$\ell_d = \frac{\ell}{2} - \ell_t \qquad (7.31)$$

7.4 NUMERICAL EXAMPLE

Let us consider the ideal case of a fiber-reinforced concrete tensile specimen that meets the conditions mentioned in the development of the model (perfect alignment as well as square packing, ...). The prism has an assumed square cross section, 3" x 3" (76.2 mm x 76.2 mm). The force applied is P = 4500 lbs (20000 N), the modular ratio n =8 , the modulus of elasticity of the steel fibers E_f = 29,000 ksi (2x105 MPa), the fiber length ℓ = 2in. (50.8 mm), the factor χ = 0.5 (arbitrarily chosen). The bond stress - slip relationship is assumed to be as in Fig. 7.6, hence the bond modulus κ = 40,000 ksi/in (10900 MPa/mm), the bond strength τ_{max} equals the frictional bond τ_f = 400 psi (2.76 MPa).

Case 1:

In this case, it is assumed that the diameter of the fibers d = 0.01 in (0.254 mm), and that the fiber volume fraction V_f = 1%. χ_{crit} = 0.075.

First, the applied stress σ_c is found:

$$\sigma_c = \frac{P}{A_c}$$

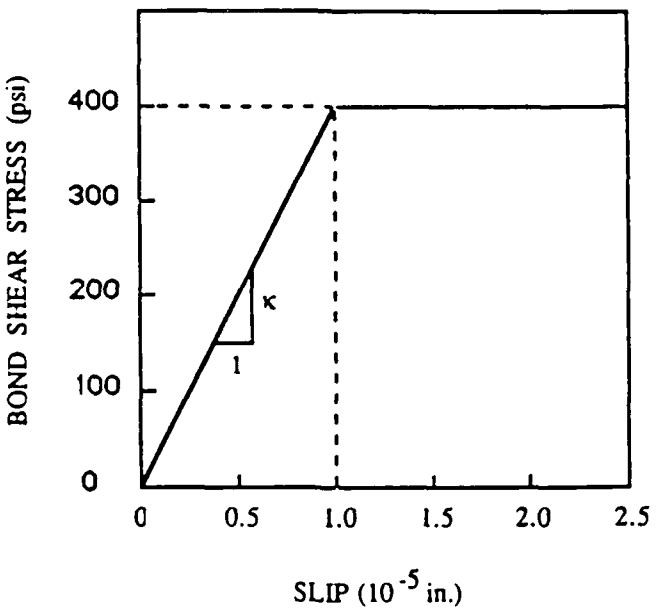

Fig. 7.6 - Assumed bond shear stress versus slip relationship in numerical example.

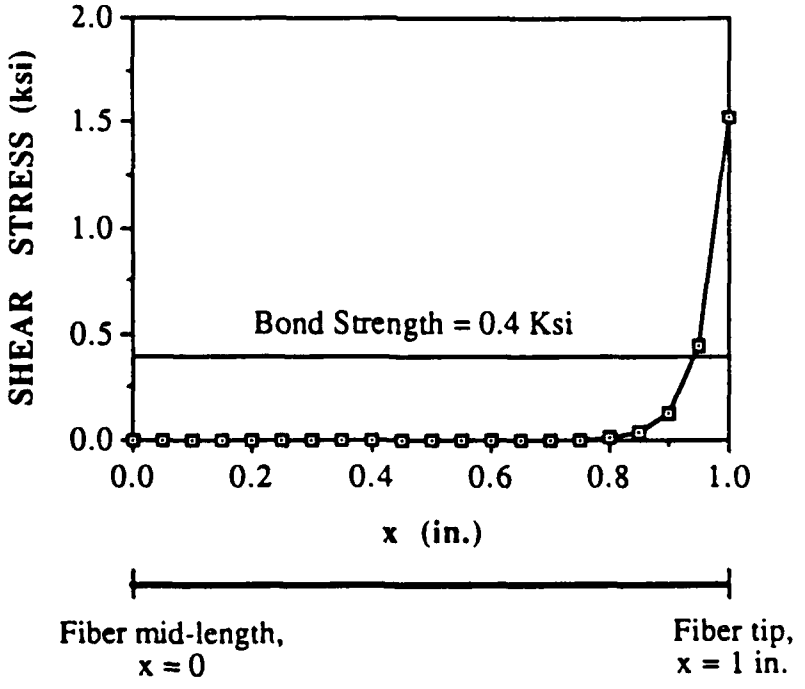

Fig. 7.7 - Predicted bond stress distribution - Case 1.

$$= \frac{4500 \text{ lbs}}{(3 \times 3) \text{ in}^2} = 500 \text{ psi} = 0.5 \text{ ksi } (3.45 \text{ MPa})$$

The force F_o applied on the representative unit is hence equal to:

$$F_o = \frac{\pi d^2}{4} \frac{\sigma_c}{V_f}$$

$$= \frac{\pi (0.01)^2 \times 0.5}{4 \times 0.01} = 0.003927 \text{ Kips } (17.5 \text{ N})$$

From Eq. 7.16 , K is such that:

$$K^2 = \frac{4}{E_f} \left(1 + n \frac{V_f}{1 - V_f} \right) \frac{\kappa}{d}$$

$$= \frac{4}{29000} \left(1 + 8 \frac{0.01}{1 - 0.01} \right) \frac{40000}{0.01}$$

or $K = 24.42 \text{ in}^{-1} (0.961 \text{ mm}^{-1})$

The bond distribution is described by Eq. 7.24, or:

$$\tau(x) = \left(\frac{\chi F_o K}{\pi d \cosh(K\frac{\ell}{2})} \right) \sinh (Kx)$$

$$= \left(\frac{0.5 \times 0.003927 \times 24.42}{\pi (0.01) \cosh(24.42 \times \frac{2}{2})} \right) \sinh (24.42x)$$

$= 7.572 \times 10^{-11} \sinh (24.42 x)$ (ksi) where x is in inche

$= 5.221 \times 10^{-10} \sinh (0.961 x)$ (MPa) where x is in mm.

To check if debonding has occurred, the maximum theoretical bond stress τ_1 is obtained @ $x = \frac{\ell}{2}$, or:

$\tau_1 = 7.572 \times 10^{-11} \sinh (24.42 \times \frac{2}{2}) = 1.53$ ksi (10.5 MPa) > τ_{max}

$= 0.4$ ksi (2.76 MPa)

therefore debonding occurs, over a length = 2 ℓ_d. To obtain ℓ_d, the value of ℓ_t has to be solved for as in Eq. 7.30:

$$\frac{\chi\ F_o - \tau_{max}\ \Psi\left(\frac{\ell}{2} - \ell_t\right)}{\pi\ d}\ K \tanh(K\ \ell_t) = \tau_{max}$$

or $$\left(\frac{0.5x0.003927 - 0.4x\pi x0.01x\left(\frac{2}{2} - \ell_t\right)}{\pi\ x\ 0.01}\right) x24.42 \tanh\left(24.42x\ell_t\right) = 0.4$$

hence ℓ_t = 0.885 in (22.5 mm).

$$\ell_d = \frac{\ell}{2} - \ell_t$$

$$= \frac{2}{2} - 0.885 = 0.115 \text{ in } (2.92 \text{ mm})$$

The bond shear stress distribution over half the fiber length is shown in Fig. 7.7.

Case 2:

The diameter of the fibers d is now assumed to be 0.02 in (0.508 mm), while the fiber volume fraction V_f is taken as 10%. $\chi_{crit} = 0.47$.

$$\sigma_c = \frac{4500\ \text{lbs}}{(3\ x\ 3)\ \text{in}^2} = 500 \text{ psi} = 0.5 \text{ ksi } (3.45 \text{ MPa})$$

The force F_o is now equal to:

$$F_o = \frac{\pi\ d^2}{4}\frac{\sigma_c}{V_f}$$

$$= \frac{\pi\ (0.02)^2}{4}\frac{0.5}{0.1} = 0.001571 \text{ Kips } (6.988 \text{ N})$$

$$K^2 = \frac{4}{E_f}\left(1 + n\ \frac{V_f}{1 - V_f}\right)\frac{\kappa}{d}$$

$$= \frac{4}{29000}\left(1 + 8\ \frac{0.1}{1 - 0.1}\right)\frac{40000}{0.02}$$

or $K = 22.83\ in^{-1}\ (0.899\ mm^{-1})$

The bond stress at any point can be found from:

$$\tau(x) = \left(\frac{\chi\ F_o\ K}{\pi\ d\ \cosh(K\frac{\ell}{2})}\right) \sinh(Kx)$$

$$= \left(\frac{0.5x0.001571x22.83}{\pi x(0.02)x\cosh(22.83x\frac{2}{2})}\right) \sinh(22.83x)$$

$= 6.943 \times 10^{-11} \sinh(22.83\ x)$ (ksi) where x is in inches.

$= 4.787 \times 10^{-10} \sinh(0.899\ x)$ (MPa) where x is in mm.

The maximum theoretical bond stress τ_1 is obtained @ $x = \frac{\ell}{2}$, or:

$\tau_1 = 6.943 \times 10^{-11} \sinh(22.83x\frac{2}{2}) = 0.285$ ksi (1.97 MPa) $< \tau_{max} = 0.4$ ksi (2.76 MPa)

therefore there is no debonding.

The bond shear stress distribution over half the fiber length for Case 2 is shown in Fig. 7.8.

7.5 CONCLUDING REMARKS

1. The analytical bond model developed in this chapter for fiber reinforced concrete composites is, to the authors' knowledge, the first attempt to predict analytically the bond stress distribution at the interface between fibers and the surrounding matrix using experimentally obtainable data, namely the bond shear stress-slip relationship.

2. The model predicts the shear stresses at the interface at any section, as well as the force distributions within the fibers and the matrix.

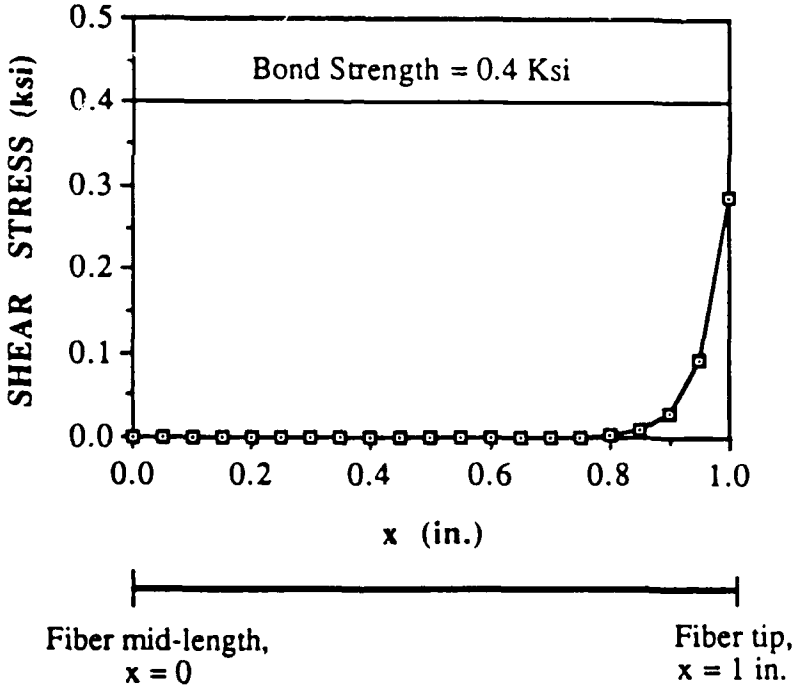

Fig. 7.8 - Predicted bond stress distribution - Case 2.

3. The method followed in deriving the model analytically can be applied to different assumed bond stress-slip relationships, whether linear or nonlinear. Experimentally derived bond stress-slip relationships can be easily accomodated.

4. The model presented incorporates all the important geometric and mechanical properties of both the fibers and the matrix.

5. In the course of the development of the model, no properties specific to the matrix or the fiber were made (except that they both behave linear-elastically). Hence, the same model can be used for all fibrous composites.

6. The model can be generalized to the case of random distribution and orientation by introducing adequate correction factors to the value of the volume fraction used.

CHAPTER VIII

MODELING OF BOND IN FIBER-REINFORCED CONCRETE BASED ON FORCE TRANSMISSION MECHANISM

8.1 INTRODUCTION

The model to be developed in this chapter, just like the one derived in Chap. 7 analytically predicts the interfacial bond shear stress, as well as the normal stress distributions in both the fiber and the matrix, when a fiber-reinforced concrete specimen is subjected to tensile stresses. However, while the model in Chap. 7 is based on an assumed bond shear stress versus slip relationship, the model of this chapter uses an assumed mechanism of force transmission between the fibers and the surrounding matrix to predict the bond and normal stress distributions at the interface and in the fibers and matrix. In both models, a perfect alignment of the fibers, as well as a square packing are assumed.

This model is furthermore used to analytically predict the interfacial bond modulus (ratio of the local shear stress and local slip under elastic conditions), which is shown to be location independent. An expression for the pre-cracking strength of a cementitious fiber composite is also derived and parametrically analyzed. Finally, the debonding stress of the composite is derived from the model.

The model developed here is essentially based on Yankelevsky's work [65], with the proper modifications and additions. Yankelevsky's work was centered on the problem of axially loaded specimens, where a single deformed bar is encased concentrically in a long concrete cylinder with the bar ends exposed.

The present model is based on an assumed interaction between uncracked concrete and a deformed bar through a mechanical system that uses the same approach as that of Yankelevsky [65]. Hence, it assumes the same mode of load transfer between the reinforcement and the matrix. The model applies primarily to continuous fibers and to long discontinuous fibers where it can be observed that one or more crack will cross the fiber so that the load is applied to the fiber.

8.2 BASIC ASSUMPTIONS

a) The structural model used by Yankelevsky for a reinforced bar embedded in concrete applies to fibers.

b) The angle α that is used in the derivation is constant.

c) The fibers are asssumed aligned within the specimen, and are squarely packed (Fig. 7.2).

d) Each individual fiber, along with its share of matrix acts and behaves independently of other fibers and the rest of the matrix body. The representative unit is further simplified to a cylinder of matrix encasing one fiber (Fig. 7.3).

e) Finally, the tensile load acting on the representative unit is assumed applied directly at the fiber tip.

8.3 MATHEMATICAL DERIVATION OF THE SHEAR STRESS DISTRIBUTION

A typical representative unit of the specimen is analyzed. This unit consists of one fiber and a cylinder of matrix that encases it, even though when a square packing is assumed, a typical unit would be expected to be a fiber encased by a prism of matrix with a square cross section. However, a circular cylinder with a cross sectional area equal to that of the prism is chosen to ensure that all the matrix area is accounted for. The length of the cylinder would be ℓ, same as the length of the fiber (see Fig. 7.3). Since a

uniform packing is assumed, the exterior diameter of this cylinder D can be directly found from the fiber diameter d and the volume fraction of the fibers V_f. The area of the fiber A_f and that of the matrix A_m are interrelated with the volume fraction, thus:

$$V_f = \frac{A_f}{A_f + A_m}$$

$$= \left(\frac{\frac{\pi\ d^2}{4}}{\frac{\pi\ D^2}{4}} \right)$$

thus:

$$V_f = \frac{d^2}{D^2}$$

or:

$$D = \frac{d}{\sqrt{V_f}} \qquad (8.1)$$

A tensile force F_o is applied to the representative unit. This force is a fraction of the total tensile force P applied to the specimen. A fraction of F_o is applied to the fiber end, while the balance of it is applied to the matrix directly. One extreme case would be to assume that the whole force F_o is applied at the fibers' ends, while nothing is given to the matrix (Fig. 8.1-a). Under this assumption, the tensile force in the fiber is maximum at the fiber's ends, decaying to a minimum at the middle. Thus, the tensile force in the matrix would be zero at the ends, and maximum at the middle. The bond shear stress and the slip at the interface between the fiber and the matrix would be maximum at the ends, and zero at the middle. The other extreme case would be to assume that the matrix takes the force at the ends in its entirety (Fig. 8.1-c). In that case, the force in the fiber would be zero at the ends, reaching a maximum in the middle, while the tension in the matrix would decrease from a maximum at the ends to a minimum at the middle. The bond stress and the slip would behave in a similar way as in the first case. If one is to assume that the force F_o is shared between the

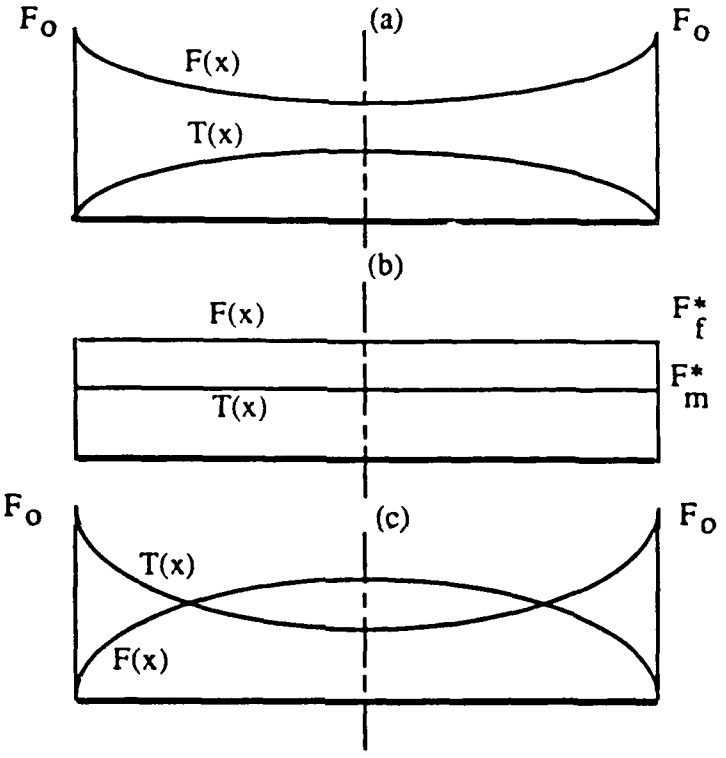

Fig. 8.1 - Typical force distribution in fiber F(x) and matrix T(x), assuming that the unit force F_o:
(a) is applied at the fibers' ends
(b) is shared by the matrix and the fiber in proportion to their relative stiffnesses
(c) is taken entirely by the matrix ends.

matrix and the fiber in proportion to their relative stiffnesses, then the tension in the fiber would be constant throughout the fiber length, and so would the force in the matrix (Fig. 8.1-b). The bond shear stress as well as the slip between the fiber and the matrix would both be nil. The model presented herein is derived based on the first assumption, i.e. that the force F_o is directly applied to the fibers' ends (Fig. 8.2) as in Yankelevsky's model [65].

Defining the x-axis as being the fiber axis with the origin at one of the ends, say the left one, a differential element of length dx of the fiber, located at a distance x from the origin is considered (Fig. 8.3-a). The tensile force in the fiber is resisted by inclined compressive forces dC, thus reducing the axial force F in the fiber as x increases. The structural model through which the resisting force dC is transferred to the matrix is shown in Fig. 8.3-b. The compressive struts AB and A'B' make an angle α with the x-axis, and react on the fiber by a force dC per unit length of fiber perimeter, hence creating a compressive stress dC/dx on the fiber periphery that makes an angle α with the fiber axis. As was mentioned before, the angle α is assumed to be location independent. α is indeed assumed to be a material property directly related to the interfacial properties of the composite. The circumference BB' is the locus of segment centroids of a typical disc EE' (Fig. 8.3-b). This disk would have an external diameter D and an internal diameter d. The forces dN, dC, and dT as shown in Fig. 8.3-b are in equilibrium. By such a mechanism, the tensile force is reduced at a rate of dF/dx in the fiber, and is increased at an equal rate in the matrix. The centroid location r (Fig. 8.3-b) is equal to:

$$r = \frac{D}{3} \cdot \left(\frac{1 + \frac{d}{D} + \frac{d^2}{D}}{1 + \frac{d}{D}} \right) \qquad (8.2)$$

but can be usually taken as D/3, especially for lower reinforcement ratios or higher D/d such as in the case of FRC.

Forces are then interrelated through static equilibrium and compatibility. A differential equation in F (the axial force in the steel) is obtained

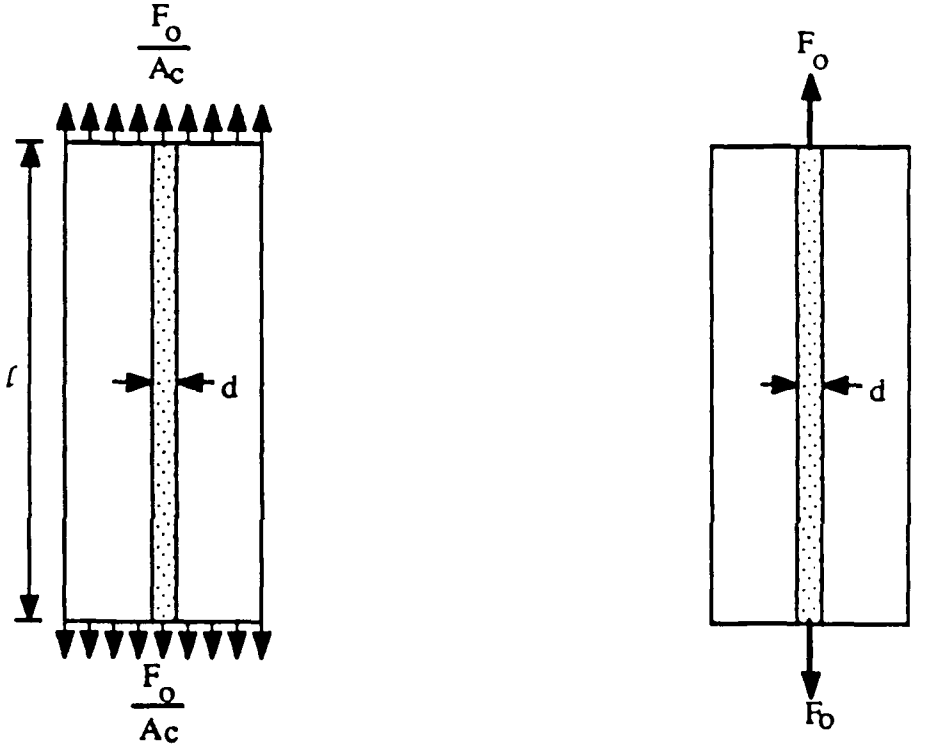

a. Actual load on representative unit

b. Assumed load on representative unit

Fig. 8.2 - Load on representative unit.

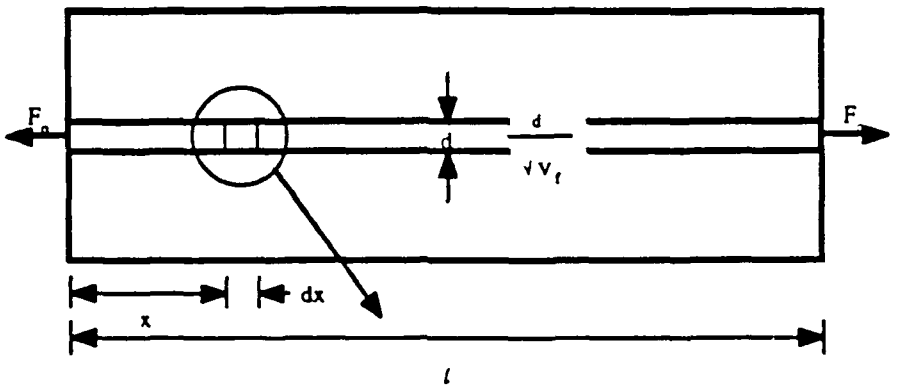

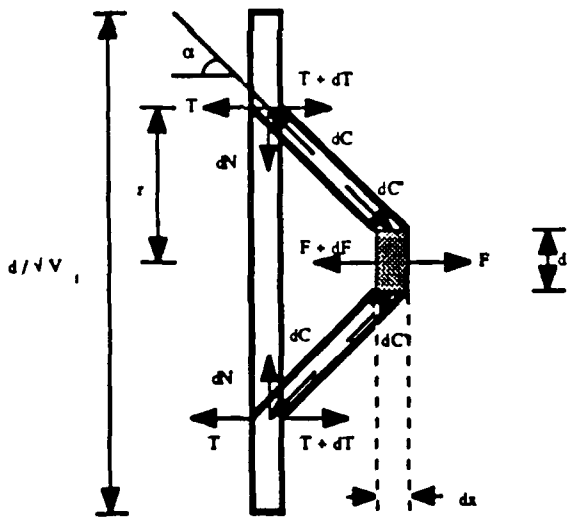

Fig. 8.3 - (a) Representative unit to be analyzed
(b) Structural model used in the development of the model, as adopted from Yankelevsky.

from compatibility equations (for more details, see Ref. 6). The general form of the differential equation was given as:

$$A_1 \frac{d^2F}{dx^2} - A_2 F = - A_3 \tag{8.3}$$

The coefficients A_1, A_2, and A_3 have been modified from their values given in [65] to accommodate the problem at hand (fiber-reinforced concrete), as well as to include the Poisson's ratio effect. These coefficients are found to be:

$$A_1 = \frac{\frac{\ln\left[\frac{4}{9 V_f}\right]}{\sin^2 \alpha} + \frac{3}{2} \sin^2 \alpha \frac{M}{q (m^2 - 1)}}{4 \pi E_m \cos^2 \alpha} \tag{8.4}$$

$$m = \frac{1}{\sqrt{V_f}} \tag{8.5}$$

$$q = \frac{2}{3}\left(1 + \frac{V_f}{1 + \sqrt{V_f}}\right) \tag{8.6}$$

$$M = [(1 + q^2) + \nu (1 - q^2)]\,[(1 + q^2 m^2) + \nu (1 - q^2 m^2)] \tag{8.7}$$

$$\begin{aligned} A_2 &= \frac{1}{E_f A_f} + \frac{1}{E_m A_m} \\ &= \frac{1}{E_f A_f}\left(1 + \frac{E_f}{E_m}\frac{A_f}{A_m}\right) \\ &= \left(\frac{4}{\pi d^2 E_f}\right)\left(1 + n \frac{V_f}{1 - V_f}\right) \\ &= \left(\frac{4}{\pi d^2 E_f}\right)\left(\frac{1 + (n - 1)V_f}{1 - V_f}\right) \end{aligned} \tag{8.8}$$

where:

$$\begin{aligned} n &= \text{modular ratio} \\ &= \frac{E_f}{E_m} \end{aligned} \tag{8.9}$$

ν = Poisson ratio of matrix

$$A_3 = \frac{F_o}{E_m A_m}$$

$$= F_o n \left(\frac{V_f}{E_f A_f (1 - V_f)} \right)$$

$$= \left(\frac{4}{\pi d^2 E_f} \right) F_o n \left(\frac{V_f}{1 - V_f} \right) \qquad (8.10)$$

where:

$$F_o = \left(\frac{\pi d^2}{4 V_f A_c} \right) P_c \qquad (8.11)$$

in which:

P_c = Total force on the composite

A_c = Cross-sectional area of composite

d = diameter of fiber

The solution to Eq. 8.3 is of the form:

$$F(x) = C_1 e^{\beta x} + C_2 e^{-\beta x} + \frac{A_3}{A_2} \qquad (8.12)$$

where:

$$\beta = \sqrt{\frac{A_2}{A_1}} \qquad (8.13)$$

$$\frac{A_3}{A_2} = F_o \left(\frac{n V_f}{(n-1) V_f + 1} \right) = F_f^* \qquad (8.14)$$

β can also be expressed in the following form:

$$\beta = \left(2 \frac{\sin(2\alpha)}{d} \right) \sqrt{\frac{Z_2}{Z_1}} \qquad (8.15)$$

in which:

$$Z_1 = \ln\left(\frac{4}{9V_f}\right) - \frac{3}{2}\sin^4\alpha\left(\frac{M}{q\,(m^2 - 1)}\right) \tag{8.16}$$

$$Z_2 = \frac{1}{n} + \frac{V_f}{1 - V_f} \tag{8.17}$$

Factors Z_1 and Z_2 are introduced for mathematical convenience and have no particular physical significance.

The factor F_f^* is the product of the overall force F_o times the fiber's relative stiffness (Eq. 8.14), while the balance of F_o, $F_m^* = F_o - F_f^*$ is proportional to the relative stiffness of the matrix.

$$F_m^* = F_o - F_f^*$$

$$= F_o \frac{1 - V_f}{(n-1)\,V_f + 1} \tag{8.18}$$

To coefficients C_1 and C_2 are obtained from the following boundary conditions:

(1) @ $x = 0$, $F = F_o$ (8.19)

$$\therefore \quad C_1 + C_2 + F_f^* = F_o$$

or

$$C_1 + C_2 = F_m^* \tag{8.20}$$

(2) @ $x = \frac{\ell}{2}$, $\tau = 0$, and hence $\frac{dF}{dx} = 0$. (8.21)

$$\frac{dF}{dx} = C_1 \beta e^{\beta x} - C_2 \beta e^{-\beta x} \tag{8.22}$$

$$\therefore \quad C_1 \beta e^{\beta \ell/2} - C_2 \beta e^{-\beta \ell/2} = 0$$

or

$$C_1 = C_2 e^{-\beta \ell} \tag{8.23}$$

$$(1) + (2) \Rightarrow C_2 e^{-\beta \ell} + C_2 = F_m^*$$

therefore:

$$C_1 = F_m^* \frac{e^{-\beta \ell}}{1 + e^{-\beta \ell}} \tag{8.24}$$

and

$$C_2 = F_m^* \frac{1}{1 + e^{-\beta \ell}} \tag{8.25}$$

$$F(x) = F_m^* \left(\frac{e^{-\beta \ell}}{1 + e^{-\beta \ell}} e^{\beta x} + \frac{1}{1 + e^{-\beta \ell}} e^{-\beta x} \right) + F_f^* \tag{8.26}$$

and $T(x) = F_o - F$

$$= F_m^* \left(1 - \frac{e^{-\beta \ell}}{1 + e^{-\beta \ell}} e^{\beta x} - \frac{1}{1 + e^{-\beta \ell}} e^{-\beta x} \right) \tag{8.27}$$

$$\tau(x) = \frac{-dF}{dx} * \frac{1}{\pi d}$$

$$= \frac{-\beta F_m^*}{\pi d} \left(\frac{e^{-\beta \ell}}{1 + e^{-\beta \ell}} e^{\beta x} - \frac{1}{1 + e^{-\beta \ell}} e^{-\beta x} \right)$$

$$= \frac{\beta F_o}{\pi d} \frac{1 - V_f}{(n-1) V_f + 1} \frac{e^{-\beta x} - e^{-\beta \ell} e^{\beta x}}{1 + e^{-\beta \ell}} \tag{8.28}$$

8.4 FIBER DEBONDING

Eq. 8.28 gives the theoretical bond or shear stress distribution along the fiber interface. However, it must be recognized that there is a limit that the shear stress τ cannot exceed, namely the bond shear strength of the interface, τ_{max} (Fig. 8.4). The maximum theoretical bond shear stress, referred to as τ_1, is given by Eq. 8.28, with $x = 0$.

$$\tau_1 = \frac{\beta F_o}{\pi d} \frac{1 - V_f}{(n-1) V_f + 1} \frac{1 - e^{-\beta \ell}}{1 + e^{-\beta \ell}} \tag{8.29}$$

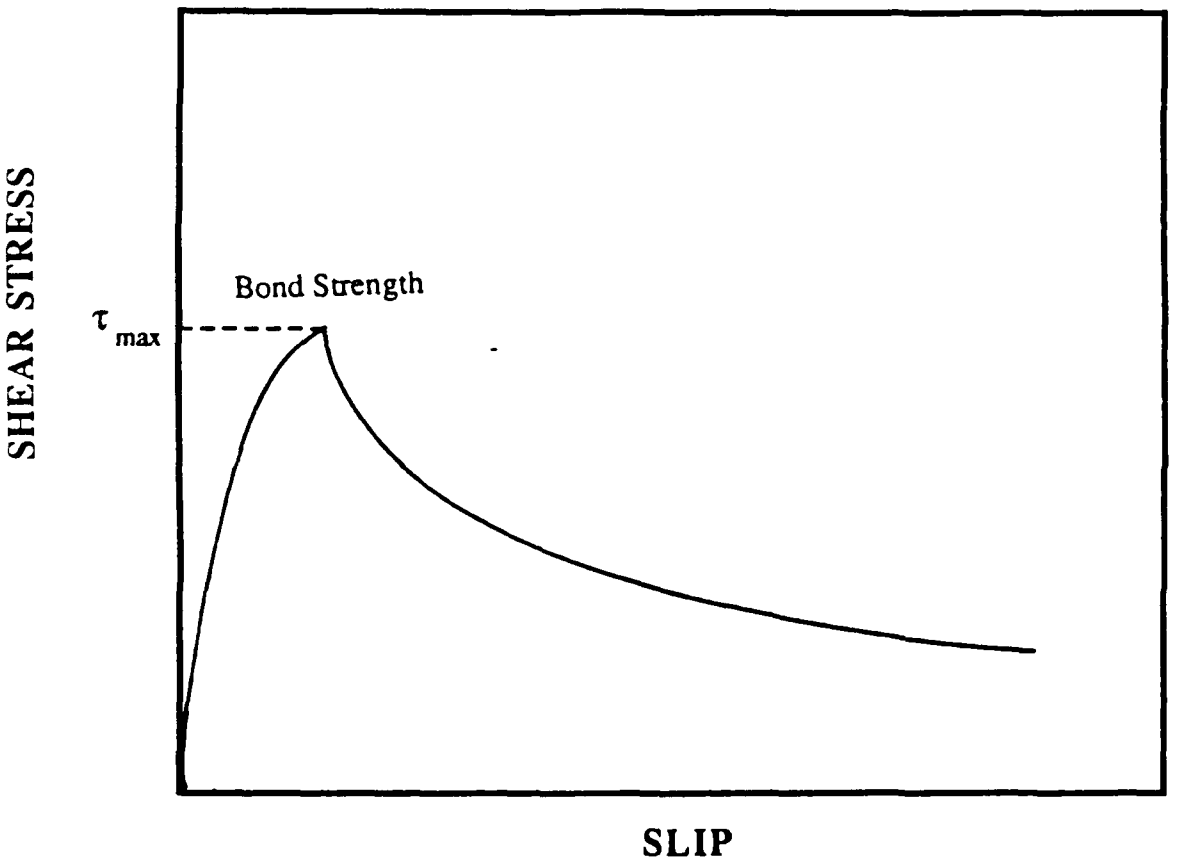

Fig. 8.4 - Example of a bond-slip relationship; the bond stress doesnot exceed the bond strength.

If τ_l does not exceed τ_{max}, the bond distribution, as predicted in Eq. 8.28 holds. This means that the stress σ_c applied to the composite does not cause any fiber debonding. Debonding will occur when $\tau_l = \tau_{max}$. The force F_o that would cause debonding can hence be found:

$$(F_o)_{deb} = \tau_{max} \left(\frac{(n-1)\ V_f + 1}{(1 - V_f)\ \beta} \right) \left(1 + e^{-\beta \ell}\right) \pi\, d \qquad (8.30)$$

But the stress in the composite $\sigma_c = P/\mathring{A}_c$ can be related to F_o through Eq. 8.11. The applied composite stress that would initiate debonding $(\sigma_c)_{deb}$ can hence be found as:

$$(\sigma_c)_{deb} = 4\, V_f\, \tau_{max}\, \frac{(n-1)\ V_f + 1}{(1 - V_f)\ \beta\ d}\ \frac{1 + e^{-\beta \ell}}{1 - e^{-\beta \ell}} \qquad (8.31)$$

$$= \rho\ \tau_{max} \qquad (8.32)$$

In Eq. 8.32, ρ is a dimensionless factor that is indicative of the strength of the bond within the composite. Here, ρ will be termed the Debonding Index. Fig. 8.5 shows the variation of this factor with the volume fraction, for different values of α. These were all chosen less than 45° in recognition of the fact that ρ is almost perfectly symmetrical about $\alpha = 45°$; in other words, ρ will have almost the same value for $\alpha = 45° + \alpha_1$ and $\alpha = 45° - \alpha_1$, when $\alpha_1 \leq 45°$. It is clear from the figure that for a given angle α, the Debonding Index ρ increases almost linearly with the volume fraction V_f. This curve would, nevertheless, only apply to fiber-reinforced composites in which the fiber volume fraction is relatively low, say $V_f \leq 5\%$. For higher volume fractions, the interaction between the fibers comes into the picture, hence changing the mechanics of the problem. Furthermore, everything else being equal, the closer α is to 45°, the lower the value of ρ.

Fig. 8.6 shows the variation of the Debonding Index with the modular ratio n, for different values of the volume fraction. As expected, higher values of n, meaning stronger relative fiber moduli, lead to higher factors. This means that everything else being equal, the higher the modulus of the fiber, the higher the debonding stress.

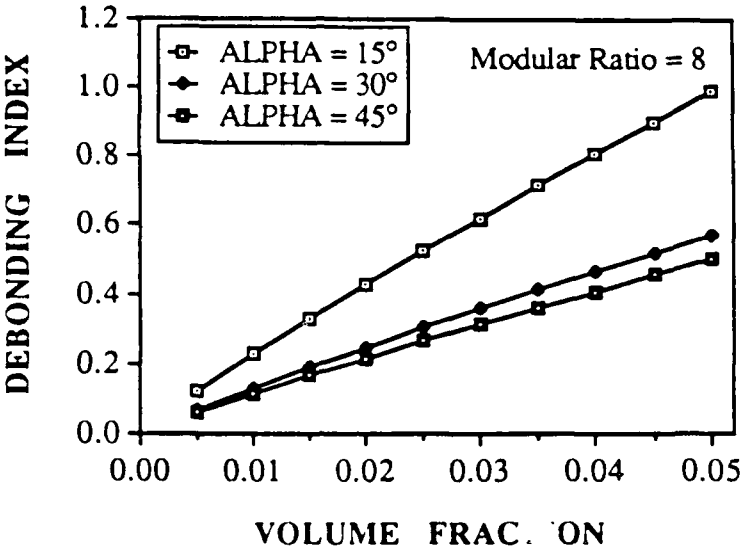

Fig. 8.5 - Debonding index versus volume fraction for different values of α.

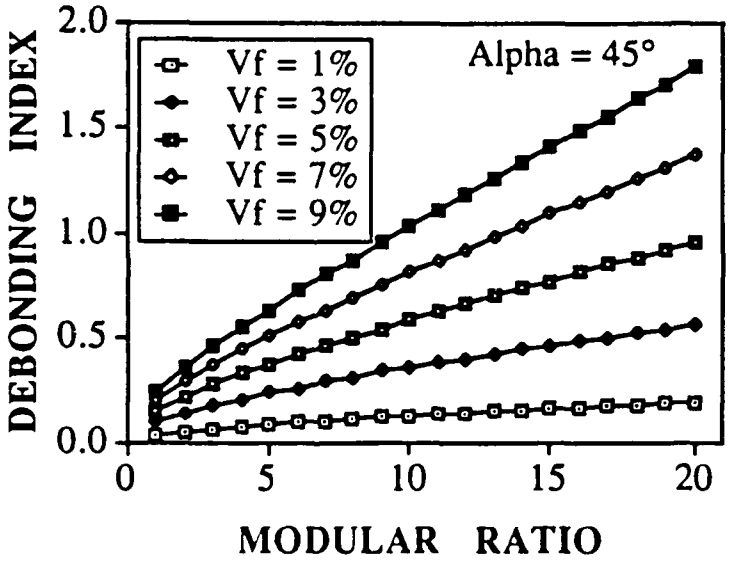

Fig. 8.6 - Debonding index versus modular ratio for different values of the volume fraction.

In the majority of cases, the factor $e^{-\beta \ell}$ can be neglected in Eq. 8.31, as the Debonding Index turned out to be basically independent of the fiber aspect ratio.

8.5 DEBONDING LENGTH

If the applied stress on the composite σ_c is less than $(\sigma_c)_{deb}$, the bond distribution along the interface between a given fiber and the matrix is as given in Eq. 8.28. On the other hand, if the composite stress exceeds $(\sigma_c)_{deb}$, then the fiber-matrix interface can be divided into two parts: a debonded part, $2\ell_d$ long, at both ends of the fiber, and the other, $\ell - 2\ell_d$ long, that is bonded. The higher the composite stress σ_c, the larger the value of the debonded length $2\ell_d$. There is no closed form solution for the general case where $0 \leq \ell_d \leq \ell/2$. To find the value of half the debonded length ℓ_d, the same differential equation described in Eq. 8.3 has to be solved, with the following differences:

a) The length ℓ is to be replaced with $\ell - 2\ell_d$

b) The force F_o is to be replaced with $F_o - \tau_{max}\, \psi\, \ell_d$

The interfacial shear stress distribution in the bonded zone becomes:

$$\tau_b(x) = \frac{\beta\, F_o'}{\pi\, d}\left(\frac{1 - V_f}{(n-1)\, V_f + 1}\, \frac{e^{-\beta x} - e^{-\beta(\ell - \ell_d)} e^{\beta x}}{1 + e^{-\beta(\ell - \ell_d)}} \right) \qquad (8.33)$$

where

$$F_o' = F_o - \tau_{max}\, \psi\, \ell_d$$

For a given P, hence ℓ_d, the length of the debonded zone can be found by solving the equation:

$$\tau_b(0) = \tau_{max}$$

or

$$\tau_{max} = \frac{\beta\,(F_o - \tau_{max}\,\psi\,\ell_d)}{\pi\,d}\left(\frac{1 - V_f}{(n-1)\,V_f + 1}\;\frac{1 - e^{-\beta(\ell-\ell_d)}}{1 + e^{-\beta(\ell-\ell_d)}}\right) \tag{8.34}$$

Therefore, to find the debonded length for a given F_o such that $(F_o)_{deb} \le F_o \le (\tau_{max}\,\pi d\ell)$, the non-linear Eq. 8.34 has to be solved by trial and error.

The bond distribution along the interface between the reinforcement and the matrix in the case where debonding occurs is as follows:

$$\tau(x) = \tau_{max} \qquad \text{for } 0 \le x \le \ell_d$$

and

$$\tau(x) = \frac{\beta\,F_o'}{\pi\,d}\left(\frac{1 - V_f}{(n-1)\,V_f + 1}\right)\frac{e^{-\beta x} - e^{-\beta(\ell-\ell_d)}e^{\beta x}}{1 + e^{-\beta(\ell-\ell_d)}} \qquad \text{for } \ell_d \le x \le \ell/2 \tag{8.35}$$

Fig. 8.7 shows two cases of loading: in one case, τ_1 is less than τ_{max}, and hence no debonding occurs, while in the other, the applied stress is larger than $(\sigma_c)_{deb}$, and hence the bond distribution at the interface is described by Eq. 8.34. Fig. 8.8 shows the variation of the interfacial bond shear stress distribution as the applied composite stress σ_c increases.

8.6 APPLICATION OF THE MODEL

8.6.1 Bond Modulus

The slip S is the relative displacement of the reinforcement with respect to the matrix, or:

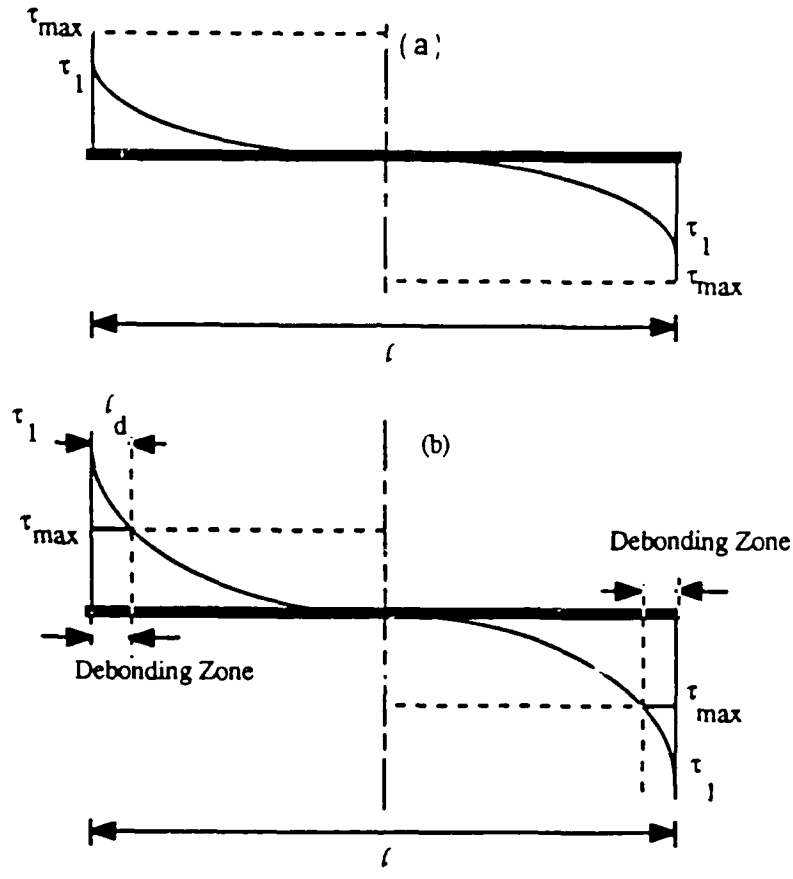

Fig. 8.7 - Interfacial bond distributions in the cases of: a) no debonding, and b) debonding occuring.

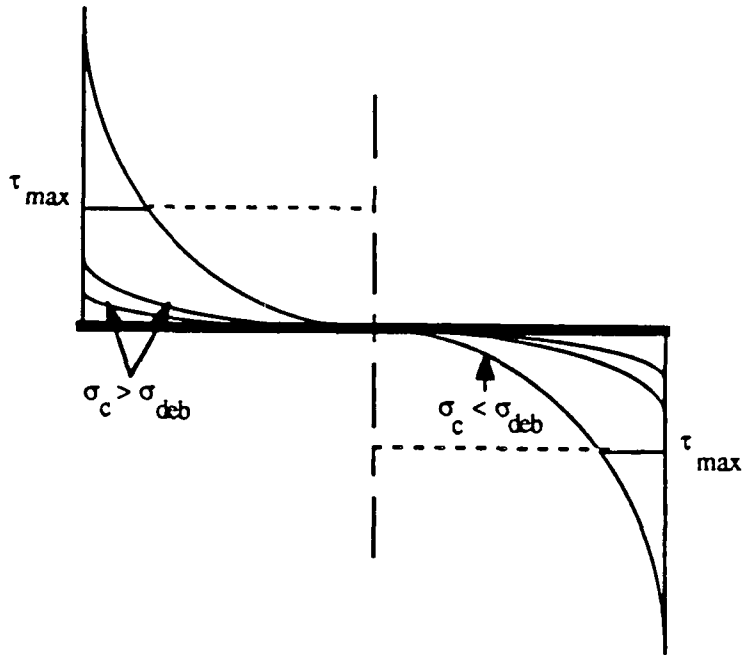

Fig. 8.8 - Variation of bond distribution with increasing applied composite stress.

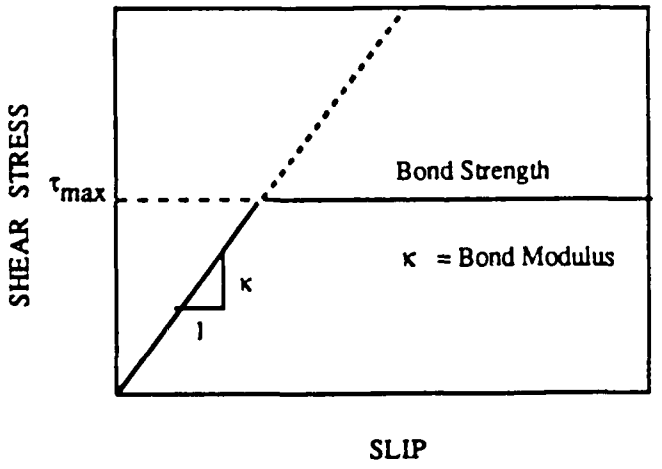

Fig. 8.9 - Bond shear stress versus slip relationship based on predicted bond modulus and on bond strength.

$$S(x) = \delta_m - \delta_f \tag{8.36}$$

$$= \int (\varepsilon_m - \varepsilon_f)\, dx$$

$$= \int \left(\frac{T}{E_m A_m} - \frac{F}{E_f A_f} \right) dx$$

$$= \frac{1}{E_f A_f} \int \left(\frac{A_f}{A_m} \frac{E_f}{E_m} T - F \right) dx$$

$$= \frac{1}{E_f A_f} \int \left(\frac{V_f}{1 - V_f} n T - F \right) dx \tag{8.37}$$

Replacing F and T by the expressions in Eqs. 8.26 and 8.27, and replacing F_f^* and F_m^* by their respective values given in Eqs. 8.14 and 8.15, it can be shown that the slip S can be expressed as follows:

$$S(x) = \frac{4 F_o}{\beta \pi d^2 E_f} \frac{e^{-\beta x} - e^{-\beta \ell} e^{\beta x}}{1 + e^{-\beta \ell}} \tag{8.38}$$

It can be noticed from Eqs. 8.59 and 8.69 that the ratio of the shear stress to the slip in the elastic range (τ-to-S ratio) is independent of x, and hence of the location. Furthermore, this ratio is constant given the volume fraction, the type of fibers and the matrix. This ratio, the bond modulus, is equal to:

$$\kappa = \frac{\beta^2 (1 - V_f) d E_f}{4 [1 + (n - 1) V_f]} \tag{8.39}$$

Recalling the expression of β given in Eq. 8.17, Eq. 8.39 can be rewritten as:

$$\kappa = \frac{\sin^2(2\alpha) Z_2 (1 - V_f) E_f}{Z_1 [1 + (n - 1) V_f]} \frac{1}{d} \tag{8.40}$$

Z_2 can be replaced by its value as given in Eq. 8.17. Eq. 8.40 hence becomes:

$$\kappa = \frac{\sin^2(2\alpha)}{Z_1} \frac{E_m}{d}$$

$$= \kappa_1 \frac{E_m}{d} \qquad (8.41)$$

where:

$$\kappa_1 = \frac{\sin^2(2\alpha)}{Z_1} \qquad (8.42)$$

The bond modulus κ is the slope of the bond stress versus slip curve in its elastic ascending portion (Fig. 8.9).

Since the ratio $\frac{E_m}{d}$ has the same units as κ, κ_1 is hence a dimensionless factor referred to as the Bond Modulus Index (BMI). This factor increases almost proportionally with increasing volume fraction. Figs. 8.10 and 8.11 show the variation of κ_1 as a function of the volume fraction for different values of the angle α and as a function of the angle α for different volume fractions V_f, respectively. As can be seen in Fig. 8.10, for a given volume fraction, the highest κ_1 is obtained for an angle α = 45°. For angles less than or greater than 45°, κ_1 is less. The bond modulus κ is hence directly proportional to the elastic modulus of the matrix E_m, inversely proportional to the fiber diameter d, almost directly proportional to $\sin^2(2\alpha)$, of the volume fraction V_f, but is almost insensitive to the value of the Poisson's ratio of the matrix ν, even though ν is included in the expression of κ_1.

The bond modulus κ is usually thought of as being an interface property. Therefore, its dependency on the fiber volume fraction V_f is somehow unexpected. Nevertheless, this dependency can be accounted for by relating it to the confining effect of fibers. Indeed, the higher the volume fraction, the closer the fibers and the smaller the diameter D of the representative unit.

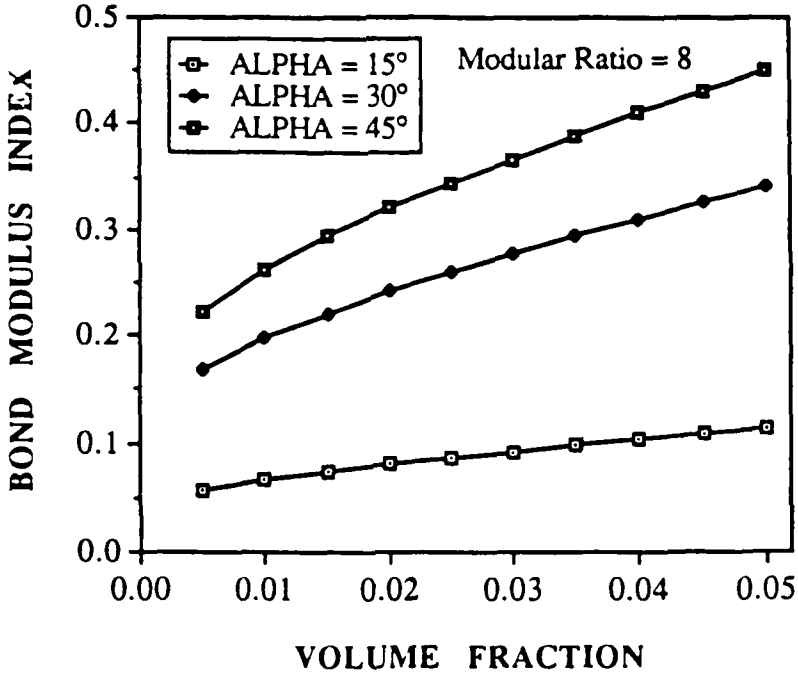

Fig. 8.10 - Bond modulus index versus volume fraction for different values of α.

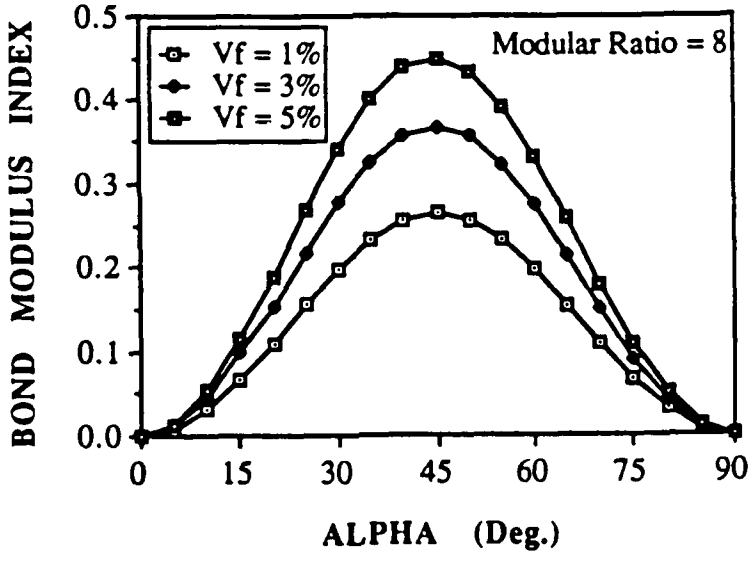

Fig. 8.11 - Bond modulus index versus α for different values of the volume fraction.

8.6.2 Composite Pre-cracking Strength

The model presented here can be used to predict the pre-cracking strength in tension of fiber-reinforced cement composites, assuming the fibers to be perfectly aligned and squarely packed. A typical stress-elongation relationship for a fiber-reinforced cementitious composite would display an almost linear behavior up to cracking. Beyond this point, a different behavior is observed. The maximum pre-cracking stress or the pre-cracking strength is hence significant and is addressed in what follows.

From Eq. 8.27, the maximum tensile force in the matrix can be found by setting $x = \frac{\ell}{2}$. Or:

$$T_{max} = F_m^* \left(1 - \frac{2\ e^{-\beta\ell/2}}{1 + e^{-\beta\ell}}\right) \tag{8.43}$$

$$= \Omega\ F_m^* \tag{8.44}$$

where:

$$\Omega = 1 - \left(\frac{2\ e^{-\beta\ell/2}}{1 + e^{-\beta\ell}}\right) \tag{8.45}$$

The maximum tensile stress in the matrix is hence the ratio of this force to the area of the matrix, A_m, that is:

$$\sigma_m = \frac{T_{max}}{A_m}$$

$$= \frac{\Omega\ F_m^*}{A_m} \tag{8.46}$$

where:

$$A_m = \frac{\pi}{4}(D^2 - d^2) \tag{8.47}$$

$$= \frac{\pi\, d^2}{4}\left(\frac{D^2}{d^2} - 1\right)$$

$$= \frac{\pi\, d^2}{4}\left(\frac{1 - V_f}{V_f}\right) \tag{8.48}$$

The composite is assumed to crack when the tensile stress in the matrix F_f^* reaches the tensile strength of the matrix, f_t. Setting σ_m equal to f_t, F_m^* is then found:

$$F_m^* = \frac{A_m\, f_t}{\Omega} \tag{8.49}$$

but F_m^* is related to F_o as in Eq. 8.18, therefore the following F_o is found:

$$(F_o)_{cr} = \frac{\pi\, d^2}{4}\,\frac{(n - 1)V_f + 1}{V_f\, \Omega}\, f_t \tag{8.50}$$

F_o in turn could be related to the composite stress $\sigma_c = \frac{P}{A_c}$ through the following expression:

$$F_o = \frac{\pi\, d^2}{4\, V_f}\, \sigma_c \tag{8.51}$$

Combining Eqs. 8.50 and 8.51, and solving for σ_c will give the composite cracking strength $(\sigma_c)_{cr}$, hence:

$$(\sigma_c)_{cr} = \frac{1}{\Omega}\,[(n - 1)\, V_f + 1]\, f_t \tag{8.52}$$

Therefore, the cracking strength of the composite is the product of a factor times the tensile strength of the matrix.

It is worth noting that in the development of this equation, it was assumed that the matrix is weaker than the reinforcement. Eq. 8.52 would therefore only pertain to composites that meet this condition.

A closer look at the factor Ω ought to be taken. From Eq. 8.15, the following can be written:

$$\beta \ell = \frac{2 \sin(2\alpha)}{d} \sqrt{\frac{Z_2}{Z_1}}\, \ell \tag{8.53}$$

$$= \omega \frac{\ell}{d} \tag{8.54}$$

where

$$\omega = 2 \sin(2\alpha) \sqrt{\frac{Z_2}{Z_1}} \tag{8.55}$$

Ω can now be expressed as follows:

$$\Omega = 1 - \frac{2\ \mathrm{Exp}\left(-\omega \frac{\ell}{2d}\right)}{1 + \mathrm{Exp}\left(-\omega \frac{\ell}{d}\right)} \tag{8.56}$$

Ω is thus a function of the fiber aspect ratio $\frac{\ell}{d}$, rather than the fiber length ℓ. It is also function of ω, which in turns depends on the angle α, on the volume fraction V_f, on the modular ratio n, and on the Poisson ratio of the matrix ν.

The factor Ω, which will be referred to as the Bonding Factor, reflects the quality of bond that exists between the matrix and the reinforcement. In the theoretical case of a "perfect bond", Ω can be taken equal to 1, whereas where there is no bond at all between the fiber and the matrix at the interface, $\Omega = 0$, in which case Eq. 8.52 does not apply. In the case of a perfect bond, Ω would be equal to 1 and the cracking strength of the composite would then be:

$$(\sigma_c)_{cr} = [(n - 1)\, V_f + 1]\, f_t \tag{8.57}$$

which is the same as the equation that could be predicted from a transformed section analysis, assuming perfect strain compatibility, linear elastic materials, continuous reinforcement, as well as a matrix weaker than the

reinforcement. Fig. 8.12 shows the variation of the bonding factor Ω versus the fiber aspect ratio.

In Fig. 8.13, the cracking strength ratio, $\frac{(\sigma_c)_{cr}}{f_t}$ is plotted against the fiber volume fraction V_f, for different values of the aspect ratio. It can be seen from the graph that for $\frac{\ell}{d} \geq 60$, the cracking strength ratio becomes insensitive to the bonding factor and approaches the values predicted in Eq. 8.57. It can also be seen from Fig. 8.13 that everything else being equal, composites reinforced with lower aspect ratio fibers have higher cracking strengths. This could be explained by observing that a shorter fiber would display a more uniform bond shear stress distribution at the interface. The fibers are hence more efficient as far as bond goes. However this result is surprizing, since the theory on which the model is based assumes that the load is applied to the fibers thus is applicable primarily to long fibers. While the theory predicts a peak, followed by a dip in the case of fibers with aspect ratio = 10 (Fig. 8.13), no reasonable explanation can be provided for such a behavior.

Fig. 8.14 shows that the cracking strength is not very sensitive to the angle α, so long as a does not approach the extremes values of 0 or 90°. Finally, the cracking strength ratio as per Eq. 8.57 is plotted in Fig. 8.15 versus the modular ratio for different values of the volume fraction. It can be observed that the cracking strength increases with both the volume fraction of fibers and the modular ratio.

8.7 CONCLUDIND REMARKS

The following remarks can be made about this model:

1. This model predicts the bond shear stresses at the interface between the fibers and the surrounding matrix in a pure tension specimen. It also predicts the tension stresses in the fibers and in the matrix.

2. The model was used to determine theoretically the bond modulus, which is the slope of the bond shear stress-slip curve. It was shown that the bond modulus is location-independent.

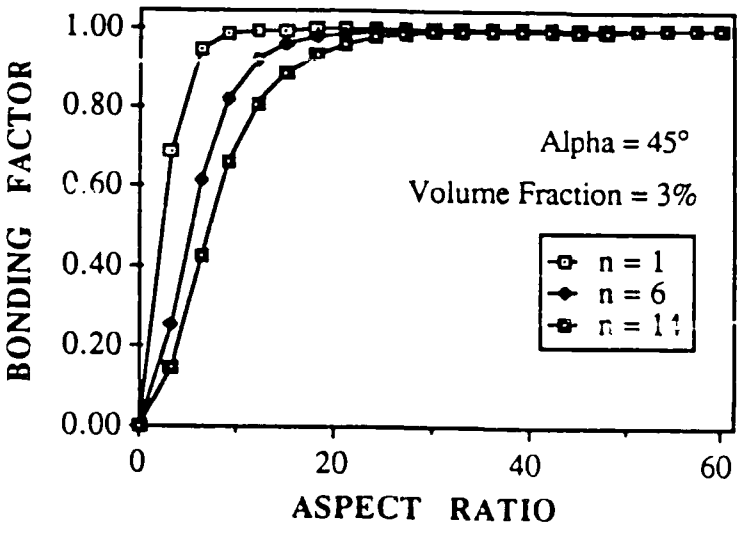

Fig. 8.12 - Bonding factor versus aspect ratio for different values of the modular ratio.

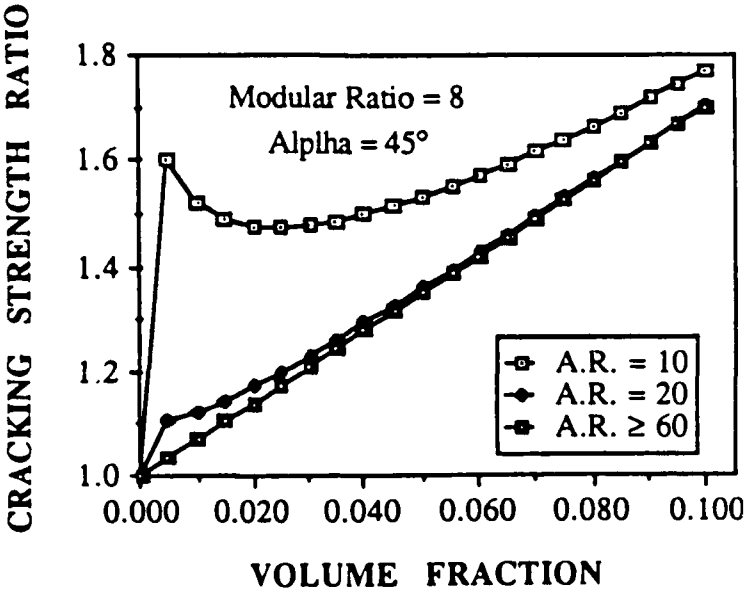

Fig. 8.13 - Cracking strength ratio versus volume fraction for different values of the aspect ratio.

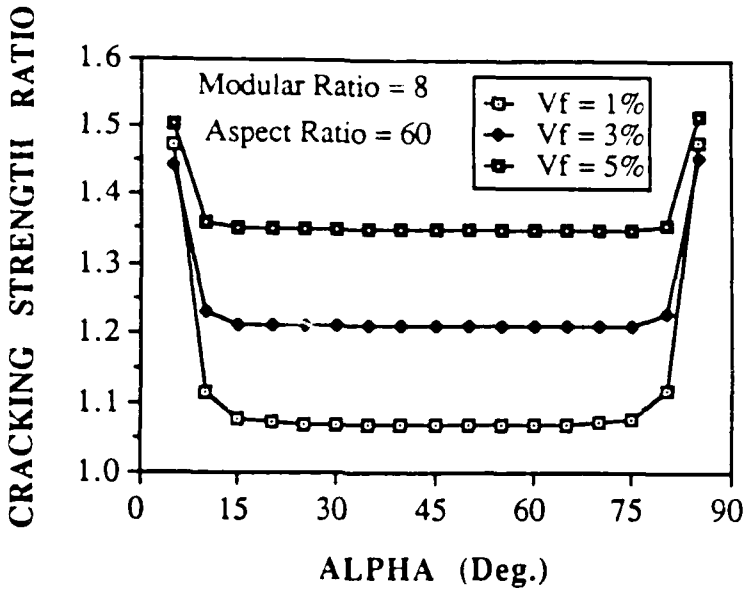

Fig. 8.14 - Cracking strength ratio versus α for different values of the volume fraction.

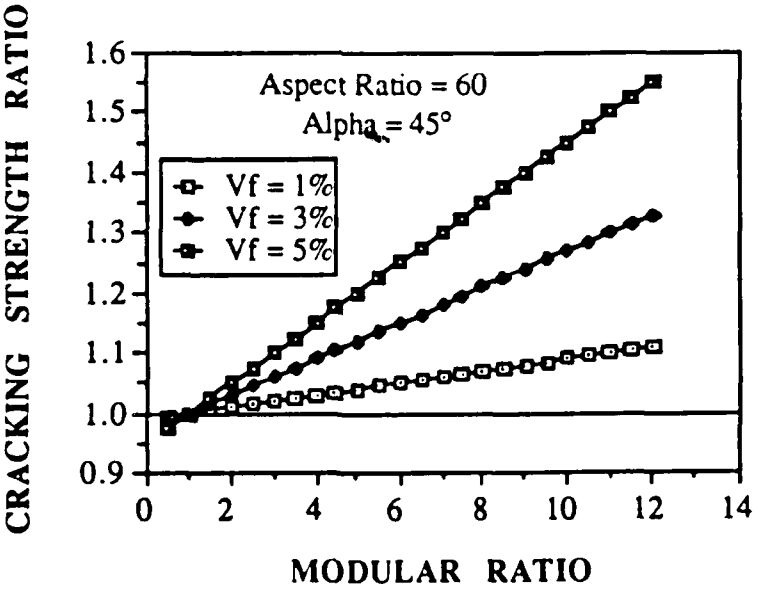

Fig. 8.15 - Cracking strength ratio versus modular ratio for different values of the volume fraction.

3. The model was also used to predict the pre-cracking strength of the composite as a function of the tension strength of the matrix. The expression derived for the pre-cracking strength is based on the assumption that the matrix is weaker in tension than the fiber.

4. An expression for the debonding stress, which is the stress that needs to be applied to the composite to impend debonding, was also derived from the model. It was a direct function of the strength of the bond between the fiber and the matrix.

6. While the mathematical expression for the bond modulus was derived based on the assumption that the force F_o is applied in its entirety to the fibers' ends, it can be shown that this expression (of bond modulus) is actually independent of this assumption. This result came as no surprise, since the bond modulus should be a material property that is independent of the load, or its mode of application. As for the other expressions derived, i.e. bond stress, tension stress, precracking strength, they were dependent on the load application assumption.

BIBLIOGRAPHY

BIBLIOGRAPHY

1. ACI Committee 408, "Bond Stress- The State of the Art," (ACI 408R-66), ACI Journal, Proceedings Vol. 63, No. 11, Nov. 1966, pp. 1161-1189.

2. Allen, H. G., "Glass Fibre Reinforced Cement: Strength and Stiffness," CIRIA Report 55, Construction Industry Research and Information Association, London, Sept. 1975.

3. Aveston, J.; Mercer, J. M.; and Sillwood, J. M., "Fibre Reinforced Cements-Scientific Foundations for Specifications," Proceedings, Conference on Composites, Standards, Testing and Design, London, Apr. 1974, IPC Science and Technology Press, 1974, pp. 93-102.

4. Bartos, Peter, " Review Paper: Bond in Fibre Reinforced Cements and Composites," The International Journal of Cement Composites, Vol. 3, No. 3, Aug. 1981, pp. 159-177.

5. Beaumont, P. W. R., and Aleszka, J. C., "Cracking and Toughening of Concrete and Polymer-Concrete Dispersed with Short Steel Wires," Journal of Material Science, Vol. 13, No. 8, Aug. 1978, pp. 1749-60.

6. Bertero, V. V.; Popov, E. P.; and Viwathanatepa, S., "Bond of Reinforcing Steel: Experiments and a Mechanical Model," Paper presented at the Annual ACI Convention, Toronto, Apr. 1978.

7. Betz, E., "Experimental Studies of the Fibre Pull-out Problem," Journal of Materials Science, Vol. 17, Jan.-Mar. 1982, pp. 691-700.

8. Borges, J. F., "Structural Behavior under Repeated Loading," Working Group on the Resistance of Structures, European Association for Earthquake Engineering, Lisbon, 1973.

9. "Bond Action and Bond Behaviour of Reinforcement: State-of-the-Art Report," Bulletin d"Information No. 151, Comité Euro-International du Béton, Paris, Apr. 1982.

10. Burakiewicz, A., "Testing of Fiber Bond Strength in Cement Matrix," Proceedings, RILEM Symposium on Testing and Test Methods of Fibre Cement Composites, Edited by R. N. Swamy, The Construction Press, 1978, pp. 355-365.

11. Edward, A. D., and Picard, A., "Bond Properties of 1/2" Strands," ACI Journal, Proceedings, Vol. 69, No. 11, Nov. 1972, pp. 684-689.

12. Edwards, A. D., and Yannopoulos, P. J., "Local Bond-Stress to Slip Relationships for Hot Rolled Deformed Bars and Mild Steel Plain Bars," ACI Journal, Proceedings Vol. 76, No. 3, Mar. 1979, pp.405-420.

13. Edwards, A. D., and Yannopoulos, P. J., "Local Bond Stress-Slip Relationships under Repeated Loading," Magazine of Concrete Research (London), Vol. 30, No. 103, June 1978, pp. 62-72.

14. Eligehausen, R.; Popov, E. P.; and Bertero, V. V., "Local Bond Stress-Slip Relationships of Deformed Bars under Generalized Excitations," Earthquake Engineering Research Center, Report No. UCB/BERC-83/23, University of California, Berkeley, California, 1983, 169 pp.

15. Ferguson, Phil M., "Bond Stress - The State of the Art," ACI Journal, Proceedings Vol. 63, No. 11, Nov. 1966, pp. 1161-1188.

16. Gokoz, Ulker N., and Naaman, Antoine E., "Effect of Strain-Rate on the Behaviour of Fibres in Mortar," The International Journal of Cement Composites, Vol. 3, No. 3, Aug. 1981, pp. 187-202.

17. Gopalaratnam, G. S., and Shah, S. P., "Tensile Failure of Steel Fiber-Reinforced Mortar," ASCE Journal of Engineering Mechanics, Vol. 113, No. 5, May 1987, pp. 635-652.

18. Goto, Y., "Cracks Formed in Concrete around Deformed Tension Bars," ACI Journal, Proceedings Vol. 68, No. 4, Apr. 1974, pp. 244-251.

19. Gray, R. J., and Johnston, C. D., "The Measurement of Fibre-Matrix Interfacial Bond Strength in Steel Fibre-Reinforced Cementitious Composites," Proceedings, RILEM Symposium on Testing and Test Methods of Fibre Cement Composites, Edited by R. N. Swamy, The Construction Press, 1978, pp. 317-328.

20. Gray, R. J., "Analysis of the Effect of Embedded Fibre Length on Fibre Debonding and Pull-out from an Elastic Matrix; Part 1, Review of Theories," Journal of Materials Science, Vol. 19, No. 3, Jan.-Mar. 1984, pp. 861-870.

21. Gray, R. J., "Analysis of the Effect of Embedded Fibre Length on Fibre Debonding and Pull-out from an Elastic Matrix; Part 2, Application to a Steel Fibre-Cementitious Matrix Composite System," Journal of Materials Science, Vol. 19, Apr.-June 1984, No. 5, pp. 1680-1691.

22. Hawkins, N. M., and Lin, I. J., "Bond Characteristics of Reinforced Bars for Seismic Loadings," Proceedings, 3rd Canadian Earthquake Engineering Conference, McGill University, Montreal, June 1979,, pp. 1225-1252.

23. Houde, J., and Mirza, M. S. " A Study of Bond Stress-Slip Relationships in Reinforced Concrete," Structural Concrete Series No. 72-8, McGill University, Montreal, Apr. 1972.

24. Hughes, B. P., and Fattuhi, N. I., "Fibre Bond Strengths in Cement and Concrete," Magazine of Concrete Research, Vol. 27, No. 92, Sept. 1975, pp. 161-166.

25. Jiang, D. H.; Shah, S. P.; and Andonian, A. T., "Study of the Transfer of Tensile Forces by Bond," ACI Journal, Proceedings Vol. 81, No. 3, May-June 1984, pp. 251-259.

26. Jimenez, R.; White, R. N.; and Gergely, P., "Bond and Dowel Capacities of Reinforced Concrete," ACI Journal, Proceedings Vol. 76, No. 1, Jan. 1979, pp. 73-92.

27. Kar, J. N., and Pal, A. K., "Strength of Fibre Reinforced Concrete," Proceedings, American Society of Civil Engineers Journal, Structural Division, Vol. 98, ST5, May 1972, pp. 1053-68.

28. Kemp, E. L., and Wilhelm, W. J., "Investigation of the Parameters Influencing Bond Cracking," ACI Journal, Proceedings, Vol. 76, No. 1, Jan. 1979, pp. 47-71.

29. Laws, V., "Mechanical Aspects of the Fibre-Cement Bond," Journal of Composites, Vol. 13, No. 2, Apr. 1982, pp. 145-151.

30. Losberg; Anders; Olsson; and Per-Åke, "Bond Failure of Deformed Reinforcing Bars based on the Longitudinal Splitting Effect of the Bars," ACI Journal, Proceedings Vol. 76, No. 1, Jan. 1979, pp. 5-18.

31. Lutz LeRoy, A.; Gergely, P.; and Winter, G., "The Mechanics of Bond and Slip of Deformed Reinforcing Bars in Concrete," Structural Engineering Report No. 324, Cornell University, Aug. 1966.

32. Lutz Leroy, A., and Gergely, Peter, "Mechanics of Bond and Slip of Deformed Bars in Concrete," ACI Journal, Proceedings Vol. 64, No. 11, Nov. 1967, pp. 711-721.

33. Lutz, L. A., "Analysis of Stresses in Concrete near a Reinforcing Bar due to Bond and Transverse Cracking," ACI Journal, Proceedings Vol. 67, No. 10, Oct. 1970, pp. 778-787.

34. Maage, M., "Steel Fibre Bond Strengths in Cement-Based Matrices Influenced by Surface Treatments," Cement and Concrete Research, Vol. 7, No. 6, Nov. 1977, pp. 703-710.

35. Maage, Magne, "Fibre Bond and Friction in Cement and Concrete," Proceedings, RILEM Symposium on Testing and Test Methods of Fibre Cement Composites, Edited by R. N. Swamy, The Construction Press, 1978, pp. 329-336.

36. Mangat, P. S., and Motamedi Azari, M., "A Theory for the Free Shrinkage of Steel Fibre Reinforced Cement Matrices," Journal of Materials Science, Vol. 19, No. 7, July 1984, pp. 2183-2194.

37. Mirza, Saeed M., and Houde, Jules, "Study of Bond Stress-Slip Relationships in Reinforced Concrete," ACI Journal, Proceedings Vol. 76, No. 1, Jan. 1979, pp. 19-46.

38. Morita, S., and Kaku, T., "Local Bond Stress-Slip Relationship under Static and Dynamic Repeated Loadings," Proceedings, IABSE Symposium on the Resistance and Ultimate Deformability of Structures (Lisbon, 1973), International Association for Bridge and Structural Engineering, Zurich, 1973, pp. 221-226.

39. Morita; Shiro; Kaku; Tetsuzo, "Splitting Bond Failures of Large Deformed Reinforcing Bars," ACI Journal, Proceedings Vol. 76, No. 1, Jan. 1979, pp. 93-110.

40. Naaman, A. E. and Shah, S. P., "Pull-out Mechanism in Steel Fibre Reinforced Concrete," ACI Journal, Structural Division, Proceedings Vol. 102, No. ST8, Aug. 1976, pp. 1537-58.

41. Naaman, A. E.; Nammur, G.; Najm, Husam; and Alwan, Jamil; "Bond Mechanisms in Fiber Reinforced Cement-Based Composites", a report on research sponsored by the United States Air Force Office of Scientific Research. Report UMCE 89-6, Department of Civil Engineering, University of Michigan, Ann Arbor, to be released in Aug. 1989.

42. Nair, N. G., "Mechanics of Glass Fibre Reinforced Cement," RILEM Symposium, London, 1975, Fibre Reinforced Cements and Concrete, The Construction Press Ltd, Hornby, 1975, p. 459.

43. Nammur, G. Jr.; Naaman, A. E.; and Clark, S. K., "Analytical Prediction of the Pull-out Behavior of Steel Fibers in Cementitious Matrices," to be published in the Proceedings of the Materials Research Society Symposium on "Cement Based Composites: Bonding in Cementitious Composites," S. Mindess and S. Shah, Editors.

44. Nilson, A. H., "Bond Stress-Slip Relationships in Reinforced Concrete," Report No. 345, Department of Structural Engineering, Cornell University, Ithaca, Dec. 1971.

45. Nilson, Arthur H., "Internal Measurement of Bond Slip," ACI Journal, Proceedings Vol. 69, No. 7, July 1972, pp. 439-441.

46. Orangun, C. O.; Jirsa, J. O.; and Breen, J. E., "A Reevaluation of Test Data on Development Length and Splices," ACI Journal, Vol. 74, No. 3, Mar. 1977.

47. Otter, D. E., and Naaman, A. E., "Fiber Reinforced Concrete Under Cyclic and Dynamic Compressive Loadings," a report on research sponsored by the National Science Foundation. Report UMCE 88-9, Department of Civil Engineering, University of Michigan, Ann Arbor, Oct. 1988, 178 pp.

48. Parameswaran, V. S., and Rajagopalan, K., "Discussion of a Paper: A Theory for the Flexural Strength of Steel Fiber Reinforced Concrete," Cement and Concrete Research, Vol. 5, No. 2, Mar. 1975, pp. 179-87.

49. Perry, Ervin S., and Jundi, Nabil, "Pull-out Bond Stress Distribution under Static and Dynamic Repeated Loadings," ACI Journal, Proceedings Vol. 66, No. 5, May 1969, pp. 377-380.

50. Pinchin, D. J., and Tabor, D., "Interfacial Contact Pressure and Frictional Stress Transfer in Steel Fiber," Proceedings, RILEM

Symposium on Testing and Test Methods of Fibre Cement Composites, Edited by R. N. Swamy, The Construction Press, 1978, pp. 337-344.

51. Popov, E. P.; Bertero, V. V.; Cowell, A. D.; and Viwathanatepa, S., "Reinforcing Steel Bond under Monotonic and Cyclic Loadings," SEAOC Conference, Lake Tahoe, Sept. 1978, Structural Engineers Association of California, San Francisco.

52. Proceedings of the Materials Research Society Symposium on "Cement Based Composites: Bonding in Cementitious Composites," held in Boston, December 2 to 4, 1987, S. Mindess and S. Shah, Editors.

53. Rehm, G., "The Fundamental Law of Bond," Proceedings, Symposium on Bond and Crack Formation in Reinforced Concrete (Stockholm, 1957), RILEM, Paris, (published by Tekniska Hogskolans Rotaprinttrychkeri, Stockholm, 1958).

54. Romualdi, J. P., and Batson, G. B., "Mechanics of Crack Arrest in Concrete," Proceedings, American Society of Civil Engineers Journal, Engineering Mechanics Division, Vol. 89, EM3, June 1963, pp. 147-68.

55. Somayaji, S., "Composite Response, Bond Stress-Slip Relationships and Cracking in Ferrocement and Reinforced Concrete," PhD Thesis, University of Illinois at Chicago Circle, 1979.

56. Somayaji, S., and Shah, S. P., "Bond Stress Versus Slip Relationship and Cracking Response of Tension Members," ACI Journal, Proceedings Vol. 78, No. 3, May-June 1981, pp. 217-225.

57. Soretz, S., and Hölzenbein, H., "Influence of Rib Dimensions of Reinforcing Bars on Bond and Bendability," ACI Journal, Proceedings Vol. 76, No. 1, Jan. 1979, pp. 111-125.

58. Stocker, M. F., and Sozen, M. A.,"Investigation of Prestressed Concrete for Highway Bridges, Part V: Bond Characteristics of

Prestressing Strands," Bulletin No. 503, Engineering Experiment Station, University of Illinois, Urbana, 1970, 119 pp.

59. Stroenen, P.; de Haan, Y. M.; and Bouter, C., "Pull-Out Tests of Steel Fibers," Proceedings, RILEM Symposium on Testing and Test Methods of Fibre Cement Composites, Edited by R. N. Swamy, The Construction Press, 1978, pp. 345-353.

60. Swamy, R. N.; Mangat, P. S.; and Rao, C. V. S. K., "The Mechanics of Fibre Reinforcement of Cement Matrices," Special Publication, SP-44, American Concrete Institute, Detroit, 1974, pp. 1-28.

61. Swamy, R. N., and Mangat, P. S., "A Theory for the Flexural Strength of Steel Fiber-reinforced Concrete," Cement and Concrete Research, Vol. 4, No. 3, pp. 313-25.

62. Tassios, T.P., and Yannopoulos, P. J., "Analytical Studies on Reinforced Concrete Members under Cyclic Loading Based on Bond Stress-Slip Relationships," ACI Journal, Proceedings Vol. 78, No. 3, May-June 1981, pp. 206-216.

63. Tatersall, G. H., and Urbanowicz, C. R., "Bond Strength in Steel - Fibre-Reinforced Concrete," Magazine of Concrete Research, Vol. 26, No. 87, June 1974, pp. 105-113.

64. Viwathanatepa, S.; Popov, E. P.; and Bertero, V. V., "Effects of Generalized Loadings on Bond of Reinforcing Bars Embedded in Confined Concrete Blocks," Report No. VCB/EERC-79/22, Earthquake Engineering Research Center, University of California, Berkeley, Aug. 1979, 304 pp.

65. Yankelevsky, D. Z., "Bond Action Between Concrete and a Deformed Bar - A New Model," ACI Journal, Proceedings Vol. 82, No. 2, Mar.-Apr. 1985, pp. 154-161.

66. Gopalaratnam, V. S., and Abu-Mathkour, H. J., "Investigation of The Pull-Out Characteristics of Steel Fibers From Mortar Matrices,"

Proceedings of the International Symposium on Fibre Reinforced Concrete, December 1987, Madras, India, pp. 2.201-2.2.211.

67. Mandel, J. A., Wei, S., and Said, S., "Studies of The Properties of The Fiber-Matrix Interface In Steel Fiber Reinforced Mortar," ACI Materials Journal, March-April 1987, pp. 101-109.

68. Wei, S., Mandel, J., and Said, S., "Study of The Interface Strength In Steel Fiber-Reinforced Cement-based Composites," ACI Materials Journal, July-August 1986, pp. 597-605.

69. Larson, B. K., and Bayasi, Z., "Carbon Fiber-Cement Adhesion in Carbon Fiber Reinforced Cement," a thesis submitted to Michigan State University in partial fulfillment of the requirements for the degree of MASTER OF SCIENCE, Department of Chemical Engineering, 1988.

70. Wang, Y., Li, V. C., and Backer, S., "Analysis of Synthetic Fiber Pullout From a Cement Matrix," Materials Research Society, symposium proceedings, V. 114, December 1987, pp. 159-165.

71 Shah, S. P., and Jenq, Y. S., "Fracture Mechanics of Interfaces," Materials Research Society, symposium proceedings, V. 114, December 1987, pp. 205-216.

72. Gao, Y. C., Mai, Y. W., and Cotterell, B., "Fracture of fiber-reinforced materials," Journal of Applied Mathematics and Physics (ZAMP), Vol. 39, July 1988, pp. 550-572.

73. Gopalaratnam, V. S., and Cheng, J., "On the Modeling of inelastic Interfaces in Fibrous Composites," Materials Research Society, symposium proceedings, V. 114, December 1987, pp. 225-231.